Volume 33 No. 1 | JNSChE Mar/Apr 2018 | ISSN 0794-6759

JOURNAL OF THE NIGERIAN SOCIETY OF CHEMICAL ENGINEERS

Published by,
THE NIGERIAN SOCIETY OF CHEMICAL ENGINEERS
National Secretariat: Infinite Grace House, Plot 4, Oyetubo Street,
Off Obafemi Awolowo Way, Ikeja, Lagos State, Nigeria.
E-mail: nationalhqtrs@nsche.org, nsche_headquarters@yahoo.com
Website: http:www.nsche.org.ng

JOURNAL OF THE NIGERIAN SOCIETY OF CHEMICAL ENGINEERS
A Publication on the Science and Technology of Chemical Engineering

EDITORIAL BOARD

2018 NIGERIAN SOCIETY OF CHEMICAL ENGINEERS

BOARD OF DIRECTORS AND OFFICIALS			CHAPTER CHAIRMEN	
Prof. Sam S. Adefila, *FNSChE*	National President		**Engr. G. H. Abubakar, MNSChE**	Kogi
Engr. O. A. Anyaoku, FNSChE	Deputy National President		**Engr. (Mrs.) Rosemary O. Imhanwa, MNSChE**	Edo/Delta
Prof. E. N. Wami A, *FNSChE*	Immediate Past President		**Engr. I. A. Dirani, MNSChE**	ABBYGOT
Engr. D. Uweh, *MNSChE*	Publicity Secretary		**Prof. I. A. Mohammed-Dabo, MNSChE**	Kaduna
Engr. Ben Akaakar, *FNSChE*	Asst. Publicity Secretary		**Dr. M. S. Nwakaudu, FNSChE**	Imo/Abia
Engr. Anthony Ogheneovo, *MNSChE*	National Treasurer		**Prof. G. O. Mbah, FNSChE**	Anambra/Enugu/ Ebonyi
Engr. (Mrs.) Edith A. Alagbe, *MNSChE*	Asst. National Treasurer		**Dr. A. A. Ujile,FNSChE**	RIVBAY
S. O. Bosoro, *MNSChE*	Executive Secretary		**Engr. N. A. Akanji,MNSChE**	Niger
			Engr. O. O. Onugu, MNSChE	FCT/Nasarawa
INTERNAL AUDITORS			**Prof. F. A. Akeredolu, FNSChE**	Oyo/Osun/Kwara
Engr. Dr. Mrs. G. Akujobi-Emetuche, *FNSChE*			**Dr. K. F. K. Oyedeko, FNSChE**	Lagos/Ogun
Engr. Edwin N.Ikezue, *FNSChE*			**Engr. T. S. Soom, MNSChE**	Benue Industrial
SUBSCRIPTION			**Dr. I. O. Oboh , MNSChE**	Akwa Ibom/Cross River
a. Individual Readers	₦1,500.00		**Dr. E. I. Dada, FNSChE**	USA
b. Overseas Subscribers	US$30.00			
c. Institution, Libraries, etc	₦2,500.00			

APPLICATION OF ZEOLITE 3A SYNTHESIZED FROM KANKARA CLAY FOR DEHYDRATION OF ETHANOL

[*]Olawale A. S., Ajayi O. A. and Bello M.
Department of Chemical Engineering,
Ahmadu Bello University, Zaria. Nigeria
[*]Corresponding author: asolawale@yahoo.com

ABSTRACT

In this work zeolite 3A pellets produced from Kankara kaolin through the normal hydrothermal (3AH) and fusion-hydrothermal (3AFH) routes and, commercial zeolite 3A (3AC) were characterized and used to dehydrate water-ethanol mixture at 90^{o}C. The pore size of 3AFH, 3AH and 3AC were 3.09, 3.78 and 2.82 Å respectively. The corresponding specific surface areas were 254.60, 177.0 and 225.5 m^{2}/g. The respective bulk densities of samples' pellets were 0.687. 0.673 and 0.91 g/cm^{3}. The properties compare well with the literature values except 3AH pore size. The breakthrough curves were obtained with 80 – 95 wt.% ethanol-water mixtures on 3AFH and 3AC pellets. However, only 95 wt% ethanol feed produced fuel grade (≥99.5 wt%) ethanol. The respective breakthrough times at inlet/outlet water concentrations (C/C$_{o}$) of 0.1 were 50 and 75 min on 3AFH and 3AC. Thus 3AFH pellets performed fairly well in comparison with commercial zeolite (3AC) pellets.

Keywords: *Molecular sieve, kaolin, water adsorption, isotherm models, breakthrough curve.*

INTRODUCTION

Bioethanol is a renewable energy source, which contributes to the reduction of the negative environmental impact of fossil fuels and has been of interest since the oil crisis of the 1970s (Anuradha, 2009). With the rising crude oil price, its continual depletion and environmental challenges coupled with the political instability in producing regions, biomass (a biofuel source) appears strongly, as pointed out by Hidayah (2010), capable of producing sustainable supply of energy needs into the future. It is no surprise then that a great deal of efforts in research and development have been directed at sourcing feedstocks and developing technologies for producing bioethanol (Agboola and Agboola, 2011 and Ogbonna and Eric, 2013).

Bioethanol produced through fermentation route require distillation and a further dehydration step beyond the water-ethanol azeotropic composition to give fuel grade product having ethanol purity in excess of 99.5 wt%. The commonly utilized processes for ethanol-water mixture include azeotropic distillation, extractive distillation, pervaporation and adsorption through zeolite or activated carbon bed (Antoine *et al*., 2012; Udeye *et al*., 2009; Anwar and Neni, 2012; Simo *et al.*, 2009; Al-Asheh *et al*, 2004; Okewale *et al*, 2013 and Yi *et al*, 2006). Adsorption using molecular sieve have been found to account for energy saving of up to 840 kJ/L when compared to distillation (Zainudeen, 2011).

Zeolite 3A has been established to be efficient for the dehydration of ethanol-water mixture beyond the azeotropic point of the mixture from many studies (Abdeen *et al*, 2011, Al-Ashieh *et al*, 2004 and Ben-Shebil, 1999). This zeolite could be produced from pure chemicals as well as alumino-silicate deposits and wastes such as kaolinite clay, fly ash and rice husk (Chairwat and Sopajaree, 2007; Tanaka and Fuji., 2009 and Mohamed *et al.*, 2015). The huge kaolin deposits of about two billion metric tons scattered in different parts of Nigeria have been found to be suitable for synthesis of zeolite 4A, which is a good precursor of zeolite 3A (Abdul-Salam *et al*, 2012 and Aderemi, 2003).

However, zeolite 4A produced from the natural deposits and their wastes have been found to require rigorous purification in order to compete with the relatively high cost commercial zeolites which are usually produced from very pure silicate and aluminate reagents. Efforts to utilize the abundant kaolin deposits available in Nigeria and elsewhere have been intensified (Aderemi, 2003; Kovo and Edoga, 2005; Omisanya *et al*, 2012; Bello *et al*, 2016 and Ugal *et al*, 2010). Bello *et al.*, (2016) reported the synthesis of a relatively purer zeolite 4A, than previously achieved, from Kankara clay by fusing the clay with sodium hydroxide prior to hydrothermal treatment of the reaction mix. Zeolite 3A which was synthesized from the relatively purer zeolite 4A described above was found to be relatively purer and

possessed physicochemical, structural and morphological characteristics (as observed from XRF, XRD, SEM results) that bear close similarity with those of some commercial zeolite 3A (Bello *et al.*, 2017). However, it is known that similar product which are derived from different sources may display differences in their performances due to the inevitable minute differences confer by the nature and sources of the material from which they are derived. (Murat *et al.*, 1992; Rios *et al*, 2007, 2010; Ugal *et al*, 2010). There is no available work on production of zeolite 3A from Kankara kaolin before now. It is thus worthwhile to investigate the characteristics and performance of zeolite 3A synthesized from this clay deposit.

Therefore, in this work two zeolite 3A samples produced from Kankara kaolin by Bello *et al.* (2017) were characterized, pelletized and used in a fixed bed adsorption experiments to study their capacity and ability to remove water from ethanol-water mixtures in comparison with commercial zeolite 3A, at 90^{o}C.

MATERIALS AND METHODS

The two zeolite 3A powder samples produced through the normal hydrothermal and fusion-hydrothermal methods by Bello *et al.,* (2017) were labelled 3AH and 3AFH respectively. The samples were pelletized; the powder and pellet samples of 3AH and 3AFH were characterized for physicochemical properties and adsorptive parameters. The powder samples were also subjected to isotherm studies. Finally, the adsorptive performance of the two pellet samples on ethanol-water mixtures of initial concentrations ranging between 80 and 95 wt% ethanol were determined. All these procedures except the pelletization steps were repeated with a commercial zeolite 3A pellets. Detailed procedures are described below.

Pelletization of Zeolite 3A

Powdered zeolite 3A sample (3AH) was mixed with beneficiated bentonite (binder) in 5:1 mass ratio. The mixture was ball-milled and passed through a 250 µm pore size sieve. Distilled water was added in small measures, to the resulting mixture, until a moldable slurry was obtained. The slurry was then forced through 2.45 mm perforations on a steel plate and the resulting cake molded into spherical pellets. The pellets were pre-dried in the sun (ca. 35^{o}C) and passed into an oven (NYC-101) to dry at 105^{o}C before subsequently calcined in an electric furnace (LH 120/14) at 650^{o}C for 18 h. (Golovko *et. al.*, 1976). This procedure was repeated on the second zeolite 3A sample synthesized (3AFH).

Characterization of Zeolite 3A Samples

This was carried out on the three zeolite 3A samples, namely a commercial zeolite 3A, 3AH and 3FAH. The pore size, pore volume and specific surface area of these zeolite samples were determined using Bennet-Emmett-Teller (BET) analytical method (Baldania *et al.*,2012; Khair *et al.*, 2009; Yi Li *et al.*, 2006 and Azarfar *et al.*, 2015). Other characterizations such as XRF, XRD and SEM of the samples are already reported by Bello *et al.*, (2017). The voidage, size, densities and crush strength of the three samples' pellets were determined as described by Ugal *et al.* (2008) and Igathinathane *et al.*, (2010).

Adsorption Isotherm Studies

Equilibrium adsorption study was carried out on the three zeolite 3A (3AC, 3AH and 3AFH) powder samples using the method described by Okewale *et al.*, (2013). Five ethanol-water solutions with initial concentrations between 50 and 90 wt% ethanol were used on 1 g. zeolite 3A samples placed in 50 ml Erlenmeyer flasks at 30^{o}C for 1 h. Filtration of the slurries were effected with Whatman filter No. 1 and the refractive index of each filtrate was determined using refractometer (MAR-33). The ethanol content of each filtrate was subsequently obtained. The amount of water adsorbed was obtained using Equation 1.

$$q_{(e)} = \frac{V}{W}\frac{(C_0 - C_e)}{C_e} \qquad 1$$

where: C_e is the equilibrium concentration, C_o is initial concertation, V is volume of solution and W is mass of zeolite used.

The equilibrium data were then fitted to Freundlich, Temkin and Langmuir adsorption isotherm models.

Adsorption Performance of Zeolite Pellets

The adsorptive performance experiments were carried out on a laboratory fixed bed adsorption column. The experimental rig was made up of water bath, lagged adsorption column (diameter: 2 cm; length: 40 cm), condenser and conical flask (250 ml) as shown in Figure 1.

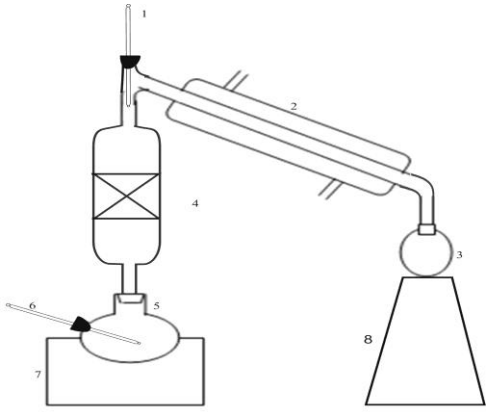

Figure 1: Adsorption rig

1, 6 - thermometer; 2 – condenser; 3 – collector; 4 - column containing zeolite bed; 5 - round bottom flask containing ethanol-water mixture; 7 - water bath; 8 – collector's support.

Different initial aqueous ethanol solutions' concentrations (80, 85, 90 and 95 wt % ethanol) and 20 g. zeolite 3A dose were used in this water adsorption study. A preliminary study indicated that 20 g. adsorbent dose was adequate for water adsorption (Bello, 2016). The ethanol-water mixture was vaporized from the 250 ml flask immersed in a thermostated water bath and made to pass through the zeolite 3A bed placed inside a glass column at 90^{o}C and atmospheric pressure (≈ 1atm). The effluent from the column was collected as condensate in a glass receiver at 10 min. interval. The condensate was then analyzed by refractometer (MAR-33) to obtain the purity of the condensate using a previously prepared calibrated curve. The procedure was repeated with all ethanol-water mixture concentrations and the three zeolite 3A samples.

RESULTS AND DISCUSSION

Characteristics of Zeolite 3A Samples

The XRF, XRD and FTIR results of the two zeolite 3A (3AH and 3AFH) samples gave indication of synthesis of zeolite 3A of varying purity as could be seen from Table 1a, Figures 2a-b and 3 which were presented in previous works (Bello, 2016 and Bello *et al.,* 2017). Table 1b gives additional properties of the two synthesized zeolite 3A (3AFH and 3AH) and commercial zeolite 3A (3AC) samples investigated in this work.

Table 1a: Composition of zeolite 3A developed from 4AFH, 4AH and commercial 3A using x-ray florescence analysis

Composition (wt.%)	3AFH*	3AH*	3AC*
SiO_2	31.47	30.90	48.2
Al_2O_3	19.50	18.00	31.4
K_2O	34.60	36.56	17.62
Na_2O	0.99	1.06	-
TiO_2	0.094	0.07	0.246
V_2O_5	-	0.03	0.021
Pr_2O_3	0.019	-	-
BaO	-	0.25	0.087
ZnO	-	-	-
Fe_2O_3	0.22	0.24	2.28
Eu_2O_3	0.06	-	0.01
Si/Al (molar ratio)	2.73	2.86	2.61

Table 1b: Properties of zeolite 3A samples

Properties/adsorbent	3AFH*	3AH*	3AC*	Specifications[a]
Pore size (Å)	3.09	3.73	2.82	2.76-3.0
Pore volume (cm^3/g)	0.0873	0.063	0.0802	-
Surface area (m^2/g)	245.6	177.0	225.5	-
Diameter of pellets (mm)	3.25	3.25	3.3	2.5- 5
Crush strength (N)	12.5	12.5	13.8	≥80
Voidage	0.623	0.615	0.716	-
Bulk density (gcm^{-3})	0.687	0.673	0.910	0.7-0.76
Particle density (gcm^{-3})	1.825	1.750	3.210	-

*3AFH: zeolite 3A developed through fusion - hydrothermal route; *3AH: zeolite 3A developed through the normal hydrothermal route; *3AC: commercial zeolite 3A

a: Sources - Baldania *et al.,* 2012; Khair *et al.,* 2009; Fasanya, 2009

The pore dimensions and specific surface area of 3AFH sample are better than those of 3AH sample and are comparable to those of typical commercial zeolite 3A and or specifications (Baldania *et al.,* 2012; Khair *et al.,* 2009; Fasanya, 2009). The pore size of 3AH is far higher than the commercial zeolite and specification. This may be traced to the difference in the synthesis methods employed for the two samples. The properties of the zeolites' pellets presented in Table 1b are not too different from those of the commercial samples and not

too far from indicated specifications. The crush strength of the three zeolite samples used in this work are far lower than the specification. This would be due to the non-mechanized pelletization method used in this work, especially for 3AFH and 3AH samples.

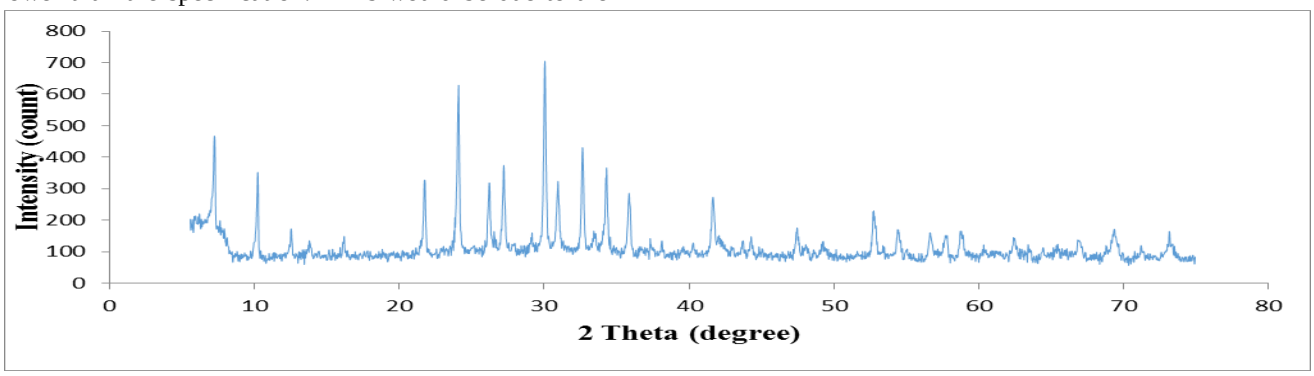

Figure 2a: XRD of zeolite 3A produced through fusion - hydrothermal route (3AFH).

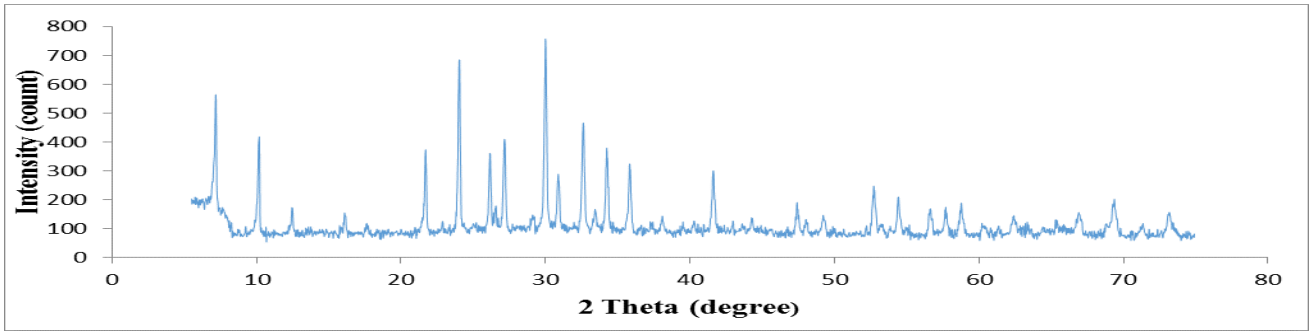

Figure 2b: XRD of zeolite 3A produced through straight hydrothermal route (3AH).

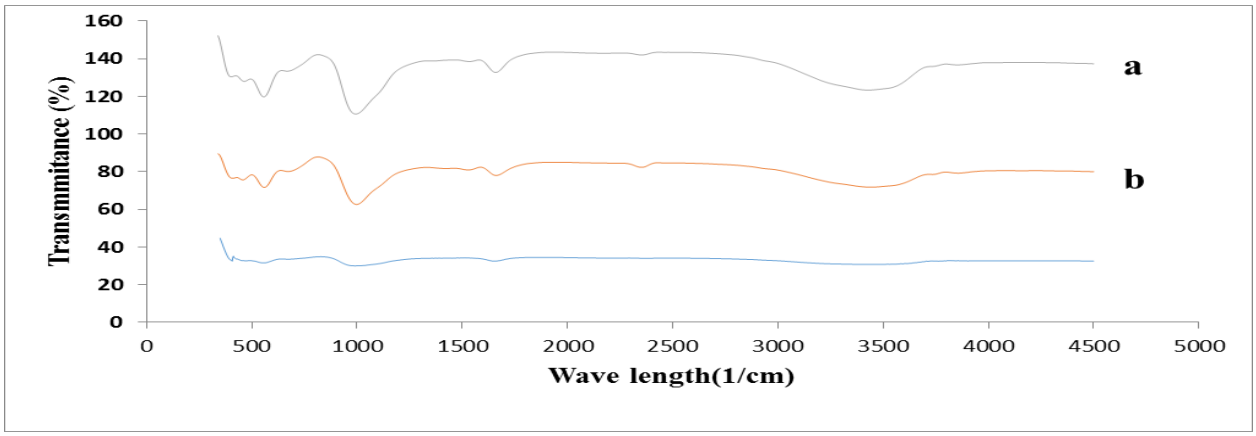

Figure 3: FTIR of zeolite 3A samples – (a) 3AFH (b) 3AH and (c) 3AC

Adsorption Isotherm Studies

The equilibrium data from the isotherm studies were fitted to Langmuir, Freundlich and Temkin isotherm models (see Table 2a) for the zeolite 3A samples labelled 3AH, 3AFH and the commercial zeolite used in this study. Langmuir isotherm model gave the best fit of water adsorption on the two synthesized adsorbents.

This is reflected in their respective coefficient of determination (R^2) values of 0.931 and 0.95 (see Table 2a). The values of Langmuir constant (b) indicates a favourable adsorption of water on zeolite 3A samples investigated as b<<<1. The adsorption capacities of 3AFH and 3AH were 2.193 g/g and 1.653 g/g respectively. Commercial zeolite was best fitted with Freundlich isotherm model. The difference in the fitted isotherm models between the commercial and synthesized zeolite 3A might be traced to the binder materials used in the commercial sample.

Table 2a: Adsorption isotherm equations

Isotherm	Normal Equation	Linear Form	Plot
Langmuir	$q_e = \frac{q_m b C_e}{1 + bC_e}$	$\frac{C_e}{q_e} = \frac{1}{q_m} Ce + \frac{1}{q_m b}$	$\frac{C_e}{q_e}\ vs. C_e$
Freundlich	$q_e = K_f Ce^{1/n}$	$\log q_{e=} \frac{1}{n} logC_e + logK_f$	$log\ q_e$ vs log C_e
Temkin	$q_e = \frac{RT}{b_T} In(K_T Ce)$	$q_e = \frac{RT}{b_T} InCe + \frac{RT}{b_T} InK_T$	$q_e\ vs\ In\ C_e$

q_e: mass of water adsorbed/mass of the adsorbent at equilibrium, C_e: equilibrium concentration, q_m: maximum capacity of the adsorbent, b: Langmuir constant related to the affinity of the binding site, 1/n: adsorption intensity, K_f: multilayer adsorption capacity, K_T: Temkin constant related to adsorption capacity, R: universal gas constant and T: absolute temperature

Table 2b: Isotherm parameters of the different adsorbents used.

Isotherm models and parameters									
Sample	**Langmuir**			**Freundlich**			**Temkin**		
	B	**q_m**	**R^2**	**1/n**	**K_f**	**R^2**	**b_T**	**K_T**	**R^2**
3AFH	0.1356	2.193	0.93	0.456	0.456	0.86	2.8665	0.414	0.73
3AH	0.082	1.653	0.95	0.432	0.432	0.86	0.8367	0.359	0.85
3AC	1.345	1.972	0.583	0.266	0.9750	0.674	9.641	0.425	0.642

Langmuir isotherm model has been found to describe the equilibrium isotherm of zeolite 3A by Sumo *et. al*. (2009) and Ben-Shebil (1999), though other models, including Freundlich model, have been identified as appropriate for zeolite 3A as well (Al-Asheh *et al.*, 2004 and Ben-Shebil, 1999). Though the other two models recorded R^2 values between 0.73 and 0.86 for the synthesized zeolite 3A samples, a cursory look at their associated parameters shows that the zeolite sample labelled 3AFH possesses better adsorption potential (from K_T values) and greater water affinity (as shown by its K_f and 1/n values) than 3AH sample.

Adsorption Performance of Zeolite 3A Pellets

The breakthrough curves of water adsorption from ethanol-water mixtures of various initial concentrations (80-95 wt%) with 20 g. adsorbents are presented in Figures 4a and 4b. These curves are for the synthesized zeolite 3A sample labelled 3AFH and the commercial zeolite 3A respectively. No breakthrough curve was achieved with the synthesized zeolite 3A labelled 3AH. This might be due to the relatively impure nature of this zeolite (3AH) sample as seen from the XRF (Table 1a) and SEM (Figure 5) results reported by Bello *et al.*, (2017) and the BET results presented in Table 1b.

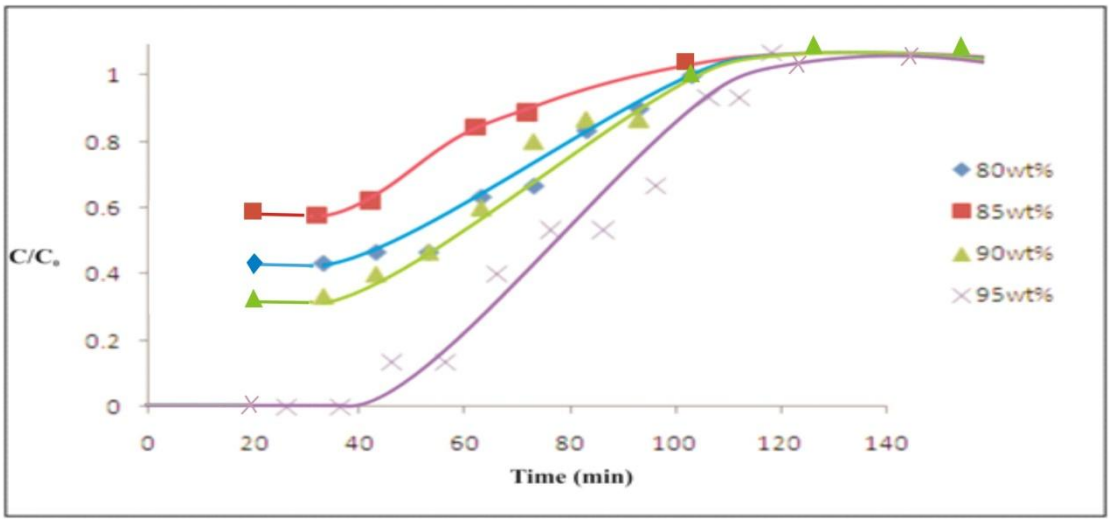

Figure 4a: Breakthrough curves of ethanol-water mixtures (80-95 wt%) on 3AFH

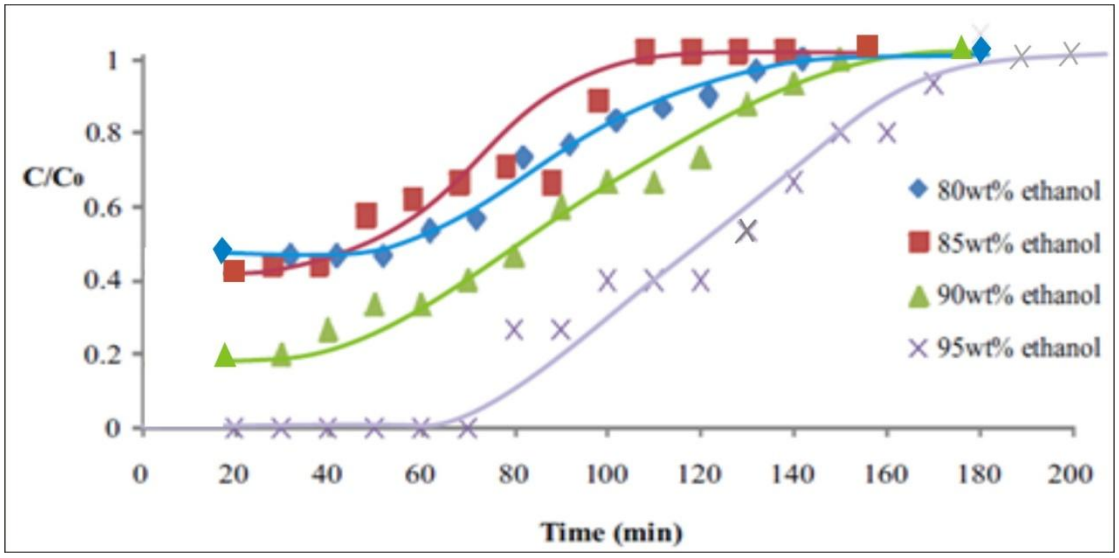

Figure 4b: Breakthrough curves of ethanol-water mixtures (80-95 wt%) on commercial zeolite 3A

C - water concentration at an arbitrary time
C_o - initial water concentration in the mixture

With the break point set at adsorbent bed's inlet/exit water concentrations (C/C_o) of 0.1 (McCabe *et. al*., 1985), commercial zeolite 3A and 3AFH samples were able to meet the required adsorptive removal of water from ethanol-water mixtures up to 50 min and 75 min respectively, when the initial (feed) concentration was 95 wt% ethanol. Fuel grade bioethanol is usually of 99.5 wt% ethanol purity or higher (Panitchakarn *et al.*, 2014). Actual exit concentration of 100 wt% ethanol was obtained up to 45 and 70 min with 3AFH and commercial zeolite respectively. The first distillate (effluent) was collected at about 20 min in each run. However, the two synthesized and commercial zeolite 3A samples could not achieve the breakthrough (at C/C_o = 0.1) when the feeds of 10, 15 and 20 wt% water were used. This could be due to the inadequate capacity of the 20 g adsorbents used here for these three feed concentrations. The exit concentrations obtained from the four feed concentrations on commercial zeolite 3A and 3AFH samples are presented in Table 3.

Table 3: Exit concentration of ethanol-water mixtures on 3AFH and commercial zeolite 3A

Initial mixture conc., (water wt%)	Exit conc. (wt% ethanol) of condensate (and time)	
	3AFH	Commercial
5	100.0	100.0
10	96.67	97.88
15	91.33	93.33
20	91.33	90.67

From Figures 2 and 3 as well as Table 3 it is seen that the concentration of ethanol in the effluent increases with increased feed concentration as expected (Pruksathorn *et al.*, 2009; Al-Asheh *et al.*, 2004; McCabe *et al., 1985*). Although the synthesized zeolite (3AFH sample) performed comparatively well in dehydration of bioethanol, it is still a little inferior to commercial zeolite 3A as seen from the exit/breakthrough time recorded with 95 wt% feeds. This relatively lower adsorption performance of 3AFH could be traced to the impurities shown in XRF and SEM results (Table 1a and Figure 5) of the sample as reported by Bello *et al.*, (2017).

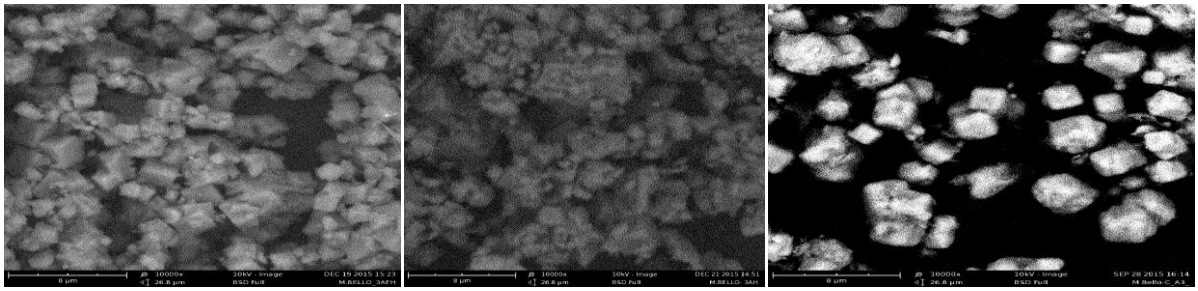

(a) (b) (c)

Figure 5: SEM micrograph of zeolite 3A samples – (a) 3AFH (b) 3AH and (c) 3AC

CONCLUSION

The zeolite 3A produced through the fusion-hydrothermal route (3AFH) was found to possess morphological characteristics and pore size which fall within the standard specifications and are comparable to those of commercial zeolite 3A. Langmuir isotherm best fitted the two zeolite 3A samples synthesized from kaolin (3AFH and 3AH) in this work, with respective R^2 values of 0.931 and 0.950. The commercial zeolite used in this study was best fitted with Freundlich isotherm model.

The pellets of 3AFH was able to produce ethanol of fuel grade purity from 95 wt% ethanol feed, while the pellets of the other sample (3AH) was not successful in this regard. The breakthrough time values for pellets of zeolite 3AFH and commercial zeolite 3A were 50 and 75 min respectively. This indicated superiority of commercial zeolite over 3AFH could be traced to the raw material sources employed.

REFERENCES

Abdulsalam, S., Misau, M. I., Abdulkarim, A. (2012). Potentials of Alkaleri and Kankara kaolinite clay for the production of aluminum sulphate. *International Journal of Engineering Research and Applications*. **2**, 2248-9622.

Aderemi, B. O. (2003). Synthesis and application of zeolite A from Kankara kaolin clay. *Nigeria Journal of Engineering*. **11** (2), 77-81

Abdeen, F. R. H., Maizirwan, M., Maan, K. and Azlin, S. A. (2011). Dehydration of ethanol on zeolite based media using adsorption process. Proceedings of the 3rd CUTSE International Conference. Miri, Sarawak, Malaysia. 8-9th November, pp 312-322

Agboola, O. P. and Agboola, M. O. (2011). Nigeria's bio-ethanol: Need for capacity building strategies to prevent food crisis. World Renewable Energy Congress. Linkoping, Sweden. 8-13th May, pp 258-265.

Al-Asheh, S., Banat, E. and Al-Lagtah, N. (2004). Separation of ethanol-water mixture using molecular sieve and bio-mass adsorbents. *Chemical Engineering Research and Design*. **83** (A7), 855 – 861.

Anuradha, M. (2009). On farm ethanol dewatering: Detailed design of distillation unit. M.Sc. Thesis, Department of Chemical Engineering, Oklahoma State University, U.S.A.

Anwar, M and Neni, D. (2012). Sythesis of zeolite pellets from natural zeolite and starch as adsorbent for fuel grade bio-ethanol production. Proceedings of International Conference on Chemical and Material Engineering. 12-13th September, Semarang, Indonesia, BRE 5 pp 1-5

Baldania, A. D and Choksi, H. C. (2012). Purification of ethanol by adsorption using 3A zeolite adsorbent under static condition. *International Journal of Biotechnology, Chemical and Environmental Engineering.* **1** (2), 6-8

Ben-Shebil, S. M. (1999). Effects of heat adsorption on the adsorptive drying at equilibrium in a packed bed of zeolite. *Chemical Engineering Journal.* **74**, 197-204

Bello, M. (2016). Adsorption performance of zeolite 3A synthesized from Kankara kaolin on water-ethanol; mixture. M. Sc. Thesis, Department of Chemical Engineering Ahmadu Bello University Zaria.

Bello, M., Olawale A.S. and Ajayi O. A. (2016). Fusion/hydrothermal synthesis of zeolite 4A from Kankara kaolin. Proceedings of National Conference of Material Society of Nigeria. 2-3rd November, Zaria, Nigeria. pp 422-426

Bello, M., Olawale A.S. and Ajayi O. A. (2017). Development of zeolite 3A from Kankara kaolin, *Nigeria Journal of Engineering*. **23** (2), 22-30

Chairwat, R. and Sopajaree, K. (2007). Modification of synthetic zeolite pellet from lignite fly ash: The pelletization. World of Coal Ash (WOCA). 7-10th May, Northern Kentucky, USA. 9 pages.

Fasanya, O. (2009). Modeling and adsorption process for the production of fuel grade ethanol from and water-ethanol; mixture. MSc. Thesis, Department of Chemical Engineering Ahmadu Bello University Zaria.

Golovko, G. A., Lipkind, B. A., Slepneva, A. T., *et. al.* (1976). Process for the preparation of synthetic zeolite. United States Patent 3,979,335; 252/455Z, 7th Sept. http://www.freepatentsonline.com/3979335.html

Hidayah, N. (2010). Effect of substrate concentration and agitation rate on butanol production from palm oil mill effluent using C*lostridium acetobutyllicum*. B Eng. Research Report, Department of Chemical Engineering

and Natural Resources, University of Malaysia, Pahang, Malaysia.

Igathinathane, C., Tumuluru, J. S., Sokhansanj, S., Bi, X., Lim, C. J., Melin, S. and Mohammad, E. (2010). Simple and inexpensive method of wood pellets macro-porosity measurement. *Journal of Bioresource Technology*. **101**, 6528-6537

Kovo, A. S. and Edoga, M. O. (2005). Production and Characterisation of Zeolite from
Ahoko clay in Kogi State, Nigeria. *Leonardo Electronic Journal of Practices and Technologies*. Issue **7**, 31-40

Khaidir, D., Setyaningsih, H. and Dan, H. H. (2009). Modification of natural zeolite as molecular sieve material on bioethanol dehydration. *Journal of Indonesia Zeolites.* **8** (2), 97-105.

McCabe, L.M., Smith, J. C. and Harriot, P. (1985). Unit Operations of Chemical Engineering. 4th ed. McGraw-Hill Book Co., New York, U.S.A, pp 818-819

Mohamed, M. R., M, I. A. and Barakat, M. A. (2012). Rice husk ash as a renewable source for the production of zeolite NaY and its characterization. *Arabian Journal of Chemistry*. **8** (1), 48-53

Murat, M., Amokrane, A., Bastide, J. P. and Montanaro, L. (1992). Synthesis of zeolites from thermally activated kaolinite: Some observations on nucleation and growth. *Clay Minerals.* **27**, 119-131

Ogbonna, C. N. and Eric, C. O. (2013). Economic feasibility of on farm fuel ethanol production from cassava tubers in rural communities. *African Journal of Biotechnology*. **12** (37), 5618-5626.

Omisanya, N. O., Folayan, C. O., Aku, S. Y. and Adefila, S. S. (2012). Synthesis and characterization of zeolite A for adsorption refrigeration application. *Pelagia Research Library: Advances in Applied Science Research.* **6**, 3746-3754

Okewale, A. O., Babayemi, K. A. and Olalekan, A. P. (2013). Adsorption isotherm and kinetics models of starchy adsorbents on uptake of water from ethanol water system. *International Journal of Applied Science and Technology.* **3**(1), 35-42

Panitchakarn, P., Klamrassamee, T., Laosiripojana, N., Viriya-empikul, N. and Pavasant, P. (2014). Synthesis and testing of zolite from industrial-waste coal fly ash as sorbent for water adsorption from ethanol solution. *Engineering Journal.* **18** (1), 37-44. http://www.engj.org/ DOI:10.4186/ej.2014.18.1.1

Rios, C. A., Williams, C. D. and Maple, M. J. (2007). Synthesis of zeolites and zeolite types by hydrothermal transformation of kaolinite and metakaolinite. *Inglaterra.* **5** (1), 15-36

Rios, C. A., Williams, C. D. and Castellanos, O. M. (2010). Synthesis of zeolite LTA from thermally treated kaolinite. *Rev. Fac. Ing., Univ. Antioquia.* No. 53, 30-44.

Simo. M., Christopher J. B. and Vladimir H. (2008). Simulation of pressure swing adsorption in fuel ethanol production process. *Journal of Computer and Chemical Engineering.* **32** 1635-1649

Simo. M., Shivashanmugam S., Christopher J. B. and Vladimir H. (2009). Adsorption/desorption of water and ethanol on 3A zeolite in near adiabatic fixed bed. *Industrial Engineering Chemistry Research.* **48**, 9247-9260

Tanaka, H. and Fuji, A. (2009). Effect of stirring on the dissolution of coal fly ash and synthesis of pure form Na-A and –X zeolites by two step process. *Advanced Powder Technology*. **20**,473-479.

Trent, R. E. (1993). Fundamentals of molecular sieve design. Presented at the AIChE Spring National Meeting, Houston Texas. April.

Udeye, V. S., Vorasingh, A. and Amornsakchai, P. (2009). Ethanol heterogeneous azeotropic distillation design and construction. *International Journal of Physical Sciences.* **4**(3), 101-106

Ugal, R. J., Mustafa, M. and Abdulhadi, A. A. (2008). Preparation of zeolite type 13X from locally available raw materials. *Iraqi Journal of Chemical and Petroleum Engineering*. **9,** (1) 51-56

Characterization and properties measurements. *Journal of the Association of Arab Universities for Basic and Applied Sciences.* **9**, 1-8

Yi, L., Huai, M. G., Tai-Shung, C. and Santi, K. (2006). Effects of novel silane modification of zeolite surface on polymer chain regasification and partial pore blockage

in polyethersulfone (PES)-zeolite A mixed matrix membrane. *Journal of Membrane Science.* **275**, 17-28.

Zainudeen, M. (2011). Pervaporative separation of ethanol-water mixtures using Ghanian zeolite-clay filled PVA composite membrane. M. Sc. Research Project. Department of Chemical Engineering, Kwame Nkrumah University of Science and Technology, Kumasi, Ghana.

TRANSALKYLATION OF BENZENE WITH XYLENE ON ZnO SUPPORTED ALUMINA CATALYSTS

AbdulAzeez, R. I.[1], Gbadamasi, S.[1], Fasanya, O. O.[1], Yusuf, A. I.[1], Osigbesan, A.[1], *Atta, A. Y[2] and Jibril, B. Y.[2]

[1]Petrochemical & Allied Department, National Research Institute for Chemical Technology, Zaria
[2]Department of Chemical Engineering, Ahmadu Bello University, Zaria
*Corresponding author: zeezoatta@yahoo.com

ABSTRACT

Screening of a synthesized ZnO-supported alumina catalyst for benzene transalkylation with xylene was carried out in a batch reactor at atmospheric pressure. The catalyst was prepared via the incipient wet impregnation method and calcined under air at 600˚C for 3 hours. The catalyst characterized with XRD and FTIR shows the deposition of ZnO (2 wt%) on the alumina support. The performance of the catalyst was assessed through reactant (benzene) conversion and product (ethylbenzene) yield. Catalytic experiments were conducted within the temperature range of 60-80˚C to elucidate the transformation of these aromatics over the prepared catalyst. The effects of reaction parameters such as temperature, time and catalyst dosage (from 0-1.3% wt/wt) on benzene conversion and ethylbenzene yield were also studied. A maximum benzene conversion (46.70%) with ethylbenzene yield (63.50%) was obtained at 70˚C for 45 mins and 0.7 wt% catalyst dosage. The study revealed that the catalyst is active and holds potential for benzene transalkyaltion reactions for industrial application.

1. INTRODUCTION

Aromatics are known to be the key raw materials for petrochemical and chemical industries. Key amongst them are benzene, toluene and xylene, which are the most important intermediates for the manufacture of materials such as plastic, fibers, resins, dyestuffs and detergents (Dias *et al*., 2007). Catalytic transalkylation and disproportionation of aromatic hydrocarbons are among the processes employed to produce suitable intermediate products for use in the petrochemical industries (Xu *et al*., 2007). The recent stringent regulations on the use of benzene in reformulated gasoline has increased the importance of benzene transalkylation with methylated benzenes as a potential reaction for commercial applications and its investigation is attracting interest both in the industry and academia (Dias *et al.*, 2007). In the traditional process, transalkylation is performed in the presence of strong mineral acids or Lewis acids (e.g. HF, H_2SO_4, and $AlCl_3$) but they have been recently substituted by zeolites owing to the latter's environmental friendliness (Perego and Ingallina, 2002). Transalkylation of alkyl benzenes with benzene has been studied extensively over several zeolitic and non zeolitic catalysts. Catalytic transformations of methyl benzenes on zeolite catalysts were investigated and it was found that the pore structure of the zeolite controls the reactivity of the reactants (Al-Khattaf *et al.*, 2011). Zeolites, particularly, with 12 member rings pore aperture, including BETA, mordenite and ultra-stable Y (USY) have been exploited as catalysts for transalkylation processes (Tsai *et al.*, 2002). However, these catalysts are prone to deactivation especially when heavy aromatics feed are employed. This lowers the catalysts' efficiencies and cycle lives. Studies have shown that the coke formed over USY during toluene disproportionation is mostly polyaromatic, and its structure is dependent on the reaction temperature. The higher the temperature the more condense rings are formed. However, incorporating certain metals (Cu, Ni, Pt, etc) with the zeolites was found to inhibit the aging problem as the metals are believed to hydrogenate the polyaromatic coke precursors (Magnoux *et al.*, 1992). Different zeolites incorporated with these metals have been studied for transalkylation and disproportionation. Toluene disproportionation over modified ZSM-5 with Ni, Cr, Mg, Bi and Zn in a fixed bed reactor has been investigated. It was found that toluene conversion and *p*-xylene yield was highest on Ni/ZSM-5 catalysts while Mg- and Cr/ZSM-5 showed the lowest yields (Abdal-Kareem and Mishra, 2002).

Roldán and co-workers studied the gas phase transformation of mixtures of benzene and xylene over several zeolite catalysts in the temperature range of 250-350˚C. They found that large pore zeolites (H-mordenite, USY, and BETA) are more active towards transalkylation of benzene and xylene and disproportionation of xylene, exhibiting different activities and selectivities depending on their acidity and pore geometry. They showed that medium pore zeolites

(ZSM-5 and FER) were inactive for the reaction (Roldán *et al.*, 2004).

Also, transalkylation of benzene with C_9^+ aromatics on silica-supported 12-tungstophosphoric acid was carried out by Dias and co-workers. The catalytic activity and selectivity to xylene formation was found to be affected by H_3PW acid loading (Dias *et al.*, 2007). In another report, the performance of triflic acid in the transformation of mixtures of metha diethylbenzene (*m*-DEB) and benzene into ethylbenzene was investigated. The study showed a maximum conversion of 57 mol% for *m*-DEB and selectivity of 80% to ethylbenzene at 35˚C with a 1:1 mole ratio. The high yield of ethylbenzene obtained from *m*-DEB showed that triflic acid was active as a catalyst for the system (Al-Dosari, 2010). Similarly, the activity of triflic acid on the conversion of *o*-DEB and benzene into ethylbenzene was evaluated. It was observed that at a certain temperature, *o*-DEB conversion to ethylbenzene strongly depended on the mole ratio of benzene/*o*-DEB (Al-Kinany *et al.*, 2005). An earlier work on the kinetics for the liquid-phase transalkylation, disproportionation and isomerization of *m*-DEB with benzene using triflic acid as catalyst was reported. The kinetic expression for the reaction was found to be first order with respect to *m*-DEB and benzene while the rate of disproportination reaction was second order (Al-Zahrani *et al.*, 2003). Furthermore, a comprehensive kinetic model for transformation of methyl benzenes over zeolite catalysts using reactant conversion (RC) models and time on stream (TOR) models has been developed. The report asserted that pore structure of the zeolites play critical role in transformations of aromatics (Al-Khattaf *et al.*, 2011).

Although numerous studies have been reported in open literature on transformations of alkyl benzenes with benzene, reports on low temperature transformation of benzene and xylene to ethylbenzene over ZnO supported on alumina catalyst is not available. Considering the importance of the system, the catalytic transformation of benzene and xylene over ZnO/Al_2O_3 catalyst under liquid phase conditions at low temperatures and atmospheric pressure is investigated. The effect of reaction time, temperature and catalyst dosage on benzene conversion and ethylbenzene yield are studied.

2. MATERIALS AND METHODS

2.1 Chemicals and raw materials

The materials used in this study are alumina, zinc nitrate hexahydrate, $Zn(NO_3)_2.\ 6H_2O$ and distilled water. Analytical grade Alumina and zinc nitrate were obtained from BDH Chemicals, Poole England. General purpose reagent xylene and benzene were also obtained from Johnson Solomon Ltd., London England. All chemicals were used as received.

2.2 Catalyst preparation

ZnO-Alumina supported catalyst [ZnO/Alumina (2 wt% ZnO)] was prepared via the standard incipient wetness impregnation technique because of the simplicity of the method and its minimal material waste (Munnik, *et al*., 2015). This was achieved by weighing a known quantity of alumina and mixing with an aqueous solution of zinc nitrate containing 2 wt% of ZnO. A glass vessel with a mechanical stirrer was used to prepare the catalyst at a temperature of 80˚C slowly evaporating the mixture to dryness. The dried mixture was placed in an oven at 100˚C overnight. The final dried sample was calcined under air at 600˚C for 3 hours.

2.3 Characterization

The calcined sample was characterized by Fourier transform infrared spectrometer (FT-IR) and X-ray diffractometer (XRD). Fourier transform infrared spectra were obtained with a Shimadzu FT-IR 8400S spectrometer with a normal detector. The sample was mixed with KBr and pressed to produce discs that were analyzed in the range of 4000–400 cm^{-1} with 4 cm^{-1} resolution and 10 scans.

The structure and crystallinity of the calcined sample was obtained using a Philips PW1710 X-ray diffractometer. The 2θ angles were varied between 5˚ to 70˚ at 0.02˚ ramp min^{-1} using CuKα (40kV, 40 mA) radiation. Nitrogen sorption isotherms were performed at liquid nitrogen temperature (−196˚C) on a GoldApp F-Sorp 2400 surface area analyzer to determine the specific surface area. Prior to the sorption measurements, 500 mg of the prepared catalyst was out gassed at 200˚C until constant pressure was achieved.

2.4 Reaction System

The reaction was performed in a closed liquid batch reactor with continuous stirring over a water bath at a constant temperature of 80˚C. The batch reactor was equipped with a thermometer to monitor the reaction temperature. The reaction procedure involved first raising the temperature of the reactants to 80˚C separately, mixing the reactants and then introducing weighed sample of the catalyst (0-1.3 wt% of the reactants (benzene and xylene). Transalkylation reaction was carried out at reaction times of 0, 15, 30 and 45 mins and reaction temperatures of 60, 70 and 80˚C. The

analysis of the reaction mixture was carried out using a Schimadzu GC-MS QP 2010Plus chromatograph. This chromatograph is equipped with a 30 m × 0.25 mm id capillary RTX-1 column (film thickness of 0.25 µm) and a flame ionization detector. n-hexane was used as a diluent prior to the GC-MS analysis. In all the different experiments, the product distributions were determined by analyzing samples of the reacting mixtures after quenching in an iced bath.

3. RESULTS AND DISCUSSION

3.1 Characterization

Figure 1 shows X-ray diffractograms of Al_2O_3 and ZnO/Al_2O_3 in the 2θ range 10-70. The peaks have been identified as belonging to the phases of ZnO, $ZnAl_2O_4$ and Al_2O_3. The relatively high intensity counts and sharp peaks showed that the Al_2O_3 was a crystalline material. The occurrence of additional peaks in X-ray pattern of ZnO/Al_2O_3 became evident, indicating the presence of the Zn-O phases, as confirmed by IR spectra in Figure 2 with characteristics peaks at 450-600 cm^{-1}. Also, traces of spinel, $ZnAl_2O_4$, were observed as a weak peak appeared at 65.2° 2θ supporting spinel phase formation. This is also collaborated by FTIR spectra, as there are characteristic peaks at 810 and 610 cm^{-1} corresponding to a normal spinel structure with tetrahedrally and octahedrally coordinated Al-O respectively (Kim, 2008). Surface area of the alumina and ZnO/Al_2O_3 catalyst was determined to be 1.10 m^2/g and 1.70 m^2/g respectively. The deposition of ZnO particles on the alumina support created heterogeneity that resulted in a higher surface area of the resultant catalyst. This value satisfies the minimum requirement to be termed "active solid" for used in chemical reactions (Kiyohara, *et al*., 2000).

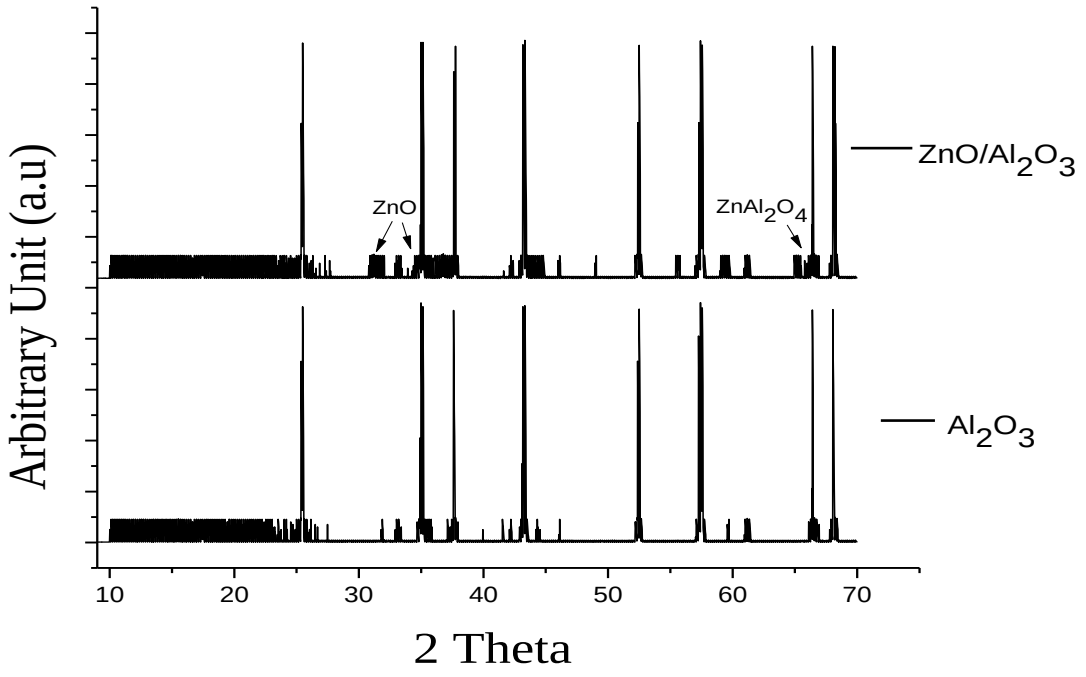

Figure 1. XRD diffractograms for Al_2O_3 and ZnO/Al_2O_3

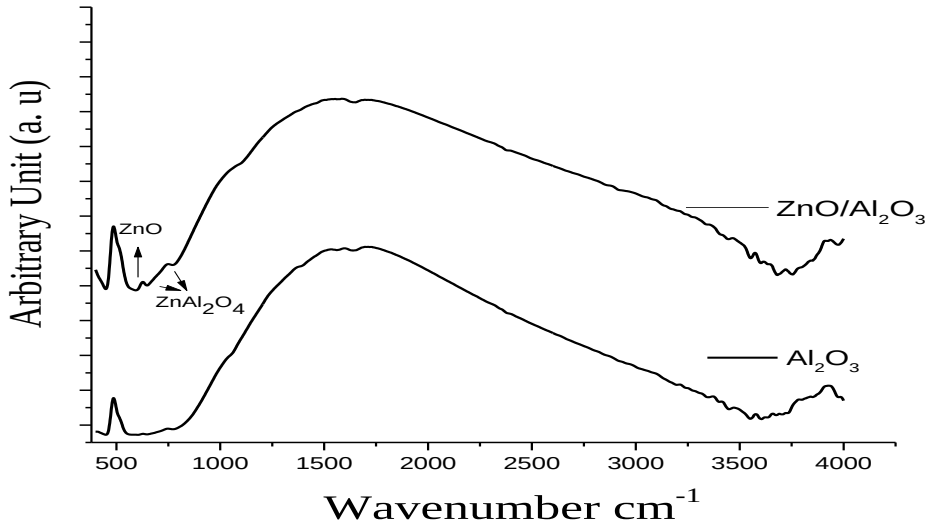

Figure 2. FTIR spectra for Al_2O_3 and ZnO/Al_2O_3

3.2 Benzene and xylene Transformation Reactions Using ZnO/Al_2O_3 Catalyst

Generally, chemical reactions are enhanced by increase in temperature. The effect of reaction temperature on the transalkylation reaction was studied by varying the temperature between 60 and 80˚C. This is to generate results for further kinetic investigations. As shown in Figure 3(a), benzene conversion increases with both reaction time and temperature. A lower reaction temperature of 60˚C showed low reactant conversion and product yield. As the reaction temperature was increased to 70˚C, it resulted in a significant increase in the ethylbenzene yield. However, increasing the reaction temperature to 80˚C resulted in a decrease on the reactant conversion which is attributed to catalyst deactivation. In order to optimize the energy required for the reaction, a reaction temperature of 70˚C was chosen. At this temperature, a high ethylbenzene yield of 63.5% and 46.7% conversion of benzene to ethylbenzene was obtained. Ethylbenzene yield and benzene conversion with respect to reaction temperature and time are shown in Figure 3 (a) and (b). The study revealed that transalkylation, disproportionation and isomerization reactions were taking place concurrently. Transalkylation reaction resulted in the formation of toluene. Benzene and ethylbenzene are believed to be formed through disproportionation of toluene. The reaction pathway for the transformation of benzene and xylene to ethylbenzene is shown in Figure 4. Typical results on the effect of catalyst dosage on ethylbenzene yield and benzene conversion are shown in Figure 5. The yield of ethylbenzene after 45 min reached a maximum of 59.50% with a catalyst dosage of 0.70% at 80˚C. This suddenly decreased to 34.40% with increase in catalyst dosage to 1.00%. Similar trends were observed on benzene conversion for 45 min at 80˚C and 0.70% catalyst dosage. A maximum benzene conversion of 43.70% was obtained at catalyst dosage of 0.70% after 45 min and this decreased to 25.30% when the dosage was increased to 1.00%. This suggests that higher reaction temperature and catalyst dosage resulted in an equilibrium shift that favours the production of toluene as proposed in schemes 2 and 4.

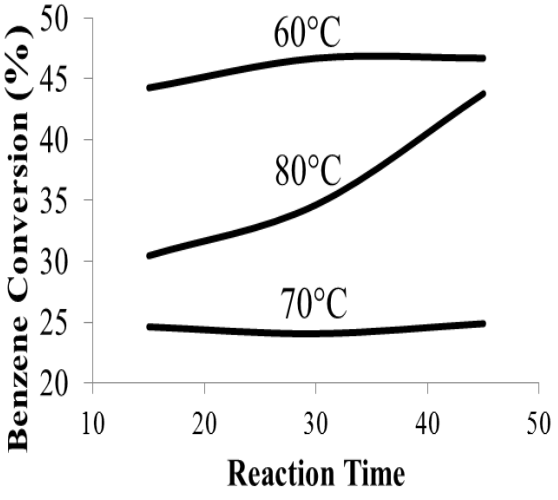

Figure 3(a) Benzene conversion against temperature and time

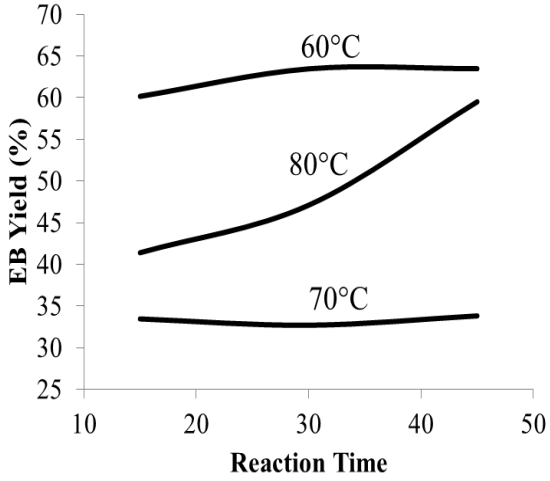

Figure 3(b). Ethylbenzene yield against temperature and time

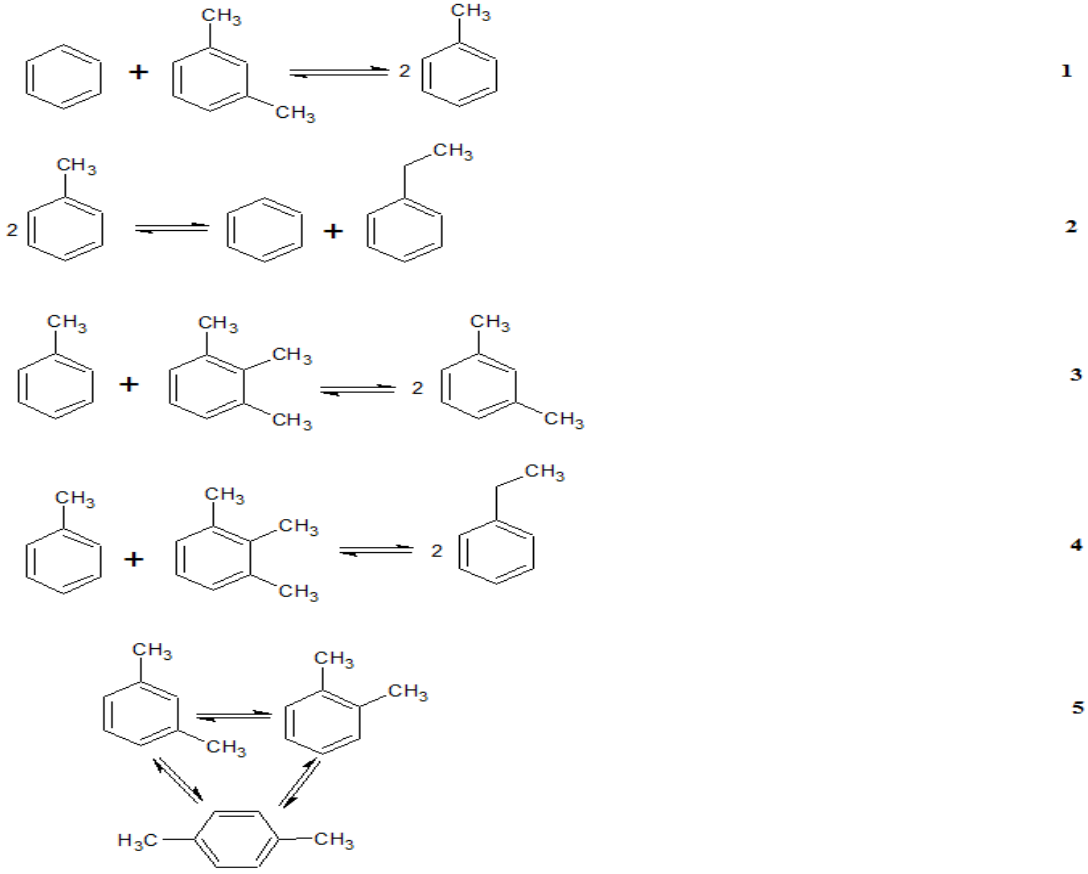

Figure 4. Proposed reaction scheme for transalkylation of benzene and xylene to ethylbenzene

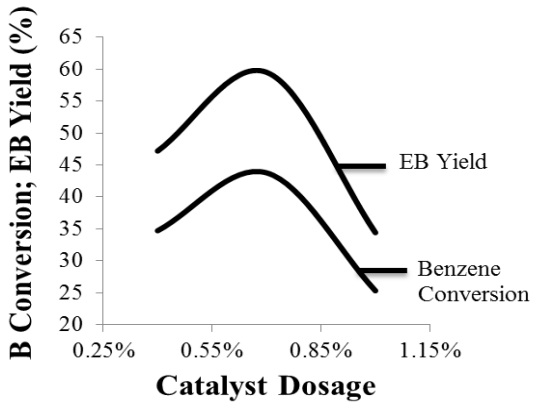

Figure 5. Effect of catalyst Dosage on Benzene conversion and Ethylbenzene yield

When the mole ratio of benzene to ethylbenzene (B/EB) was plotted against reaction time and temperature, in Figure 6, the benzene to ethylbenzene ratio was found to be greater than unity in all cases. It has been shown that this ratio signifies the importance of ethyl group transfer (Al-Khattaf, 2008). At 70˚C, the optimum temperature established for the reaction, the ratio was observed to be relatively constant. This is a deviation from what other researchers have reported because of the difference in the catalyst systems. They claimed that product selectivity increases with temperature during catalytic transformation of methylbenzenes over zeolite based catalysts. Furthermore, the report also observed that benzene to ethylbenzene ratio increases with temperature and decreases with time. The variation was attributed to the increase in undesirable reactions (Al-Khattaf, 2008). However, in this case, traces of cumene, a product of side reaction, were observed. The decreased presence of side reactions is believed to be responsible for the almost

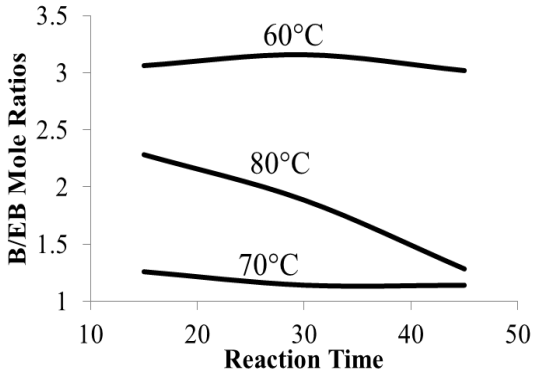

Figure 6. Product Selectivity against reaction temperature and time

constant benzene to ethylbenzene ratio observed. At lower reaction temperature of 60˚C, disproportionation has been reported to be controlling. This resulted in the high benzene/ethylbenzene mole ratios observed. However, increasing the reaction temperature to 80˚C favored the transalkylation step which lowered the benzene/ethylbenzene mole ratios.

Xylene isomerization was observed in the experiments and only two isomers of xylene were detected by the GC-MS. The ratios of *p-/o*-xylene in the product mixtures suggests the acidity and porosity of solid catalysts *(Guisnet et al.,* 2000). Al-Khattaf *et al.,* (2011) reported that large *p/o* values indicate smaller channels while lower values establish the presence of large pores. At 80˚C, ZnO/Al_2O_3 catalyst revealed a *p/o* ratio between 1 and 3 depending on the catalyst dosage. This shows that under the reaction conditions, ZnO/Al_2O_3 pore systems facilitated the formation of these two isomers and the diffusivities of the individual isomers added to the high *p/o* values obtained.

The effect of temperature on *p-/o*-xylene ratios is well reported in the literature. Al-Khattaf (2007) reported that the ratio decrease with increase in temperature. High temperatures significantly influence the configurational diffusion of *o*-xylene. This leads to low *p/o* ratios because of the difference in diffusion rates of *p*-xylene *and o*-xylene. Figure 7 shows the variation of *p-/o*-xylene ratios with temperature. A high *p/o* ratio obtained at reaction temperature of 60˚C and 45 min reaction time was found to be 3.17. However, this ratio decreased with temperature increase reaching a minimum value of 1.62 at 80˚C. Interestingly, the observed value (1.39) for *p/o* ratio at 70˚C is close to literature value of 1.4 reported for silica-alumina catalyst as it has been established that *p/o* selectivity is dependent on the catalyst (Guisnet *et al*., 2000).

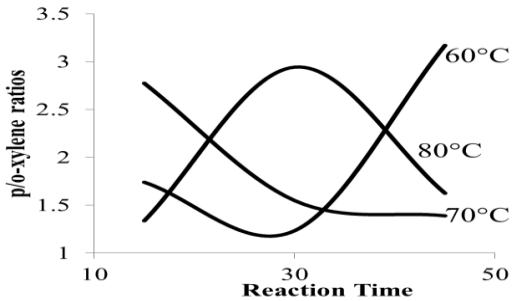

Figure 7. *P/O*-xylene ratio against reaction time and temperature

CONCLUSION

ZnO supported on alumina with a loading of 2 wt% ZnO, was found to be an active catalyst for the liquid

transalkylation of benzene with xylene in the temperature range of 60-80˚C. The batch with 0.7 wt% catalyst dosage was the most active and selective to produce ethylbenzene at 70˚C for 45 min under atmospheric pressure, which was related to the adequate and high active sites. This catalyst thus presents promising potentials to improve the industrial production of ethylbenzene.

REFERENCES

Abdal-Kareem M. A., Chand S. & Mishra I. (2002). Toluene Disproportionation Over Modified ZSM-5 Zeolite Catalysts. *Journal of Institution of Engineers (India)-Chemical Engineering Division*, 83**,** 6-8.

Al-Dosari, M. A. (2010). Transformation of mixture of benzene and m-diethylbenzene into ethylbenzene by transalkylation using triflic acid as catalyst at low temperatures. *Arabian Journal For Science And Engineering*, 35**,** 7-17.

Al-Khattaf, S. (2007). Xylenes reactions and diffusions in ZSM-5 zeolite-based catalyst. *Industrial & engineering chemistry research*, 46**,** 59-69.

Al-Khattaf, S. (2008). Catalytic transformation of ethylbenzene over Y-zeolite-based catalysts. *Energy & Fuels*, 22**,** 3612-3619.

Al-Khattaf, S., Akhtar, M. N., Odedairo, T., Aitani, A., Tukur, N., Kubů, M., Musilová-Pavlačková, Z. & Čejka, J. (2011). Catalytic transformation of methyl benzenes over zeolite catalysts. *Applied Catalysis A: General*, 394**,** 176-190.

Al-Kinany, M. C., Jibril, B. Y., Al-Khowaiter, S. H., Al-Dosari, M. A., Al-Megren, H. A., Al-Zahrani, S. M. &

Al-Humaizi, K. I. (2005). Low temperature transalkylation of o-diethylbenzene with benzene to ethylbenzene using triflic acid as a catalyst. *Chemical Engineering and Processing: Process Intensification*, 44**,** 841-846.

AL-Zahrani, S. M., AL-Kinany, M. C., AL-Humaizi, K. I. & AL-Khowaiter, S. H. (2003). Kinetics and mechanisms of transalkylation and disproportionation of meta-diethylbenzene by triflic acid catalyst. *International journal of chemical kinetics*, 35**,** 555-563.

Dias, J. A., Rangel, M. D. C., Dias, S. C. L., Caliman, E. & Garcia, F. A. C. (2007). Benzene transalkylation with C9+ aromatics over supported 12-tungstophosphoric acid on silica catalysts. *Applied Catalysis A: General*, 328**,** 189-194.

Guisnet, M., Gnep, N. S. & Morin, S. (2000). Mechanisms of xylene isomerization over acidic solid catalysts. *Microporous and Mesoporous Materials*, 35**,** 47-59.

Kim, M. (2008). Mixed-Metal Oxide Nanopowders By Liquid-Feed Flame Spray Pyrolysis (Lf-Fsp): Synthesis And Processing Of Core-Shell Nanoparticles (PhD Dissertation). Horace H. School of Graduate Studies, University of Michigan.

Kiyohara, P. K., Santos, H. S., Coelho, A. C. V. & Santos, P. D. S., (2000). Structure, Surface Area and Morphology of Aluminas from thermal decomposition of Al(OH)(CH3COO)2 Crystals. *Anais da Academia Brasileira de Ciências*, 27 April/June, 72(4), pp. 471-495

Magnoux, P., Canaff, C., Machado, F. & Guisnet, M. (1992). Coking, aging, and regeneration of zeolites xiii. Composition of the carbonaceous compounds responsible for the deactivation of a ushy zeolite during toluene disproportionation. *Journal of Catalysis*, 134**,** 286-298.

Munnik, P., de Jongh, P. E. & de Jongh K. P. (2015). Recent Developments in the Synthesis of Supported Catalysts. *Chemical Reviews*, p. 6687−6718.

Perego, C. & Ingallina, P. (2002). Recent advances in the industrial alkylation of aromatics: new catalysts and new processes. *Catalysis Today*, 73, 3-22.

Roldán, R., Romero, F. J., Jiménez, C., Borau, V. & Marinas, J. M. (2004). Transformation of mixtures of benzene and xylenes into toluene by transalkylation on zeolites. *Applied Catalysis A: General*, 266**,** 203-210.

Tsai, T-C., Chen, W-H., Liu, S-B., Tsai, C-H. & Wang, I. (2002). Metal zeolites for transalkylation of toluene and heavy aromatics. *Catalysis Today*, 73**,** 39-47.

Xu, O., Su, H., Ji, J., Jin, X. & Chu, J. (2007). Kinetic Model and Simulation Analysis for Toluene Disproportionation and C9-romatics Transalkylation *Chinese Journal of Chemical Engineering*, 15**,** 326-332

EMPIRICAL MODELING OF THIN LAYER DRYING CHARACTERISTICS OF *NAUCLEA LATIFOLIA* LEAVES

***Adeyi, O.[1] , Adeyi, A. J.[2] and Oke, O. E.[3]**

[1]Chemical Engineering Department, Landmark University, Omu Aran, Kwara State, Nigeria
[2]Mechanical Engineering Department, Ladoke Akintola University of Technology Ogbomoso, Oyo-State, Nigeria
[3]Chemical Engineering Department, Micheal Okpara University of Agriculture, Umudike, Abia State, Nigeria
adeyioladayo350@yahoo.com

ABSTRACT

The thin layer drying characteristics of Nauclea latifolia leaves were studied at four drying temperatures of 35, 45, 55 and 65^oC and a constant air velocity of 1.5 m/s in a convective dryer. Experimental kinetic data were fitted to four established drying models available in the literature, namely: the Newton, Henderson and Pabis, Page and Logarithmic models. Model parameters were determined by using non-linear regression analysis while the goodness of fit was assessed by the coefficient of determination (R^2), root mean square error (RMSE) and the standard error (SE). Fick's diffusion model and Arrhenius-type equation were used to determine the effective diffusivity and activation energy, respectively. The increase in air temperature significantly reduced the drying time of the Nauclea latifolia leaves. Among the models proposed, the Page model was found satisfactory for describing the air-drying kinetics of Nauclea latifolia leaves. The effective diffusivity increases as temperature increases and ranged between 3.3841 E-08 - 1.1202 E-07 m^2/s while the activation energy of diffusion was estimated to be 40.55 kJ/mol.

***Keywords**: Nauclea latifolia leaves, Convective drying, Modeling, Activation energy, Moisture diffusivity.*

1. INTRODUCTION

Nauclea latifolia, a member of plant family Rubiaceae, is known to be of high medicinal value (Deeni and Hussain, 1991). *Nauclea latifolia* often known as African peach or pin cushion tree is a straggling evergreen, multi-stemmed shrub or small tree native to tropical Africa and Asia. The leaves, stems, roots and fruits of *Nauclea latifolia* are of high, significant medicinal importance. The extracts of *Nauclea latifolia* have been reported to be potent against bacterial (Okwori *et al*., 2008; Doughari, 2008), viral (Donalisio *et al*., 2013), diabetic (Gidado and Ameh, 2005), and plasmodia (Benoit-Vical *et al*., 1998) activities. The phytochemicals found in *Nauclea latifolia* are indole alkaloids, triterpenes, steroids and saponins (Donalisio *et al.*, 2013). Traditional use of the various parts of the plant include the treatment of jaundice, yellow fever, rheumatism, abdominal pains, loss of appetite, malaria, diarrhea, dysentery, hypertension, diabetes and hepatitis (Donalisio *et al*., 2013). Ayeleso *et al*. (2014) also reported that *Nauclea latifolia* has strong antioxidant potentials with the leaves demonstrating higher *in vitro* antioxidant activities than the fruits. The leaves were found to contain polyphenols, flavanol, and flavonol which further encourage the use of the leaves of *Nauclea latifolia.* The high moisture content of the leaves however, makes it perishable and significantly affects its shelf life and quality. To preserve the quality (including bio-activities) of the leaves for effective utilization at any time and enhanced shelf-life, postharvest processing aspect is very important (Rayaguru and Routray, 2011). One of the oldest and most widely employed technologies to avoid spoilage and improve shelf life is drying.

Drying is a method of reduction of water activity values through moisture removal to achieve physicochemical and microbiological stability (Nag and Dash, 2016). Drying removes moisture through simultaneous heat and mass transfer and it provides longer shelf life, lighter weight for transportation and smaller space for storage (Karimi *et al.*, 2012). However, drying is not only affecting the water content of the product, but also alters other physical, biological and chemical properties such as aroma, bioactivity, colour, antioxidant activities as well as palatability of foods (Rayaguru and Routray, 2011; Wojdyło *et al.*, 2009). Therefore, appropriately controlled drying of the leaves appears to be the only means of preserving the quality of the leaves. Hence standardization of drying operation specific to leaves of *Nauclea latifolia* is a necessity in order to achieve the simultaneous purpose of quality preservation and

increased self-life. Literature revealed the documentation of drying behaviour of some medicinal plants such as *Adathoda vasica* leaves (Ganesapillai *et al.*, 2015), ginger and Javanese pepper (Tambunan et al., 2001), rosemary leaves (Arslan and Özcan, 2008), mint leaves (Doymaz, 2006), meadowsweet (*Filipendula ulmaria*) and willow (*Salix alba*) (Harbourne *et al.*, 2009) and bay leaves (Demir *et al.*, 2004). However, investigations on the drying characteristics of *Nauclea latifolia* leaves are scarce in the literature.

The traditional method of drying agricultural products is sun drying. However, the drying time by this method can be quite long, it has associated problems of contamination with dust, soil, sand particles and insects (Afolabi, and Agarry, 2014) and also it is weather dependent and hence difficult to control. Therefore, the drying process should be undertaken in closed equipment to improve the quality of the final product (Ertekin and Yaldiz, 2004; Doymaz, 2006). Hot air drying method has been widely investigated in the literature and identified by some researchers as a more efficient drying method. This is because heat and mass transfer can be controlled during the drying process to achieve desired product quality (Tunde-Akintunde *et al*., 2014). Factors having a significant effect on drying characteristics of a particular plant material include drying temperature, relative humidity, product size, pre-treatment method (Tunde-Akintunde and Afon, 2010), air velocity and type of drying equipment.

An important aspect of drying technology is the empirical modelling of the drying process. This is because it enables design engineers to choose the best operating conditions for the development of drying equipment according to desired conditions. It can as well be used for improving existing drying systems or even for the control of the drying process. Thin layer drying model remains the best model to describe the food drying process since all commercial flow dryers are designed on thin-layer drying principles (Tahmasebi *et al.*, 2010). Many researchers have investigated the drying kinetics of several medicinal plants to determine the best empirical models for describing thin-layer drying. Such plants include coriander (Coriandrum sativum) leaf and stem (Silva *et al.*, 2008), mint leaves (Doymaz, 2006), *Adathoda vasica* leaves (Ganesapillai *et al.*, 2015), and *Pandanus amaryllifolius* leaves (Rayaguru and Routray, 2011). Other agricultural products properties of interest which are necessary for designing and modelling the mass transfer processes of dehydration or moisture adsorption during storage are effective moisture diffusivity and activation energy. The activation energy indicates the minimum amount of energy required to initiate moisture diffusion from a solid matrix (Nag and Dash, 2016). A Literature survey has revealed that there is a dearth of substantial research on the preservation and drying behavior of *Nauclea latifolia* leaves despite its medicinal importance. Therefore, the objectives of this work are to investigate the thin layer drying characteristics of *Nauclea latifolia* leaves as a function of time at fixed air temperatures, fit the drying data into four thin layer models and determine the effective diffusivities and activation energy of moisture diffusion.

2. MATERIAL AND METHODS

Raw materials

Nauclea latifolia plants freshly harvested from the commercial farm of Landmark University, Omu-Aran, Nigeria were used in this study. It was later identified at the botany unit of the Department of Biological Science of the same institution. When received in the laboratory, the leaves were separated from the stem and root by carefully plucking the leaves. The leaves were later cleaned and washed with water to remove the extra soil. Then, the leaves were sanitized by washing with 25% vinegar solution, wiped with a cloth and cut into 10 cm-long pieces. The thickness of the 20 samples was measured using vernier caliper and the average thickness of the leaves was found as 0.45 mm. The leaves were put into polyethylene bag in a domestic refrigerator operating at 4^{o}C, prior to the drying experiment.

Drying procedure

The drying of the leaves was performed in a hot air convective dryer at temperatures of 35, 45, 55 and 65 °C and drying air velocity of 1.5 m s^{-1}. Prior to placing the sample on the tray, the drying system was run for at least 30 min to obtain steady conditions. Then, the sample was placed on the drying tray in a single thin-layer. Samples of approximately 30 g (± 0.5g) were individually identified and used for all experimental runs. The moisture loss was recorded at 10 min intervals by discontinuous weighing of the experimental sample on digital scales, with a ± 0.01g precision, up to a constant weight that is, the samples reached the equilibrium moisture content with conditions of the drying air. Each experiment was performed twice and averages were reported. The initial moisture content of the leaves was determined by using the oven drying method at 105^{0}C for 5 h (AOAC, 1990). The initial moisture content of the *Nauclea latifolia* was 196.96% dry basis (db).

Empirical modelling of drying curves

Four thin-layer empirical drying models, namely: the Newton (Ganesapillai *et al.*, 2015; Ayensu, 1997), the Henderson and Pabis (Doymaz, 2006; Silva *et al.*, 2008), the Page (Rayaguru and Routray, 2011; Nag and Dash, 2016) and the Logarithmic (Tahmasebi *et al.*, 2010; Aregbesola *et al.*, 2015) models were used to analyse and represent experimental drying data and are shown in Table 1. In the models a, c and n are parameters of the models, k is the drying constant for a particular temperature, (min^{-1}), and t is the drying time (min). During the drying experiment, the moisture ratio of *Nauclea latifolia* leaves was calculated by using Equation (1).

$$\text{Moisture ratio (MR)} = \frac{M - M_e}{M_o - M_e} \quad (1)$$

where, MR, M, M_0, M_e are the moisture ratio, moisture content at any time, initial moisture content and equilibrium moisture content, respectively.

Table 1: Thin-layer drying models considered

Model name	Model equation	References
Newton	MR = $\exp(-kt)$	Ganesapillai et al., 2015; Ayensu, 1997
Henderson and Pabis	MR = $a\exp(-kt)$	Doymaz, 2006; Silva et al., 2008
Page	MR = $\exp(-kt^n)$	Rayaguru and Routray, 2011; Nag and Dash, 2016
Logarithmic	MR = $a\exp(-kt) + c$	Tahmasebi et al., 2010; Aregbesola et al., 2015

Curve fittings for thin-layer kinetic models were performed using the solver function in Microsoft Excel adopting the generalized reduced gradient (GRG2) nonlinear optimization code to determine the model parameters. The best fit line with the minimum sum of square errors (SSE) was used as the sole criterion during curve fitting.

The goodness of fit, R^2, was calculated using Equation 2:

$$R^2 = 1 - \frac{SSE}{SST} \quad (2)$$

where SST is the total corrected sum of square (Walpole *et al.*, 2002).

SSE measures variation due to error or variation unexplained while SST represents variation in the response values that ideally would be explained by the model. SSE and SST were calculated using Equations 3 and 4 respectively.

$$\text{SSE} = \sum_{i=1}^{n}\left(MR_{exp,i} - MR_{pre,i}\right)^2 \quad (3)$$

$$\text{SST} = \sum_{i=1}^{n}\left(MR_{exp,i} - MR_{mean}\right)^2 \quad (4)$$

The best fit model was selected on the basis of high coefficient of determination, R^2; low root mean square error, RMSE, as given in Equation 5; and standard error, SE, as given in Equation 6.

$$\text{RMSE} = \left[\frac{\sum\left(MR_{pre,i} - MR_{exp,i}\right)^2}{n}\right]^{1/2} \quad (5)$$

$$\text{SE} = \left[\frac{\sum\left(MR_{pre,i} - MR_{exp,i}\right)^2}{n-1}\right]^{1/2} \quad (6)$$

where, $MR_{exp,i}$ is the experimental moisture ratio at observation *i*, $MR_{pre,i}$ is the predicted moisture ratio at this observation, MR_{mean} is the overall mean moisture ratio of all observations and n is the number of observations.

3. RESULTS AND DISCUSSION

3.1. Influence of drying temperature

Figure 1 shows thin layer drying curves of *Nauclea latifolia* leaves at the different drying air temperatures considered. Drying air temperature has a significant effect on drying behaviour of *Nauclea latifolia* leaves. At higher temperature, the drying time was shorter due to the fast removal of moisture from the leaves (Revaskar *et al.*, 2014). Similar observations were reported for hot air drying of dika nuts and kernels (Aregbesola, 2015) and hot air drying of elephant apple (Nag and Dash, 2016). The total drying times for *Nauclea latifolia* leaves to reach final moisture content were 80, 120, 180 and 290 min at drying temperatures of 65, 55, 45 and 35^0C respectively.

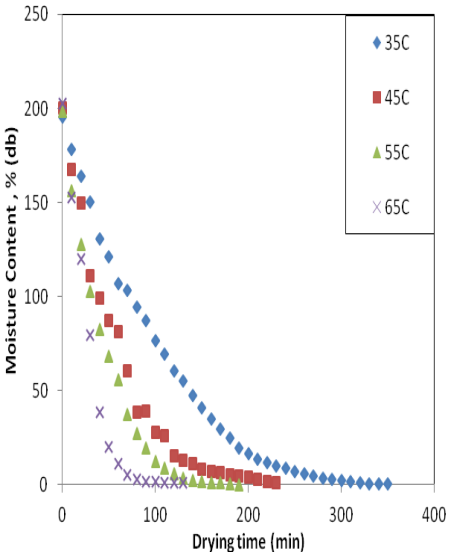

Fig. 1. Moisture content versus time for *Nauclea latifolia* leaves

The graph showing the relationship between moisture ratio and time for *Nauclea latifolia* leaves at all investigated temperature is presented in Fig. 2. It is apparent from the plot that drying occurred predominately during the falling rate period for the leaves. Hence it may be inferred that the dominant physical mechanism governing the moisture movement in *Nauclea latifolia* leaves was diffusion along the moisture concentration gradient as obtained for most agricultural products (Aregbesola *et al.*, 2015).

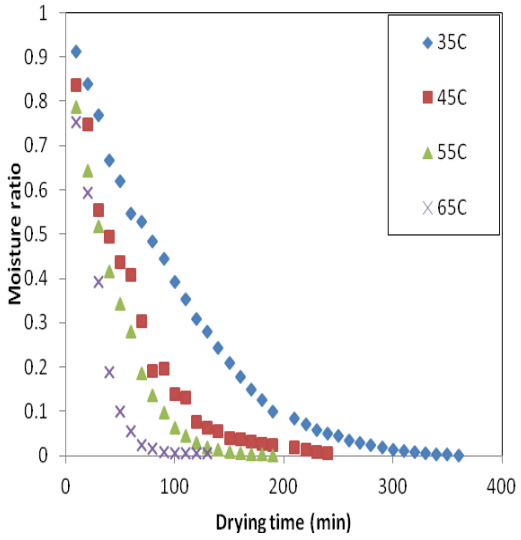

Fig. 2. Moisture ratio versus time for *Nauclea latifolia* leaves

3.2. Evaluation of the models

The empirical drying models of Newton, Henderson and Pabis, Page and Logarithmic were fitted to experimental drying data to determine the model that best fit the data. The summary of the statistical analysis values used to judge the performance of each model is presented in Table 2. All the tested models described the experimental data well with high coefficient of determination (R^2) values in the range 0.9761 - 0.9960. This is an indication that all the models could satisfactorily describe the air-drying of *Nauclea latifolia* leaves. However, the Page model had the highest R^2 values and the lowest RMSE and SE values compared to other examined thin layer drying models in the range of temperature studied. As indicated in Table 2, the RMSE and SE values of Page model were in the range of 0.017000 - 0.022000 and 0.018000 - 0.023000, respectively. Thus, this model may be assumed to describe best the thin-layer drying behaviour of the *Nauclea latifolia* leaves. Examination of the R^2, RMSE and SE values showed that Newton model gave the least description of the experimental data with lower R^2 and higher RMSE and SE when compared with other tested thin layer models. The parameters of Page model are as well presented in Table 2.

Both parameter *k* (drying constant) and *n* of Page model are in the range of 0.0043825 - 0.0149455 and 1.1061461 - 1.4262697, respectively. Similar ranges of values were reported for sun and solar drying of chilli pepper (Tunde-Akintunde, 2011); hot air-drying of *dika* (*Irvingia gabonensis*) nuts and kernels (Aregbesola, 2015) and vacuum drying of fenugreek, mint, leek and parsley leaves (Zakipour and Hamidi, 2011). Plots of experimental and Page model predicted moisture ratio values with drying time are presented in Fig. 3. As shown in Figure 3, the Page model provided a good description of the experimental kinetic drying data in terms of moisture ratio values. Similar findings were reported by Revaskar *et al.* (2014) for onion slices and Demir *et al.* (2004) for bay leaves.

Table 2: Coefficient of thin layer empirical models and goodness of fit for *Nauclea latifolia leaves.*

Model	Temp (°C)	Parameters	R^2	RMSE	SE
Newton	35	*k* = 0.0104	0.9877	0.032340	0.032799
	45	*k* = 0.0182	0.9913	0.026724	0.027299
	55	*k* = 0.0245	0.9937	0.023131	0.023732
	65	*k* = 0.0363	0.9761	0.049158	0.051014
Henderson and Pabis	35	*k*= 0.0108, a =1.0448	0.9897	0.029638	0.030058
	45	*k*= 0.0186, a =1.0236	0.9919	0.025857	0.026413
	55	*k*= 0.0238, a =1.0172	0.9940	0.022581	0.023167
	65	*k*= 0.0379, a =1.0550	0.9790	0.046068	0.047807
Page	35	*k*= 0.0044. n = 1.1807	0.9955	0.019622	0.019901
	45	*k*= 0.0116, n =1.1061	0.9940	0.022000	0.023000
	55	*k*= 0.0149, n =1.1124	0.9960	0.017000	0.018000
	65	*k*= 0.0080, n =1.4262	0.9960	0.021000	0.022000
Logarithmic	35	*k*= 0.0109, a = 1.0448			
		c = 0.000001	0.9897	0.029638	0.030059
	45	*k*= 0.0186, a =1.0236			
		c = 0.000001	0.9919	0.025857	0.026413
	55	*k* = 0.0238, a = 1.0172			
		c = 0.000001	0.9939	0.022581	0.023168
	65	*k*= 0.0380, a =1.0550			
		c = 0.000001	0.9790	0.046067	0.047807

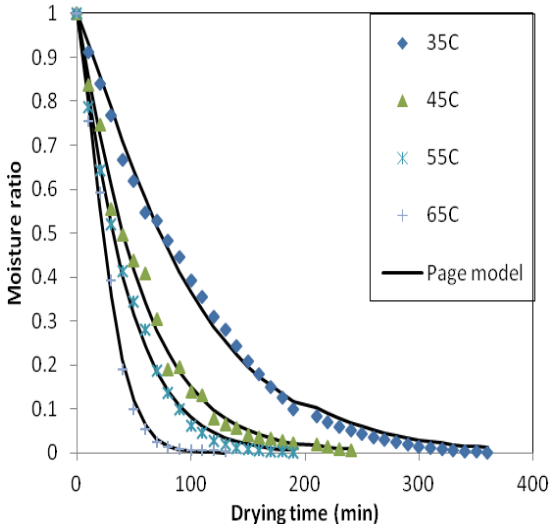

Fig. 3: Influence of air-drying temperature on drying curves and prediction of drying curves by using the proposed Page model.

3.3. Determination of the effective moisture diffusivity

The Fick's second diffusion equation (Equation 7) was used to interpret the experimental drying data for the determination of effective diffusivity coefficients at different drying temperatures.

$$\frac{\partial M}{\partial t} = D_{eff}\nabla^2 M \quad (7)$$

Considering the *Nauclea latifolia* plant leaves to conform to slab geometry, the solution of the diffusion equation (Eq.5) assuming: (a) unidimensional moisture movement volume change (b) constant temperature and diffusivity coefficients, and (c) negligible external resistance (Crank, 1975), is presented in Equation 8:

$$\text{MR} = \frac{8}{\pi^2}\sum_{n=1}^{\infty}\frac{1}{(2n-1)^2} exp\left(-\frac{(2n-1)^2\pi^2 D_{eff}t}{4L^2}\right) \quad (8)$$

For long drying times, according to Doymaz (2006), Equation (8) is simplified to give Equation (9).

$$\text{MR} = \frac{8}{\pi^2} exp\left(-\frac{\pi^2 D_{eff}t}{4L^2}\right) \quad (9)$$

Where D_{eff} is the effective moisture diffusivity (m^2/s), L is the half thickness of the plants leaves of *Nauclea latifolia* (m), and t is drying time (s).

The linearized form of Eq. (9) is expressed in Eq. (10) according to Zakipour and Hamidi, (2011).

$$\ln(\text{MR}) = \ln\left(\frac{8}{\pi^2}\right) - \left(\frac{D_{eff}\pi^2}{4L^2}t\right) \quad (10)$$

The effective moisture diffusivity was calculated from the slope (k_o) of the plot of ln (MR) versus drying time (t) in Figure 4.

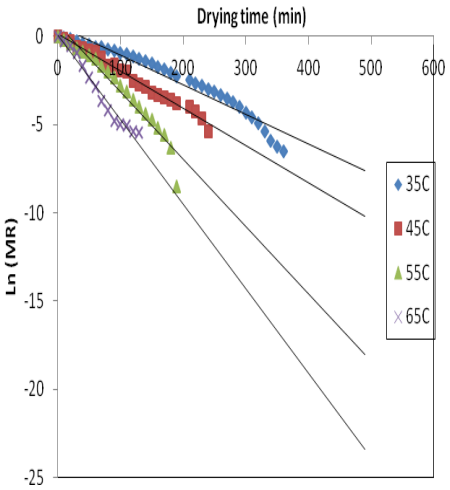

Fig.4.Plot of ln (MR) versus time for *Nauclea latifolia* leaves.

$$k_o = \frac{\pi^2 D_{eff}}{4L^2} \quad (11)$$

Table 3 shows the values of D_{eff} obtained for different drying temperatures. Effective diffusivity values ranged from 7.7017 E -09 at 30°C to 1.1202 E -07 m^2/s at 70 °C. These values compare well with values reported for Pandanus amaryllifolius leaves (Rayaguru and Routray, 2011) and mint leaves (Doymaz, 2006). However, the corresponding expressions in Table 3 show that the best fit for each drying temperature is given by a linear relationship ($R^2 > 0.97$).

Table 3: Values of effective diffusivity obtained for *Nauclea latifolia* leaves at different drying temperatures

Temperature (°C)	Effective diffusivity (D_{eff}) (m^2/s)	Equation of fit	R^2
35	3.3841 E -08	- 0.0145x +0.3419	0.9740
45	5.1111 E -08	- 0.0219x +0.1837	0.9812
55	8.0984 E -08	- 0.0347x + 0.4722	0.9812
65	1.1202 E -07	- 0.0480x + 0.1042	0.9681

As indicated in the table, the values of D_{eff} increased greatly as the drying temperature increased. Similar observations were reported for mint leaves (Doymaz, 2006); fenugreek, mint and parsley leaves and vegetative parts of leek leaves (Zakipour and Hamidi 2011); aromatic Pandanus amaryllifolius leaves (Rayaguru and Routray, 2011); elephant apple (Nag and Dash, 2016) and *dika* (*Irvingia gabonensis*) nuts and kernels (Aregbesola *et al*., 2015). Increase in moisture diffusivity as drying temperature increased has been explained regarding increase in the average energy for transitional, rotational and vibrational motion of vapour which ultimately resulted in higher moisture gradient and increased mass transfer rate and hence increase in moisture diffusivity (Nag and Dash, 2016).

3.4. Activation energy

The temperature dependence of effective diffusivity by Arrhenius relationship is described by Aregbesola *et al.* (2015) as:

$$D_{eff} = D_o exp\left(-\frac{E_a}{RT}\right) \quad (12)$$

where D_o is the pre-exponential factor of the Arrhenius equation (m^2/s); E_a the activation energy (kJ/mol); R the universal gas constant (kJ/mol K) and T is the absolute air temperature (K). The linearized form of Eq. (12) is presented in Eq. (13).

$$ln\left(D_{eff}\right) = lnD_o - \frac{E_a}{R(T)} \quad (13)$$

Figure 5 shows the plot of $ln\left(D_{eff}\right)$ against the inverse of absolute temperature. The graph obtained was essentially a straight line ($R^2 > 0.99$) which indicated Arrhenius relationship. Activation energy of *Nauclea latifolia* leaves (the minimum amount of energy required to initiate moisture diffusion) was calculated from the slope of the straight line described by Arrhenius equation to be 40.55KJ/mol. The corresponding value of the pre-exponential factor of the Arrhenius equation, D_o, which represents the diffusivity constant equivalent to the diffusivity at infinitely high temperature (Nag and Dash, 2016) was 3.044 E-2 m^2/s. The values of the energy of activation lie within the general range of 12.7 – 110 kJ/mol for food materials (Stamatios and Vassilios 2004).

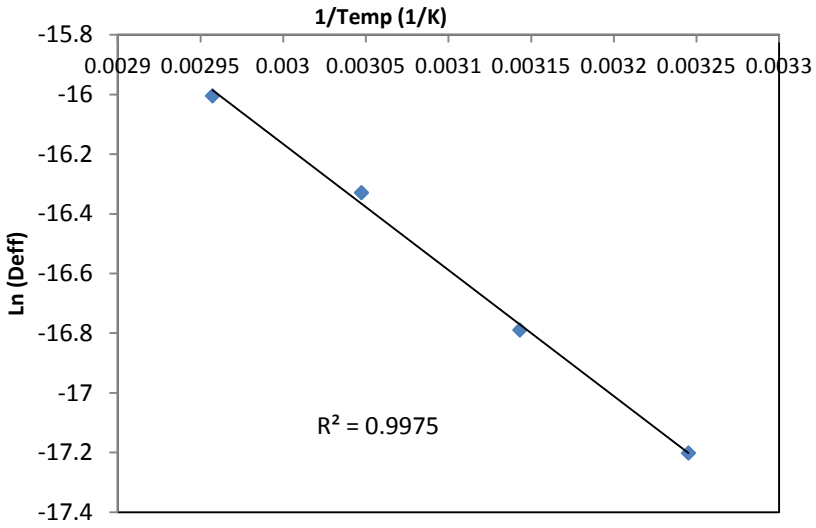

Fig. 5. Influence of air temperature on the effective diffusivity

.

Table 4 compares the activation energy value obtained for *Nauclea latifolia* leaves with various vegetables and fruits found in literature. It is similar to the activation energy of red pepper drying (Vega-gálvez *et al.*, 2007) and Cape gooseberry (Vega-gálvez *et al.*, 2014), higher than the activation energy of drying elephant apple (Nag and Dash, 2016) and lower than the activation energy of mint leaves drying (Doymaz, 2006) and fever leaves drying (Sobukola and Dairo, 2007).

Table 4: Comparison of activation energy values with literature values

Material	**Activation energy (E_a) (KJ/mol)**	**Reference**
Nauclea latifolia leaves	40.55	Present work
Red peppers	40.80	Vega-gálvez *et al.* (2007)
Mint leaves	62.96	Doymaz (2006)
Fever leaves	80.78	Sobukola and Dairo (2007)
Elephant apple	21.95	Nag and Dash (2016)
Cape gooseberry	38.78	Vega-galvez *et al.* (2014)

4. CONCLUSION

Thin layer drying characteristics of *Nauclea latifolia* leaves was studied at four drying temperatures in an air oven. The data obtained was processed and after that fitted into four established semi-empirical equations.

From the study, the following conclusions can be drawn:

i) The increase in air temperature significantly reduced the drying time of the *Nauclea latifolia* leaves.

ii) Thin layer drying of *Nauclea latifolia* leaves did not show a constant rate drying period but predominately occurred in the falling rate period; hence, the drying process for *Nauclea latifolia* leaves could be said to be dominantly driven by diffusion.

iii) The Page model gave the best fit for the description of experimental kinetic data with the highest coefficient of determination (R^2) values and lowest root mean square error (RMSE) and standard error (SE) values compared with other investigated model.

iv) The values of effective diffusivity for drying at 35 - 65^{0}C of air temperature and 1.5 m/s of air velocity ranged from 3.3841 E-08 to 1.1202 E-07 m^2/s. The effective diffusivity increased with the air temperature. The activation energy for moisture diffusion was found as 40.55 kJ/mol.

Nomenclature

a, c	model coefficient
db	dry basis
SE	standard error
RMSE	root mean square error
SSE	sum of square error
SST	total sum of squares
k	drying rate constant (min^{-1})
M	moisture content (% db)
MR	moisture ratio
MR_{mean}	overall mean moisture ratio

M_0	initial moisture content (% db)
M_e	equilibrium moisture content (% db)
$MR_{exp,i}$	i^{th} Experimental moisture ratio
$MR_{pre,i}$	i^{th} Predicted moisture ratio
n	exponent
R^2	coefficient of determination
t	time (min)
D_{eff}	effective diffusivity, m^2/s
D_0	pre-exponential factor of Arrhenius equation, m^2/s
E_a	activation energy, kJ/mol
k_0	slope
R	gas constant
L	half slab thickness

REFERENCES

Afolabi, T.J. and Agarry, S.E., (2014), *Thin layer drying kinetics and modelling of okra(Abelmoschus esculentus (L.) Moench) slices under natural and forced convective air drying. Food Science & Quality Management*, 28, pp.35-49.

AOAC (1990). *Official method of analysis. No. 934.06 Association of Official Analytical Chemists, Arlington, USA.*

Aregbesola, O.A., Ogunsina, B.S., Sofolahan, A.E. and Chime, N.N., (2015), *Mathematical modeling of thin layer drying characteristics of dika (Irvingia gabonensis) nuts and kernels. Nigerian Food Journal*, 33(1), pp.83-89.

Ayeleso, A.O., Oguntibeju, O.O. and Brooks, N.L., (2014), *In vitro study on the antioxidant potentials of the leaves and fruits of Nauclea latifolia. The Scientific World Journal*, vol. 2014, 437081, pp.1-8.

Ayensu, A., (1997), *Dehydration of food crops using a solar dryer with convective heat flow Solar energy*, 59(4-6), pp.121-126.

Arslan, D. and Özcan, M.M., (2008), *Evaluation of drying methods with respect to drying kinetics, mineral content and colour characteristics of rosemary leaves. Energy Conversion and Management*, 49(5), pp.1258-1264.

Benoit-Vical, F., Valentin, A., Cournac, V., Pélissier, Y., Mallié, M. and Bastide, J.M.,(1998), *In vitro antiplasmodial activity of stem and root extracts of Nauclea latifolia SM (Rubiaceae). Journal of Ethnopharmacology*, 61(3), pp.173-178.

Deeni, Y.Y. and Hussain, H.S.N., (1991), *Screening for antimicrobial activity and for alkaloids of Nauclea latifolia. Journal of ethnopharmacology*, 35(1), pp.91-96.

Demir, V., Gunhan, T., Yagcioglu, A.K. and Degirmencioglu, A., (2004), *Mathematical modelling and the determination of some quality parameters of air-dried bay leaves. Biosystems Engineering*, 88(3), pp.325-335.

Donalisio, M., Nana, H.M., Ngane, R.A.N., Gatsing, D., Tchinda, A.T., Rovito, R., Cagno, V.,Cagliero, C., Boyom, F.F., Rubiolo, P. and Bicchi, C., (2013), *In vitro anti-Herpes simplex virus activity of crude extract of the roots of Nauclea latifolia Smith (Rubiaceae). BMC complementary and alternative medicine*, 13(1), p.266.

Doughari, A.M., (2008), *In vitro antibacterial activities of crude extracts of Nauclea latifolia and Daniella oliveri. Scientific Research and Essays*, 3(3), pp.102-105.

Doymaz, İ., (2006), *Thin-layer drying behaviour of mint leaves. Journal of Food Engineering*, 74(3), pp.370-375.

Ertekin, C. and Yaldiz, O., (2004), *Drying of eggplant and selection of a suitable thin layer drying model. Journal of food engineering*, 63(3), pp.349-359.

Gidado, A. and Ameh, D.A., (2005), *Effect of Nauclea latifolia leaves aqueous extracts on blood glucose levels of normal and alloxan-induced diabetic rats. African Journal of Biotechnology*, 4(1), p.91.

Ganesapillai, M.A.H.E.S.H., Singh, A.S.H.I.S.H., Rao, B., De, D.E.B.I.P.A.R.N.A. and

Juneja, U.P.N.Y.A.A.S., (2015), *Extraction of alkaloids from microwave dried Adathoda Vasica leaves-a comparative study. International Journal of Pharma and Bio Sciences*, 6(1), pp.121-139.

Harbourne, N., Marete, E., Jacquier, J.C. and O'Riordan, D., (2009), *Effect of drying methods on the phenolic constituents of meadowsweet (Filipendula ulmaria) and willow (Salix alba). LWT-Food Science and Technology*, 42(9), pp.1468-1473.

Karimi, F., Rafiee, S., Taheri-Garavand, A. and Karimi, M., (2012), *Optimization of anair drying process for Artemisia absinthium leaves using response surface and artificial neural network models. Journal of the Taiwan Institute of Chemical Engineers*, 43(1), pp.29-39.

Nag, S. and Dash, K.K., (2016). *Mathematical modeling of thin layer drying kinetics and moisture diffusivity study of elephant apple. International Food Research Journal*, 23(6).

Okwori, A.E.J., Okeke, C.I., Uzoechina, A., Etukudoh, N.S., Amali, M.N., Adetunji, J.A.and Olabode, A.O., (2008), *The antibacterial potentials of Nauclea latifolia. African Journal of Biotechnology*, 7(10).

Rayaguru, K. and Routray, W., (2011), *Microwave drying kinetics and quality characteristics of aromatic Pandanus amaryllifolius leaves. International Food Research Journal*, 18(3).

Revaskar, V.A., Pisalkar, P.S., Pathare, P.B. and Sharma, G.P., (2014), *Dehydration kinetics of onion slices in osmotic and air convective drying process. Research in Agricultural Engineering*, 60(3), pp.92-99.

Silva, A.S., Almeida, F.D.A., Lima, E.E., Silva, F.L.H. and Gomes, J.P., (2008), *DRYING KINETICS OF CORIANDER (Coriandrum sativum) LEAF AND STEM CINÉTICAS DE SECADO DE HOJA Y TALLO DE CILANTRO (Coriandrum sativum). CYTA-Journal of Food*, 6(1), pp.13-19.

Sobukola, O.P .and Dairo, O.U. (2007), *Modeling drying kinetics of fever leaves (Ocimum viride) in a convective hot air dryer. Nigerian Food Journal*, 25 (1), pp146 -154.

Stamatios J. B. and Vassilios G. B. (2004), *Influence of the drying conditions on the drying constants and moisture diffusivity during the thin-layer drying of figs. Journal of Food Engineering* 65, pp.449–458.

Tahmasebi, M., Tavakkoli Hashjin, T., Khoshtaghaza, M. H., and Nikbakht, A. M. (2010), *Evaluation of thin-layer drying models for simulation of drying kinetics of quercus (Quercus persica and Quercus libani). Journa of Agricultural Science and Technology*, 13, pp.155-163.

Tambunan, A. H., Yudistira, Kisdiyani, and Hernani. (2001), *Freeze drying characteristics of medicinal herbs. Drying Technology*, 19(2), pp.325-331.

Tunde-Akintunde, T., Oyelade, O., and Akintunde, B. (2014), *Effect of drying temperatures and pre-treatments on drying characteristics, energy consumption, and quality of bell pepper. Agricultural Engineering International: CIGR Journal*, 16(2), pp.108-118.

Tunde-Akintunde, T., and Afon, A. A. (2010), *Modeling of hot-air drying of pretreated cassava chips. Agricultural Engineering International: CIGR Journal*, 12(2), pp.34-41.

Tunde-Akintunde, T.Y., (2011), *Mathematical modeling of sun and solar drying of chilli Pepper. Renewable Energy*, 36, pp.2139 – 2145.

Vega-Galvez, A., Puente-Diaz, L., Lemus-Mondaca, R., Miranda, M. and Torres, M.J. (2014), *Mathematical modeling of thin-layer drying kinetics of cape gooseberry (Physalis peruvianaL.). Journal of Food Processing and Preservation:* 38(2), pp.728-736.

Vega-gálvez. A. Lemus-mondaca R, Bilbao-sáinz. C., Vagnam F. and Rojas A. (2008),*Mass transfer kinetics during convective drying of red pepper var. hungarian (capsicum annuuml.): mathematical modeling and evaluation of kinetic parameters. Journal of Food Process Engineering* 31, pp.120 – 137.

Wojdyło, A., Figiel, A., and Oszmiański, J. (2009), *Effect of drying methods with the application of vacuum microwaves on the bioactive compounds, color, and antioxidant activity of strawberry fruits. Journal of Agricultural and Food Chemistry*, 57(4), pp.1337-1343.

Walpole, R.E., Myers, R.H., Myers, S.L. and Ye, K., (1993), *Probability and statistics forengineers and scientists (Vol. 5). New York: Macmillan.*

Zakipour, E. and Hamidi, Z. (2011), *Vacuum Drying Characteristics of Some Vegetables.Iran. J. Chem. Chem. Eng.*30 (4), pp.97 -105.

MODELING OF BIODIESEL YIELD FROM AFRICAN PEAR SEED (*DYACRODES EDULIS*) OIL USING ARTIFICIAL NEURAL NETWORKS

***Esonye, C.[1], Onukwuli, O. D.[2], Ofoefule, A. U.[3] and Momoh, S. O.[4]**

[1]*Department of Chemical and Petroleum Engineering, Federal University, Ndufu Alike Ikwo , P.M.B 1010 Abakaliki, Ebonyi State Nigeria; eso_vic@yahoo.com*

[2]*Department of Chemical Engineering, Nnamdi Azikiwe University, P.M.B 5025 Awka, Anambra state, Nigeria; onukwuliod@yahoo.com*

[3]*Department of Pure and Industrial Chemistry, University of Nigeria, 410001 Nsukka, Enugu State, Nigeria; akuzuoo@yahoo.com*

[4]*Research and Development Unit, National Agency for Science and Engineering Infrastructure, Abuja, Nigeria. stevmomoh@yahoo.com*

ABSTRACT

The present study involves the application of artificial neural network (ANN) model to predict the yield of methyl ester derived from the seed oil of African pear (Dyacrodes edulis) using Levenberg-Marquardt algorithm. The propagation algorithm used for network training where 52 percent of the data was taken for training set, 13 percent for validation and the rest of the data for the test set. The regression coefficients of training, testing, validation and overall model developed using ANN had very good values of correlation coefficient 'R' (1.000, 0.9951, 0.8456 and 0.97171). It consists of three layers: input layer with four input variables, hidden layer with ten hidden neurons and an output layer with single output variable. The statistical analysis of the ANN model performance gave a mean squared error (MSE) of 1.3110, mean absolute error (MAE) of 1.6588, mean absolute deviation (MAD) of 1.3112 and a high value of correlation coefficient (R^2 = 0.9447. This shows that the model performance is statistically validated. The overall result shows that ANN is an efficient method for empirical modeling and optimization of biodiesel yield. The results recommend that ANN provides an excellent means of identifying patterns in data and effectively predicting biodiesel yield based on investigating inputs.

Keywords: *Artificial Neural Networks; African Pear; methyl ester; Prediction; Yield; Statistics*

1. INTRODUCTION

The gradual depletion of fossil fuel and the biological environmental degradation resulting from the over usage of petroleum derived transportation fuels have attracted serious attentions and makes it imperative to develop alternatives that are renewable and eco-friendly. Vegetable oils hold promise as alternative fuels for diesel engines but undesirable properties like high viscosities, low volatilities and poor cold flow properties have led to the development of various derivatives in order to improve its qualities. Out of these, fatty acid methyl esters derived from triglycerides by transesterification with methanol known as biodiesel have received the most attention (Bhattacharyulu *et al.*, 2013). The production of biodiesel using feedstocks that do not compete with food sources is the best approach in biomass selection. However, costs of production are still rather high compared to petroleum based diesel fuel making improvement in the biodiesel yield from the different vegetable oil feedstocks an urgent need. The biodiesel yield is strongly influenced by several factors such as molar ratio of alcohol to oil, catalyst Conc concentration, reaction temperature and time. These independent parameters are used in estimation of the dependent parameters like viscosity and fatty acid methyl esters (FAME) (Pariwa et al., 2004). Different correlation techniques such as Response Surface Methodology (RSM), Genetic Algorithm, Waveleth Theorem, Fuji Logic and Artificial Neural Network (ANN) can be adopted to predict the effect of these parameters on biodiesel yield (Ghorbani *et al.*, 2011). Many research works have been carried out on the application of ANN as superior linear and quasi non linear calibration techniques in conversion of non-edible vegetable oils from several tropical trees in Africa into methyl esters (Roman, 2011) but none has been reported in the literature being carried out using African Pear seed oil.

The African Pear belongs to the family of *Burseracea* and botanically known as *Dacryodes edulis*. It is an indigenous fruit tree grown in low lands and plateau regions of West Central Africa and Gulf of Guinea (Ogunsuyi, 2015). In the Southern part of Nigeria, the trees are grown around homestead and flowering takes

place from January to April with the major fruiting season between May and October. It is an annual fruit of about 3cm in diameter and contains a leathery shelled stone surrounded by a pulpy pericarp of about 5mm thick. It is this potion that is consumed while the seeds are discarded. The major work carried out on the industrial application of African Pear seed oil was reported by Ogunsuyi, 2015 where he investigated on the application of the seed oil in biodiesel production. He discovered that the seed is a viable feedstock considering the fact that the seed contained about 59% oil and yielded an optimum value of 64.24% biodiesel at 60ºC, 7:1 methanol /oil molar ratio, at 850rpm for 120 minutes reaction time with KOH catalyst. Bull and George, 2015 equally assessed the fuel properties of biodiesel from African seed oil and obtained 80% biodiesel yield at 60 ºC , for 50 minutes reaction time using 1:6 oil/methanol molar ratio using 0.25g of NaOH as catalyst. However, there has not been a literature report on the application of modeling techniques to provide an accurate, time saving and concise effect of operating parameters on the biodiesel production from this feedstock.

The present work aims to develop models inculcating the effect of the following operating conditions: catalyst conditions, temperature, reaction time and methanol to oil molar ratio as independent variables to estimate the biodiesel (methyl ester) yield as the dependent parameter using Artificial Neural Network model (ANN) on MATLAB platform using African Pear (*Daycrodes edulis*) seed oil as the feedstock.

2. MATERIALS AND METHODS

Materials

Sodium hydroxide (99% Sigma-aldrich), potassium hydroxide (loba chemie, gmbH 85%), methanol (Merck, Germany 99.5 % purity)**,** carbon tetrachloride (chloroform), Wij's solution (iodine monochloride), potassium iodide solution and phenolphthalein (Merck Germany) were all of analytical grade. The seed oils used in this work were extracted by solvent extraction method and the fruit seed biomass was gathered from Onitsha City in Anambra State of Nigeria.

Biodiesel Production

The oil was heated fairly at 80°C for 30 minutes using Gallenkamp Magnetic Stirrer thermostat hot plate (Weiss Technik England) to reduce the viscosity of the oil while the catalyst was prepared by adding 2% weight of the oil of NaOH to 175ml of methanol and stirred at 300rpm until it dissolved completely for about two minutes in the reaction vessel.

An esterification was carried out using 50ml of methanol and 0.2ml of concentrated H_2SO_4 mixed together inside a 250 ml conical Flask. The conical Flask was inserted into a water bath at 50 °C. The mixture was later added to200ml warmed (preheated) APSO inside a 500ml conical flask and placed on magnetic stirrer with heater, continuously stirred for 1 hour 30 minutes for the acid transesterification to take place.

The product of acid transesterification was subjected to base transesterification. The calculated amount of NaOH (Catalyst) and methanol was added for each reaction for the temperature and reaction time specified. The Base transesterification was carried out in a Sohxlet extractor fitted with thermo-regulator heater and stirrer. The calculated amount of oil was measured into the flask and was heated to the specified temperature. The sodium methoxide was then poured into the flask containing oil and was immediately covered. The temperature was maintained for the specified time at constant agitation.

After the base transesterification process the biodiesel was allowed to settle for at least 24h inside a separating funnel to allow clear separation of biodiesel from glycerin by gravity. The layer on the top is the biodiesel while the bottom layer is the glycerol. The Biodiesel separation was carried out by decanting as the glycerol was drained off while the biodiesel remained.

Warm distilled water at 50ºC was added to the separated biodiesel and the mixture was shaken vigorously. The water was allowed to drain through the bottom of the separating funnel. This was carried out five times until a clear biodiesel was obtained.

Anhydrous $CaCl_2$ was added to the biodiesel and heated gently at 50°C. The anhydrous $CaCl_2$ was later separated from the biodiesel to obtain a clean dry biodiesel. The volume of the biodiesel obtained from each sample was determined while the percentage yield of biodiesel was calculated.

Physico-chemical Characterization of the Biodiesel

The fuel properties of the synthesized biodiesel were determined by ASTM standards: the kinematic viscosity was determined by ASTM D-445 method, the density was determined by ASTM D-1298 method, and the pour point determination was made using ASTM D-97

methods. The flash point of the fuel was determined as ASTM D-93, the value of cloud point was estimated according to ASTMD-2500, and Acid value was measured following the ASTM D-664 method. The Calorific value and cetane number were calculated according to the correlation developed by Patel, 1999.

GC-MS Analysis of the Fatty Acid Profile of the seed oil

The fatty acid composition of the African pear seed oil was analyzed by Gas –Chromatography coupled with Mass Spectrometer. The gas Chromatographic analysis was made using GCMS-QP2010 plus, Shimadzu, Japan instrument. The GC column used was calibrated by inject ting methyl ester standards, good separations were achieved by diluting the sample in a small amount of ethyl acetate. The carrier gas used was hydrogen and its flow rate was regulated at 41.27ml/mins while the column lows at 1.82ml/mins. The oven temperature was set at 80ºC before ramping up at 6ºC/min until 340ºC.the identification of peaks was done by comparison of their retention time and mass spectra with mass Spectra Library (NIST05s LIB.).

Experimental Design

In order to optimize operating parameters, a five –level – four factor statistical design was employed for this study. It generated twenty five (25) runs. The factors investigated in this study were reaction time (minutes), catalyst amount (weight %), Temperature (ºC), and oil/methanol ration). The coded and uncoded factors (X_1, X_2, X_3 and X_4) and levels used are shown in Table 1. The variables ranges were selected based on results obtained from preliminary studies and literature (Awolu and Layokun, 2013).

Table 1: Factors and their levels for the biodiesel productions

Variable	Symbol	Coded levels				
		-2	-1	0	1	2
Temperature ($^{\circ}$C)	X_1	30	40	50	60	70
Catalyst Conc. (wt %)	X_2	0.5	1.0	1.5	2.0	2.5
Reaction Time (mins)	X_3	45	50	55	60	65
Oil/methanol ratio	X_4	1:3	1:4	1:5	1:6	1:7

Development of Artificial Neural Network (ANN) Model

A consolidated data set comprising of twenty five (25) data set are compiled and parameters like temperature at which the reaction is carried out, the time of reaction in minutes, the catalyst concentration as weight percent and the oil to methanol ratio were used as the independent input parameters. In this study, a three-layered feed-forward neural network with tangent sigmoid transfer function (tansig) at hidden layer and linear transfer function (purelin) at output layer was used. The sigmoid transfer function is given by Equation 1 and the linear activation function by Equation 2;

$$f(x) = 2[\frac{1}{1+e^{-2x}}] - 1 \quad (1)$$

$$f(x) = x \quad (2)$$

The models developed are used for the production of the one dependent parameter: the biodiesel yield in each of the 25 independent runs. ANN model is developed using MATLAB 7.9 software. The propagation algorithm was used for network training, 52 percent of the data was taken for training set, 13 percent for validation and the rest of the data for the test set. The accuracy of the models was determined by using equations 3 to 5 as applied by Ahmadian -Morghadam *et al.*, 2013.

$$MAD = \sum_{i=1}^{n}(\left|\text{yi} - \text{y\^{}i}\right|)/\text{n} \quad (3)$$

$$MAPE = \sum_{i=1}^{n}\{(\left|\text{yi} - \text{y\^{}i}\right|)/\text{yi}\}/n \quad (4)$$

$$MSE = \sum_{i=1}^{n}\{(\left|\text{ y\^{}i} - \text{ yi }\right|)\text{\^{}2}\}/n \quad (5)$$

Where MSE – Mean Squared Error (Standard Deviation)
MAD- Mean Absolute Deviation
MAPE- Mean Absolute percentage Error
yi – Actual biodiesel yield (%)
y^i- Predicted biodiesel yield

3. RESULTS AND DISCUSSION

Table 2: Physico-chemical parameters of African Pear Seed Oil (APSO) and its biodiesel in relation with standards

Parameters	Results	Standards			
	APSO	APSO FAME	ASTM D 9751	ASTMD 6751	DIN 14214
Yield (%)	55.70	93.025	-	-	-
Colour	Pale yellow	Light brown	-	-	-
Specific gravity	0.8885	0.8517	0. 850	0.880	0.860-0.900
Moisture content (%)	0.55	0.031	-	-	-
Refractive Index	1.4269	1.4269	-	-	-
Acid value (mgKOH/g)	6.57	0.92	0.062	0.50	0.50
Free fatty acid (%)	3.28	0.46	0.31	0.25	0.25
Iodine value (mgKOH/g)	50.96	45.06	42-46	-	120max.
Peroxide Value (milli eq. oxy/kg)	1.88	-	-	-	-
Saponification value **(mgKOH/g Oil)**	250.72	242.51	-	-	-
Ash Content (%)	1.50	0.10	0.01	0.02	0.02
Viscosity (cp)	5.82	2.31	2.6	1.9-6.0	3.5-5.0
Smoke point (^{o}C)	30	24	-	-	-
Titre Value (^{o}C)	36	-	-	-	-
Fire point (^{o}C)	40	27	-	-	-
Flash point (^{o}C)	149	125	60-80	100-170	120
Cloud point (^{o}C)	10	10	-20	-3 to 12	-
Pour point (^{o}C)	-6	4	-35	-15 to -16	-
Calorific Value (KJ/Kg)	-	34,421.50	42-46	-	35
Conductivity (Us/CM)	-	0.86	-	-	-
Cetane Index	-	57.80	-	-	-
Cetane Number	-	55.20	40-55	47min	51min
Higher Heating Value(HHV)[a] (MJ/kg)	-	34.50	-	-	-
Higher Heating Value(HHV)[b] (MJ/kg)	-	40.52	-	-	-
Higher Heating Value(HHV)[c] (MJ/kg)	-	63.75	-	-	-

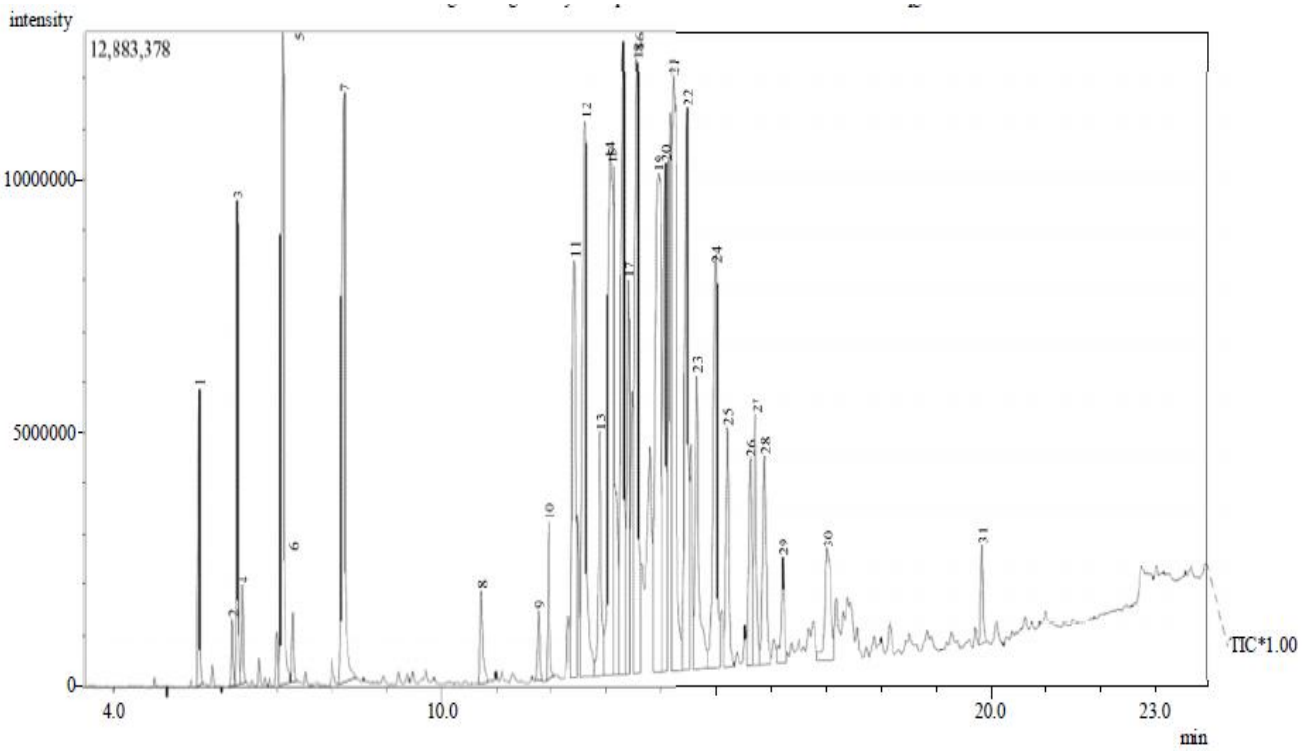

Figure 1: GC-MS Spectrum for African Pear seed Oil

Table 3: CCD matrix of four independent variables along with experimental and predicted response

Run	Factor 1 X_1 (°C)	Factor 2 X_2 (wt %)	Factor 3 X_3 (mins)	Factor 4 X_4 (mol/mol)	Actual Value (%)	Predicted Value (%)
1	40	1.0000	50	1:4000	80.2600	80.0910
2	60	1.0000	50	1:4000	67.8200	73.0778
3	40	2.0000	50	1:4000	69.5600	69.5676
4	60	2.0000	50	1:4000	68.2500	68.3166
5	40	1.0000	60	1:4000	86.6200	86.7414
6	60	1.0000	60	1:4000	85.3100	85.2270
7	40	2.0000	60	1:4000	87.0500	88.2719
8	60	2.0000	60	1:4000	85.7400	86.5910
9	40	1.0000	50	1:6000	69.1300	69.4590
10	60	1.0000	50	1:6000	66.8200	67.7630
11	40	2.0000	50	1:6000	69.6600	66.4099
12	60	2.0000	50	1:6000	67.2500	68.1794
13	40	1.0000	60	1:6000	86.8200	86.2429
14	60	1.0000	60	1:6000	85.3500	79.6197
15	40	2.0000	60	1:6000	87.6500	87.1192
16	60	2.0000	60	1:6000	85.8400	85.6321
17	30	1.5000	55	1:5000	78.7450	78.9258
18	70	1.5000	55	1:5000	76.1250	76.0502
19	50	0.5000	55	1:5000	77.0050	76.6884
20	50	2.5000	55	1:5000	77.8650	74.0572
21	50	1.5000	45	1:5000	59.9450	60.0572
22	50	1.5000	65	1:5000	94.9250	95.3069
23	50	1.5000	55	1:3000	77.4350	77.5250
24	50	1.5000	55	1:7000	78.5142	79.2240
25	50	1.5000	55	1:5000	80.2193	81.0040

Table 4: Model Statistics and Information for the Artificial Neural Network Model of APSOME

Performance	Biodiesel
MSE	1.3112
MAE	1.6588
MAD	1.3112
Minimum Absolute Error	0.009
Maximum Absolute Error	5.7303
R^2	0.944706

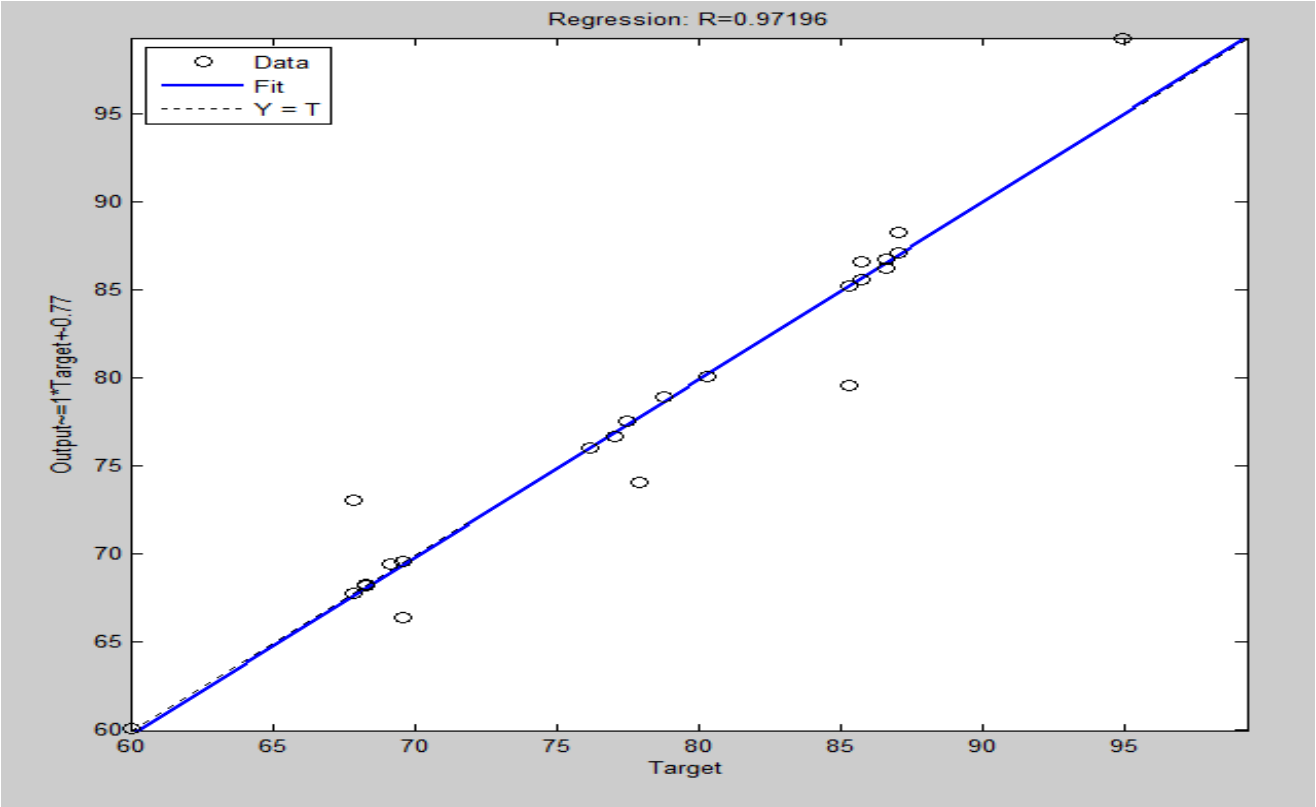

Figure 2: Desired output and actual network base on randomized data

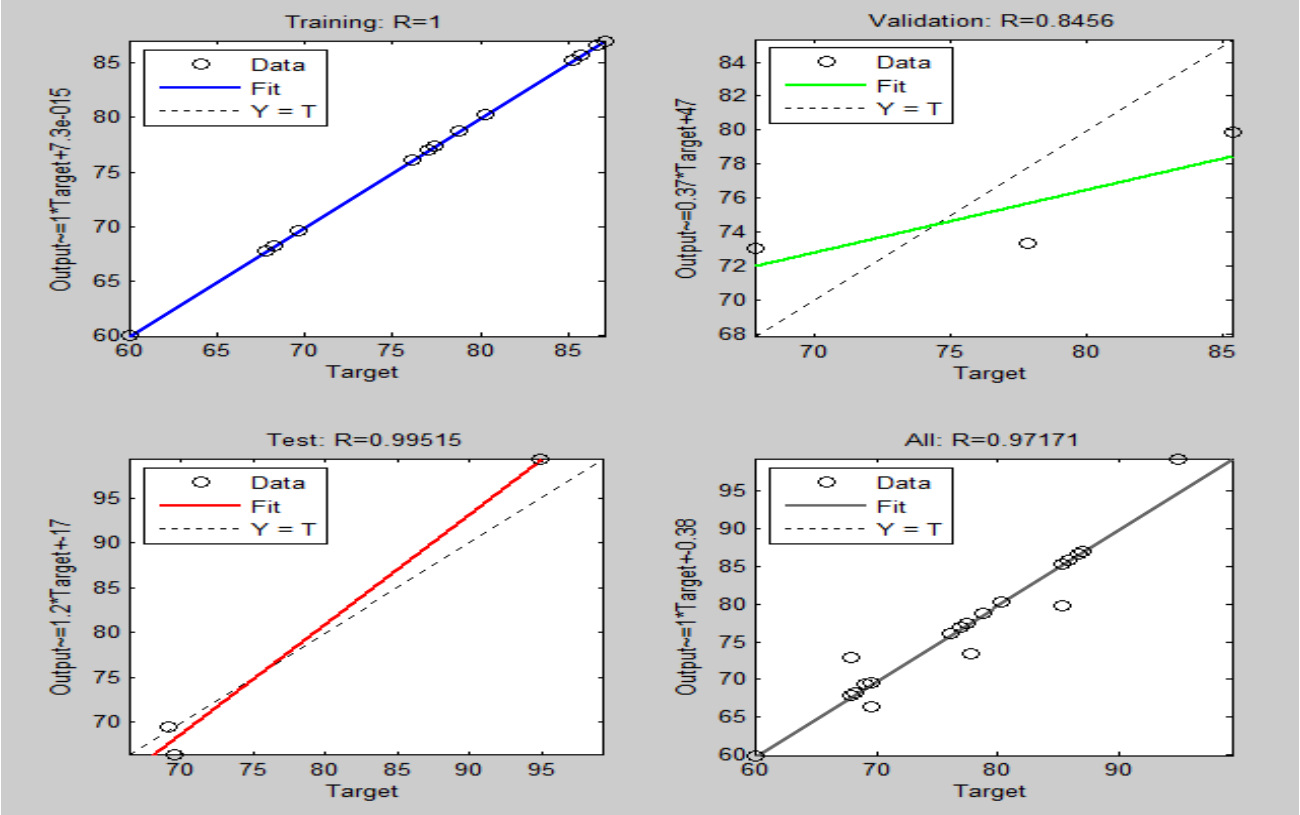

Figure 3: Regression values for Training Data, Test data, Validation data and overall model

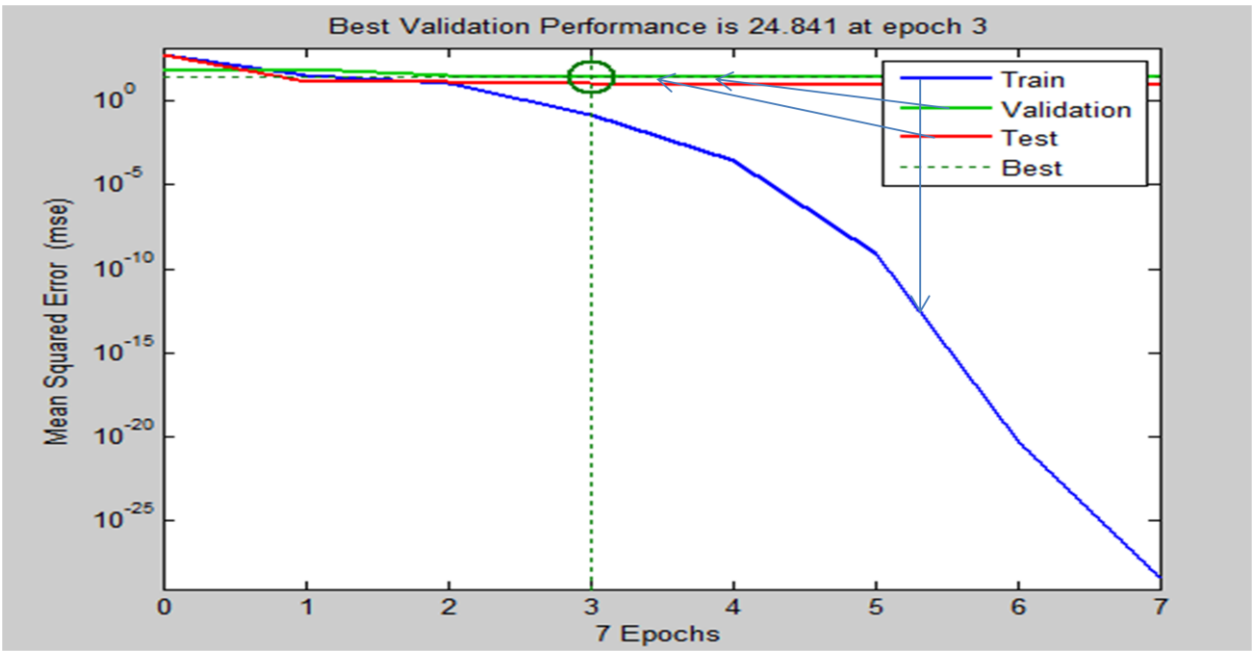

Figure 4: RMSE for training, testing and validation data for the ANN model developed

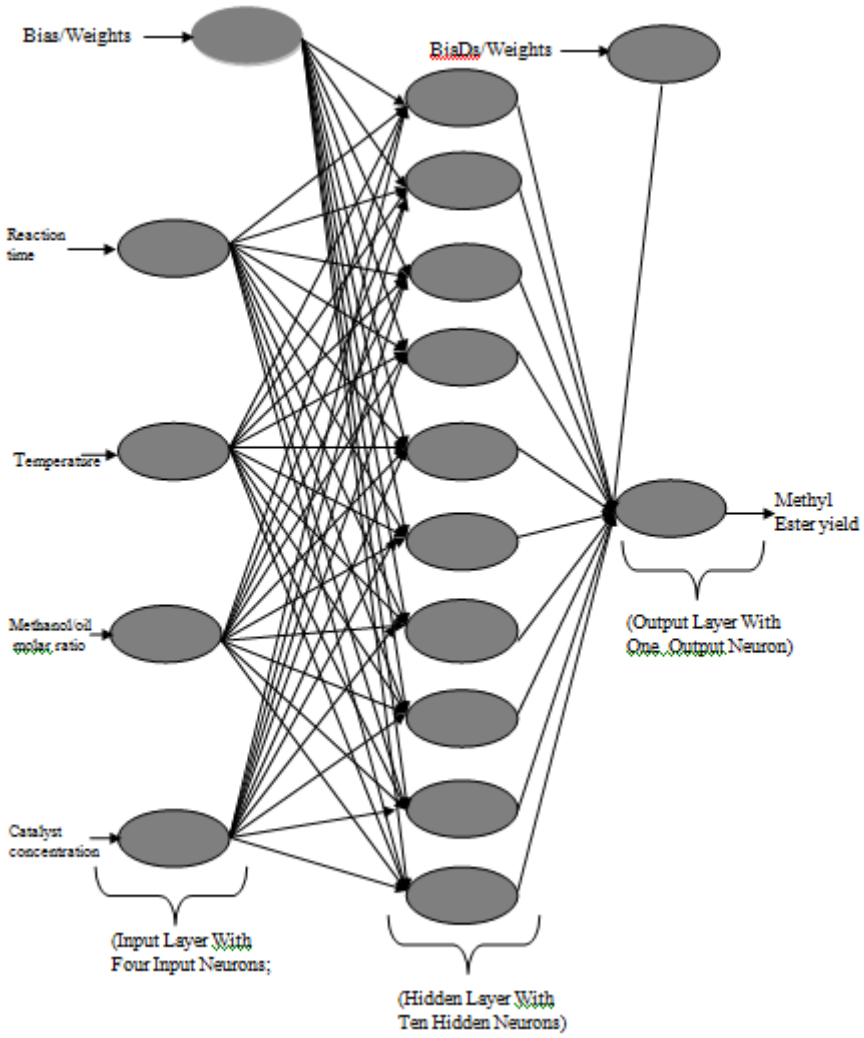

Figure 5: A typical architecture of the topology of the ANN model with three layers

The physico-chemical characterization of the APSO and APSOME are shown in Table 2. It is observed that the oil contains high yield (55.70%) with high FFA (3.25)mg/KOH/g. The high FFA gave the need to apply two-step transesterification which brought down the FFA to 0.46 in order to prevent soap formation which might lower the biodiesel yield. The quality of the oil compared well with result of other studies in the literature (Ogunsuyi, 2015). The raw oil had higher values of viscosity, smoke point, flash point and fire point than the corresponding biodiesel as an indication of improved fuel properties upon transesterification process. The results of the biodiesel compares well with the ASTMD 9751 and EN 14214 standards. Also the result of the GC-MS analysis showed that the African pear seed oil is non-dry and belongs to the oleic category with total saturated fatty acids of 33.56%, monounsaturated fatty acids of 59.88% polyunsaturated fatty acid of 6.01%. The most dominant fatty acids were oleic acid (53.13%), stearic acid (12.54%), palmitic (10.65%) and Eicosenoic acid (4.71%) (Figure 1).

Total data set of 25 points as shown in Table 3 was used in developing ANN model by MATLAB 7.9. All models constructed from the data set were characterized by a great response for all input variables from the leaning set. Figure 2 shows the relationship between the output and the target with high coefficient of determination (R=0.97196) and low standard error of estimation using ANN as contained in Table 4.0. Almost all the data scattered around the 45° line and that shows excellent compatibility between the experimental results and ANN predicted data. The regression coefficients of training, testing, validation and overall model developed using ANN is shown in Figure 3 and all prediction set had very good values of R (1.000, 0.9951, 0.8456 and 0.97171 respectively). The values on the x-axis are the

target values or the experimental values used to develop the model while the values on the y-axis are the values predicted by the model. The models constructed from this data set were characterized by a huge response for all input variables from the learning set which exhibited good relation between inputs (reaction temperature, reaction time, oil to methanol molar ratio and catalyst concentration) and the output (biodiesel yield) As mentioned earlier, the validation of results was tested using 25 sets of data. The comparison showed the behavior of such neural network models in predicting biodiesel yield. In addition, Table 4 summarizes the statistical results. These results indicate forecasting error measurements based on differences between the model and actual values. For validation data, the low standard deviation, mean absolute deviation, mean absolute percentage error and high R^2 were observed for biodiesel yield. The calculated statistics indicate that ANN provides a desirable way of understanding the patterns in data and predicating methyl ester yield based on investigating parameters (inputs). The genetic approach could be applied to provide optimal neural networks in terms of hidden layers, number of neurons and their configurations of connections. The results of this study is in agreement with the works available in literature (Bhattacharyulu *et al.*, 2013; Ahmadian-Morgan *et al*., 2013).

The optimum architecture topology of ANN (4:10: 1) model in this case is shown Figure 5. It consists of three layers: input layer with four input variables, hidden layer with ten hidden neurons and an output layer with single output variable. All neurons from hidden layer have tan-sigmoid transfer function (tansig) and the output layer neuron has linear transfer function (purelin).As can be seen from Figure 5, the connections consist of weights and biases between inputs and neurons as well as between neurons from different layers.

3. CONCLUSION

This study was able to develop a correlation between the operating parameters and biodiesel yield in a batch two-step transesterification process using Artificial Neural Networks (ANN) as a modeling technique. The comparison of the methyl ester yield as well as percentage error for all the data points are well in acceptable limits. Therefore, ANN has a great potential in providing solutions to the predicting problems related to yields of biodiesel production. This renewable and eco-friendly process has the potential to provide a sustainable route for the production of high quality methyl ester using underutilized African pear seed oil. This result may find useful application in large scale biodiesel production process by using artificial neural network model to predict final biodiesel yield through investigation of quantitative relationship between temperature of reaction, residence time, methanol to oil molar ratio and catalyst concentration. Further research shall involve comparing the ANN model with resonance surface methodology (RSM) model techniques so as to find the best network architecture. Also, extended exploration on this technology is necessary for scale up of process design, reaction kinetics study and application of the biodiesel fuel in diesel engine.

Nomenclature

ANN	Artificial Neural Network
APSO	African Pear Seed Oil
APSOME	African Pear Seed Oil Methyl Ester
b	Based on Viscosity
c	Based on Density
CCD	Central Composite Design
FAME	Fatty Acid Methyl Ester
FFA	Free Fatty Acid
HHV	Higher Heating Value (mg/kg)
MAD	Mean Absolute Deviation
MAE	Mean Absolute Error
MAPE	Mean Absolute Percentage Error
max	Maximum
Min	Minimum
MSE	Mean Squared Error
n	number of iterations
R	Correlation Coefficient
RSM	Resonance Surface Methodology
RMSE	Root Mean Square Error
X_1	temperature (˚C)
X_2	Catalyst Concentration (wt%)
X_3	Reaction time (˚C)
X_4	Oil/Methanol Ratio (mol/mol)
y_1	Actual Biodiesel Yield (%)
$y^\wedge_2$	Predicted Biodiesel Yield

REFERENCES

Ahmadian-Morghadam, H., Elegado, F. B. and Nayve, R. (2013). Prediction of Ethanol Concentration in Biofuel production Using Artificial Neural Networks, *American Journal of Modeling and Optimization* Vol. 1, No. 3, 31-35.

Awolu, O. O. and Layokun, S. K. (2013). Optimization of two-step transesterification production of biodiesel from Neem (*Azadirachta indica*) oil, *Int. J of Energy and Environmental Engineering*, 4: 39,

Bhattacharyulu, Y. C, Ganvir, V. N., Aditaya, A. and Ramming, A. (2013). Modeling of Neem Oil Methyl Esters Production using ANN, *International Journal of Computer Application*, Vol.70. No. 27, (0925-8887)

Bull, O. S. and George, D. Mc. (2015). Assessment of fuel properties of biodiesel obtained from African Pear (Dyocrodes edulis) seed oil, *Int J. of Advanced research in Science, Engineering and Technology*, Vol.2, Issue 10, pp 894-898

Ghorbani, H., Nikbakht, A. M., Tahatabaei, M., Hosseini, M. and Mohammadi, P. (2011). Application of modeling techniques for prediction and optimization of biodiesel production process, Int. Conf. on Biotechnology and Environment Mgt(IPCBEE) vol 18; pp7-12.

Ogunsuyi, H. O (2015). Production of biodiesel using African Pear(*Daycrodes edulis*) seed oil as a feed stock *Academia Journal of Biotechnology* 3(5) pp085-092,

Parawira, W., Murto, M., Zvauya, R., Matthiasson, B. (2004). Anaerobic digestion of solid potato waste alone and in combination with sugar beet leaves. *Renew. Energy* : 29: 1811-1823.

Patel, V. (1999). Cetane Number of New Zealand diesel, Report, office of Chief Gas Engineer, Energy Inspection Group. Ministry of Commerce Press. Wellington, New Zealand

Roman, M. B., Ekaterina, I. L. and Rvilya, Z. S. (2011). Artificial Neural Network (ANN) approach to biodiesel analysis. Analysis of biodiesel density, kinematic viscosity, methanol and water contents using near Infrared (NIR) Spectroscopy. *Fuel* 90: 2007 – 2015.

MODELLING THE CASCADE CYCLES AND THEIR IMPACTS ON DOWNSTREAM FRACTIONATION IN NATURAL GAS LIQUEFACTION PROCESS

Okeke, E. O.
MERCOGAS, Port Harcourt Nigeria,
eric.okeke@mercogasgroup.com

ABSTRACT

The study was designed to further advance our earlier model on natural gas processing. The objective is to efficiently evaluate all field natural gas in a region in Nigeria and decide on processing and utilization requirements. The region has large reserve of natural gas: associated and non-associated from the production fields. These need to be recovered, processed and utilized, to the benefit of all stakeholders. A generalized algorithm was developed and modelled on ASPEN HYSYS, in the context of processing field natural gas of varied compositions: C_1H_4 of range 78-97% or wider, and the balance other components. The model employs the LNG unit operation with cascade refrigerant cycles. Each cycle which uses refrigerants: methane, ethane and propane separately and/or mixed in appropriate ratios, is in a process loop consisting of a compressor, condenser, a throttle valve and the LNG unit operation. Along the process flowsheet sequence, downstream the cascades cycles loop is the fractionation train which separates the desired components. Overall, identified critical parameters, such as refrigerants compositions in the cycles and compressors process conditions, are used to optimize the model. The model was tested and applied to various field data in the region and confirmed to be robust and reliable. This model now provides solution to specific and specialized natural gas processing; supplies data and process information for both engineering and investment decisions on the hydrocarbon utilization, optimization and applications.

Key words *natural gas, field, evaluate, cascade, cycle, process*

INTRODUCTION

The Federal Government of Nigeria has made it a priority to unlock and harness the potential of natural gas resource to increase domestic and industrial power supply, raise living standards and support sustainable economic growth and diversification. According to the Oil Producers Trade Section (OPTS) of the Lagos Chamber of Commerce and Industry, Nigeria has around 181 trillion cubic feet (TCF) of proven gas reserves plus much more in undiscovered gas resources. However, despite having the largest gas reserves in Africa, only about 25% of those reserves are being produced or are under development today.

Available data shows Nigeria gas reserves and production over the years, and the potential to harness this resource to the benefit of all stakeholders. The main objective of this study is to develop a robust and reliable model for comprehensive evaluation of the natural gas reserves, determine processing requirements and prepare for investments. Data on Nigerian oil and gas is available and can be obtained outside the producers from the Nigerian National Petroleum Corporation and the Department of Petroleum Resources where they are domiciled. This study has therefore taking advantage of these, to do the design and simulation of natural gas and test such models with data from these sources.

CONCEPT

The concept attempts to expand and develop robust models for the technical and commercial evaluation of natural gas. Natural gas can be wet or dry, hence for full processing and greater end-use application, liquefaction/refrigeration are the processes used to separate the various components and deploy same, for specified domestic and industrial uses..

A refrigeration cycle uses changes in pressure and temperature on a mixed or pure compound (named refrigerant) in order to transfer heat from a cold zone (or fluid) to a hot zone (or fluid).

When there is a great gap between the temperature of the hot and cold zones (or fluids) and it is not possible to use only one refrigerant, the cascade cycles are used[1]. This configuration uses more than one individual cycle in a loop[2]. This arrangement guarantees very low temperatures on the desired natural gas stream. Different refrigerants have been recommended[3], with different

purities. Different cascade cycles have been modelled here on ASPEN HYSYS and they are shown latter here.

LIQUEFACTION CYCLES MODEL

Thermodynamic model is required for the liquid vapour equilibria and their energy properties for the work and heat calculations. Peng & Robinson[4] equation of state modelled as one of the physical property data correlation on ASPEN HYSYS was selected for this simulation.

Different arrangements of the multiple cascade cycles have been evaluated[3]; we have adopted and modelled various configurations. The model uses refrigerants in process cycles consisting of the evaporator, the compressor, the condenser and an expansion valve.

The cycles are configured to be a cascade or cascades depending on the type. The model defines specific parameters of the unit operations and streams, and calculates key process conditions:

$Q_{cm,i,j}$, $Q_{cn,i,j}$, , $Q_{LN,i,j}$ and $W_{cm,i,j}$;

where ***i*** represents the natural gas feed case (Cases 1-4), ***j***, the configuration of cascade (Traditional Triple Cascade[T3C], Triple Cascade [TPC] and Triple Hybrid Cascade [TPH])

The model has two segments: liquefaction and fractionation. Overall, the concept operates in layers with the liquefaction as the heart of the process; generating the outputs for fractionation, power and cascade cycle's performance analysis. The model has been developed to also handle multiple refrigerants in each cycle and the cycles in the cascade range from 1-3, as well as hybrid of cascade in one larger or separated sub-system. Figure 1 shows the general configuration while other configurations have also been studied. The streams and equipments have been defined as stated: numbers for streams and codes ***(Cm, compressor, Cn, condenser, JT, JT valve, LN, evaporator here modelled as LNG, FrT, downstream fractionation section).***

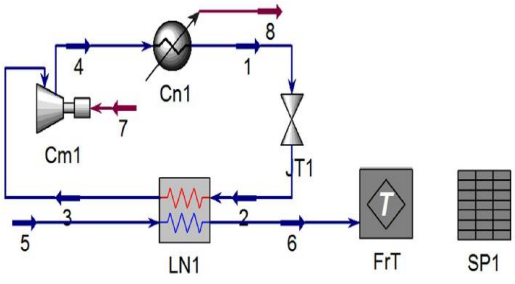

Figure 1a: Single Cycle

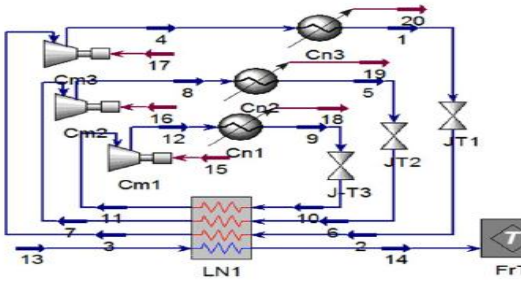

Figure 1b: 3 Cycle Cascade [T3C]

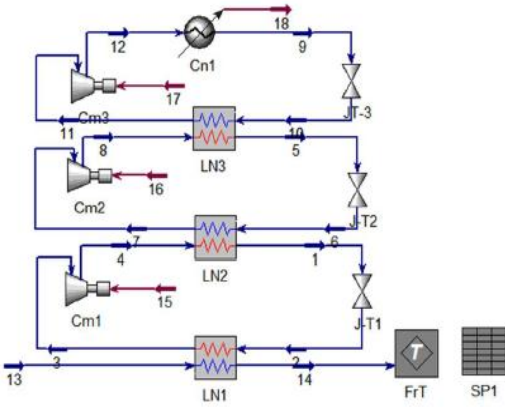

Figure 1c: Triple Cascade]3PC]

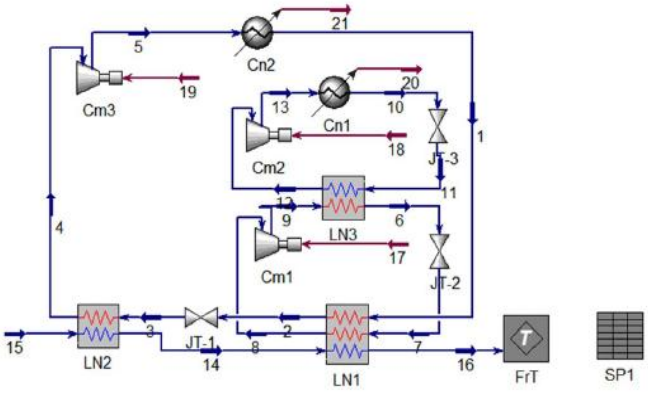

Figure 1d: Triple Hybrid Cascade [3HC]

These cascades were defined by flowsheet matrices describe below showing the contents ***i,j where i=0*** when there is no connection between stream ***i (i=1,21)*** with equipment or unit operations ***j (j is defined above in Figure 1 and in the matrix vertically- Cn, Cm, JT, LN, FrT)***, or ***i=1*** showing that stream ***i*** enters equipment ***j,*** and ***i=-1,*** stream ***i*** leaves equipment ***j.*** The matrix streams are balanced on both axis with ***StB*** (stream balance) and ***EqB*** (equipment to stream).

Single Cycle [T1C]

	1	2	3	4	5	6	7	8	EqB
Cn1	-1	0	0	1	0	0	0	-1	-1
JT1	1	-1	0	0	0	0	0	0	0
LN1	0	1	-1	0	1	-1	0	0	0
Cm1	0	0	1	-1	0	0	1	0	1
FrT	0	0	0	0	0	1	0	0	1
StB	0	0	0	0	1	0	1	-1	1

3 Cycle Cascade [T3C]

	1	2	3	4	5	6	7	8	9	10	11	12	13	14	15	16	17	18	19	20	EqB
Cn1	0	0	0	0	0	0	0	0	-1	0	0	1	0	0	0	0	0	-1	0	0	-1
Cn2	0	0	0	0	-1	0	0	1	0	0	0	0	0	0	0	0	0	0	-1	0	-1
Cn3	-1	0	0	1	0	0	0	0	0	0	0	0	0	0	0	0	0	0	0	-1	-1
JT1	1	-1	0	0	0	0	0	0	0	0	0	0	0	0	0	0	0	0	0	0	0
JT2	0	0	0	0	1	-1	0	0	0	0	0	0	0	0	0	0	0	0	0	0	0
JT3	0	0	0	0	0	0	0	0	1	-1	0	0	0	0	0	0	0	0	0	0	0
LN1	0	1	-1	0	0	1	-1	0	0	1	-1	0	1	-1	0	0	0	0	0	0	0
Cm1	0	0	0	0	0	0	0	0	0	0	1	-1	0	0	1	0	0	0	0	0	1
Cm2	0	0	0	0	0	0	1	-1	0	0	0	0	0	0	0	1	0	0	0	0	1
Cm3	0	0	1	-1	0	0	0	0	0	0	0	0	0	0	0	0	1	0	0	0	1
FrT	0	0	0	0	0	0	0	0	0	0	0	0	0	1	0	0	0	0	0	0	1
StB	0	0	0	0	0	0	0	0	0	0	0	0	1	0	1	1	1	-1	-1	-1	1

Triple [3] Cascade [3PC]

	1	2	3	4	5	6	7	8	9	10	11	12	13	14	15	16	17	18	19	20	EqB
Cn1	0	0	0	0	0	0	0	0	-1	0	0	1	0	0	0	0	0	-1	0	0	-1
JT1	1	-1	0	0	0	0	0	0	0	0	0	0	0	0	0	0	0	0	0	0	0
JT2	0	0	0	0	1	-1	0	0	0	0	0	0	0	0	0	0	0	0	0	0	0
JT3	0	0	0	0	0	0	0	0	1	-1	0	0	0	0	0	0	0	0	0	0	0
LN1	0	1	-1	0	0	0	0	0	0	0	0	0	1	-1	0	0	0	0	0	0	0
LN2	-1	0	0	1	0	1	-1	0	0	0	0	0	0	0	0	0	0	0	0	0	0
LN3	0	0	0	0	-1	0	0	1	0	1	-1	0	0	0	0	0	0	0	0	0	0
Cm1	0	0	1	-1	0	0	0	0	0	0	0	0	0	0	1	0	0	0	0	0	1
Cm2	0	0	0	0	0	0	1	-1	0	0	0	0	0	0	0	1	0	0	0	0	1
Cm3	0	0	0	0	0	0	0	0	0	0	1	-1	0	0	0	0	1	0	0	0	1
FrT	0	0	0	0	0	0	0	0	0	0	0	0	0	1	0	0	0	0	0	0	1
StB	0	0	0	0	0	0	0	0	0	0	0	0	1	0	1	1	1	-1	0	0	3

Triple [3] Hybrid Cascade [3HC]

	1	2	3	4	5	6	7	8	9	10	11	12	13	14	15	16	17	18	19	20	21	EqB
Cn1	0	0	0	0	0	0	0	0	0	-1	0	0	1	0	0	0	0	0	0	-1	0	-1
Cn2	-1	0	0	0	1	0	0	0	0	0	0	0	0	0	0	0	0	0	0	0	-1	-1
JT1	0	1	-1	0	0	0	0	0	0	0	0	0	0	0	0	0	0	0	0	0	0	0
JT2	0	0	0	0	0	1	-1	0	0	0	0	0	0	0	0	0	0	0	0	0	0	0
JT3	0	0	0	0	0	0	0	0	0	1	-1	0	0	0	0	0	0	0	0	0	0	0
LN1	1	-1	0	0	0	0	1	-1	0	0	0	0	0	1	0	-1	0	0	0	0	0	0
LN2	0	0	1	-1	0	0	0	0	0	0	0	0	0	-1	1	0	0	0	0	0	0	0
LN3	0	0	0	0	0	-1	0	0	1	0	1	-1	0	0	0	0	0	0	0	0	0	0
Cm1	0	0	0	0	0	0	0	1	-1	0	0	0	0	0	0	0	1	0	0	0	0	1
Cm2	0	0	0	0	0	0	0	0	0	0	0	1	-1	0	0	0	0	1	0	0	0	1
Cm3	0	0	0	1	-1	0	0	0	0	0	0	0	0	0	0	0	0	0	1	0	0	1
FrT	0	0	0	0	0	0	0	0	0	0	0	0	0	0	0	1	0	0	0	0	0	1
StB	0	0	0	0	0	0	0	0	0	0	0	0	0	0	1	0	1	1	1	-1	-1	2

The concept has been modelled on ASPEN HYSYS using available natural gas data, with results relating to previous studies and consolidated as contributions to engineering.

MODELLING WITH ASPEN HYSYS

A stage-wise approach was adopted as follows:

(i) Selection of refrigerants. Refrigerants have been identified and studied for natural gas processing[1-6]. Here we are using methane, ethane and propane available on ASPEN HYSYS data base.

(ii) Selection of physical and thermodynamic property data. The physical and thermodynamic data model by Peng Robinson is the most appropriate.

(iii) Selection of the components and characterization of the natural gas feed. The feed is characterized based on available laboratory data showing the composition and the condition of the field gas for different cases (Table 1).

Table 1: Composition of the design field natural gas feed.

Components	*Gas 1*	*Gas 2*	*Gas 3*	*Gas 4*
Nitrogen	0.0050	0.0004	0.0019	0.0020
H2S	0.0000	0.0000	0.0000	0.0000
CO2	0.0052	0.0001	0.0430	0.0243
Methane	0.7923	0.9962	0.8615	0.8260
Ethane	0.1304	0.0031	0.0420	0.0889
Propane	0.0491	0.0002	0.0215	0.0149
i-Butane	0.0071	0.0000	0.0094	0.0258
n-Butane	0.0059	0.0000	0.0070	0.0074
i-Pentane	0.0025	0.0000	0.0047	0.0008
n-Pentane	0.0016	0.0000	0.0026	0.0055
n-Hexane	0.0003	0.0000	0.0028	0.0008
n-Heptane	0.0003	0.0000	0.0026	0.0004
n-Octane	0.0001	0.0000	0.0011	0.0033
H2O	0.0000	0.0000	0.0000	0.0000
Totals	1.0000	1.0000	1.0000	1.0000

(iv) Configuration of the cascade liquefaction model. The different cascade models have been configured as required for basic traditional, hybrid and triple cascade, each consisting of mixed or pure refrigerants.

(v) Downstream the cascade model is the fractionation section, designed to separate and

recover lean gas (methane and ethane), propane and butane.

(vi) Simulation to determine

- ***a.*** Refrigerants' thermodynamic and physical property data at varied purities in each cycle,
- ***b.*** Determine conditions that provide lowest temperatures of outlet natural gas,
- ***c.*** Define configurations for downstream fractionation of the natural gas.

(vii) The models of the cascade liquefaction and the fractionation sections converged as required. Specifications are set for all cases in both the cascade and the downstream fractionation to define and meet targeted duties, heat loads, and components' yields as required for analysis of the model.

All the models described for different configurations as contained Figures 1, were run on ASPEN HYSYS: basic cycle, generalized for traditional three-cascade, hybrid and triple cascade. The cascade segment is the upstream and links into the downstream fractionation ***[T]*** segment shown in Figure 2.

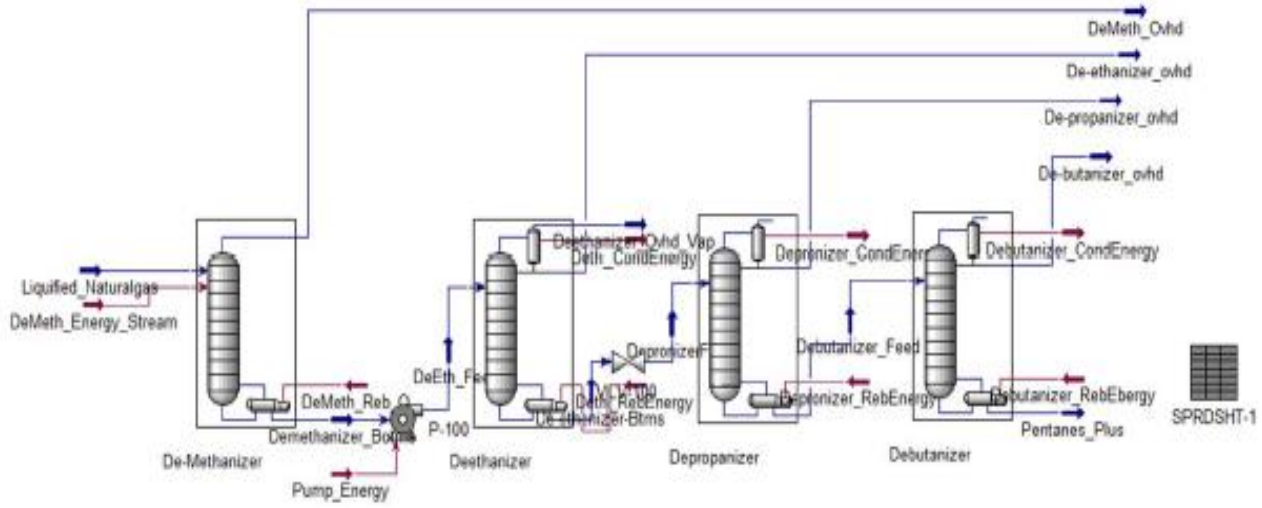

Figure 2: Downstream fractionation configuration showing the de-methenizer, the de-ethanizer, de-propanizer and de-butanizer columns inside the [T] sub-flowsheet.

RESULTS ANALYSIS

A very wide range of application of the model was considered: the simple cascade with one cycle and other cascade models were studied, for varied natural gas feed properties and process conditions. The consolidated result showing the loads for the cases are contained here in Table 2:

Table 2: Cascade refrigeration results analysis

		Load at x 1E6			
Traditional [3] Cascade [T3C]		***Gas 1***	***Gas 2***	***Gas 3***	***Gas 4***
Qcm, KJ/hr	***Qcm***	9.1688	9.1688	9.1688	9.1688
Qcn,, KJ/hr	***Qcn***	20.0907	20.0907	20.0907	20.0907
QLNG, KJ/hr	***QLN***	21.9509	17.4927	13.0553	20.0763
Wcm, KW	***Wcm***	0.0022	0.0022	0.0022	0.0022
Triple [3] Cascade [3PC]		***Gas 1***	***Gas 2***	***Gas 3***	***Gas 4***
Qcm, KJ/hr	***Qcm***	0.1852	0.1852	0.1852	0.1852
Qcn,, KJ/hr	***Qcn***	0.1850	0.1850	0.1850	0.1850
QLNG, KJ/hr	***QLN***	1.6972	5.0946	3.1084	6.2573
Wcm, KW	***Wcm***	0.0016	0.0019	0.0017	0.0019
Triple [3] Hybrid [3HC]		***Gas 1***	***Gas 2***	***Gas 3***	***Gas 4***
Qcm, KJ/hr	***Qcm***	5.4857	5.4799	5.4741	5.4833
Qcn,, KJ/hr	***Qcn***	26.7036	0.1852	17.7965	24.8265
QLNG, KJ/hr	***QLN***	41.5197	33.4617	29.0185	37.7681
Wcm, KW	***Wcm***	0.0015	0.0015	5.4741	5.4833

Result for downstream fractionation for Case Gas 1 for ***3PC*** is shown here in Table 3.

Table 3: Downstream Fractionation showing products streams compositions

.

Fractionation Data for Tripple Hybrid Wet Gas

Composition	*NG_Fd*	*DM_Ov*	*DE_Fd*	*DE_Ov*	*DP_Fd*	*DP_Ov*	*DB_Fd*	*DB_Ov*	*Pe_Plus*
Nitrogen	0.0050	0.0069	0.0000	0.0000	0.0000	0.0000	0.0000	0.0000	0.0000
H2S	0.0000	0.0000	0.0000	0.0000	0.0000	0.0000	0.0000	0.0000	0.0000
CO2	0.0052	0.0016	0.0148	0.0161	0.0000	0.0000	0.0000	0.0000	0.0000
Methane	0.7923	0.9772	0.2946	0.1412	0.0000	0.0000	0.0000	0.0000	0.0000
Ethane	0.1304	0.0136	0.4449	0.8420	0.3105	0.4997	0.0000	0.0000	0.0000
Propane	0.0491	0.0007	0.1795	0.0006	0.5038	0.4983	0.5128	0.8695	0.4840
i-Butane	0.0071	0.0000	0.0263	0.0000	0.0739	0.0019	0.1922	0.0977	0.1998
n-Butane	0.0059	0.0000	0.0218	0.0000	0.0612	0.0001	0.1614	0.0328	0.1718
i-Pentane	0.0025	0.0000	0.0094	0.0000	0.0264	0.0000	0.0697	0.0000	0.0753
n-Pentane	0.0016	0.0000	0.0058	0.0000	0.0163	0.0000	0.0431	0.0000	0.0466
n-Hexane	0.0003	0.0000	0.0012	0.0000	0.0034	0.0000	0.0089	0.0000	0.0096
n-Heptane	0.0003	0.0000	0.0011	0.0000	0.0030	0.0000	0.0079	0.0000	0.0085
n-Octane	0.0008	0.0000	0.0005	0.0000	0.0015	0.0000	0.0041	0.0000	0.0044
H20	0.0000	0.0000	0.0000	0.0000	0.0000	0.0000	0.0000	0.0000	0.0000
Total	1.0007	1.0000	1.0000	1.0000	1.0000	1.0000	1.0000	1.0000	1.0000

Where

NG_Fd	Natural gas feed	***DM_Ov***	De-methanizer overhead
DE_Fd	De-ethanizer feed	***DE_Ov***	De-ethanizer overhead
DP_Fd	De-propanizer feed	***DP_Ov***	De-propanizer overhead
DB_Fd	De-butanizer feed	***DB_Ov***	De-butanizer overhead
Pe_Plus	Pentanes plus compounds		

Over 80 simulation runs were performed for various cases using the ASPEN HYSYS.

CONCLUSIONS

The results show the loads/duties obtained from the cascade liquefaction model (heart of the process) and these are similar to those obtained elsewhere[3]: Compressor load for ***T3C*** is highest, followed by ***3HC*** and then ***3PC*** cascade configurations. Downstream data also shows composition of the products and intermediates, revealing opportunities for isolation of specific compounds like methane, ethane, propane and butane, and customizing specifications for various end-use applications.

The studied field gas composition range is wide with methane as 78-97% covering the virtually the entire spectrum wet to lean gas; hence model is applicable to natural gas from any part of the world. This model can therefore be used for extensive evaluation of natural gas fields and the resource processing and applications.

NOMENCLATURE

Q	Heat load or duty
W	Power or work for compressors

REFERENCES

1. Smith, R. (2005). *Chemical Process: Design and Integration (1st. ed.)*, Wiley, 978-0471486817.
2. Okeke E. O (2017). A generalized cascade algorithm modelled on ASPEN HYSYS optimizes natural gas processing. *Presentation at the 67th Canadian Chemical Engineering Conference, Edmonton, Canada.*
3. Trigilio Alessandro, Bouza Alexis & Di Scipio Sabrina (2012) Modelling and simulation of natural gas liquification process. *Advances in natural gas technology*
4. Peng, D.-Y. & Robinson, D. B. (1976). A New Two Constant Equation of State. *Industrial & Engineering Chemistry Fundamentals*, Vol. 15, No.1, (February 1976), pp. 59-64.
5. Çengel, Y. & Boles, M. (2006). Thermodynamics: *An Engineering Approach, McGraw-Hill*, 978-0070606593.
6. Walas, S. M. (1990). *Chemical Process Equipment Selection and Design*, Butterworth-Heinemann, 0-7506-9385-1

OPERATIONAL SUSTAINABILITY THROUGH INFINITE REVIEW OF VARIABLES

[*]Akujobi-Emetuche, G. C.[1], Joel O.F. [2], Chukwuma F.O. [3] and Wami E. N. [4]

[1]NPSC/PPMC-NNPC, Alesa-Eleme

[2]Centre for Oil field Research, World Bank African Centre of Excellence,
University of Port Harcourt Choba, Nigeria·

[3]Department of Chemical Engineering, University of Port Harcourt, Choba, Nigeria;

[4]Departement of Chemical/Petrochemical Engineering, Rivers State University of Science and Technology, Nkpolu, Port Harcourt, Nigeria.

graceakujobi_emetuche@yahoo.com

ABSTRACT

One of the Federal Government mandates on the Nigerian National Petroleum Corporation is to make petroleum products available in all parts of the nation. One of the pump stations set aside to accomplish this obligation is the Port Harcourt Area Systems 2E and 2EX pump Station nearly written off due to perceived low efficiency. The aim is to certify the newly and locally developed quality assurance protocol formula using the current real time pumping parameters. The objective of this work was to establish the relationship between data used for the formulation of the previous rule of thumb and current field data irrespective of the pump used and product type being moved. The previous rule of thumb confirmed optimum operating pressure and flow rate as 26.8 bar and 240 m^3/hr respectively, against the over 30 years designed parameters. This rule can be used to predict the pressure drop in fluid flow through the referenced pipeline. The result showed 0.01% deviation from the original work. This is evidence that the formula can still be used to authenticate the efficiency of the pipeline with assured product delivery and distribution.

***Keywords**: pumping, pressure, delivery, quality assurance, parameters.*

INTRODUCTION

One of the fastest and cheapest means of transporting large volume of petroleum products from one location to another is through the pipeline network. The product delivery is enhanced by pumps which is part of the pump station configurations. The pumps are either driven by electric motors, diesel engines or gas turbines. The pumps are classified according to pipeline design, topography and capacity requirements. The pumps were designed alongside workstation that remotely control the entire pump house and other aspects of pipeline operations. The station is also designed with instruments that predict real-time information on products densities, flash points and operational parameters like suction, discharge and mainline pressure. Pipeline control rooms utilize data acquisition systems that return real-time information about the rate of flow, the pressure, the speed and other characteristics. Both computers and trained operators evaluate the information continuously, (Ross, 2014 and Runge, 2014). Pump performance can be affected by the pump's physical properties like tensile strength, limit of proportionality, elongation, reduction in area, hardness, impact strength, fatigue strength, creep resistance, chemical composition, and corrosion resistance. The effects of these are felt more when the pump factory spares are unavailable and Operators resort to in-house fabrications of parts.

The pumps used for this review are diesel engine pumps. They were designed for oil-field environments with speed range maintained between 2,975 and 2,985 rpm. The engines employ a pneumatic control system to ensure no hazard is generated, (Singh, 2013 and Goyal, 2015).The initial research consideration used field data obtained from the then lone functional diesel driven pump. The operational performance was affected by:

- Aged and upkeep issues (workshop upgrading).
- Dearth of skilled young Engineers/Operators.
- Disguised succession plan due to apprehensions; as most of the people trained to operate the pumps have retired from service.
- Observed downtime occasioned to shortage of factory spare parts.
- Micro misalliance on some fabricated parts.

The direct measurable variables considered are pressure drop, flow rate, internal diameter and length of the pipe. Other variables considered are the internal roughness of the pipe, fittings, elevation change, types of flow, Reynold's number, friction factor, and fluid velocity.

RELATIONSHIP BETWEEN FLOW RATE AND PRESSURE DROP

From the previous work, the flow rate was measured in volume per time, this gave the volumetric flow rate Q_v (m^3/s) as area A (m^2) of the pipe multiplied by the velocity *v* (m/s) of the fluid.

Thus $Q_v = A \times \boldsymbol{v} = A\boldsymbol{v}$ (1)

The mass flow rate Q_m (kg/s) of the fluid (product) is given as:

$Q_m = Q_v\rho = A\mathbf{v}\rho$ (2)

As the A in equation (1) is substituted with $\pi\frac{d^2}{4}$, it implies that

$Q_v = \pi\frac{d^2v}{4} = 0.785\, d^2\boldsymbol{v}$ (3)

Where *d i*s the internal diameter of the pipe (Ujile, 2014).

PRESSURE DROP

One of the key calculations considered in the pipeline operation is pressure. The critical pressure types are the pressure drop in a given length of pipe for a given flow volume, the allowable working pressure and the delivery pressure. The allowable working pressure of the pipe in all operation conditions is important, and is taken as the maximum gauge pressure permissible.

Darcy's equation presented in S. I Unit has pressure drop expressed as

$$\Delta P = \frac{\rho f L v^2}{2d}, N/m^2 \quad (4)$$

Where ΔP = Pressure drop (N/m^2) over the length L (m).
ρ = density of fluid, (kg/m^3);
f = friction factor, dimensionless; L = length of pipe, (m); v = velocity of the fluid, (m/sec);
d = Inside diameter of the pipe, (m) and Acceleration due to gravity (9.81 m/s^2).

The total change in the static pressure of the fluid (product) as it flows along the pipeline is determined using the components of the Bernoulli equation.

$$\Delta\left(\frac{v^2}{2}\right) + gc\Delta Z + \int_1^2 VdP + Ws + F = 0 \quad (5)$$

The work and friction were neglected in the review hence,

$$\frac{\Delta P}{\rho} + \frac{\Delta v^2}{2gc} + \frac{g}{gc}\Delta Z = 0 \quad (6)$$

g is regarded as acceleration due to gravity acting in the same direction as force and can also be expressed as $g = \frac{dv}{dt}$ *; gc = Acceleration due to gravity (9.81 m/s²)*

These components were considered separately and added together. It was observed that a change in elevation can result to pressure decrease. Also a change in velocity may cause it to increase, and that the head loss may cause it to decrease. The cumulative effect depends on the relative magnitudes of each change, (McAllister, 2015; Shashi-Menon, 2015 and Bratland, 2013). It was confirmed that in the uniform diameter pipe, the inlet flow rate cannot completely be equal to the discharge.

The previous research work revealed that the designed flows rates were never achieved and using the then available main line pumps. The optimum operating parameter was consolidated as 26.8015 bar and 240m^3/hr based on 2011 to 2014 field data. Meanwhile, the maximum and minimum designed pressure and flow rate is 35 bar to 25 bar and 290 m^3/hr to 270 m^3/hr respectively. The result led to the established confidence and commitment to run the aged pumps again in order to sustain product delivery through the pipeline.

The objective of this work was to establish the relationship between data used for the formula and current field data irrespective of the pump and product type being moved.

METHODOLOGY

This present review considered 2017 field figures as there was no tangible operation from 2015 to 2016. The 2017 available field data was for AGO only. The data was reviewed and compared with the result from the previous work. The operational field data was from Automotive Gas Oil which is the dominated product pumped in 2017.The collated hourly flow rate was averaged to daily and then compressed to weekly. The observed minimum and maximum flow rates were noted. The main line pressure was extracted from the daily log book and control room activity charts. The exit pressure was not certain due to the observed inconsistency in the data. For the observed inconsistent, quality assurance procedure was deployed to ascertain the exit/receiving pressure. The data was evaluated

using relevant empirical and statistical formulae, equations and correlations. Other analysis models used were linear, power, exponential logarithmic and polynomial functions. Linear function was used when the data appear to fall within a straight line. This was done to choose the best possible fit for the data. Power function is used by engineers and scientist in areas that require basic qualitative evaluations. Exponential function relates to the understanding of mechanisms and working of nature. Logarithmic function is a mathematical inverse of exponential and it was used as an instrument which governs growth processes. Polynomial is a quadratic equation which appears as consequences of laws of physics and other classical phenomena in certain range of parameter, (Shestopaloff, 2100; Richards, 2014; Barkech, 2015; Kalman, 1997).

The current review was compared with the results of the previous work. Additional input to this work was the rehabilitation and performance of an Allen Engine pump abandoned for over 20 years due to vandalism. The results from the previous work was compared with the recent.

FINDINGS AND DISCUSSIONS

Observed Flow rate and Mainline Pressure using different functions and the same Diesel Pump for previous research:

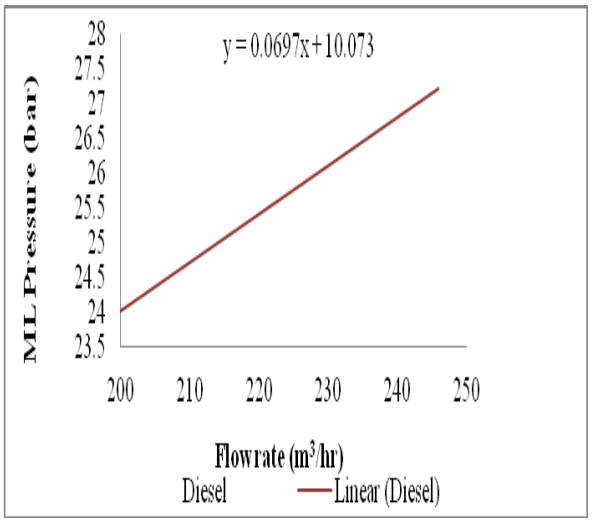

Fig 1: Linear function

At optimum flow rate of 240m^3/hr., the main line pressure was calculated as 26.973 bar

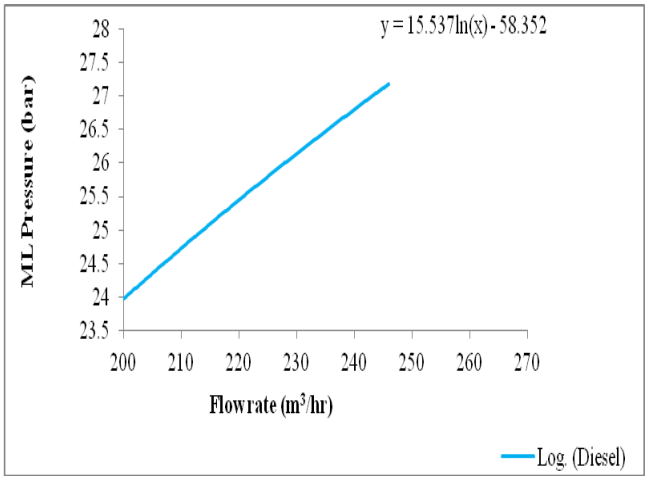

Fig 2: Logarithmic function

At optimum flow rate of 240 m^3/hr, the main line pressure is calculated as 26.801bar.

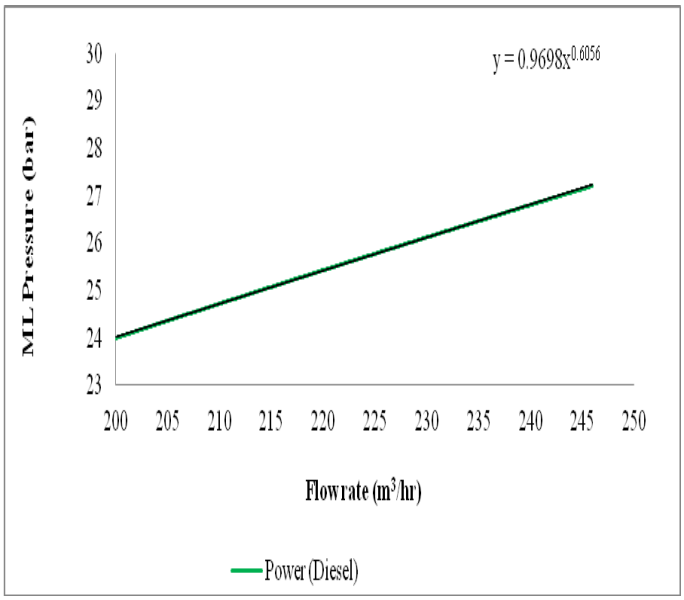

Fig 3: Power function

At optimum flow rate of 240 m^3/hr, the main line pressure was calculated as 26.80 bar

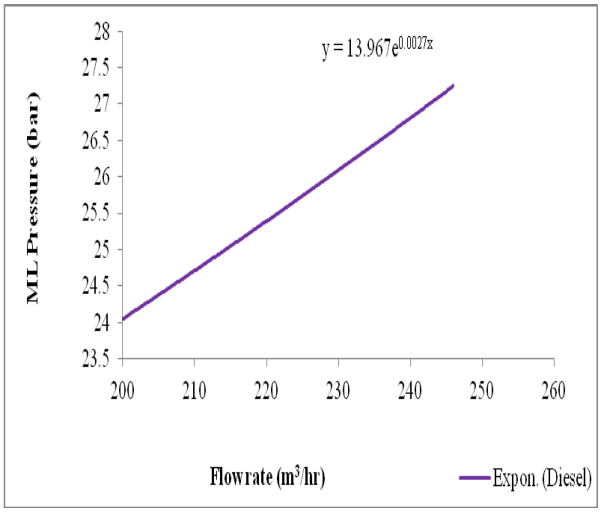

Fig 4: Exponential function

At optimum flow rate of 240m^3/hr, the main line pressure was calculated as 26.701 bar

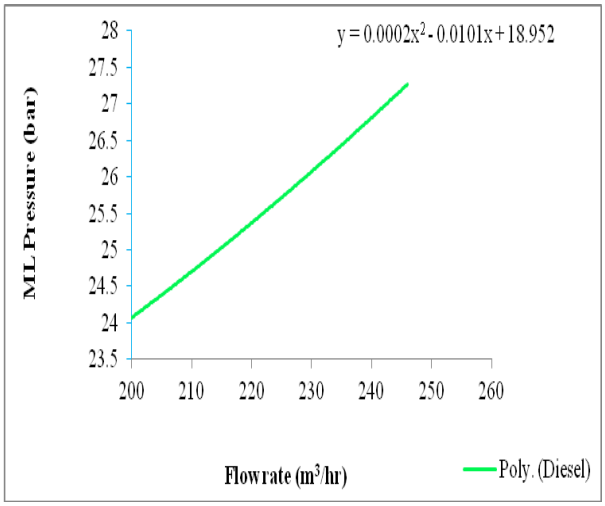

Fig 5: Polynomial function

Considering the optimum flow rate of 240 m^3/hr, main line pressure was calculated as 28.048 bar.

DEVELOPMENT WITH ALLEN ENGINEMAINLINE PRESSURE AND FLOW RATE

For the Allen Engine pump, the maximum and minimum designed pressure and flow rate is 50 bar to 35 bars and 290 m^3/hr to 270 m^3/hr respectively. The result obtained after the analysis of the field data revealed the following:

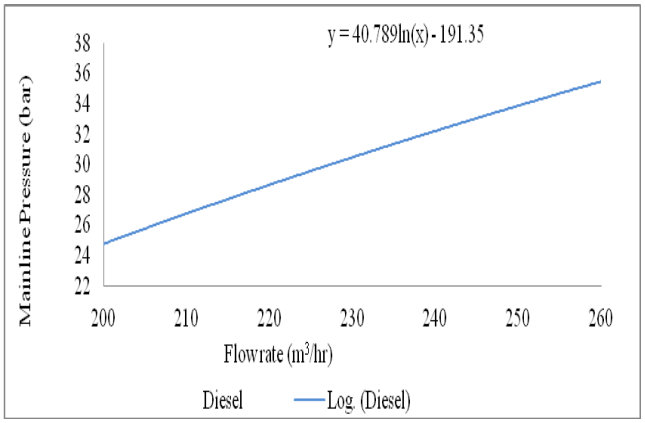

Fig. 6: Logarithmic function

With the Allen engine, the optimum mainline pressure at 240m^3/hr was calculated as 32.2 bar.

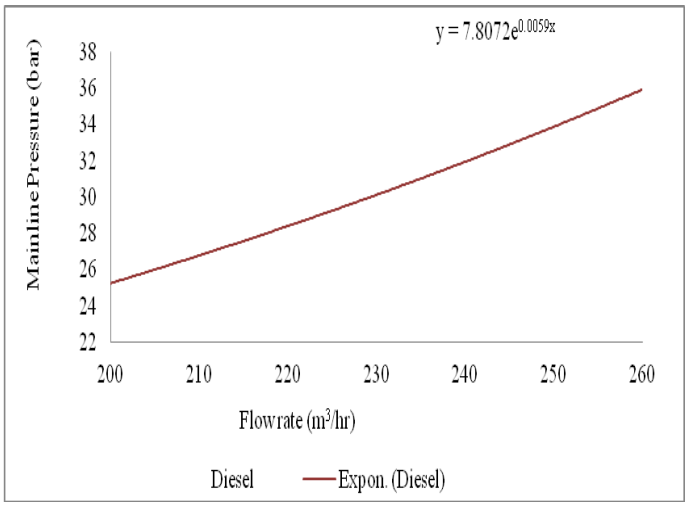

Fig. 7: Exponential function

Using optimum flow rate 240m^3/hr, the main line pressure was calculated 32.17 bar.

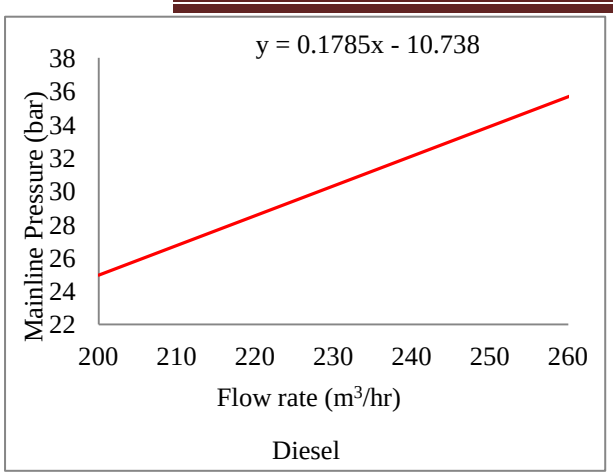

Fig. 8: Linear function

With the Allen engine, the optimum mainline pressure at 240 m^3/hr was calculated as 32.102 bar.

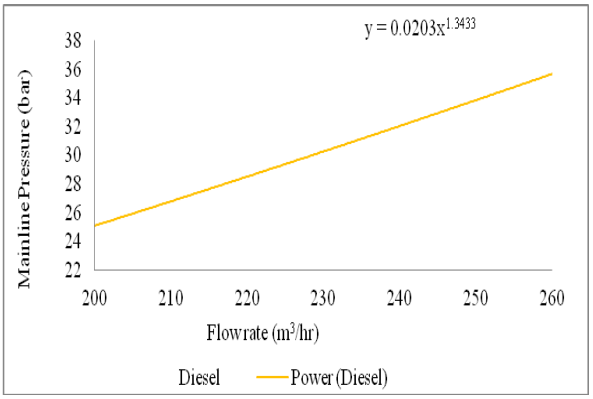

Fig 9: Power function

With Allen engine, the optimum mainline pressure at 240m^3/hr was 31.977 bar

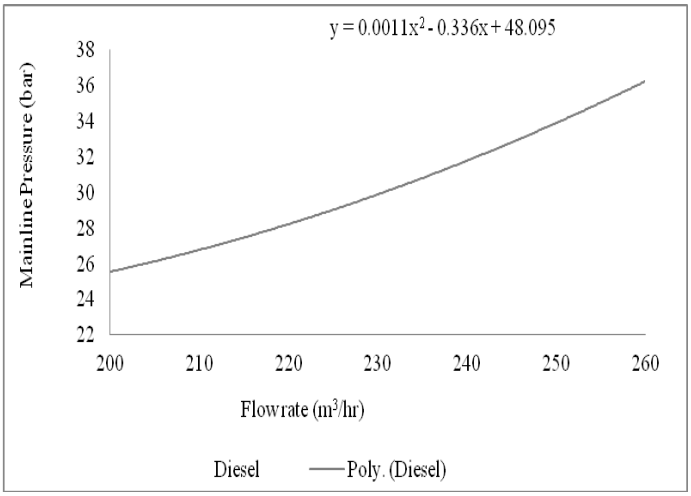

Fig 10: Polynomial function

With the Allen engine, the optimum mainline pressure at 240m^3/hr was 30.85 bar.

COMPARISON OF 2E AND 2EX DIESEL PUMP FIELD DATA

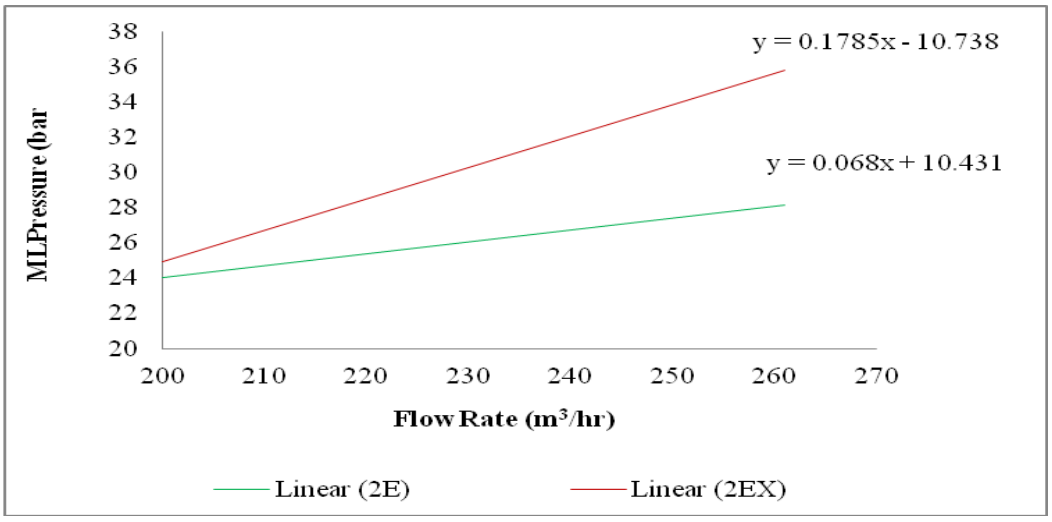

Fig 11: 2E and 2EX field data compared.

Table 1: AGO PUMPING USING 2E MAINLINE PUMP

P_{ML} (bar)	A = P_{ML} (kg/ms^2)	B = Qm (kg/s)	C = V (m/s)	D = Enhancement factor	E = d^2 (m^2)	F = (BxC) ÷ (DxE)	G = Fx56,000m in respect of the segment	P ($_{EXIT}$) = A-G (kg/ms^2)	$P_{(EXIT)}$ (bar)
24	2,400,000	47.78	0.781	21.592721	0.0919454	18.795756	1,052,184	1,347,816	13.5
24.2	2,420,000	48.73	0.796	21.592721	0.0919454	19.53764	1,094,440	1,325,560	13.3
24.3	2,430,000	49.21	0.804	21.592721	0.0919454	19.928382	1,116,107	1,313,893	13.1
24.7	2,470,000	49.69	0.812	21.592721	0.0919454	20.322992	1,137,987	1,332,013	13.3
25	2,500,000	50.17	0.820	21.592721	0.0919454	20.721471	1,160,079	1,339,921	13.4
25.2	2,520,000	51.6	0.843	21.592721	0.0919454	21.909875	1,227,153	1,292,847	12.9
25.3	2,530,000	52.56	0.859	21.592721	0.0919454	22.741083	1,273,239	1,256,761	12.6
25.7	2,570,000	53.51	0.874	21.592721	0.0919454	23.556405	1,319,681	1,250,319	12.5
26	2,600,000	54.47	0.890	21.592721	0.0919454	24.417995	1,367,458	1,232,542	12.3
26.2	2,620,000	56.38	0.921	21.592721	0.0919454	26.154554	1,465,040	1,154,960	11.5
26.4	2,640,000	56.86	0.929	21.592721	0.0919454	26.606343	1,490,091	1,149,909	11.5
26.8	2,680,000	57.33	0.937	21.592721	0.0919454	27.057281	1,514,827	1,165,173	11.7
27.1	2,710,000	57.81	0.945	21.592721	0.0919454	27.516766	1,540,299	1,169,701	11.7
27.2	2,720,000	58.29	0.952	21.592721	0.0919454	27.95076	1,565,984	1,154,016	11.5
27.4	2,740,000	58.77	0.960	21.592721	0.0919454	28.41774	1,591,881	1,148,119	11.5

Note that the density of AGO used is 860 kg/m^3

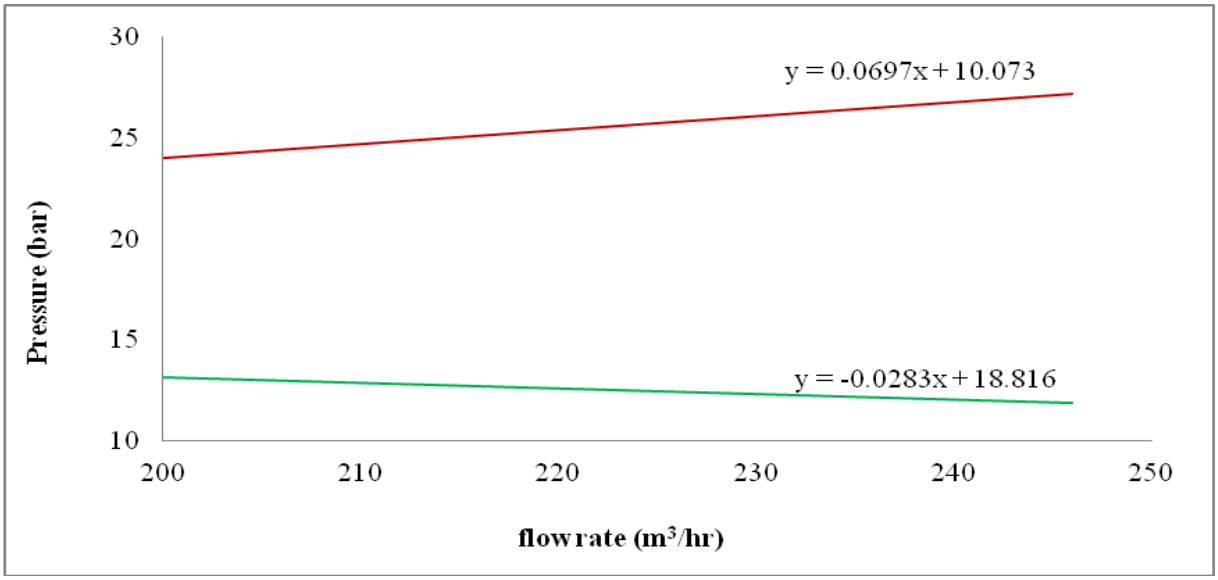

Fig 12: Comparison of 2E mainline and and stabilized reception pressure.

Table 2: AGO PUMPING USING 2EX ALLEN PUMP

P_{ML} (bar)	A = P_{ML} (kg/ms^2)	B = Qm (kg/s)	C = V (m/s)	D = Enhancement factor	E = d^2 (m^2)	F = (BxC) ÷ (DxE)	G = Fx56,000m in respect of the segment	P $_{(EXIT)}$ = A-G (kg/ms^2)	P$_{(EXIT)}$ (bar)
26	2,600,000	48.733	0.785	21.592721	0.0919454	19.268834	1,078,712	1,521,288	15.2
26.4	2,640,000	49.211	0.792	21.592721	0.0919454	19.631342	1,099,977	1,540,023	15.4
27	2,700,000	49.689	0.800	21.592721	0.0919454	20.022249	1,121,449	1,578,551	15.8
27.2	2,720,000	50.167	0.808	21.592721	0.0919454	20.417009	1,143,129	1,576,871	15.8
27.6	2,760,000	51.6	0.831	21.592721	0.0919454	21.59799	1,209,368	1,550,632	15.5
28	2,800,000	52.556	0.846	21.592721	0.0919454	22.395218	1,254,595	1,545,405	15.5
28.6	2,860,000	53.272	0.858	21.592721	0.0919454	23.022311	1,289,012	1,570,988	15.7
30	3,000,000	54.944	0.885	21.592721	0.0919454	24.492108	1,371,196	1,628,804	16.3
30.6	3,060,000	56.378	0.908	21.592721	0.0919454	25.784466	1,443,705	1,616,295	16.2
31.4	3,140,000	56.856	0.916	21.592721	0.0919454	26.232181	1,468,289	1,671,711	16.7
31.7	3,170,000	57.333	0.923	21.592721	0.0919454	26.654405	1,493,029	1,676,971	16.8
32	3,200,000	57.811	0.931	21.592721	0.0919454	27.10958	1,518,029	1,681,971	16.8
32.8	3,280,000	58.767	0.946	21.592721	0.0919454	28.001886	1,568,650	1,711,350	17.1
33	3,300,000	59.244	0.954	21.592721	0.0919454	28.467896	1,594,218	1,705,782	17.1
34	3,400,000	59.722	0.962	21.592721	0.0919454	28.938235	1,620,047	1,779,953	17.8
35	3,500,000	60.2	0.969	21.592721	0.0919454	29.382104	1,646,084	1,853,916	18.5
35	3,500,000	60.439	0.973	21.592721	0.0919454	29.620524	1,659,180	1,840,820	18.4

Note that the density of AGO used is 860 kg/m^3

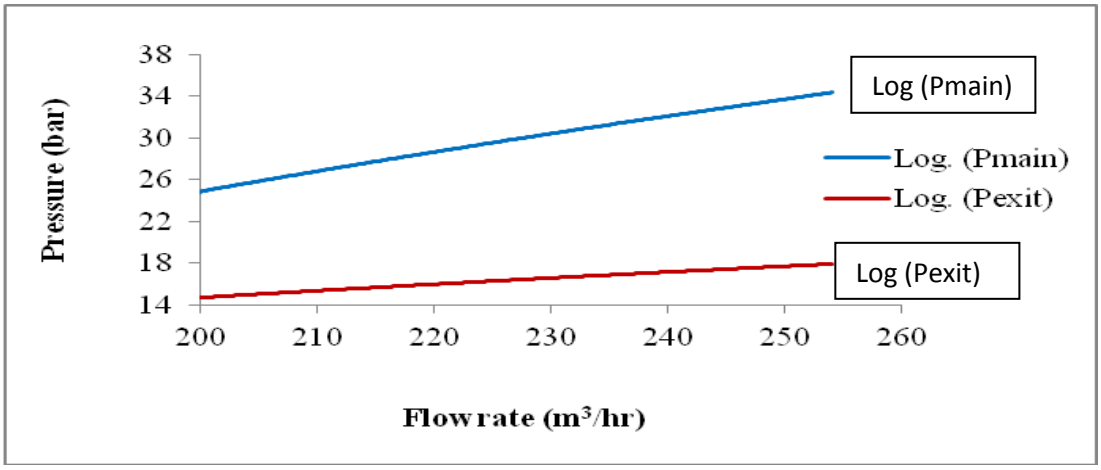

Fig 13: Comparison of 2EX main line and stabilized reception pressure.

Table 3: Summary of calculations using the 2E Main line pump

S/N	PROCEDURE	PRESSURE (bar)	PREVIOUS RESEARCH	DEVIATION	% DEVIATION
1	Linear	26.801	26.8015	0.001	0.004
2	Logarithmic	26.801		0.001	0.004
3	Power	26.8		0.002	0.007
4	Exponential	26.701		0.101	0.378
5	Polynomial	28.048		-1.246	-4.442

Table 4: Summary of calculations using 2EX Allen Engine Pump

S/N	PROCEDURE	MAINLINE PRESSURE (bar)	REMARKS
1	Linear	32.2	All results are within the range of 30.5 to 32.5
2	Logarithmic	32.1	
3	Power	31.98	
4	Polynomial	30.85	
5	Exponential	32.17	

CONCLUSION

Comparison of the respective plots shows that the current individual and average flow rate are still below the designed value, but the previous optimum mainline pressure and flow rate are still valid. The deviation from the optimal flowrate on the 2E main was below 0.01% using linear, logarithmic and power functions. The objective of this work and the relationship between data used for the formula and current field data was a success, However, the values for exponential and polynomials functions are still within operational range.

Using the quality assurance parameters, the uncertain field data for exit pressure was ascertained both for 2E and 2EX. Meanwhile the calculation with the Allen has the optimal flow rate and the mainline pressure as 240 m^3/hr and 32 bar. Using the quality assurance parameters, the uncertain field data for exit pressure was established both for 2E and 2EX. The newly restored Allen engine pump that has been dormant for over 20 years is established to be delivering at optimal flow rate and mainline pressure of 240 m^3/hr and 32 bar respectively. The pump is transporting products optimally and smoothly to the designated Depot

.

REFERENCES

Ross, D. F. (2014): Distribution Planning and Control: *Managing in Era of Supply Chain Management,* 3rd ed. Springer. Pp 708.

Runge, W. (2014): *Technology Entrepreneurship: A* Treatise on Entrepreneurs and Entrepreneurship for and in Technology ventures. Vol 1 & 2, Kit Scientific Publishing. Pp.1003.

Ujile, A. A, (2014): *Chemical Engineering Unit Operations, Synthesis and Basic Design calculations, Vol 1.BOMN P*rints Nigeria. Pp 21.

Barkech, K. (2015): Studies in Systems, Decisions and Control: *Modelling and Analysis of Linear Hyperbolic Systems of Balanced Laws",* Sprinter. Pp 15.

Bratland, O. (2013): Pipe Flow 2; Multi-phase Flow Assurance", ISBN 978-616-335-926-1; Pp 8.

Goyal, M. K. (2015): Fluid Mechanics and Hydraulic Machines", *Eastern Economy Edition. PHI Learning Private Limited.* Pp 4-16.

Kalman, D. (1997): Elementary Mathematical Models: Order Aplenty and a Glimpse of Chaos *Mathematical Association of America*. Pp 265.

McAllister, E. W. (2009): Pipeline Rules of Thumb Handbook. A Manual of quick, accurate to everyday pipeline Engineering problems. 7th ed., Oxford OX2 8DP, UK: *Gulf Professional Publishing*, Jordan Hill. Pp 389, 399-401, 418, 421-422, 477.

Menon, E. S. (2015): *Transmission Pipeline Calculations and Simulations Manual, Elsevier Press*. Pp 15-18, 93-94, 174.

Richards, K. (2014): Design Engineer's Reference Guide, *Mathematics, Mechanics and Thermodynamics", Elsevier*. Pp 239-246.

Shestopaloff , Y. K, (2010): Properties and Interrelationships of Polynomial, *Exponential, Logarithmic and power functions with the applications to modelling natural phenomena* Akvy Press, USA. Pp 21-64.

Singh, R. (2013): Artic Pipeline Planning: Design, Construction and Equipment, GPP. Pp 75-76.

INVESTIGATION ON THE USE OF BLENDS OF *MORINGA OLEIFERA* AND PUMPKIN SEEDS CAKE EXTRACTS IN THE TREATMENT OF SHIKA DAM RAW WATER

[*]Jumare, S.A,[1], Mohammed-Dabo, I.A.[2] and Muhammad, J.A.[2]

[1]Department of Food Tech., Federal Polytechnic Kaura Namoda, P.M.B 1012, Zamfara State.

[2]Department of Chemical Engineering, Ahmadu Bello University, Zaria, P.M.B 1013, Kaduna State.

Corresponding author: sanijumare@yahoo.com, sanijumare@gmail.com.

ABSTRACT

A preliminary investigation was carried out for the feasibility of using blends of Moringa Oleifera Seed Extract (MOSE) and Pumpkin Seed Extract (PSE) to treat surface water. The two seed extracts were mixed in proportions ranging from 100 % Moringa Oleifera (MO) and 0 % Pumpkin (PPK) to 0 % MO and 100 % PPK. 5.0, 5.5, 6.0, 6.5 and 7.0 ml of the blends were used to treat 500 ml of raw water on a jar test apparatus. The contents of the jar were stirred rapidly for 5 min at 100 rpm and slowly stirred for 15 min at 50 rpm. The water was then allowed to settle, filtered and analysed for; turbidity, hardness, pH, biological oxygen demand (BOD), chemical oxygen demand (COD) and bacterial load (E-coli.). From the results obtained, it showed that the 100 % MO had maximum reduction in turbidity and bacterial load of 97 % and 67 %, whereas, 100 % PPK had maximum reduction in turbidity and bacterial load of 89 % and 100 % respectively. Furthermore, the results for the blends showed that blends with more concentrations of Moringa Oleifera had more effect on the reduction of; turbidity by 98 %, hardness by 78 %, and COD by 82 %. On the other hand, blends with more concentrations of pumpkin had more effect on the reduction of; BOD by 43 %, COD by 82 % and bacterial load by 100 %. However, analyses on the treated water showed that Moringa Oleifera and Pumpkin did not significantly affect the pH (1.5 – 5.8 %) after treatment. Certainly, the results obtained in this research are in agreement with the standards by Standards Organisation of Nigeria (SON) and World Health Organisation (WHO). Therefore, the study showed the possibility of blending Moringa Oleifera and Pumpkin seeds cake extracts as a viable and indigenous pretreatment approach in raw water treatment.

***Key Word**: Blends, Moringa Oleifera, Pumpkin, Extracts, Seeds, Treatment*

INTRODUCTION

Turbidity removal is one of the important steps in water treatment process and it is generally achieved using coagulation with metal salts followed by aggregation of particles through flocculation and separation through sedimentation and filtration. Aluminium (e.g. $Al_2(SO_4)_3 .18H_2O$) and iron salts are mostly used as coagulant reagents. Studies by (Ngabigengesere & Narasiah, 1998; Katayon *et al.,* 2005) have indicated a number of serious drawbacks linked to the use of aluminium salts such as Alzheimer's disease associated with high aluminium residuals in treated water, excessive sludge production during water treatment and considerable changes in water chemistry due to reactions with the OH– and alkalinity of water.

A number of studies have pointed out that the introduction of natural coagulants as a substitute for metal salts may ease the problems associated with chemical coagulants (Katayon *et al.,* 2005). Using natural coagulants such as the seeds from the *Moringa Oleifera* MO tree instead of aluminium salts might give advantages, such as smaller costs of water production, less sludge production and ready availability of reagents.

In this paper, the potentials of using *Moringa Oleifera* and pumpkin as an alternative to aluminium sulphate for drinking water treatment in zaria, kaduna state is evaluated, its limits analyzed and the optimal use and dosage assessed. Standard Jar-test experiments performed with solutions prepared from *M.O* and pumpkin seeds cake extracts were used to compare the efficiency in turbidity, pH, COD and Bacterial load of Shika dam raw water, Zaria, Kaduna State, Nigeria.

WATER TREATMENT WITH NATURAL COAGULANTS

Many coagulants are widely used in conventional water-treatment process for turbidity removal during potable water production. These coagulants may be classified as inorganic, synthetic organic polymer, and natural polymer. These coagulants are used for various purposes

depending on the chemical characteristics of the water to be treated.

Moringa Oleifera

With its origin in India and Pakistan *M. Oleifera* was brought to the Africa continent and Sudan in particularly for ornamental purposes during the colonial era. The women of Sudan soon discovered the abilities of the tree and have used the seeds for water treatment since the beginning of the 20th century. The natural coagulant found in *Moringa Oleifera* is present in 6 of the 14 species of *Moringa* growing in Africa, Madagascar, India and Arabia. *Moringa Oleifera* is the only one of the species in the botanic family that is present in tropical and subtropical regions around the world, and is therefore the most famous. The various forms in which *Moringa Oleifera* exist are presented in figure 1.0.

(a)

(b)

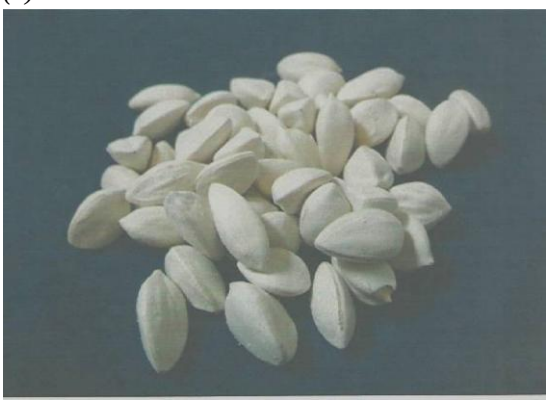

(c)

Figure 1: (*a-c*) *Moringa Oleifera* Tree, Pods, and Seeds. (Pragnya, 2005).

The tree was given names by the most popular tribes in Nigeria and is presented in table 1.0 as;

Table 1. Various names given to *Moringa Oleifera* by some Nigerian tribes.

Tribe	Name
Fulani	Kabije or Gawara
Hausa	Zogale Gandi
Igbo	Owe Igbale
Yoruba	Ewe Igbale/Ewe ile

Source: (Nwali *et al.*, 2013)

Pumpkin

Pumpkin can be found in many shapes, sizes and colours, which have a moderately hard rind, with a thick, edible flesh below, and a central seed cavity. There are numerous seeds in the fruit. Most seeds are plump and tan or soft white. They are all covered with a testa that serves as a protectant around the seeds (Robinson and Decker- Walters, 1997).

Pumpkin fruit and pumpkin-derived products in the past few years because of the nutritional and health protective value of the proteins (25.2-37%) and oil (37.8-45.4%) from the seeds as well as the polysaccharides from the fruit (Sojak & Głowacki, 2010). Figure 2.0 depicted the pumpkin seeds.

Figure 2a: Pictorial View of Pumpkin

Figure 2b: Pictorial View of Pumpkin

The pumpkin kernel was given names by the most popular tribes in Nigeria and is presented in table 2.1 as;

Table 2: Various names given to Pumpkin by some Nigerian tribes.

Tribe	Name
Fulani	Kabayel/Hadera
Hausa	Goji or Kabewa
Igbo	Ugwu
Yoruba	Elegede/Agbeje

Source: (Nwokolo and Sim, 2007)

MATERIALS AND METHODS

Good quality dry seeds of *Moringa Oleifera* were selected from the pods which were ensured to be completely dry on the tree (i.e. until the pods turns brown in colour) because the green pods do not possess any coagulation activity (Ndabigengesere *et al.,* 1995). The seeds coat and wings were removed manually. The seeds were grounded to a fine powder with a domestic food blender and sieved through sieve 210 μm (Gassenschmidt *et al.,* 1995).

On the other hand, the ripe pumpkins were cut and then the seeds were separated. The separated seeds were washed and air dried at room temperature. The dried seeds were then grounded to a fine powder using blender and sieved through sieve 210 μm. The powder with < 250 μm was used in this research work.

Extraction of Oil

100 g of the crushed seeds of both *Moringa* and Pumpkin were weighed separately and placed on a thimble. The thimble containing the sample was then inserted into the Soxhlet apparatus. 500 *ml* of the solvent (hexane) was measured using a measuring cylinder and then poured into a round bottom flask with the sample and heated at 60 ^oC for 5 *hours* after which the sample was removed and transferred into the air oven to dry at 105 ^oC for 15 *minutes*. This sample was then weighed and the difference was calculated as:

$$\%\, Yield\ of\ Oil = \frac{\text{Wt of sample before extraction} - \text{Wt of sample after extraction}}{\text{Initial weight of sample}} \times 100 \ldots\ldots Eqn\ 1.0$$

The oil was recovered by solvent evaporation. It was collected into a beaker and left open at room temperature (24 Ex2221d^oC) until the solvent finally evaporates leaving behind the oil extracted.

Coagulants Preparation

The coagulant solution of *Moringa Oleifera* and pumpkin were prepared and used on the same day. For the preparation of standard solution of *Moringa oleifera* and Pumpkin, for each 3g of *Moringa oleifera* and Pumpkin seeds pulp, were added to 100ml of distilled water containing 0.1M NaCl to form 3% solution.

The solution was thoroughly stirred for 3 minutes to extract the active ingredients which were then filtered to remove the cake and a clear solution was obtained (Cardoso *et al.,* 2008, Madrona *et al.,* 2010 and Jaju, 2012).

Jar Test

The coagulation and floc formation process was simulated. The jar test apparatus consists of six paddle stirrers and 6 jars filled with sample. A pictorial representation of jar test setup is shown in figure 3.0.

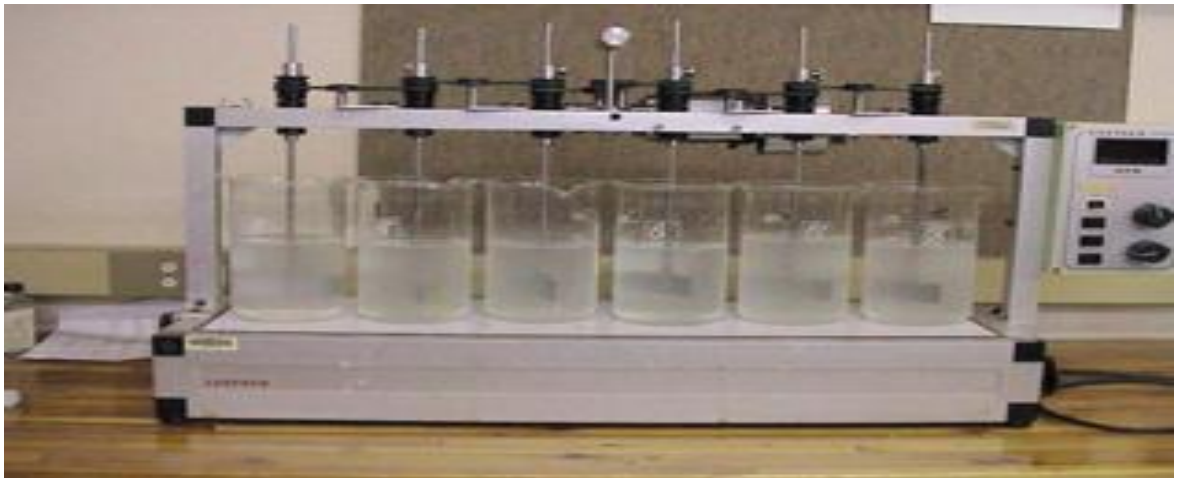

Figure 3: Jar Test Equipment.

To each jar a certain dose (5, 5.5, 6.0, 6.5 and 7.0 *ml* respectively as presented in appendix A) of coagulant was added subjected to rapid mixing (coagulation process) and then slow mixing (flocculation process). After rapid mixing at 100 rpm for 5 *minutes*, a slow stirring at 50 rpm for approximately 15 *minutes* and then the propellers were stopped and the content of the jars left to settle under quiescent condition. After sedimentation, samples were filtered and taken for water quality determination.

RESULTS

Raw Water Characteristisation

An initial experiment was carried out to determine the preliminary characteristics of the raw water for examining the effectiveness of *Moringa Oleifera* and Pumpkin as Coagulants in the treatment process. The characteristics of the raw water were measured at the Ahmadu Bello University, Water Treatment Plant laboratory, except for Bacteriological analyses, BOD, COD and TSS which were respectively made at Department of Veterinary Medicine and Department of Chemical Engineering of Ahmadu Bello University, Zaria. These samples were taken straight from Shika Dam, which is a major river that supplies potable water to Zaria town and its environs. The results of shika dam raw water characteristics were presented in Table 3.0.

Table 3: Shika Raw Water Analysis

Parameters	Values	Standard Organisation of Nigeria (SON)
Turbidity (*NTU*)	107	5
pH	6.9	6.5 – 8.5
Hardness (*mg/l*)	50	150
BOD (*mg/l*)	3.0	5
COD (*mg/l*)	190	100
Bacterial load (*cfu/100ml*)	21	0/100 ml

DISCUSSION OF RESULTS

Effect of Dosage on the Turbidity

The initial turbidity of Shika dam raw was recorded as 107 *NTU* before coagulation. Using MOSE for the treatment gave turbidity values in the range of 3.3 to 3.9 *NTU* and using PSE gave values between 11.5 to 15.7 *NTU*. The results as presented graphically in fig. 4.0 confirmed a gradual increase in turbidity of 3.1, 3.6, 4.0, 4.3, 4.7, 4.9, 5.1, 5.5 and 6.2 *NTU* obtained by 90:10,

80:20, 70:30, 60:40, 50:50, 40:60, 30:70,20:80 and 10:90 dosage ratios of *MO*: PPK respectively. From the results obtained as presented in figure 4.1, it evidently proved, the best turbidity was obtained to be 3.1 *NTU* (97%) at 90:10 dosage ratio of *MO*: PPK. However, blending of the two seeds extract (MOPE) in the treatment process was aimed to strike a balance by augmenting the efficiency of one over the other. Certainly, the results here showed that MOSE was more effective in turbidity reduction than PSE hence, MOSE is the augmenting agent.

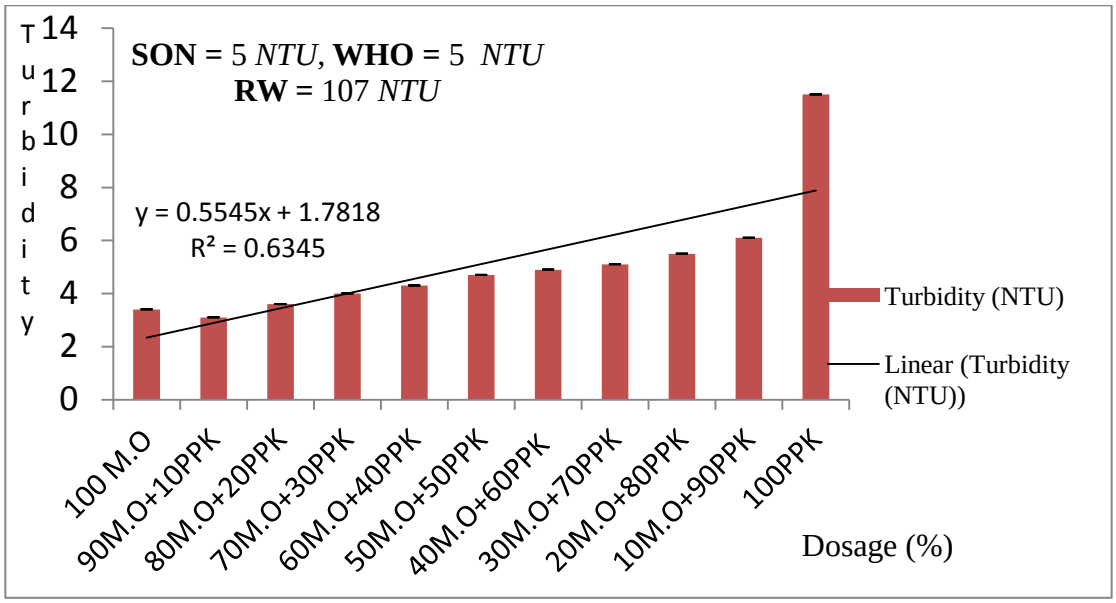

Figure 4: Effect of Dosage (%) on the Turbidity (*NTU*)

Effect of Dosage on the Hardness

Based on the analysis conducted on the Shika dam raw water, the hardness value was obtained to be 50 *mg/l*. Treatment carried out using MOSE revealed that, the hardness was in the range of 10.1 to 11.7 *mg/l* and that conducted with PSE gave 15.6 to 17.1 *mg/l*. The results for the blends (*MO*: PPK) showed gradual increase in hardness of 12.6, 13.42, 14.31, 14.36, 14.89, 15.33, 17.62, 17.94 and 19.08*mg/l* which was achieved by 90:10, 80:20, 70:30, 60:40, 50:50, 40:60, 30:70, 20:80 and 10:90 dosage ratios of *MO*: PPK respectively. From the results presented in figure 5.0, it evidently proved, the best hardness was found in sample B (90:10) of 12.76 *mg/l* (74%) at 90:10 dosage ratio, this means that MOSE had better hardness reducing tendency than PSE, although PSE is still suitable for hardness reduction and all the results obtained are in agreement with the set standards of drinking water of 150 *mg/l*.

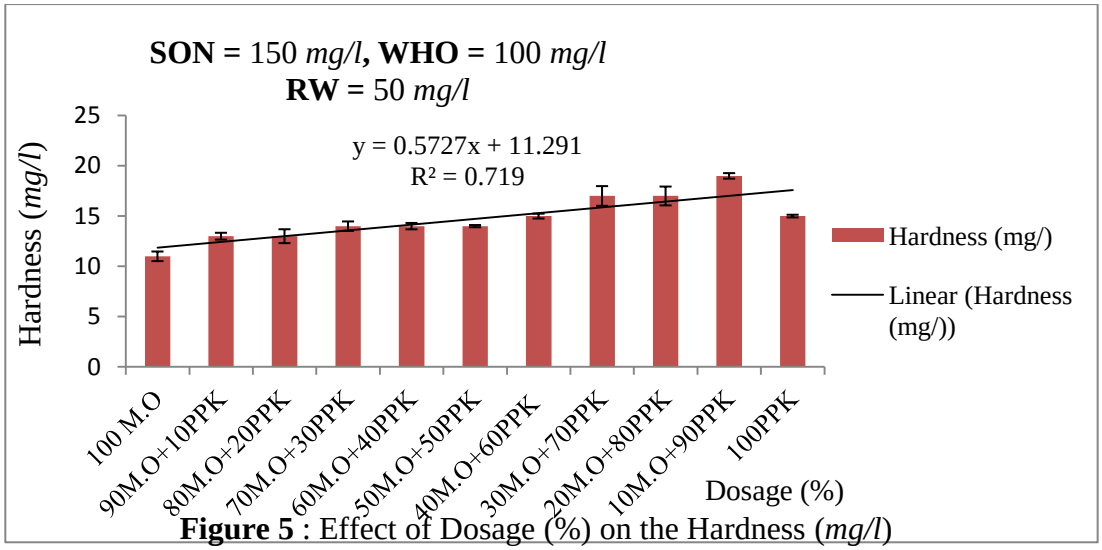

Figure 5 : Effect of Dosage (%) on the Hardness (*mg/l*)

Effect of Dosage on the pH

Analysis carried out on Shika dam raw water sample before treatment showed that the value of pH was 6.9. Consequently, the treatment conducted with MOSE showed the pH to be in the range of 6.5 to 6.6. Whereas, using PSE gave 6.7 to 6.9. Moreover, results from the blends (MOPE) showed that the pH was in the range of 6.4 to 6.8 with the highest value found in sample J (10:90) and the least found in sample B (90:10). In general, the pH results as shown in figure 6.0 of the product (treated water) were within the recommended standards (SON, 2007). The only fluctuation was in sample D (70:30) which gave a value of 6.4 slightly below the range of standard of 6.5-8.5.

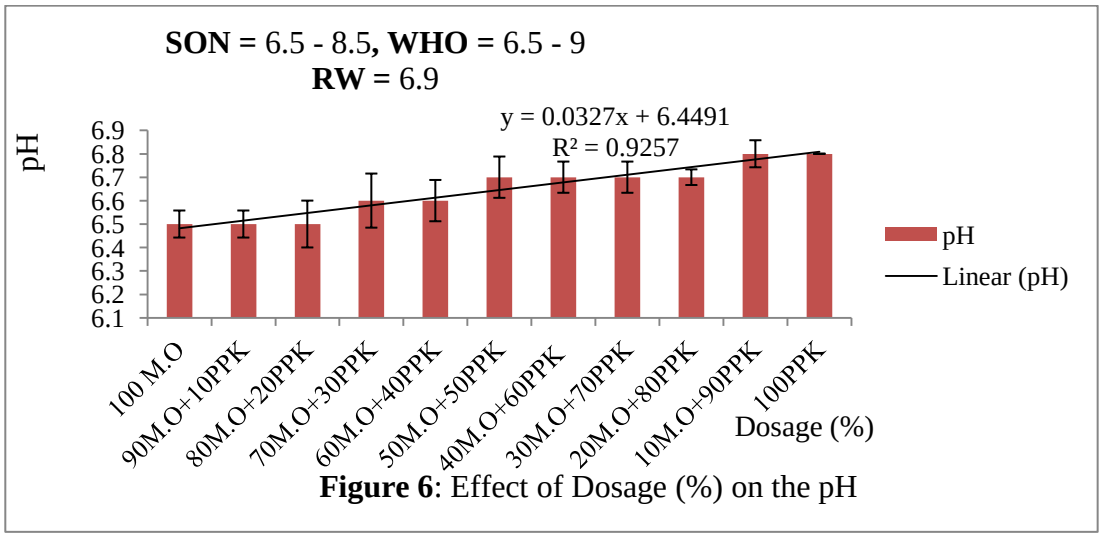

Figure 6: Effect of Dosage (%) on the pH

Effect of Dosage on the Biological Oxygen Demand (BOD)

The BOD value for the Shika dam raw water was obtained to be 3.0 *mg/l*. In the treatment process conducted, it was observed that using MOSE, the reduction tendency was observed to be in the range of 2.1 to 2.3 *mg/l*. However, using PSE gave the result in the range of 2.0 to 2.1 *mg/l*. The result presented in figure 7.0 showed that MOSE is the best in the treatment level. Moreover, the blends (MOPE) gave the reduction level in the range of 1.7 to 2.2 *mg/l* with the best found in samples; B (90:10) and C (80:20) each of 2.2 *mg/l* respectively and the least was found in samples; I (20:80) and J (10:90) of 1.7*mg/l*. Generally, unpolluted waters typically have BOD values of 2 *mg/l* O_2 or less and those receiving waste water may have values up to 10 *mg/l* O_2 or more (Chapman, 1997). Thus, a high BOD is attributed to input of decomposing organic matter through run-off.

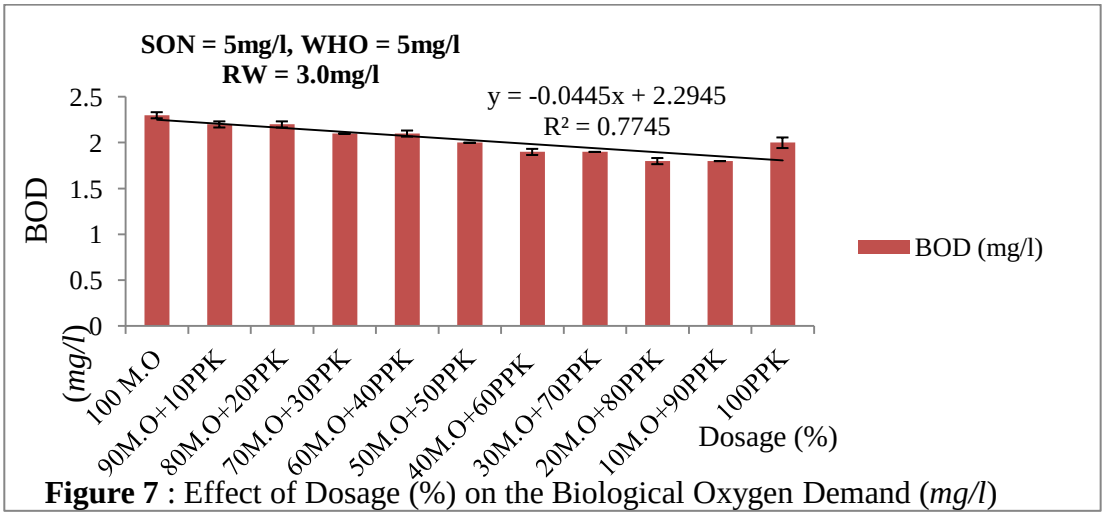

Figure 7 : Effect of Dosage (%) on the Biological Oxygen Demand (*mg/l*)

Effect of Dosage on the Chemical Oxygen Demand (COD)

The COD of Shika dam raw water was obtained to be 190 *mg/l* which indicates the measure of the oxygen equivalent of the organic matter content of water that is susceptible to oxidation by a strong chemical oxidant. The treatment level using MOSE was ascertained to be in the range of 40 to 45 *mg/l* and that using PSE was seen to be in the range of 38 to 42 *mg/l*. However, a gradual decrease in COD values of 40, 38, 37, 36 and 35 *mg/l* by 90:10, 80:20, 70:30, 60:40 and 50:50 dosage ratios of *MO*: PPK respectively. Subsequently, a further increase was observed by 40:60, 30:70, 20:80 and 10:90 dosage ratios of 36, 37, 38 and 40 *mg/l* respectively. The results from this study showed that, COD was generally within the levels expected for unpolluted water of 100 *mg/l*. Additionally, COD of water increases with increasing concentration of organic matter, which is a reliable parameter for guiding the extent of pollution in water (Boyd, 1979 and Amirkolaie, 2008).

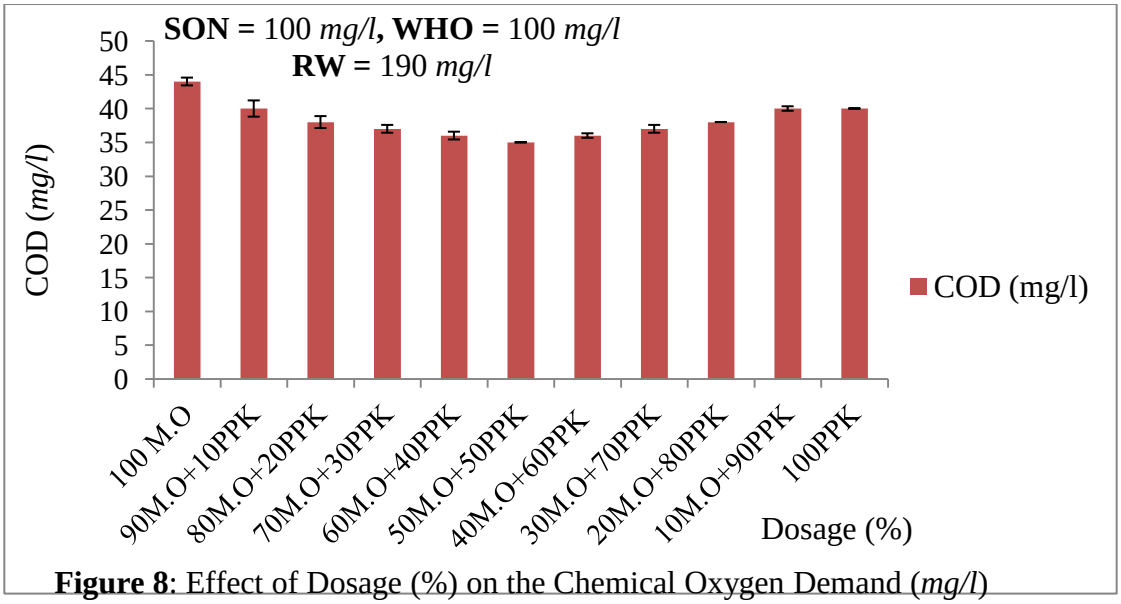

Figure 8: Effect of Dosage (%) on the Chemical Oxygen Demand (*mg/l*)

Effect of Dosage on the Bacterial Load

The reduction observed in the bacterial population of the raw water treated with MOSE and PSE can be attributed by the antibacterial properties of the bioactive ingredient. Initially, the raw water sample was analysed to have 21 *cfu*/100*ml*. Consequently, the treatment using MOSE gave the reduction efficiency at a range of 42.86% (12 *cfu*/100*ml*) to 66.67% (7 *cfu*/100*ml*) but upon using PSE gave a much higher reduction of 90% (2 *cfu*/100*ml*) to 100% (0 *cfu*/100*ml*) which indeed revealed the effectiveness of PSE in terms

of antibacterial properties than MOSE. The highest bacterial load

reduction (%) was found to be 100% at 30:70, 20:80 and 10:90 dosage ratios of *MO*: PPK respectively. Also, the results presented a step-wise decrease in the bacterial load of 7, 5, 4, 3, 3, 2, 1, 0, 0 and 0 achieved by 90:10, 80:20, 70:30, 60:40, 50:50, 40:60, 30:70, 20:80 and 10:90 of *MO*: PPK dosage ratios respectively. Therefore, the results obtained for the blends shows that, only that which has higher pumpkin concentration produced much more reduction in bacterial population and hence clearly depicted its effectiveness and suitability in augmenting *Moringa Oleifera* in water treatment most especially in area of improving its antibacterial properties.

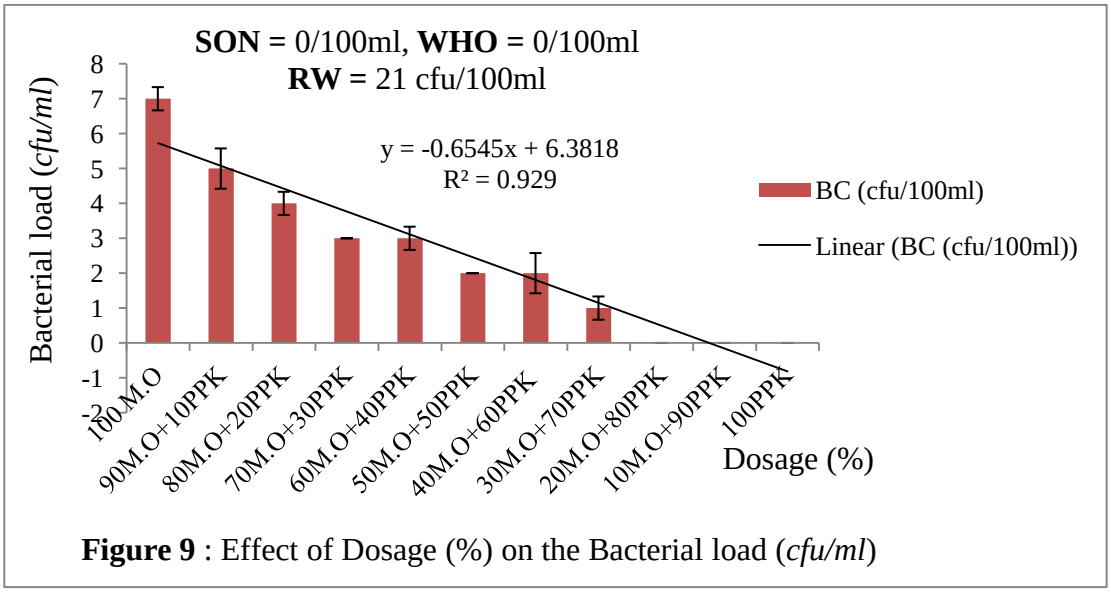

Figure 9 : Effect of Dosage (%) on the Bacterial load (*cfu/ml*)

FTIR result of *Moringa Oleifera* Oil Free Cake Powder

The FTIR spectra of *Moringa Oleifera* Oil free cake powder before dissolution and extraction of the active ingredient is shown in fig. 4.11. The spectra contain peak at 2855.1 cm^{-1} (alkane, C-H stretch), 1651.2 cm^{-1} (amides, C=O stretch), 1054.8 cm^{-1} (alcohols, C-O stretch), 1744.4 cm^{-1} (ketones, C=O stretch), 1054.8 cm^{-1} (alkyl halide, C-F stretch), 793.8 cm^{-1} (alkyl halide, C-Cl stretch), 3283.8 cm^{-1} (amines, N-H symmetric), 2922.2 cm^{-1} (carboxylic acids, O-H stretch). The results as presented in figure 10 showed that some of the peaks are shifted and new peaks are also seen to appear and can be traced to other functional groups. However, the active ingredients which served the purpose of disinfection from the function groups are; alcohols, ketones, alkyl halides and carboxylic respectively.

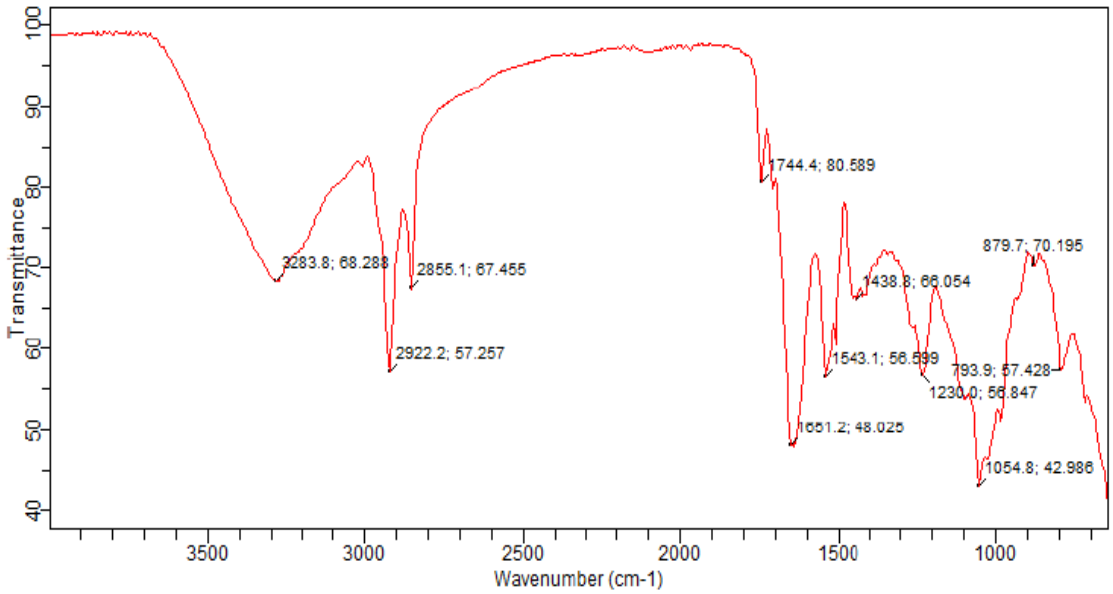

Figure 10: FTIR Spectrum of *Moringa Oleifera* Cake Powder.

FTIR result of Pumpkin Oil Free Cake Powder

The spectrum here contains some distinct peaks at 1707.1 cm^{-1} (characteristic absorption peak of aldehydic group), 1230 cm^{-1} (stretching vibration of aliphatic C-H), 1528.2 cm^{-1} (aromatic C=C in plane deformation), 2922.2 cm^{-1} (alkanes, C-H bending), 3280.1 cm^{-1} (carboxylic group, O-H stretching), 3280.1 cm^{-1} (amides, N-H symmetric) 1043.7 cm^{-1} (alcohol, C-O stretch), 1230.0 cm^{-1} (alkyl halide, C-F stretch). The differences in peak position and intensity in the spectra suggested the attachment of new functional groups. Consequently, the active ingredients which served the purpose of disinfection from the function groups obtained are; aldehydes, alcohols, aromatic compounds and carboxylic respectively.

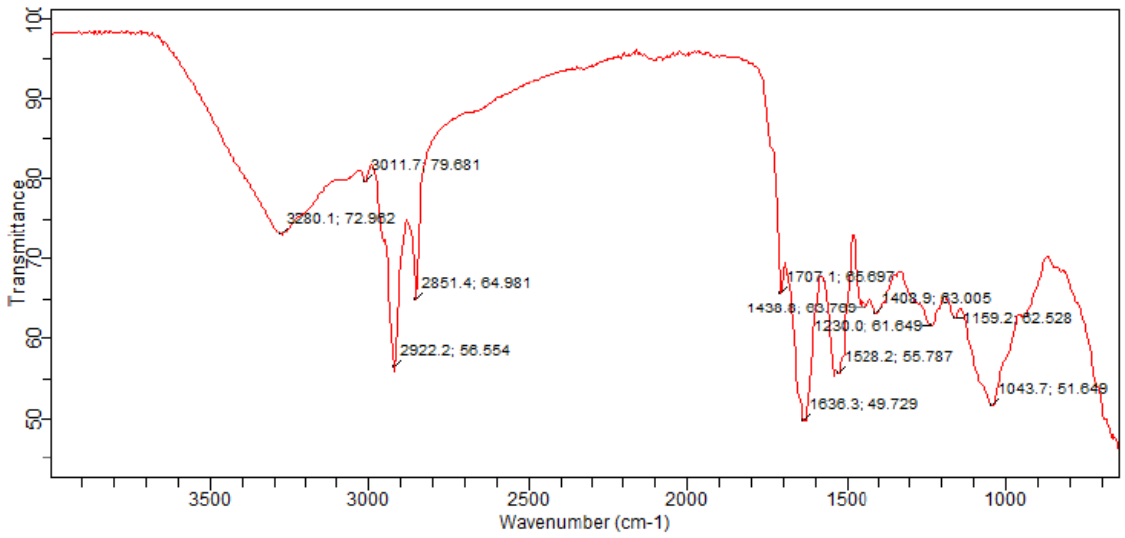

Figure 11: FTIR Spectrum of Pumpkin Cake Powder

CONCLUSIONS

i. A relatively better coagulation condition was reached using both *Moringa Oleifera* and Pumpkin dose of 6*ml:* 500*ml* (of stock solution and raw water quantity).

ii. The FTIR analysis conducted on the pumpkin cake powder revealed the presence of; alcohols, aldehydes, carboxylic acids and aromatic compound, Whereas, FTIR conducted on *Moringa Oleifera* showed the presence of;

alcohols, ketones, carboxylic acids and traces of chlorine as the active ingredients for their antimicrobial tendencies.

iii. The blends with more concentration of *Moringa Oleifera* were more effective in the reduction of; Turbidity (97%), Hardness (74%), and COD (82%). Whereas, blends with more concentration of pumpkin had more effect on; BOD (40%), COD (82%) and Bacterial load (100%).

iv. Generally, blend B (90:10) demonstrated an outstanding performance in terms of; Turbidity, pH and Hardness among other dosage ratios of *MO*: PPK.

v. Also, based on this research, *Moringa Oleifera* and Pumpkin seeds demonstrate good potential for use as viable and indigenous pretreatment alternative in raw water treatment.

REFERENCES

.

Boyd, C.E., 1979. Water quality management in pond fish culture Auburn Inter. Center. For Aquaculture A.E. Station.

Cardoso, K.C., Bergamasco, R., Cossich, E.S. & Konradt-Moraes, L.C. (2008): Otimização dos tempos de mistura e decantação no processo de coagulação/floculação da água bruta por meio da *Moringa oleifera* Lam. *Acta Scientiarum – Technology*, 30: 193-198.

Chapman, 1997. Water Quality Assessments: A Guide to
the Use of Biota, Sediments and Water in
Environmental Monitoring; London, E & FN
SPON.

Gassenschmidt, U. and Jany, K.K. (1995): Isolation and characterization of a flocculation protein from MO lam. BBA Biochem Biophys Acta 1243: 477-481.

Jaju, A. M. (2012). Design and developing of a pilot scale water treatment plant using *Moringa Oleifera* technology. PhD. Thesis Submitted to Ahmadu Bello University, Zaria, Nigeria.

Katayon S., Megat Mohd Noor M.J., Asma M., Thamer A.M., Abdullah A.G., Idris A., Suleyman A.M,, Aminuddin M.B, Khor B.C., (2004): Effects of storage duration and temperature of Moringa Oleifera stock solution on its performance in coagulation, *International Journal of Engineering and Technology*, 1(2): 146-151.

Ndabigengesere, A. & Narasiah, K.S. (1998): Quality of water treated by coagulation using *Moringa oleifera* seeds. *Water Research*, 32: 781–791.

Nwali, B.U, Aja, P.M, Ibiam, U.A Uraku, A.J, Orji, O.U and Offor, C.E (2013): Comparative Proximate and Mineral Composition of *Moringa oleifera* Leaf and Seed. *Global Advanced Research Journal of Agricultural Science* 2(5): 137-141.

Nwokolo, E.; & Sim, J.S. (2007): "Nutritional assessment of defatted oil meals of melon (*Colocynthis citrullus* L.) and fluted pumpkin (*Telfaria occidentalis* Hook) by chick assay". J. Sci. food Agric. 38: 237-246.

Pragnya Y. Alekal (2005): Appropriate Water Treatment for the Nyanza Province of Kenya An *M.Sc* Thesis Submitted to Massachusetts Institute of Technology, Pp.16-25.

Robinson, R.W. & Decker-Walters, D.S. (1997): "What are Cucurbits". In Cucurbits, R.W. Robinson & D.S. Decker-Walters, CAB International, New York. Pp.1-22.

Sojak, M. & Głowacki, S. (2010): Analysis of Giant Pumpkin (*Cucurbita maxima*) Drying Kinetics in Various Technologies of Convective Drying. *Journal of Food Engineering*, 99, 323-329.

MARGINAL FIELD DEVELOPMENT: OPPORTUNITIES AND CHALLENGES

Onojuvwevwo, D.O.
Midwestern Oil and Gas Company Limited
Plot 10, Block 12, Otunba Adedoyin Ogungbe Crescent, Lekki Phase 1, Lagos - Nigeria
dukeomonigho@gmail.com

ABSTRACT

A marginal field is an oil/gas field discovered to contain hydrocarbon deposit but left fallow for a period exceeding ten years. Such fields are awarded to Nigerian independent companies in order to encourage local participation in the upstream sector and increase the country's hydrocarbon reserve base and production capacity. The first marginal field licensing round was in 2003. Some of the awardees have developed their fields and have commenced production while others are at different levels of development. Marginal fields have increased Nigeria's oil/gas reserve base and production capacity thereby increasing revenue for the nation. Many Nigerians have become Managing Directors/Chief Executive Officers as well as other top positions in the upstream sector through the marginal field policy. The policy has thus increased local capacity in the upstream sector. Despite the huge opportunities inherent in marginal field, there are many challenges facing the development of such fields. This work reviewed the opportunities that marginal fields present to Nigerians and Nigeria as a country. The work also studied the challenges facing marginal field development in Nigeria and presented recommendations on how to mitigate such challenges.

INTRODUCTION

In Nigeria, lease administration was originally designed in favour of the International Oil Companies (IOCs). This made access to oil/gas assets very difficult for Indigenous/ Independent Operators.

IOCs left significant Oil & Gas Resources un-appraised/unproduced many years after discovery for several reasons.

The Petroleum (Amendment) Decree No. 23 of 1996 was enacted to award such fields as "marginal" to Indigenous Companies.

The first marginal field licensing round was in 2003 where twenty four fields were awarded to 31 Companies.
These fields are presently at various stages of development with some already producing.

LEGAL FRAMEWORK FOR MARGINAL FIELD DEVELOPMENT

The Marginal Field program is based on the Petroleum (Amendment) Act No 23, 1996.

PETROLEUM (AMENDMENT) ACT NO 23, 1996

A key policy of government was to enhance growth in the exploration and production of petroleum resources. In implementing this policy, government paid particular attention to a number of reported oil and gas discoveries that exist in the country, especially, the Niger Delta, some of which have been left unattended for very many years. In most cases, they have remained unproduced and only in a few cases partially appraised.

The consequence of the above was the enactment of the Petroleum Act as amended and cited as Act No. 23 of 1996 which grants access, specifically by indigenous companies, to operate and produce these un-attended fields. The marginal field policy is based on this act.

OBJECTIVES OF THE MARGINAL FIELD POLICY

i. Promote indigenous participation in the sector thereby fostering technological transfer.
ii. Provide opportunity to gainfully engage the pool of high level technically competent Nigerians in the oil & gas sector.
iii. Grow production capacity by expanding the scope of participation in Nigeria's Petroleum industry, especially, the upstream sector, through diversification of resources and inflow of investments.
iv. Increase oil and gas reserves base through aggressive exploration and development efforts, in particular the deeper hydrocarbon plays.
v. Provide opportunity for portfolio rationalization.

vi. Promote common usage of assets/facilities to ensure optimum utilization of available capacities.

DEFINTIONS OF MARGINAL FIELD

A marginal field is any field that has oil and gas reserve booked and reported annually to the Department of Petroleum Resources (DPR) and has remained un-produced for a period of over 10 years.

Specifically, marginal fields have some or all of the following characteristics:

i. Fields not considered by license holders for development because of assumed volatile economics under prevailing fiscal and market conditions.

ii. Fields with at least one exploration well drilled and reported as oil and or gas discovery for more than 10 years with no follow up appraisal or development effort.

iii. Fields with crude oil characteristics different from current streams (such as crude with very high viscosity and low API gravity), which cannot be profitably produced through conventional methods or current technology.

iv. Fields with high gas and low oil reserves.

v. Hitherto producing fields that have been abandoned by the leaseholders for upwards of three years for economic or operational reasons.

vi. Fields that the present leaseholders may consider for farm-out as part of portfolio rationalization programs.

OUTCOME OF THE 2003 MARGINAL FIELD AWARDS

In 2003, 24 marginal fields were awarded to 31 companies. The fields are presented in table 1 below:

Table 1: 2003 Marginal Field Award Structure (Osahon 2013)

S/N	FIELD	FARMOR	OML	FARMEE	TERRAIN
1	Asuokpu/Umutu	Shell	38	Platform Petroleum Limited	Land
2	Asaramatoru	Shell	11	Prime Energy (51%) / Sufolk Petroleum (49%)	Swamp
3	Atala	Shell	46	Bayelsa Oil (100%)	Swamp
4	Eremor	Shell	46	Excel E&P (100%)	Swamp
5	Ibigwe	Shell	16	Walter Smith (70%) / Morris Petroleum (30%)	Land
6	Ofa	Shell	30	Independent (100%)	Land
7	Oza	Shell	11	Millenium Oil (100%)	Land
8	Qua Ibo	Shell	13	Network Oil & Gas (100%)	Land
9	Stubb Creek	Shell	14	Universal Energy (100%)	Swamp
10	Tom Shot Bank	Shell	14	Associated (51%)/ Dansaki Pet (49%)	Offshore
11	Tsekelewu	Shell	40	Sahara (51%) & AOG (49%)	Swamp
12	Uquo	Shell	13	Frontier Oil (100%)	Swamp
13	Ororo	Chevron	95	Guarantee Oil / Owena Oil	Offshore
14	Akepo	Chevron	90	Sogenal (100%)	Offshore
15	Ogedeh	Chevron	90	Bicta (100%)	Offshore
16	Ajapa	Chevron	90	Britania –U (100%)	Offshore
17	Dawes Island	Chevron	54	Eurafic (100%)	Swamp
18	KE	Chevron	54	Del-Sigma (100%)	Swamp
19	Oriri	Chevron	88	Goland (100%)	Offshore

S/N	FIELD	FARMOR	OML	FARMEE	TERRAIN
20	Ekeh	Chevron	88	Movido	Offshore
21	Umusadege	Elf	56	Midwestern Oil & Gas (70%) / Suntrust (30%)	Land
22	Obodugwa / Obodeti	Elf	56	Pillar Oil (100%)	Land
23	Umusati/Igbuku	Elf	56	Energia (55%) / Oando (45%)	Land
24	Amoji/Matsogo/Igbolo	Elf	56	Chorus (100%)	Land

OTHER MARGINAL FIELD AWARDS

- Awards of Okwok field in 2006 and Ebok field in 2007 to Oriental Energy were made to compensate the company for losing part of its OML 115 to Equatorial Guinea due to boundary adjustment.
- Ogbelle field was awarded to the Niger Delta Petroleum Resources Limited in 1999. The company was the first beneficiary of marginal field in the country.
- In 2010, Otakikpo and Ubima fields were awarded to Green Energy Ltd and Allgrace Energy Ltd respectively as part of a lingering award process that commenced in 2004.

SCORECARD OF MARGINAL FIELD INITIATIVE

Out of the 24 + 5 marginal fields, twelve have started production

The twelve producing fields are:

1. Umusadege (Midwestern Oil & Gas)
2. Umusati (Pillar Oil)
3. Ibigwe (Waltersmith)
4. Egbaoma (Platform Petroleum)
5. Obodugwa / Obodeti (Energia Petroleum / Oando)
6. Ajapa (Britania-u)
7. Ogbelle (Niger Delta Petroleum)
8. Ebok (Oriental Energy)
9. Uquo (Frontier) 1st Marginal Gas Operator
10. Asaramatoru (Prime Exploration)
11. Stubb Creek (Universal Energy)
12. Qua Ibo (Network Oil and Gas)

RESEARCH METHODOLOGY

Data were obtained from the database of Department of Petroleum Resources (DPR) and Nigerian National Petroleum Corporation (NNPC). These data were analyzed with charts generated, using Microsoft Excel.

RESULTS/DISCUSSION

Figure 1 shows how marginal field contribution to total crude oil production in Nigeria increased from 0.09% in 2006 to 3.01% in 2015.

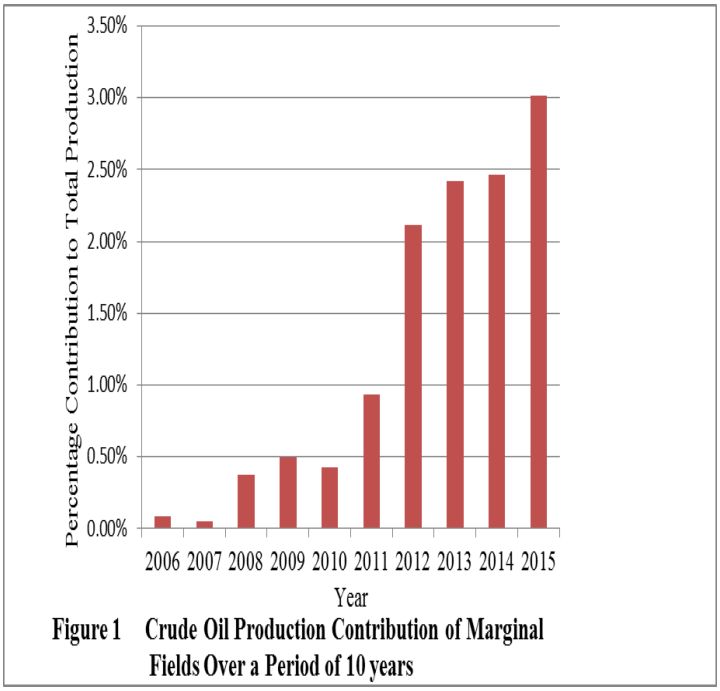

Figure 1 Crude Oil Production Contribution of Marginal Fields Over a Period of 10 years

In terms of volume, marginal field production increased from 2,366bopd in 2006 to 70,274bopd in 2015 (Figure 2).

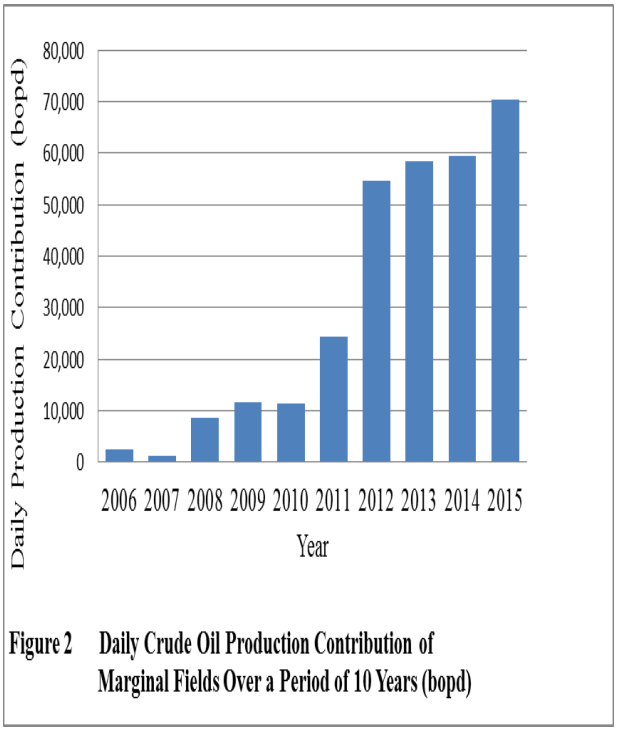

Figure 2 Daily Crude Oil Production Contribution of Marginal Fields Over a Period of 10 Years (bopd)

Gas production data was not available from 2006 to 2010. From 2011 to 2015, gas production increased from 4.2mmscfd to 150mmscfd as shown in figure 3.

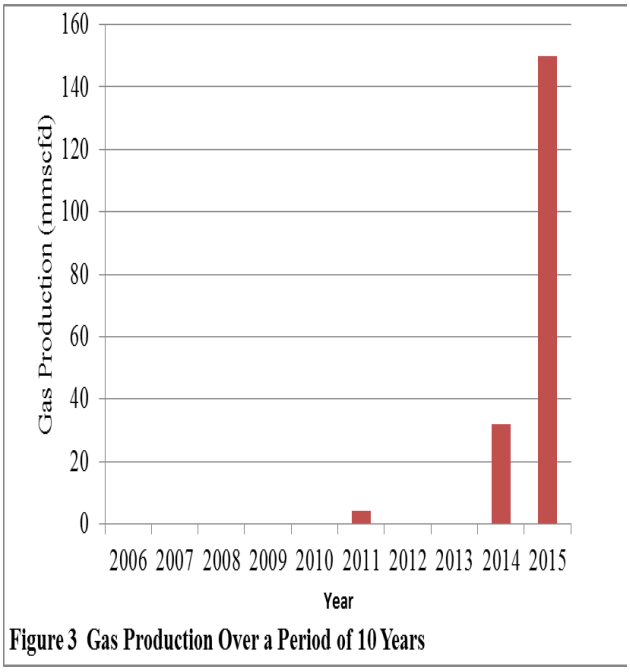

Figure 3 Gas Production Over a Period of 10 Years

The production distribution chart of figure 4 shows that marginal field contributed about 3% to Nigeria's total crude oil production for the year 2015. Joint Venture contracts gave the highest contribution of 48%. The least percentage (about 1%) was contributed by the Service Contract type.

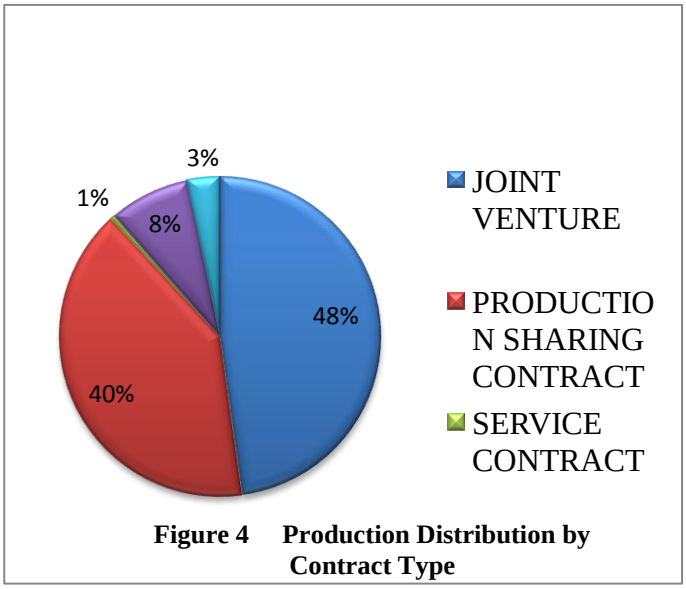

Figure 4 Production Distribution by Contract Type

OTHER BENEFITS OF MARGINAL FIELD

- Integrating value
  - ✓ Producing crude oil
  - ✓ Monetizing gas
  - ✓ Small scale refining
- Unlocking stranded molecules through deployment of new technologies
- Creating opportunity for employment and empowerment
- Better handle of local communities

CHALLENGES FACING MARGINAL FIELD DEVELOPMENT/OPERATIONS

- Low oil prices
- Insecurity
- Deferred production due to attacks by militants
- Shortage of foreign exchange (Forex)
- Fiscal issues that pertain to royalty and Petroleum Profit Tax (PPT)
- Community problems
- Assets are sub-economic and hardly bankable

REMEDIES TO THE CHALLENGES FACING MARGINAL FIELD DEVELOPMENT/OPERATIONS

- Optimization of resources to minimize operating cost and capital cost.
- Collaboration with security agencies and host communities.
- Sharing and collaboration among clusters of contiguous fields.
- Amnesty for militants.
- DPR facilitation and update on guidelines.

CONCLUSION/RECOMMENDATIONS

The marginal field program has provided so much opportunity to Nigerians and Nigeria as a country. Despite the challenges facing marginal field operators, they have continued to provide employment for Nigerians and increase local capacities. The marginal field program contributes considerable volume to the nation's production capacity and reserve base.

As at 2015, marginal field contributes about 3% of Nigeria's total crude oil production. With production ramp up and more marginal fields commencing production, this figure would likely approach or even exceed 4% in 2017.

Challenges inherent in marginal field development/operations should be continuously analyzed and appropriate interventions put in place.

Introducing enablers in subsequent Marginal Fields Bid Round would be very helpful.

More Nigerians should take advantage of the Marginal Field policy and invest in the program.

LIST OF ABBREVIATION

Bopd	Barrel Oil Per Day
mmscfd	Million Standard Cubic Feet per Day
OML	Oil Mining Lease
N/A	Not Available

REFERENCES

Department of Petroleum Resources, (2013), *Guidelines for Farmout and Operation of Marginal Fields*, Lagos.

Department of Petroleum Resources, (2015), *Oil and Gas Annual Report*, Lagos.

Idigbe, K.I. & Bello, K. O., (2013), 'Sustainable Operation of Marginal Fields in Nigeria: Opportunities, Challenges and Best Practices', *Journal of Emerging Trends in Engineering and Applied Sciences (JETEAS)* 4(4): 686-691.

Nigerian National Petroleum Corporation, (2015), *Annual Statistical Bulletin*, 1st ed., Abuja.

Ogelle, O. & Obioma, H., (2016), 'Contractual Arrangements in the Nigeria's Oil Industry', *International Journal of Arts and Humanities (IJAH)*, Vol. 5(3), S/No 18,136-149.

Osahon, G., (2013), 'Marginal Field Development: Best Practices & Lessons Learned', paper presented at the Society of Petroleum Engineers' 37th Nigeria Annual International Conference & Exhibition, Eko Hotel, Lagos, 30th July to 1st August.

Nwokolo, E.; & Sim, J.S. (2007): "Nutritional assessment of defatted oil meals of melon (*Colocynthis citrullus* L.) and fluted pumpkin (*Telfaria occidentalis* Hook) by chick assay". J. Sci. food Agric. 38: 237-246.

Pragnya Y. Alekal (2005): Appropriate Water Treatment for the Nyanza Province of Kenya An *M.Sc* Thesis Submitted to Massachusetts Institute of Technology, Pp.16-25.

Robinson, R.W. & Decker-Walters, D.S. (1997): "What are Cucurbits". In Cucurbits, R.W. Robinson & D.S. Decker-Walters, CAB International, New York. Pp.1-22.

Sojak, M. & Głowacki, S. (2010): Analysis of Giant Pumpkin (*Cucurbita maxima*) Drying Kinetics in Various Technologies of Convective Drying. *Journal of Food Engineering*, 99, 323-329.

ELECTROCOAGULATION TREATMENT OF ABATTOIRWASTEWATER USING ALUMINIUM ELECTRODE PAIRS

Nwabanne J.T. and *Obi C.C.

Department of Chemical Engineering, Nnamdi Azikiwe University, Awka, Nigeria.

Corresponding Author: E-mail: obichristopher27@gmail.com

ABSTRACT

This work investigated the effectiveness of Electrocoagulation (EC) technique in Abattoir Wastewater (AWW) treatment using aluminum electrode pairs.The effluent was characterized before and after treatment and the performance of the treatment process was assessed by the percentage removal of turbidity of the effluent. The experimental data were used to carry out the reaction kinetics studies. The modeling and optimization of the process weredone using the Central Composite Design (CCD) of the Response Surface Methodology (RSM). The results of the experiments showed that the removal efficiency of turbidity fromabattoir wastewater increases with a decrease in pH and an increase in current intensity, electrolysis time, settling time and temperature. The reaction kinetics study showed that there is a good a correlation between the experimental data and a pseudo-second-order kinetic model with R^2 values greater 0.9700. The result of the modeling process showed that a quadratic model fitted the experimental data appropriately with a correlation coefficient (R^2) of 0.9975. The optimum conditions were initial pH of 2; thecurrent intensity of 1.9A; electrolysis time of 20 minutes; settling time of 50 minutes and operating temperature of 40^oC at an optimal turbidity removal of 96.78% and 0.28kWh/L energy consumption. The results showed that EC technique using aluminum electrode pairs is suitable for turbidity removal from abattoir wastewater.

Key Words: *Electrocoagulation (EC), wastewater, abattoir, aluminum, electrode,and turbidity.*

1.0 INTRODUCTION

Wastewaters from various domestic and industrial activities are among the major causes of environmental pollution.The variation in the nature and magnitude of the pollutants in these wastewaters is majorly dependent on the source of the wastewater.The abattoir industryis among the human activities in which large volume of wastewater is generated.

Abattoir wastewatercontains high amounts of organic matter including proteins, blood, and fat. Abattoir wastewater has been classified by Environmental Protection Agency (EPA) as one of the most harmful to the environment (Seif and Moursy, 2001).This wastewater is majorly generated in the slaughtering process and washing of equipment used for the operation.

Discharging abattoir wastewater into water bodies untreated will have anadverse impact due to the enormous amounts of organic substances contained in the effluent.There is, therefore, need for an economically viable treatment method that will enable the reduction of the pollutants in this effluent to a concentration where their impact will not have an adverse effect on the environment when discharged. Among the techniques employed in wastewater treatment, EC has the advantage of removing colloidal particles compared with traditional flocculation–coagulation. In addition, in the EC technique less sludge is produced from the treatment process and less time is taking to accomplish the operation(Impa et al, 2015 andNaje and Abbas, 2013).Many researchers have identified initial pH, current density, operating time, electrode material, and supporting electrolyte concentration to be very important process parameters that affects the effectiveness of EC in wastewater treatment (Mahajan et al, 2013;El-Shazly Daous, 2013 and Badu et al, 2007).

The EC process has been successfully used in removal of pollutants from abattoir wastewater.The performance of the EC process in abattoir wastewater treatment has been investigated using different electrode combinations; mild steel and aluminium electrodes (Asselin et al., 2008), tubular electro-coagulator (Eryuruk et al., 2011), plug flow EC reactor (Eryuruk et al., 2014) and a combination of iron (Fe) and aluminium (Al) electrode pairs (Budiyono et al., 2010 and Tezcan Un et.al 2007). The use of iron electrode pairs in EC process has also been reported (Adebayo et al, 2015 and Marconato et al. 1998).

The present study was aimed at determining the effectiveness of aluminum electrode pairs in the EC process for the treatment of abattoir wastewater. The work will evaluate the effects of the process parameters on the process, analyze the reaction kinetics and carry out the modeling and optimization of the processusing the Central Composite Design (CCD) of the Response Surface Methodology (RSM).

2.0 MATERIALS AND METHODS

2.1 Collection and Characterization of the wastewaters

The turbid effluent was collected from a local abattoir located in Anambra State, Nigeria.The sample was stored in a thoroughlycleaned polyethylene bottle and tightly closed. The bottle was rinsed with effluent sample before the finalsample collection. The analysis of the wastewater sample before and after treatment was carried out according to APHA, (1998).

2.2 Electrocoagulation Experiment

A screened raw abattoir wastewater was transferred into the electro-coagulator. The electrolytic cell used had a working volume 500ml equipped with magnetic stirrer operating at 150 rpm. A direct current power supply of (220V, 0 - 3A) capacity was used. Aluminum rods of size (100×9mm, i.e. length×thickness) were used as the electrodes. The electrode pair was dipped in the wastewater to a depth of 8.0 cm and electrode spacing of 1.0 cm apart. The effective area of the electrode pair was 48.0cm^2. The conductivity of the solution was increased by the addition of 0.001M Na_2SO_4. The effects of various process variables such as theinitial wastewater pH,current intensity, electrolysis time, settling time and operating temperature were investigated. The current intensity was regulated at 0.5A, 1.0A, 1.5A, 2.0A, and 2.5A with a constant voltage of 220V, while the EC time was varied between 5 and 30 minutes.The wastewater pH was maintained at the desired value by adding either of 1M HCl or 1M NaOH prior the start of each run. The initial solution pHstudied was ranged from 2-10. All runs were performed at 150rpm followed by varying settling time (5 – 60 mins).

Before the start of each run, thesample was tested for turbidity, representing the turbidity before treatment. At the end of each experiment, samples were collected from 2cm depth at varying settling times and were analyzed for turbidity, representing the turbidity after treatment. The efficiency of pollutant removal, R was evaluated using equation (1).

$$\%\text{Removal} = \frac{T_0 - T}{T_0} \times 100 \qquad (1)$$

Where T_o is the turbidity of raw effluent and T,theturbidity of effluent after treatment.

The electric power consumption was calculated per m^3 of the effluent solution using equation (2).

$$P = \frac{EIt}{V} \qquad (2)$$

WhereP is the specific power consumption (W.h/m^3). E is the cell voltage in volt (V). I is the current in ampere (A), t is the EC time in hour (h) and V is the solution volume in cubic meter (m^3).

The maximum dissolved mass of aluminum (theoretically) that occur during EC process for a specific electrical current flow in an electrolytic cell was calculated using equation (3) according to Vlachou et al., (2013).

$$m = \frac{ItM_r}{zF} \qquad (3)$$

Where, m is the amount of the dissolved anode material (g); I is the current (A); t is the electrolysis time (s); M_r is the specific molecular weight of the anode electrode (Al) (26.98 gmol^{-1}); z the number of electrons involved in the reaction, and F, Faraday's constant (96485.34 A s mol^{-1}). The value of z for aluminum is 3 being the number of electrons involved in the reaction(Vlachou et al., 2013).

2.3 Design of Experiment for the Modeling and Optimization Study

The modeling and optimization process was done using the Central Composite Design (CCD).The dependent variable was percentage turbidity removal while the independent variables considered were initial solution pH, current intensity, electrolysis time, settling time, and operating temperature. In order to ascertain the combined effects of the independent variables on the dependent variable, as well as develop a mathematical relationship (model) relating the dependent variables with the independent variables, 50 experiments were performed as prescribed by the central composite rotatable design. The range of the five independent variables was presented in Table 1

Table 1 Factors levels of independent variables

Independent Factors	-α	Low Level (-)	Medium level (0)	High level (+)	+α
A: pH	1	2	3	4	5
B: Current density (A)	0.5	1	1.5	2	2.5
C: Electrolysis time (min)	15	20	25	30	35
D: Settling time (min)	20	40	40	50	60
E: Temp (^{O}C)	35	40	45	50	55

3.0 RESULTS AND DISCUSSION

3.1 Characterization of AWW before and afterEC treatment

The raw and treated wastewater samples were characterized and some of the physicochemical parameters determined are presented inTable 2.The reduction of the BOD_5 and COD levels of the wastewater after treatment confirmed the effectiveness of EC process in achieving organic load reduction. While the decrease in turbidity after treatment is an indication that EC has the capability to drastically deplete the Total Dissolved and Suspended Particles (TDSP) in AWW. The values of pH, COD, BOD_5, TS, and TSS of the raw sample were found to be in close range with the findings of other authors (Verhoef, 2002; Pozo and Diez, 2005; Kwarciak-Kozłowska et al., 2011; Adebayo et al., 2015 and Ciro et al., 2016).

Table 2. Characteristics of AWW before and afterEC treatment

Wastewater Parameter	Before Treatment	After EC Treatment
pH	6.80	6.44
COD (mg/l)	1814	110.7
BOD_5 (mg/l)	920	55.8
TS (mg/l)	2660	266
Turbidity (NTU)	330	16
Total hardness (mg/l)	60.31	47.88
Sulphate (mg/l)	13.85	7.74
TSS (mg/l)	1080	42.4
Iron (mg/l)	2.09	1.64
Potassium (mg/l)	0.10	0.05
Magnesium (mg/l)	57	45.4
DO (mg/l)	2.38	6.18

Note: Al-Al EC = Aluminium – Aluminium Electrocoagulation.

3.2.1Effect of pH at Varying Current Intensity

The initial pH of the solution is one of the important factors upon which the performance of EC process depends.The effect of pH onEC of abattoir wastewater was studied and presented in Figure 1. It can be seen (Figure 1) that the removal efficiency increased by decreasing the pH from 10 to 2. This is an indication that the turbidity removal efficiency is favored by performing the experiment when the wastewater solution is in acidic medium. This is in agreement with the findings of Bayar et al., (2011) and Bayar et al., (2014) in similar studies.Acidic is considered to medium favor rapid adsorption of soluble organic compounds and trapping of colloidal particles.

On the other hand, final effluent pH fell into limits set by discharge standards of water pollution control regulations (pH 6–9) according to FEPA, (1991). This is one of the advantages of EC process. When the initial solution pH was in acidic medium the final pH after treatment increased, moving towards neutral. While for alkaline influent, the pH after treatment decreased.Vik et al.(1984) and Dermentzis, et al. (2011) reported that the observed increase of pH at low initial pH (<7) is ascribed to the hydrogen evolution and the generation of OH ions at the cathodes.

On the other hand, thecurrent intensity is also one of the important parameters that must be considered in the quest to determine the optimum condition for the performance of EC process. It can be seen in Figure 2 that the removal efficiency increased with increasing current intensity. This is because at increased current intensity there will be anincrease in the amount of aluminum ions dissolved in the wastewater and in the formation rate of the metal hydroxides ($Al(OH)_3$).However, it should be noted thathigh current intensity results in high energy consumption, hence it was necessary to determine the optimum condition for the optimal performance of the EC process.

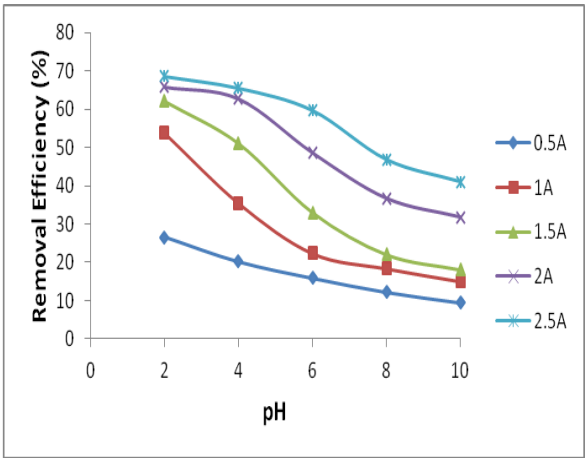

Fig1. Effect of pH at varying current intensities

3.2.2Effect of Electrolysis Time at Varying Current Intensity

The effect of electrolysis time on turbidity removal efficiency was studied at varying current intensity and the result is presented in Figure 2. It can be seen (Figure 2) that removal efficiency increased with increase in EC reaction time. This is because at an increased reaction time more metal ions would be dissolved into the solution leading to the formation of more metal hydroxides which is the main coagulating agent in EC process. Beyond the current intensity of 1.0A, the rate of increase in removal efficiency was observed to be less significant. This is an indication that at increased current intensity the influence of reaction time in the process is reduced. However, a current intensity of 2.5A and a reaction time of 30 minutes still gave the best result.

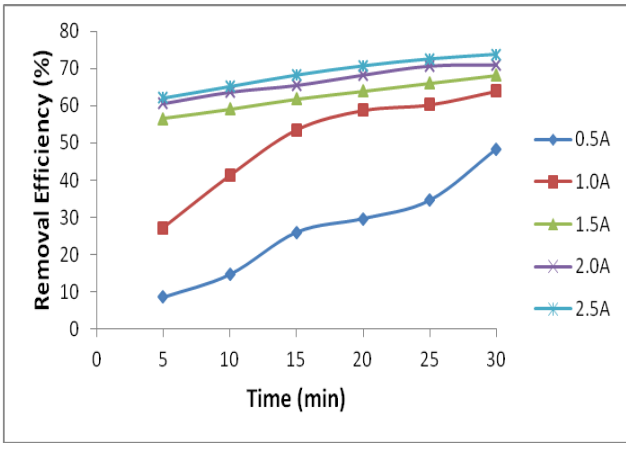

Fig.2 Effect of electrolysis time at varying current intensities

3.2.3Effect of Settling Time at Varying Current Intensity

Settling time was examined at varying current intensity to determine the optimum value. The results are presented in figure 3. The trend showed that removal efficiency increased with settling time. This is because,at an increased settling period, the flocs in the wastewater will have more time to move down to the bottom of the settling container. This results in a more turbidity-free treated effluent. The highest degree of coagulation was witnessed within the first 30 minutes in accordance with the theory of rapid coagulation (Smoluchowski, 1917).

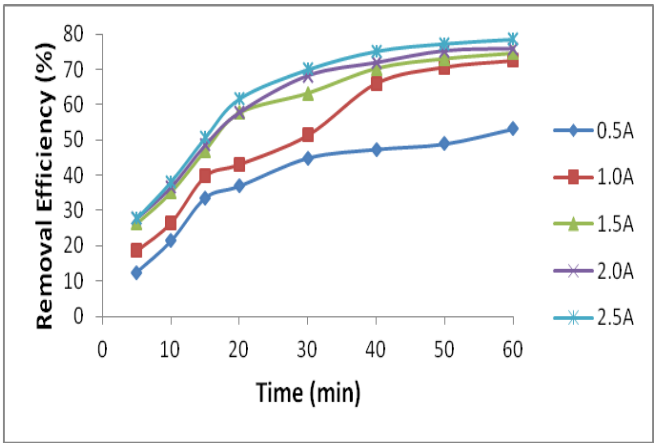

Fig 3 Effect of settling time at varying current intensity

3.2.4Effect of Solution Temperature at Varying Settling Time

Figure 4 presents the effect of solution temperature on the performance of the treatment process. It shows that the efficiency of turbidity removal from abattoir wastewater in the EC process increased by increasing solution temperature up to 50^{o}C. The increase in removal efficiency with temperature is attributed to a gain in kinetic energy by the solution. At an increased kinetic energy of the solution, the viscosity of the solution is reduced, and at a less-viscous condition of the solution, the coagulating agent can penetrate the bulk of the solution at a faster rate thereby enhancing the trapping of the colloidal particles. A further increase in the solution temperature beyond 50^{o}C had an adverse effecton the removal efficiency. This is an indication that temperature equilibrium was attained at about 50^{o}C beyond which there was a counter effect.

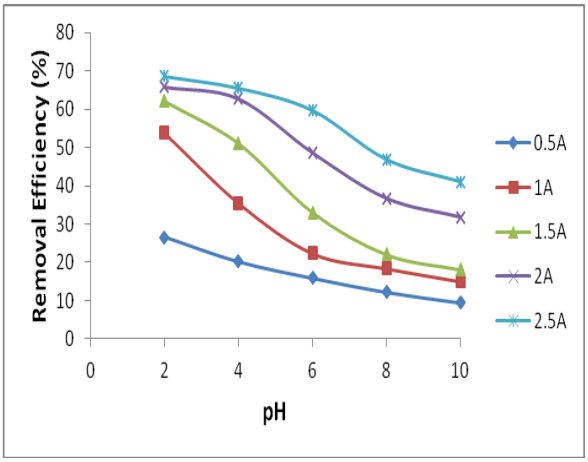

Fig1. Effect of pH at varying current intensities

3.2.2Effect of Electrolysis Time at Varying Current Intensity

The effect of electrolysis time on turbidity removal efficiency was studied at varying current intensity and the result is presented in Figure 2. It can be seen (Figure 2) that removal efficiency increased with increase in EC reaction time. This is because at an increased reaction time more metal ions would be dissolved into the solution leading to the formation of more metal hydroxides which is the main coagulating agent in EC process. Beyond the current intensity of 1.0A, the rate of increase in removal efficiency was observed to be less significant. This is an indication that at increased current intensity the influence of reaction time in the process is reduced. However, a current intensity of 2.5A and a reaction time of 30 minutes still gave the best result.

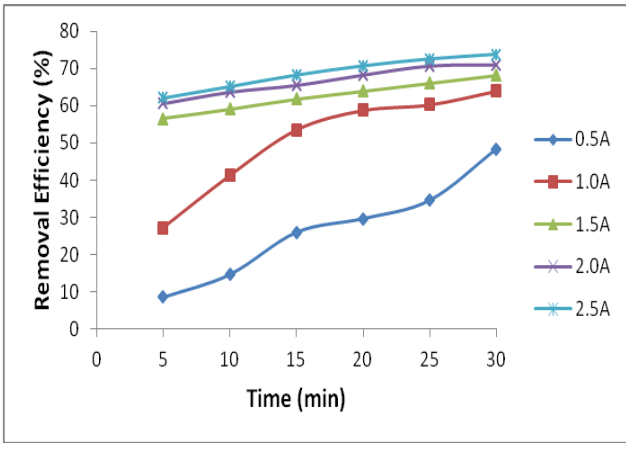

Fig.2 Effect of electrolysis time at varying current intensities

3.2.3Effect of Settling Time at Varying Current Intensity

Settling time was examined at varying current intensity to determine the optimum value. The results are presented in figure 3. The trend showed that removal efficiency increased with settling time. This is because,at an increased settling period, the flocs in the wastewater will have more time to move down to the bottom of the settling container. This results in a more turbidity-free treated effluent. The highest degree of coagulation was witnessed within the first 30 minutes in accordance with the theory of rapid coagulation (Smoluchowski, 1917

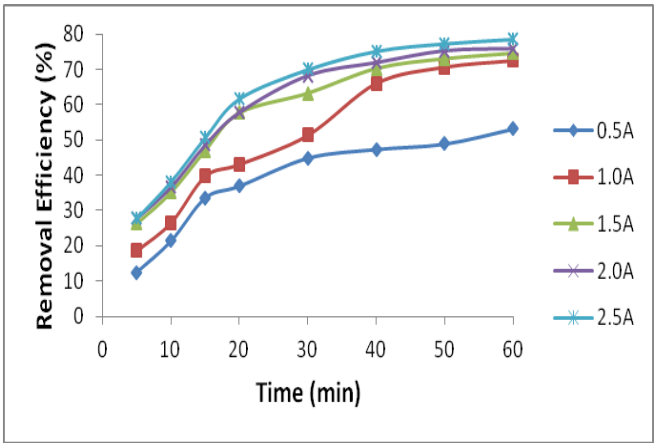

Fig 3 Effect of settling time at varying current intensity

Settling Time

Figure 4 presents the effect of solution temperature on the performance of the treatment process. It shows that the efficiency of turbidity removal from abattoir wastewater in the EC process increased by increasing solution temperature up to 50^{o}C. The increase in removal efficiency with temperature is attributed to a gain in kinetic energy by the solution. At an increased kinetic energy of the solution, the viscosity of the solution is reduced, and at a less-viscous condition of the solution, the coagulating agent can penetrate the bulk of the solution at a faster rate thereby enhancing the trapping of the colloidal particles. A further increase in the solution temperature beyond 50^{o}C had an adverse effecton the removal efficiency. This is an indication that temperature equilibrium was attained at about 50^{o}C beyond which there was a counter effect.

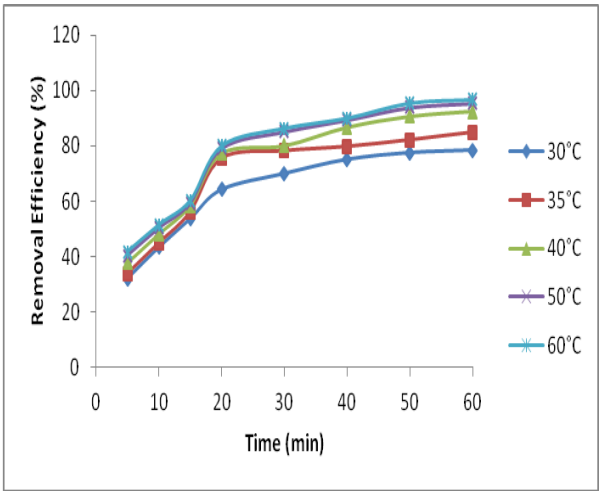

Fig. 4 Effect of operating temperature

3.3Electrical Power Consumption for the EC Process

The electric power consumption of the EC process was calculated per m^3 of the effluent solution using equation (2). The result is presented in Figure 5. It is clear that increasing the current intensity and EC time will lead to increase in power consumption as shown (Figure 5). This is because thecurrent intensity and EC time are two most important electric power parameters as they determine the dissolution rate of the metal electrodes in the solution and the amount of electrodes that will dissolve in the solution respectively. The electrical power consumption within the range of the experimental values can be determined from Figure 5 whenever a known current is applied for a specified time.

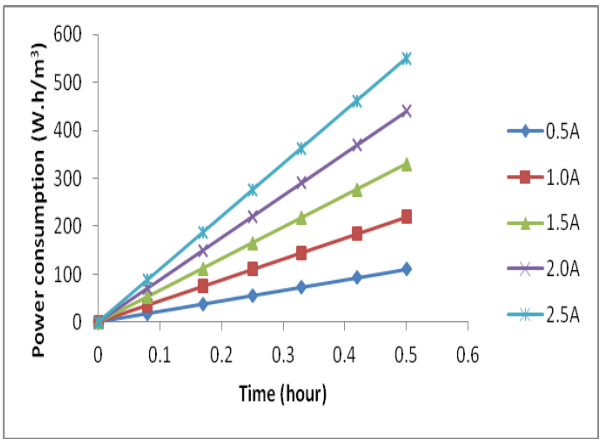

Fig 5. Power consumption (W.h/m^3) Vs Time

3.4Rate of Dissolution of Electrodes during the EC Process

The theoretically maximum dissolved mass of aluminum that occurs during EC process from the sacrificial anode for a specific electrical current flow in an electrolytic cell is calculated according to equation (3). The dissolution rate of the electrodes is presented in Figure 6. The result shows that an increase in both time and current intensity resulted in an increased rate of electrode dissolution at the anode. This is theoretically in agreement with equation 3.

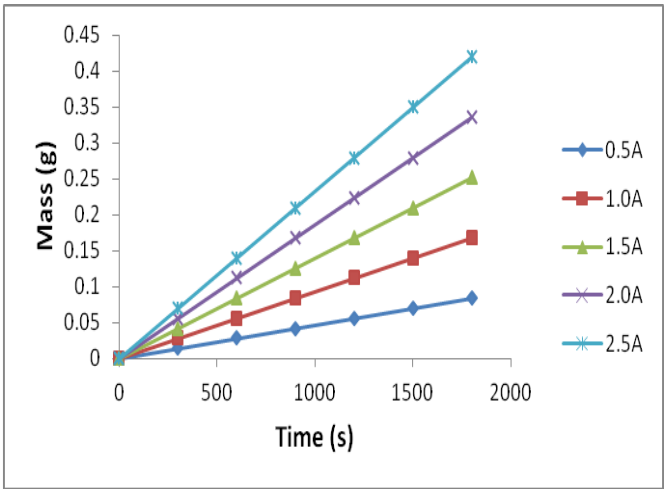

Fig 6. The dissolution rate of Al-Al electrode at varying current intensity during the EC reaction

3.5Reaction Kinetic Results and Parameters

The rate of the depletion of Total Dissolved and Suspended Particles (TDSP)was analyzed using linear – pseudo-second order equation.The EC functional parameters for a linear pseudo – second order reaction was obtained following the procedure described by Menkiti et al., (2008); Babayemi et al. (2013); and Ani et al. (2011) and presented in Table 3.Figure 7 presents the plot of 1/C against time from which the kinetic parameters were obtained. The highest value of K was obtained at the highest current intensity value of 2.5A, representing the condition with the highest reaction rate. Linear regression coefficient (R^2) was employed to ascertain the fitness of the experimental data to the kinetic model. The result as presented (Table 3) show that the values of R^2 obtained are greater than 0.9700. This result suggests that the EC treatment of AWW using aluminum electrode pair followed the second order kinetic model

Table 3. Kinetics parameters for second order reaction kinetics of Al-Al EC

Parameter	0.5A	1.0A	1.5A	2.0A	2.5A
K_2(l/mg.min)	1.00E-05	1.30E-05	2.20E-05	2.80E-05	3.10E-05
C_o (mg/l)	2518.892	2415.459	2493.766	2801.12	2906.977
α	2	2	2	2	2
R^2	0.9744	0.977	0.9943	0.9894	0.9876
Rate Equation (mg/l.min)	1.00E-05C^2	1.30E-05C^2	2.20E-05C^2	2.80E-05C^2	3.10E-05C^2

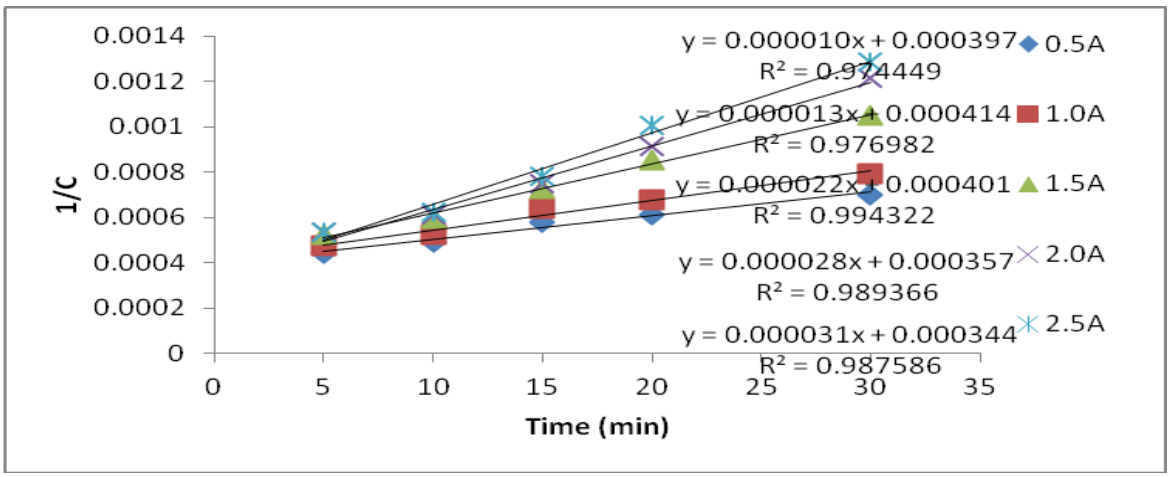

Fig 7 Kinetic plot of 1/C versus time for the pseudo second order kinetic model

3.6 Modeling and Optimization Study

3.6.1 Experimental Design Matrix

The Central Composite Design (CCD) of the response surface methodology (RSM) was used to perform the experimental design which was used for the modeling and optimization study. The independent variables for the Al-Al EC process were pH, current intensity, electrolysis time, settling time and temperature. The percentage removal of turbidity was the response variable. The design matrix together with the experimental and predicted response values are presented in Table 4, this represents the combined effects of independent variables on the response variable.

Table 4 Experimental and Predicted response of the five process variables in terms of real values

Std	pH (A)	Current Intensity(B)	Electrolysis Time(C)	Settling Time(D)	Temp (E)	Actual Result	Predicted Result
1	2	1	20	40	40	70.63	70.52
2	4	1	20	40	40	45.87	46.67
3	2	2	20	40	40	82.57	82.48
4	4	2	20	40	40	65.43	65.07
5	2	1	30	40	40	72.85	73.35
6	4	1	30	40	40	56.00	55.38
7	2	2	30	40	40	75.06	76.12
8	4	2	30	40	40	65.20	64.58
9	2	1	20	50	40	82.85	82.71

Std	pH (A)	Current Intensity(B)	Electrolysis Time(C)	Settling Time(D)	Temp (E)	Actual Result	Predicted Result
10	4	1	20	50	40	67.95	68.34
11	2	2	20	50	40	96.35	96.86
12	4	2	20	50	40	88.57	88.94
13	2	1	30	50	40	92.68	91.90
14	4	1	30	50	40	83.13	83.41
15	2	2	30	50	40	97.01	96.86
16	4	2	30	50	40	93.98	94.81
17	2	1	20	40	50	80.94	81.10
18	4	1	20	40	50	60.28	59.97
19	2	2	20	40	50	83.89	83.30
20	4	2	20	40	50	67.55	68.62
21	2	1	30	40	50	75.05	74.76
22	4	1	30	40	50	60.13	59.53
23	2	2	30	40	50	68.41	67.78
24	4	2	30	40	50	58.06	58.98
25	2	1	20	50	50	95.25	94.90
26	4	1	20	50	50	83.37	83.27
27	2	2	20	50	50	97.89	99.31
28	4	2	20	50	50	94.89	94.12
29	2	1	30	50	50	94.15	94.93
30	4	1	30	50	50	88.98	89.18
31	2	2	30	50	50	90.67	90.14
32	4	2	30	50	50	91.01	90.84
33	1	1.5	25	45	45	93.25	93.12
34	5	1.5	25	45	45	70.35	69.96
35	3	0.5	25	45	45	70.50	70.85
36	3	2.5	25	45	45	85.34	84.46
37	3	1.5	15	45	45	81.84	81.15
38	3	1.5	35	45	45	80.53	80.70
39	3	1.5	25	35	45	51.11	51.22
40	3	1.5	25	55	45	95.89	95.26
41	3	1.5	25	45	35	82.61	81.93
42	3	1.5	25	45	55	88.37	88.52
43	3	1.5	25	45	45	80.80	82.50
44	3	1.5	25	45	45	83.45	82.50
45	3	1.5	25	45	45	83.57	82.50
46	3	1.5	25	45	45	82.25	82.50
47	3	1.5	25	45	45	81.98	82.50
48	3	1.5	25	45	45	81.98	82.50
49	3	1.5	25	45	45	83.10	82.50
50	3	1.5	25	45	45	82.35	82.50

3.6.2Analysis of Variance (ANOVA) for the fitted model

Multiple regression analysis was employed in the correlation of the dependent variable with the independent variables. ANOVA was carried out to determine the significance of the fitness of the selected model as well as the significance of individual terms and their interaction on the chosen response as presented in Table 5.The summary of p-values (Table 5) indicates that a quadratic model fitted the ANOVA analysis and hence it was suggested.

The quadratic regression model obtained for the Al-Al EC process prior the elimination of the nonsignificant terms are represented by Equation 4. The alphabets, A, B, C, D,and E stand for pH, current intensity, electrolysis time, settling time and temperature respectively.

Removal (%) = +82.50 – 5.79A + 3.40B - 0.11C + 11.01D + 1.65E + 1.61AB + 1.47AC + 2.37AD + 0.68AE - 2.30BC + 0.55BD -2.44BE +1.59CD – 2.29CE +0.41DE – $0.24A^2$ - $1.21B^2$ - $0.39C^2$ - $2.32D^2$ + $0.68E^2$. (4)

The p-value (Probability of error value) is used to check the significance of each regression coefficient and the interactions between the test variables (Shrivastava et al., 2008). A significance level of 95% was used hence; all terms whose p-value is less than 0.05 are considered significant. For the EC of abattoir wastewater using aluminium electrode electrode pairs, the p-values show that among the test variables used in the study that A, B, D, E, AB, AC, AD, AE, BC, BD, BE, CD, CE, DE, B^2, C^2, D^2, $E^2$are significant model terms. Therefore, eliminating the insignificant terms, the final model Equation is obtained as Equation 5.

Removal (%) = +82.50 – 5.79A + 3.40B + 11.01D + 1.65E + 1.61AB + 1.47AC + 2.37AD + 0.68AE - 2.30BC + 0.55BD -2.44BE +1.59CD – 2.29CE +0.41DE - $1.21B^2$ - $0.39C^2$ - $2.32D^2$+$0.68E^2$. (5)

The independent variables with positive sign implies that an increase in the variable will lead to increase in the response variable; while the independent variables with negative sign implies that an increase in the variable will result in a decrease in the response variable.

Table 6. ANOVA for Response Surface model

Source	Sum of Squares	df	Mean Square	F Value	p-value Prob> F	
Model	7972.26	20	398.61	569.66	< 0.0001	significant
A-pH	1341.54	1	1341.54	1917.19	< 0.0001	
B-Current Density	463.15	1	463.15	661.88	< 0.0001	
C-Operating Time	0.51	1	0.51	0.73	0.3989	
D-Settling time	4848.14	1	4848.14	6928.46	< 0.0001	
E-Temperature	108.60	1	108.60	155.20	< 0.0001	
AB	82.98	1	82.98	118.59	< 0.0001	
AC	69.24	1	69.24	98.95	< 0.0001	
AD	180.07	1	180.07	257.34	< 0.0001	
AE	14.97	1	14.97	21.40	< 0.0001	
BC	169.14	1	169.14	241.72	< 0.0001	
BD	9.67	1	9.67	13.82	0.0009	
BE	190.08	1	190.08	271.64	< 0.0001	
CD	80.93	1	80.93	115.66	< 0.0001	
CE	167.86	1	167.86	239.88	< 0.0001	
DE	5.27	1	5.27	7.54	0.0103	

Source	Sum of Squares	df	Mean Square	F Value	p-value Prob> F
A^2	1.85	1	1.85	2.64	0.1151
B^2	46.87	1	46.87	66.98	< 0.0001
C^2	4.97	1	4.97	7.10	0.0125
D^2	171.52	1	171.52	245.12	< 0.0001
E^2	14.90	1	14.90	21.29	< 0.0001
Residual	20.29	29	0.70		
Lack of Fit	14.40	22	0.65	0.78	0.6971
Pure Error	5.89	7	0.84		
Cor Total	7992.55	49			

Std. Dev.	0.84	R-Squared	0.995
Mean	79.72	Adj R-Squared	0.997
C.V. %	1.05	Pred R-Squared	0.995
PRESS	59.74	Adeq Precision	97.14

3.6.3Test of Adequacy of the Model

The fitness of the selected model was validated using the coefficient of regression R^2. The model summary statistics is presented in Table 6. From the table (Table 6) it can be deduced that the quadratic model has the highest R^2 value justifying its selection as the model that best describes the response. The R^2 value for the quadratic model is 0.9975 showing that 99.75% of the variability in the response can be explained by the model.

Table 6 Model Summary Statistics

Source	Std. Dev.	R-Squared	Adjusted R-Squared	Predicted R-Squared	PRESS	
Linear	5.29	0.8460	0.8285	0.7936	1649.52	
2FI	2.77	0.9674	0.9530	0.9520	383.81	
Quadratic	0.84	0.9975	0.9957	0.9925	59.74	Suggested
Cubic	0.82	0.9988	0.9958	0.9760	191.62	Aliased

3.6.4Predicted Versus Actual

Figure 8 presents the predicted Vs Actual plot. The plot is used to assess the adequacy of the correlation between the experimental and the predicted responses.A close correlation is inferred when the plotted points are linearly distributed on the line of plot. It can be deduced from Figure 8 that the points were closely distributed to the straight line of the plot, hence, it can be concluded that there is a close correlation between the experimental response and the predicted response. This equally validates the adequacy of the selected model in predicting the response variables experimentally.

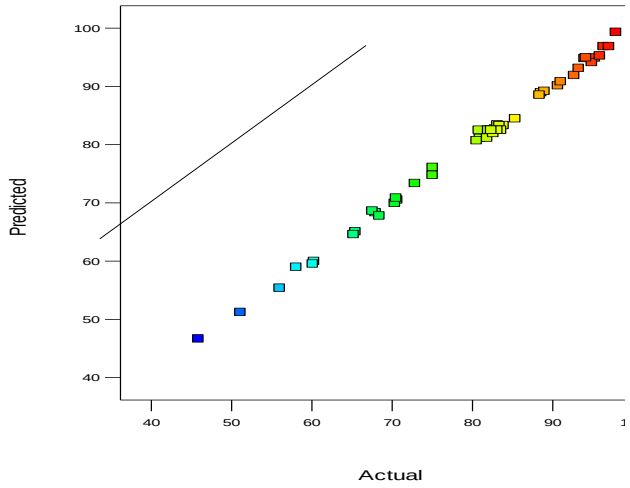

Fig 8 Predicted Vs Actual plot for the response

3.6.53D Response Surface Plots for the Treatment Process

Figures 9-15 presents the 3-D response surface plots for the EC treatment process of abattoir wastewater using aluminum electrode pairs. The response surface curves are plotted to show the effects of two variables on the responsewhen other variables are kept constant. It also helps to show the optimum level of each variable for maximum response. Fig. 15 gives the interactive effect of settling time and pH on the removal efficiency. It can be seen that the removal efficiency was positively impacted by anincrease in settling time and a decrease in pH. The impact of the interactive effect of settling time versus electrolysis time, settling time versus current intensity and temperature versus settling time is given in Figures9, 10and 14 respectively. The impact of the interaction was also influenced mainly by settling time in both cases as shown. In each case increase in settling time influenced the removal efficiency positively. This could be attributed to the fact that an increase in settling time would give more time for the formation of flocs hence a reduction in turbidity level. The independent interactions between temperature and current intensity,electrolysis time and current intensity, temperature and electrolysis time in Figures 11, 12 and 13, indicated apoor influence on the yield.

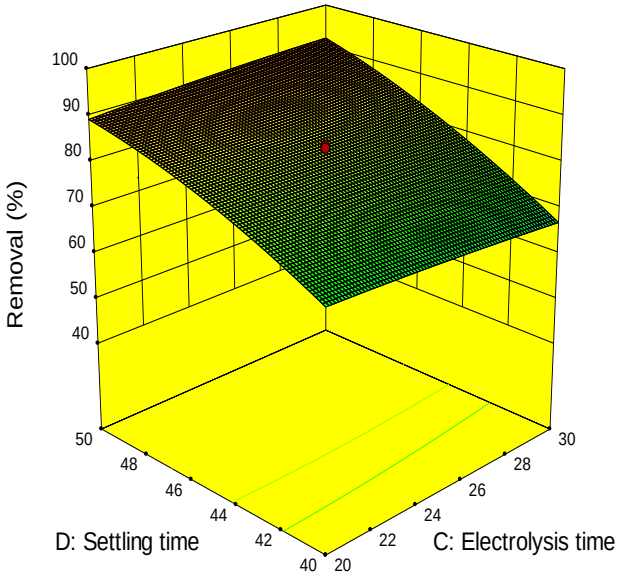

Fig. 9 Effect of settling time and electrolysis time

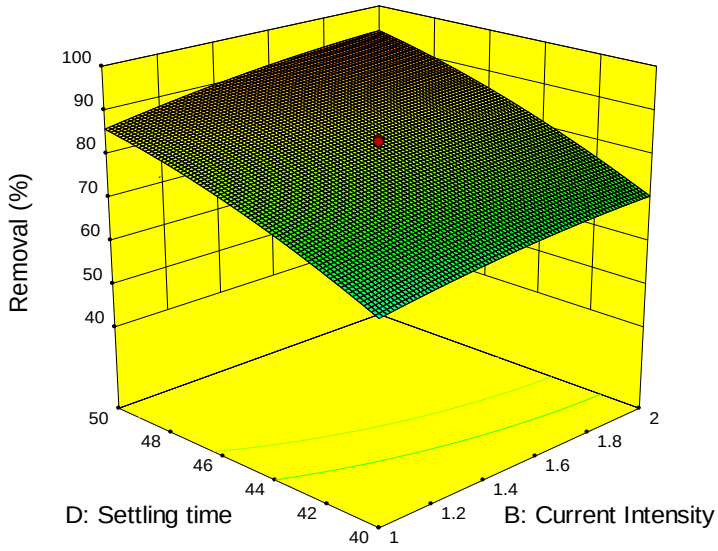

Fig. 10 Effect of settling time and current intensity

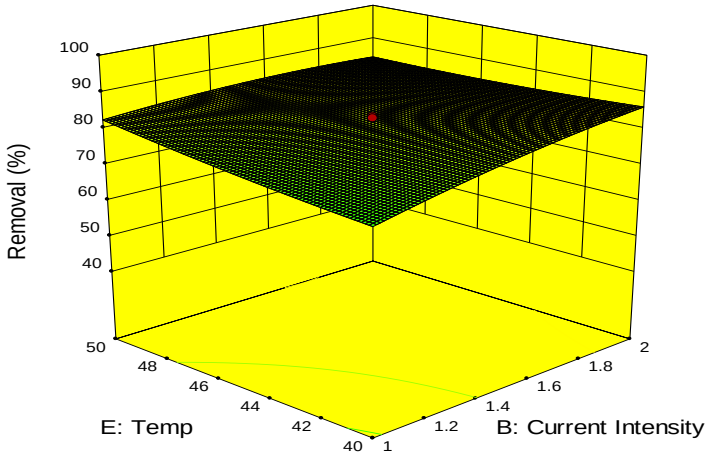

Fig. 11 Effect of temperature and current intensity

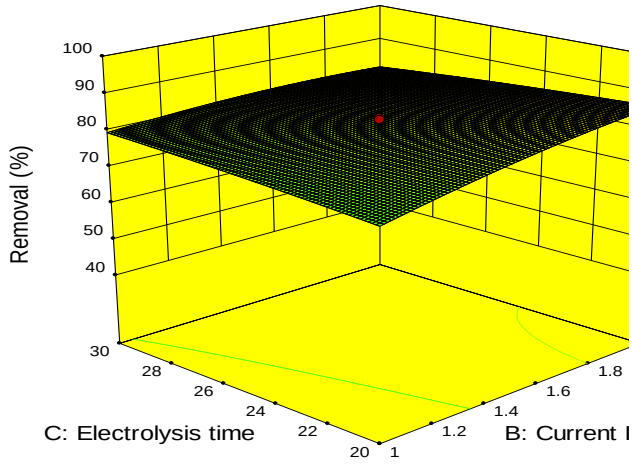

Fig. 12 Effect of Electrolysis time and current intensity

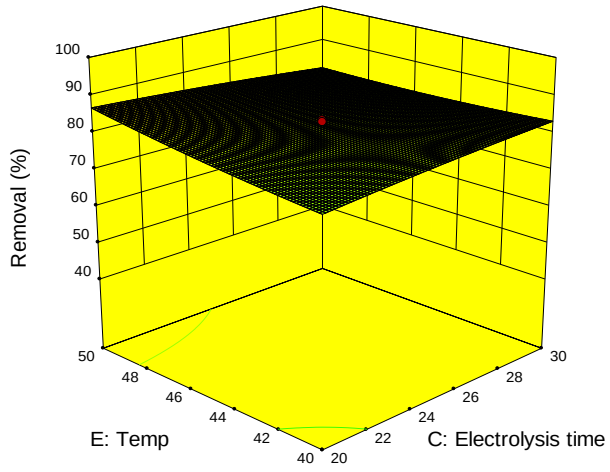

Fig. 13 Effect of temperature and electrolysis time

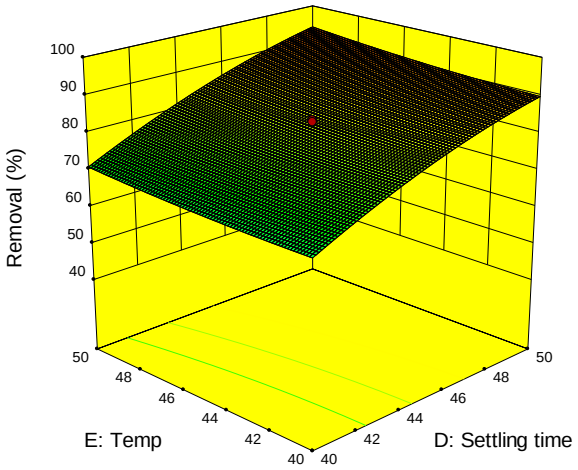

Fig. 14 Effect of temperature and settling time

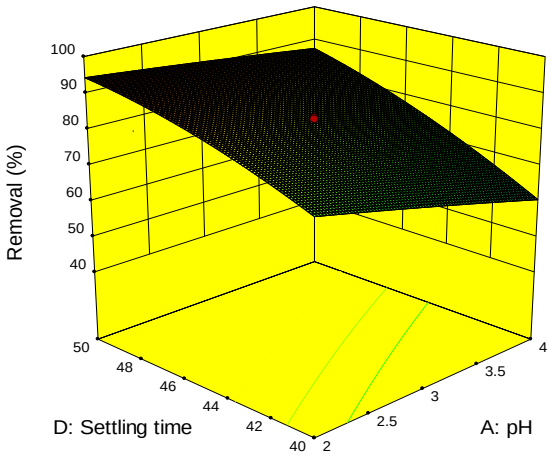

Fig. 15 Effect of settling time and pH

3.6.5Model Validation

The optimum conditions predicted for obtaining 96.78% of turbidity removal from abattoir wastewater by EC process using aluminum electrode pairs were as follows: pH of 2; thecurrent intensity of 1.9A; electrolysis time of 20 minutes; settling time of 50 minutes and operating temperature of 40^{o}C. The optimization was performed using the numerical method of the Design-Expert version 10.1 by State Ease U.S.A. this value is in close agreement with the experimental value of 95.15% performed at the same optimum values of the process variables.

4.0CONCLUSION

The present study has successfully evaluated the performance of aluminum electrode pairs in the EC treatment of abattoir wastewater. The findings of the study showed that the removal efficiency of turbidity by the EC process isincreased by a decrease in the initial solution pH, and increase in current intensity, electrolysis time, settling time and operating temperature. The reaction kinetics result is in agreement with theprevious report on similar work to be in conformity with a pseudo second order kinetic model (Adebayo et al, 2015). The modeling and optimization study was performed using the central composite design of the response surface methodology. Regression analysis showed that a quadratic model best describes the response. From the result obtained in this work, a removal efficiency of 96.78% can be achieved at the following optimum conditions: pH of 2; thecurrent intensity of 1.9A; electrolysis time of 20 minutes; settling time of 50 minutes and operating temperature of 40^{o}C. At the optimum condition for turbidity removal efficiency, 0.28kWh/L power consumption was recorded. This study shows that EC process using

aluminum electrode pairs is effective for the primary treatment of abattoir wastewater.

REFERENCES:

Adebayo A.O., Ajiboye E.A. and Ewetumo T. (2015). Removal of organic pollutants from abattoir wastewater using electro-coagulation. *FUTA Journal of Research in Sciences,* 11(1): 15-24.

Ani J.U., Menkiti M.C., Onukwuli O.D. (2011). Coagulation-Flocculation Performance of Snail Shell Biomass For Waste Water Purification. *New York Science Journal*, 4(2): 81- 90.

APHA (1998). Standard methods for the examination of water and wastewater, *20th edition, APHA/AWWA/Wef Washinton* DC, USA.

Asselin M., Drogui P., Benmoussa H. and Blais, J.F (2008). The effectiveness of electrocoagulation process in removing organic compounds from slaughterhouse wastewater using monopolar and bipolar electrolytic cells, *Chemosphere,* 72 (11):1727-1733.

Babu R. R., Bhadrinarayana N.S., Meera S. K.M., Anantharaman N. (2007). Treatment Of Tannery Wastewater By Electrocoagulation. *Journal of the University of Chemical Technology and Metallurgy*, 42(2):201-206.

Bayar S., YildizY.Ş., YilmazA.E. and Koparal A. S. (2013). The effect of initial pH on thetreatment of poultry slaughterhouse wastewater by electrocoagulation method. *Desalination and Water Treatmen*t Volume 52, Issue 16-18, pp. 3047-3053.

Budiyono, Widiasa I.N. and Johari S. (2010). Study on Treatment of Slaughterhouse Wastewater by Electro-coagulation Technique. *Internat. J. of Sci. and Eng.* 1(1):25-28.

Chaturvedi S. I. (2013). Electrocoagulation: A Novel Waste Water Treatment Method. *International Journal of Modern Engineering Research* (IJMER), 3(1):93-100.

Ciro, B.L., Mehrab, M., and Edgar Q.B. (2016). Slaughterhouse Wastewater Characterization and Treatment: An Economic and Public Health Necessity of the Meat Processing Industry in Ontario, Canada. *Journal of Geoscience and Environment Protection,* 4, 175-186.

Dermentzis K., Christoforidis A., Valsamidou E. and Kokkinos N. (2011), Removal of Hexavalent Chromium from electroplating wastewater by electrocoagulation with iron electrodes, *Global NEST Journal,* 13 (4): 412-418.

El-Shazly, Danous, M.A. (2013), Kinetics and performance of phosphate removal from hot industrial effluent using a continuous flow electrocoagulation reactor, *Electrochemical Science,* 8:184-194.

Eryuruk K., Umran T. U., Ulker B. O. (2011). Treatment of cattle-slaughterhouse wastewater using tubular electrocoagulator, 2011 *2nd International Conference on Chemical Engineering and Applications IPCBEE* vol. 23, IACSIT Press, Singapore, p. 134 – 137.

Eryuruk K., Tezcanun U. and Bakir Ogutveren U. (2014). Electrocoagulation in a Plug-flow Reactor: The Treatment of Cattle Abattoir Wastewater by Iron Rod Anodes. *Int. J. Environ. Res.,* 8(2):461-468.

FEPA, (Federal Environmental Protection Agency), (1991). *National Interim Guidelines and Standards for Industrial Effluent, Gaseous Emissions,and Hazardous Wastes. Abuja*, Nigeria, 33-63.

Fridriskhsberg D.A (1984). A course in colloid chemistry. Mir Publishers, Mosco, 22: 126-132.

Impa J.A., Nagarajappa D.P., Krishne G. K., Manjunath N.T. (2015), Domestic wastewater treatment by electrocoagulation using copper and aluminum electrodes, *International journal of innovative research in science, engineering,and technology*, 4 (6): 3844-3850.

Kwarciak-Kozłowska A., Bohdziewicz J., Mielczarek K., Krzywicka A. (2011), Treatment of meat industry wastewater using coagulation and Fenton's reagent, *civil and environmental engineering reports*, 6:45-58.

Mahajan R., Khandegar V., Saroha A. K., (2013). Treatment of hospital operation theatre effluent by electrocoagulation.*International Journal of Chemical and Environmental Engineering*, 4(2): 104 – 107.

Menkiti M.C., Igbokwe P.K., Ugodulunwa F.X.O., Onukwuli O.D. (2008). Rapid coagulation/flocculation kinetics of coal effluent with high organic content using blended and unblended chitin derived coagulant (CSC*). Research Journal of Applied Sciences,* 3(4): 317 – 323.

Naje A. S., and Abbas S. A. (2013). Electrocoagulation Technology in Wastewater Treatment: A Review of Methods and Applications. *Civil and Environmental Research*, 3(11): 29-43.

Orugba O.H., Onukwuli O.D., Njoku N.C., Ojebah C.K., and Nnanwube I.A. (2014). Process modeling of sulphuric acid leaching of iron from Ozoro clay. *European Scientific Journal* vol.10, No.30, pp. 256-268.

Pozo, R.D., and V. Diez. (2005). Integrated anaerobic-aerobic fixed-film reactor for slaughterhouse wastewater treatment. *Water Res.*, 39(6), 1114-1122.

Silva G.F., Camargo F.L. and Ferreira A.L. (2011). Application of response surface methodology for optimization of biodiesel production by transesterification of soybean oil with ethanol. *Fuel Processing Technology*, 92(3): 407-413.

Shrivastava A., Sandagar P., Baja I. and Singhal R. (2008). Media optimization for the production of U-linolenic acid by cunninghamellaechinulatavarielegans MTCC 522 using response surface methodology. *International Journal of Food Engineering*, 4(2): 1-32

Smoluchowski M. (1917), Verscuheiner Mathematischen Theorie der koagulationskineticcolloidslousungen. *Z. Phys. Chem.* 92. 129 –168.

Tezcan Ü. Ü., Koparal A. S. and Öğütveren Ü. B. (2008). Treatment of slaughterhouse wastewater with iron electrodes. *WIT Transactions on Ecology and the Environment*, Vol 111:, pp. 541-551.

Verhoef, D.G., (2002). An experimental study of abattoir wastewater treatment from an economic perspective. *A dissertation for Master of science degree, Deakin University, Warrnambool, Victoria*, 3280, Australia.

Vlachou M., Hahladakis J. And Gidarakos E. (2013). Effect of Various Parameters in Removing Cr and Ni from Model Wastewater by using Electrocoagulation. *Global NEST Journal*, 15(4):494-503.

ENVIRONMENTAL ISSUES OF THE NIGERIA CONTENT DEVELOPMENT: THE NEED FOR PARADIGM SHIFT TO RENEWABLE ENERGY USE.

***Ugbebor, J. N.[1] and Joel, O.F,[2]**

[1]Civil & Environmental Engineering Department, University of Port Harcourt

[2] World Bank African Centre of Excellence in Oil field Chemicals Research, University of Port Harcourt

johnugbebor@yahoo.com, ogbonna.joel@ipsng.org

ABSTRACT

The global outcry today of global warming and climatic change associated with the exploration and production of fossil energy has necessitated the study of reviewing the need to shift from the use of fossil fuel to using renewable energy. The methodology of study includes detail literature reviews of present practice and the environmental consequences in a developing economy like Nigeria. The study details renewable energy types, the motivation for adoption of renewable energy, the merits and accruable benefits of paradigm shift. Amongst the highlighted benefits are reduced global warming, diversification of nation's resources and economic growth; divergent academic researches; improved employment in other sectors outside the Oil and Gas, more environmentally friendly energy use, better livable environment and energy security in the near foreseeable future. The paper recommended stiff laws on environmental protection and fines for polluting practices as a panacea to achieving the needed paradigm shift.

Key words: *diversification, energy, environment, fossil, global warming and renewable.*

1. INTRODUCTION

Energy is indispensable to life and without it billions of people would go hungry, cold and eventually die (Riddell et al, 1999). Globally, over one billion people lack access to electricity. (World development indicators, 2014) This has made energy sustainability a great issue both in the developed and developing world in the 21st century. To supply hydrocarbon energy, the Oil and Gas companies have engaged in aggressive drive for exploration and production. The subsequent continuous flaring of gases from Oil and Gas facilities has caused serious environmental damage such as air, water, and land pollution; and health related challenges. The resultant imbalances from massive hydrocarbon usage are captured as global warming, climatic changes, tsunamis', flood, erosion, acid rain and drought all over the world today.

The environmental aspects from Oil and Gas industries which are of serious concerns including emission to air, discharges to water, contamination on Land, waste generation (especially hazardous waste) and discharges in the form of noise, particulate dust, heat and vibrations. Today, Nigeria is marked among the countries that are heavily polluting the environment. In fact, the rate of oil spill incidents have escalated to a dangerous and unacceptable level of about 80% between 1976-2008 in the oil producing area of Niger delta region (Egwu, 2012). It is even increasing further today with militancy and pipeline vandalization.

The union of concerned Scientists whose primary study is to ensure safer and healthier environment are encouraging the use of renewable energy as an alternative before the earth's pollution is stressed above limit. They defined 'Renewable Energy' as energy that meet today's demand of energy without putting them in danger of getting expired or depleted and is available for reuse; without necessarily causing harm to the natural environment. Such energy includes ocean energy, geothermal energy, wind energy, solar energy, hydro power energy and bio energy. The need to direct research and development to eco-friendly energy is born out of concern and alarm rose by scientists and the public that the environment is heavily polluted by energy generated from Oil and Gas industry. Since humanity and the ecosystem cannot exist in an unhealthy environment, impacts of industrial activities on the environment have become an issue of major discussion in International and National conventions. Recent scientific report indicated that above 82% of issues raise for deliberation in international assemblies are environmentally related. Since the earth is limited in size and shape, the industrial man cannot continue to ignore the consequences of his action as though the earth is finite. (Joel and Olajide, 2011). Engineers, Scientists, investors and the concerned public of the 21st century

need to weigh the benefits of Oil and Gas production against its impacts and consequences. Therefore, investments into renewable energy technologies are major priority to governments and industry players (NTWG, 2009).

2. AIM/ OBJECTIVES OF THE RESEARCH

The aim of this paper is to encourage Nigerian scientists of the 21st century to refocus research on renewable energy which will readily reduce the damaging effects on hydrocarbon energy use on the environment and human race at large. The specific objectives of this study are to:

i. Review the current global practice in the production and usage of Oil and Gas energy
ii. Evaluate the challenges and implications of over dependence on hydrocarbon based Oil and Gas energy
iii. Establish efforts towards adapting renewable energy use in the 21st century
iv. Establish the roles of renewable energy as alternative energy to oil and Gas energy through established scientific findings.
v. Evaluate environmental and social benefits of energy shift to renewable energy
vi. Make recommendations and way forward.

3. DEFINITION AND TYPES OF RENEWABLE ENERGY

Renewable energy is energy created or generated from sources other than the conventional sources like fossil fuel and nuclear reactors. It is non-conventional energy. Renewable energy can be continually replenished by natural sources (Sulphey, 2013).

These forms of energy include Solar, wind, biofuels, hydro, geothermal, wave and tidal etc.

i. **Solar**: It is directly derived from sun in the form of radiant energy. It is abundant, the fastest growing energy source and very much available for use in the world today. Scientist in the 21st century is known to convert sun energy into electricity by thermo-electric devices (converters), solar chimneys and solar ponds.
ii. **Wind energy**: Wind energy is generated in the form of electricity by converting the rotation of turbine blades into electrical current by means of electrical generators. Wind energy is plentiful, renewable, widely distributed and reduces GHGS.
iii. **Biofuels**: these are fuel sources derived from recently died plants and animals. These could produce methane from animal excrement and ethanol from plants materials. Also biodiesel could be produced from Jatropha plants (*Jatropha curucas).*
iv. **Hydro energy:** Hydro energy is produced from the fast flowing river or an ocean which is capable of turning turbines to generate electricity. This is generally cheap than other sources of energy generation though dam construction may result in environmental problems.
v. **Geothermal Energy:** Geothermal power harnesses natural flow heat from the interior of the earth, derived from natural decay of radioactive element in the earth's crust and mantle. 1st discovered in Italy, 1904. Now used in U.S.A, Japan, New Zealand, Mexico and India etc.
vi. **Wave and tidal:** The technology of being develop to harness energy from Sea or Ocean.
vii. **Hydrogen and fuel cells**: This requires electro-chemical reaction between hydrogen and oxygen gases I hydrogen and fuel cells. Hydrogen is emerging as an alternative to fossil fuels. Hydrogen can be produced from electrolysis of water using solar energy, photo-electrochemical process, thermo-chemical process; direct thermal decomposition or biochemically from water. (Sulphey, 2013)

4. REVIEW OF CURRENT PRACTICE IN OIL AND GAS PRODUCTION AND USAGE IN NIGERIA

In 2007, Nigeria was known to be among the first 10th nations in the world with proven Oil and natural gas reserves with 36.5 billion barrels and 180 trillion cubic feet respectively (NTWG, 2009). There was a near total dependence of Oil and Gas in Nigeria as her revenue source which resulted in intense exploration and exploitation of Oil and Gas in the last six decades. The oil booms of the 1970s and 21st century in Nigeria have not actually helped matters as government intensified oil production and flaring of Gases. The Oil and Gas industry today are major polluters of the Nigerian environment. It was estimated that wasted energy resources via Gas flaring in Nigeria was about 45% of the energy requirements of France, the world fourth largest economy (Ashton, et al 1999; Diugwu et al, 2013). The Department of Petroleum Resources publication indicated that over 3000 oil spills incidence have occurred in Niger Delta. This figure has astronomically increased with recent pipeline vandelization in the region. Some of the incidence which occurred in histories of Oil exploration and production in Nigeria include several Oil pipeline incidents such as

the Jesse pipeline explosion incident of 2001; Ejigbo pipeline incident in 2005 (where 350 persons were killed) and the several recent pipelines blow out by the aggrieved Niger Delta militants. (Ugbebor, 2010). Therefore, researches, technology and papers today on renewable energy are timely to salvage the embarrassing escalation of harm to the environment.

5. CHALLENGES AND IMPLICATIONS OF OVER DEPENDENCE ON OIL AND GAS ENERGY

It was reported that between 9 million to 13 million barrels of Oil have been spilled in the Niger Delta since drilling began in 1958. (Kadafa, 2012). Cleanups have been halfhearted, and compensation has been paltry. It is worthy of note that about 2,000 oil-polluted sites still need cleaning up. (Ugbebor, 2013).The implications of over dependence on fossil energy are serious environmental abuse and social problems in Nigeria such as public outcry from host communities due to destruction of rivers, lakes, wetland, farmland and sources of livelihood; global climatic changes, global warming, flooding and erosion, food insecurity due to drought, acid rain, Stratospheric Ozone layer depletion; increased poverty, unemployment, health related problems (breathing problems, neurological damage, increased heart attack and cancer) with reduced life expectancy, risk of natural disaster; destruction of flora, fauna and wildlife in the Niger Delta region, militancy and wars. These are incalculable loses (Ajienka et al, 2006). One of the major environmental problems in the Niger Delta Region of Nigeria since the inception of oil exploration, exploitation, processing and transportation by the multinational Oil Companies has been that of oil spillage. This area in particular has been greatly impacted by Oil spillage. The NNPC in its annual report, places the quantity of oil jettisoned into the Niger Delta environment yearly at two thousand, three hundred (2,300) cubic meters with an average of three hundred (300) individual spills annually (Medugu, 2012).

The impacts may keep increasing and be a night mare if nothing is done by intellectuals, the academia, professionals, and technocrats. While government smiles home with petrodollars, the fragile environmental components are destroyed. The some developed nations have made some level of progress and the developing countries must intensify efforts also to reduce the level of exposure resulting from unregulated industrial pollution. Though there may be some challenges; these challenges can be erased by leveraging on the gradual paradigm shift towards production of renewable energy as alternative energy source

The Environmental abuse in Nigeria could not be easily checked due to:

i. Lack of effective National contingency plan. Apart from establishing Ministries and lead agencies like Federal Ministry of Environment (FMEnv), Department of Petroleum Resources (DPR), Nigerian Environmental Standards and Regulations Enforcement Agency (NESREA); and National Oil Spill Detection and Response Agency (NOSDRA); realistic assessment tools and adequate strategy for protection and cleaning of polluted areas are not put in place and made public.
ii. Lack of stiff enforcement of existing legislation
iii. Government as a major player in Oil and Gas business and regulator.
iv. Poor compensation of host communities.
v. Poor compensation of host communities and victims of pollution. Hundreds of thousands of people are affected (Amnesty Int. Report, 2009).
vi. Poor surveillance of facilities
vii. Poor involvement of professional bodies as advisory organizations to government and the operating Companies.
viii. Massive unemployment and Militancy.

6. EFFORTS OF COUNTRIES TOWARDS ADAPTING RENEWABLE ENERGY IN THE 21ST CENTURY

Some Countries including Nigeria have made positive efforts towards gradually shifting ground from the over dependence on fossil to renewable energy. Prasad and Kochher (2009) in their report stated that one of the measures to mitigate the climate change is to promote hydro and renewable energy. The Nigeria efforts can be seen in the Map published by NNPC in 2009 as shown in Figure one. The Nigeria soil is so divergent that it has the potential to commercially produce fuel crop in the various regions of the country. In the Northern part of Nigeria, sugarcane, rice, wheat and millet are grown in commercial quantity while the Southern part has the potential to grow palm oil, cassava, and sugarcane. (See the Map on fig one as adopted from NNPC feasibility study, 2009) These crops need to be cultivated in commercial quantity to serve as sources of bio-energy production in Nigeria.

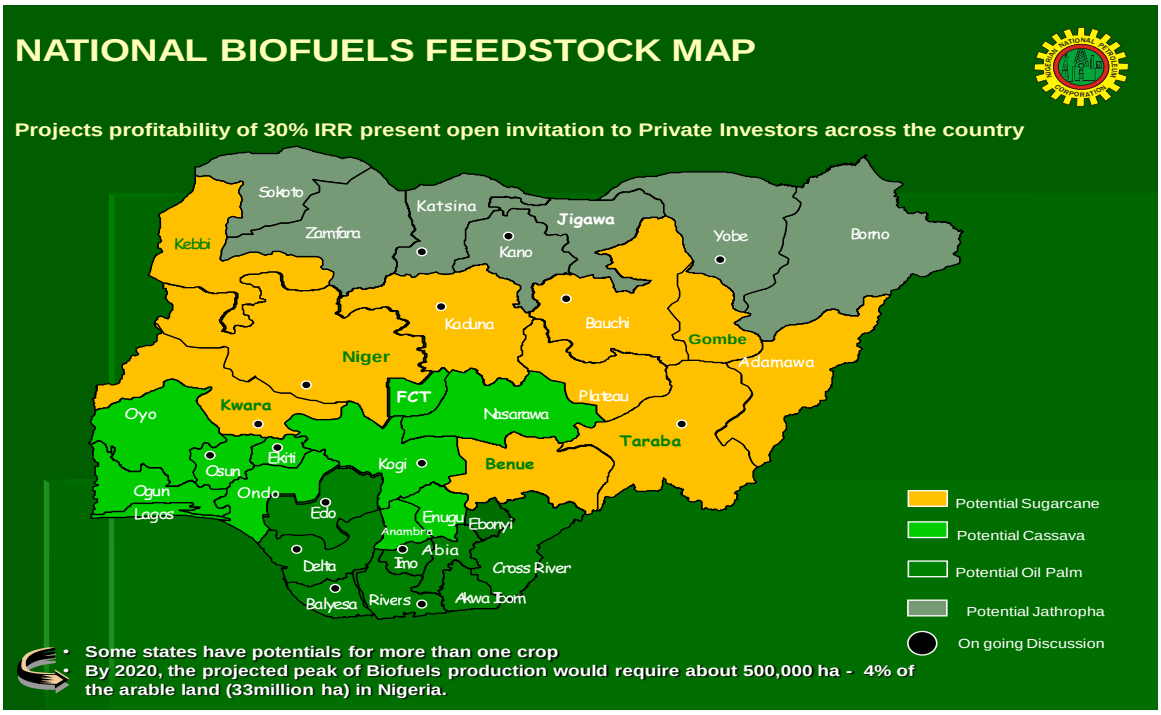

Figure 1: Map of Nigeria indicating region with potential to produce fuel crops
Source: (NNPC, 2009, Siraju, 2012).

Several ad hoc initiatives are currently being undertaken by Energy commission of Nigeria (ECN) and NNPC on renewable energy development though quite slowly. ECN has invested on technology-driven pilot projects on solar energy, wind power demonstration projects in Sokoto State and a small hydro plant in Jos (Report of vision 2020 National Technical Working Group on energy sector, july, 2009). Several State governments in Nigeria recently are making efforts to embarks on solar energy projects for homes, street lights, school, water supply, and community uses.

Some countries like USA, Argentina, Brazil, Malaysia, India, and Germany etc. are among countries in the world that have developed master
plan for using and producing renewable energy. Many more countries are encouraging research and development into the sustainable energy use on annually basis.

7. PROBLEMS MILITATING AGAINST ACCEPTANCE OF RENEWABLE ENERGY IN NIGERIA

Initial challenges and non technical barriers identified to slow down the production of alternative energy are:

i. Massive Petroleum reserve in the Delta Niger region of Nigeria
ii. Government's near total dependence on Oil revenues as major source of income.
iii. No real interest
iv. Lack of proper legislation
v. Poor organizational farming of fuel energy crops
vi. Insensitivity to environmental implication of Petroleum activities
vii. Poor values for human lives.
Viii. Weak environment laws and enforcement.

8. MOTIVATION FOR ADOPTION RENEWABLE ENERGY IN NIGERIA

"Environmental conservation have stimulated the development and utilization of biomass as vital source of renewable energy" (Lim et al, 2012) couple with increasing energy demand in Nigeria. Nigeria is known to be among major global countries that lack access to sufficient energy (electricity energy in particular). Selected countries for study include India, 269 million, Nigeria 75million, Ethiopia 68million, Bangladesh 63million, and others 555million people. (www.worldbank.org). (Solar power and other renewable energy will reduce the problem. Dr. Maikanti Baru, the new General Managing Director, NNPC in a paper titled Recession: Nigeria Oil and Gas reserves running out; when the Nigerian Association of Petroleum Explorationists (NAPE) hosted him revealed that the national oil demand forecast indicates a rapid

growth of 15 billion standard cubic feet per day (bscfd) by 2020. This shows that current reserves level can only sustain production for 35 years except more oil and gas reserves are found. He disclosed further that Nigeria drive for industrialization risks being truncated except something is done about it. The Minister of Petroleum Dr Ibe Kachukwu also in July, 2017, in a media interview cautioned that in the next eight years, some of the developed countries will be using electrically driven automobiles, reducing their hydrocarbon energy requirement drastically, in line with UN Global warming reduction agenda.

The time has come when it is desirable to look for alternative energy resources to complement fossil energy and mitigate the increasing environmental problems and eliminate possible crisis of fossil fuel production. The combined impact of fossil fuel scarcity and the current global oil price crisis make renewable energy investment increasingly attractive. Research findings have demonstrated that we can significantly supplement conventional Oil and Gas supplies with alternative energy. (Kesijav etal, 2011). Also, investing in alternative energy could extend our fossil fuel resources well into the next century and perhaps longer until fossil fuels can be replaced entirely. Moreover, energy independence can be a very important cornerstone for the economic and social development in Nigeria, as seen recently in South America. For Nigeria, Government assistance may be needed to sponsor the required local technology.

9. WAYS OF ENHANCING RENEWABLE ENERGY PRODUCTION

i. Government support for fuel crop production
ii. Government policies must stimulate farming biomass rich crops
iii. Financial incentives such as loans, subsidies and tax reductions
iv. Investment into basic researches and technologies on renewable energy.
v. Private sector investment in mechanized farming of fuel crops like palm oil, maize, cassava, millet, rice, wheat and sugar cane in the north).

Moreover, in recent years, the rising concern about environmental protection revealed the need to incorporate environmental externalities into major decision-making process (Danae & George, 2001). The substantial damage from the hydrocarbon energy production in Nigeria when translated in monetary cost, will also serve as a strong justification for paradigm shift to bio energy production.

10. INNOVATIVE SOLUTIONS AND BENEFITS OF RENEWABLE ENERGY IN NIGERIA

The wakeup call for complimentary and supplementary use of renewable energy is timely to salvage the embarrassing escalation of harm to the environment.

The benefits of renewable energy are classified under sustainable and emissions benefits. The sustainable benefits include reduce reliance on Petroleum & Crude Oil products; reduce emission of green house gases thereby reduction in Global Environmental issues; improve economic growth in form of employment in regional & rural areas; diversification of income, increase security of energy supplies, and reduce environmental pollution (air, Land & water). Better tax regime for Government, Renewable Energy also reduces the health risks associated with Petroleum energy. Renewable energy is central to sustainable development and poverty reduction efforts (Energy Commission of Nigeria (ECN) 2003; National Technical Working Group NTWG, 2009).

The emission benefits include reduction in release Particulate Matter (PM), hydrocarbon, and carbon monoxide (CO) emissions, and enhance combustion due to presence of fuel oxygen which allows better burning, so fewer unburned fuel emissions result. A paradigm shift to renewable energy use will fast track local technologies for harnessing biomass from conventional crops and trees by Biochemical and thermo chemical conversion (Simonyan & Fasina, 2013). Renewable energy production has proved to be eco-friendly far more than fossil fuel. (Buyukkaya, 2010

11. CONCLUSION AND RECOMMENDATIONS

The time has come for all stakeholders of environment to launch out a campaign for paradigm shift from Petroleum fossil fuel to renewable energy. Although we may not be able to rid the country completely of fossil fuel usage for now, we must realize that sufficient renewable energy production is achievable. The world is through organized bodies like United Nations and World Bank are driving the process. The Universities, environmental professionals and research centers should provide the technical expertise resources; while the government of Nigeria should create legislative framework and enabling environment for investors to invest in renewable energy production. The government should also incorporate renewable energy production into the national content plan and the vision 2020 agenda, leveraging on the availability of land, local

technologies, raw materials and financial resources to enhance this innovative transformation. The bottom line is that Nigeria and Nigerians will enjoy a more livable environment, energy security in the near foreseeable future, diversified income and economic growth in form of employment.

ACKNOWLEDGEMENT

The authors hereby thank University of Port Harcourt for providing the platform for this review article, NNPC for efforts already made to map out bio-energy resource regions in Nigeria and other researchers whose work were sighted.

REFERENCES:

Ajienka J.A; Jaja A.J and Ugbebor N.J (2006), *Oil and Gas pollution in the Niger Delta: causes and consequences*. A paper presented at the annual conference of national registry of environmental professionals (NREP), Nashville, Tennessee, USA, in October 16-19.

Amnesty International Report-Eyes on Nigeria (2009). *Nigerian Petroleum, Pollution and Poverty in Niger Delta*. P.27

Ashton, N.J; Arnott, S; Douglas, O (1999). *The Human Ecosytm of the Niger Delta-An Era Handbook*, Environmental Rights Action, Lagos.

Buyukkaya, E (2010); *Effect of Biodiesel on a D1 diesel engine performance, emission and combustion characteristics.* Fuel 89 (20103099-3105).

Danae, D and George, K (2001); *Cost benefit Analysis of bio-fuel oil-seed origin in Greece*. Centre for Renewable Energy Sources, Greece.

Department of Petroleum Resources (2009). *Oil spill incidents data between 1976-2008*, released at the Oil pollution workshop held in Lagos Resource Centre.

Diugwu, I. A; Ijaiya, M.A; Mohammed, M and Egila, A.E (2013). *The effect of gas production, utilization and flaring on the economic growth of Nigeria*. Published in scientific Research (Open access), Article ID 35176.

Egwu, S.A (2012); *Managing Health Challenges in the Oil and Gas Industry, "Oil spill control and management.* A paper presented at 15th International Biennial conference on the Oil and Gas industry in Nigeria held in congress Hall, Transcorp Hilton Hotel, Abuja November 5-7.

Green Peach Oil briefing, 1993.

Energy Commission of Nigeria (ECN) (2003). *National Energy Policy*. www.energy.gov.ng.

Energy Commission of Nigeria.ECN (2006). **Renewable Energy Master Plan draft**. www.energy.gov.ng.

Environment Agency (2004) M17: *Monitoring of Particulate Matter in Ambient Air around Waste Facilitie*s. Environment Agency, Bristol

Environment Agency (2008) *Environmental permitting regulations, standards and measures, getting the basics right - how to comply with your environmental permit, Environment Agency*, Bristol http://publications.environment-agency.gov.uk/pdf/GEHO0209BPHU-e-e.pdf

Intergovernmental Panel on Climate change (2011): *IPCC special report on renewable energy sources climate change mitigation.* Prepared by working group 111 of the IPCC. Cambrdge University Press, Cambridge, United Kingdom. Or New York, NY USA 1075 pp. 9.

Joel O.F and Olajide F.O (2012); *Green Economy: wake up call for the government and oil industries in Nigeria*. A paper present in 1st international conference and technical exhibition on Petroleum Refining & Petrochemicals, Port Harcourt, Nigeria.

Joel, O.F and Ugbebor, J. N (2011); *Environmental sustainability the need for holistic practical approach*. A publication in Journal of Science and sustainability. July 2011 volume 4. NREP, USA.

Kadafa, A A (2012): *Environmental impacts of oil exploration and exploitation in Niger Delta of Nigeria.* Published in Global Journal of science frontier research environment. (Publisher: Global Journal Inc USA). Online ISSN 2249-4626 & Print ISSN 0975-5896).

Keshav, B; Wayne, M. S; Scott, MCkay, Gija,G and Nimisha, B (2011); *Biofuel: An alternative to fossil fuel for alleviating world energy and economic crises*. Published by Journal of Environmental Science and health, Part A, 46:12 1424-1442. London WIT 3JH, UK.

Lim J S, Manan Z A, Wan Alwi S R, Hashim H (2012). *A review on utilization of biomass from rice industry as a source of renewable energy*. Renewable and Sustainable energy review 16, 3084-3094.

Maikanti, B. (2016): *A paper titled "Nigeria's Recession:* oil, gas reserves running out" Published by Vanguard: Exploration drill Masters (Explorationdrillmasters.com).

Medugu (2012): *Issues and Challenges*. Crude Oil Exploration and Production in Nigeria. NNPC, 2009.

Prasad, H.A.C and Kochher J.S (2009). *Climate Change and India- Some major issues and policy implications*, working paper No. 2/2009-DEA, Department of Economic Affairs, Ministry of Finance, Government of India.

National Technical Working Group (2009). *A report of vision 2020 on the energy sector in Nigeria*, July. 2009. Chairman: Funsho M Kupalokan (OFN, FNSE) and Coordinator: Abubakar, Siddique Mohammed.

Riddell, A; Ronson, S; Counts, G; and Spenser, K (1998): *Towards Sustainable Energy: the current fossil fuel problem and prospects of Geothermal* and Nuclear power.

Simonyan K.J and Fasina, O (2013). *Biomass resources and Bio-energy potentials of Nigjeria*. Published in Africaan Journal of Agricultural Research. Academic Journal. http://www.academicjournals.org/AJAR

Siraju, Y and Okonkwo, I (2012): *The use of bio-fuels as alternative Energy to crude oil in promoting Environmental sustainability*. A paper presented at 15th International Biennial conference on the Oil and Gas industry in Nigeria held in congress Hall, Transcorp Hilton Hotel, Abuja November 5-7.

Sulphey, M.M (2013): *Introduction to Environmental Management* 2nd Edition, Publication by PHI Learning Private Limited, Delhi, India Page 141, 152-156.

Ugbebor, J.N (2010): *The role of Safety in National development.* A publication in Nigeria Institute of Safety Professional's journal volume 2. No 1, November

Ugbebor, J N (2013); *Innovative Solutions to Perennial Environmental Impacts of Petroleum Industry (A wake up call for bio diesel use in Nigeria).* Environmental Engineering Department, University of Port Harcourt, Port Harcourt. Nigeria.

World Development Indicators,2014 (www.worldbank.org

OIL FIELD CHEMICALS FROM MACROMOLECULAR RENEWABLE RESOURCES IN NIGERIA: AN INTEGRATION OF HYDROCARBON RECOVERY WITH BIORESOURCE UTILIZATION

***Jimoh, K. A. [1], Muritala, K.B. [2] and Musliu, O. S. [3]**

[1]College of Petroleum Engineering & Geosciences, King Fahd University of Petroleum & Minerals, Dhahran 31261, Saudi Arabia

[2]Chemical and Polymer Engineering Department, Lagos State University, Lagos, Nigeria

[3]Department of Food Engineering, University of Ilorin, Ilorin, Nigeria.

adekayojih@yahoo.com

ABSTRACT

Nigeria is ranked as Africa's largest oil producer (the 6th largest producer globally) with a crude oil production capacity up to 2.7 million barrels per day. The country's gas production is about 1.7x10^{8}cubic meters per day. The investment in the oilfield chemical subsector of the Nigeria oil and gas industry is about 100 million dollars. On the other hand, Nigeria is blessed with various naturally occurring multi-component materials some of which are by-products of large scale industrial processes. The country is the 6th and11th largest raw cashew and coconut producer in the world, respectively. Nigeria also produces other crops such as sugar cane, plantain/banana, guava, pawpaw, and varieties of vegetables. The huge amount of waste generated from the harvesting and processing of these crops can be upgraded to value added products for application as oilfield chemicals. This paper presents an overview of the potential application of agro-biomass wastes in the oil and gas industry. Specifically, research outcomes on the use of these waste materials for drilling fluids, well completion fluids, enhanced oil recovery, and gas shut-off are discussed. The paper seeks to provide information and production technology that are needed by indigenous entrepreneurs who are interested in small and medium scale oilfield chemicals production.

1.0 INTRODUCTION

Nigeria is one of the largest oil producing countries in the world. The country is the world's eighth largest exporter of crude oil and was once a major oil exporter to the United States (Akuru and Okoro, 2011).The amount of money spent in the oilfield chemical subsector of the Nigeria oil and gas industry is about 80 to 100million dollars(This Day, 2017). A certain percentage of this cost could be offset by the involvement of the local industries in the production of these chemicals using locally available raw materials. Nigeria produces varieties of agro materials whose by-products can be used as oilfield chemicals. Major crops produced in Nigeria include coconut, cashew, mango, pineapple, plantain/banana, citrus, guava and pawpaw, (Ibeawuchi et al. 2015). Nigeria also consumed some imported crops in large quantity such as apple, date, and so on.

The production statistics of some of the agricultural produce are shown in Table 1.1 (from 1995-2004).Based on FAO report, about 3.4billion kilogram of citrus fruits are produced annually from about 3million hectares. The country is the 9th major citrus fruit producer globally. Large quantity of palm is also produced in Nigeria (Nwosu, 2016).By processing1tonne of full fruits bunches, each palm oil mill produces an average of 712.1kg of fruits, 254.7kg of empty fruits bunches, 399.8kg of palm kernel cake, 114.9kg of fiber, 0.24m^3 of palm oil mills effluent, and 0.1523m^3 of crude palm oil (Valentin et al. 2016).Nigeria is the fifth largest major producer of coconut in Africa and ranked 11th in the world with an annual production of 2.34x10^{8}kg in 2009 (following African countries such as Tanzania, Mozambique and Ghana, and other countries like Philippines, Indonesia and Brazil) (Uwubanmwen et al. 2011). Coconut trees produce 120 melon-sized fruits per year. Each fruit has approximately 1.6 kg of total mass, consisting of 35% husk, 28% copra, 12% shell, 5% milk, and 20% water (Jan et al 2004). The husk, which represented about 35% of the mass of the coconut melon, comprises 6.67% pith (a lignin which behaves like a phenolic resin), and 33% fibre (Jan et al 2004).

Table 1.1: Production Statistics of Some Major Staple Foods (Kg*10^9) (Aregheore 2009)

Staples	1995	1996	1997	1998	1999	2000	2001	2002	2003	2004
Coconut	149	151	152	152	158	160	161	161	161	162
Millet	5 563	5 881	5 902	5 956	5 960	6 105	5 530	6 100	6 100	6 100
Rice	2 920	3 122	3 268	3 275	3 277	3 298	2 752	3 192	4 952	4 952
Wheat	44	47	66	98	101	73	51	77	73	73
Cassava	31 404	31 418	32 050	32 695	32 697	32 010	32 586	34 476	33 379	33 379
Plantain	1 632	1 687	1 744	1 803	1 902	1 969	1 999	2 058	2 110	2 110
Groundnut	1 579	2 278	2 531	2 534	2 894	2 901	2 683	2 699	2 700	2 700
Mangoes	631	656	689	731	729	730	730	730	730	730
Papaya	648	662	675	751	748	748	748	755	755	755
Maize	6931	5667	5254	5127	4107	4620	4934	5150	5150	5150
Kolanut	95	85	82	82	82	82	82	85	85	85
Cashewnut	95	110	125	152	176	184	185	186	186	186

Cashew is another crop that is produced in Nigeria. It is grown in about nineteen (19) states with possibility to be grown in all other states of the country. The current cashew nuts production in Nigeria is $1.2x10^8$ kg annually (NEPC, 2015). Furthermore, according to African Development Bank (AFDB) president, and the United States Department of Agriculture (USDA), Nigeria produces an estimated $1.7000x10^9$ kg of sugarcane. A fully developed sugarcane industry can generate 117,000 jobs (Agbota, 2016) and its by products (such as bagasse, and left-over leaves/stalks) (Aina et al. 2015) could be processed and used as oilfield chemicals. Out of the 36000kg of world production of orange peels, Nigeria produces 300 million kilogram with high potential to produce more (Ndubuisi et al. 2011).A huge amount of wastes are generated by Nigerian sawmill industry inform of bark, sawdust, trimming, split wood, planer shavings and sander dust every year (Ogunwusi , 2014). The estimated amount of sawdust generated per annum is about 1.8 billion kilogram (Sambo, 2009) while the amount of wood residue is about 5.2 billion kilogram per year (Francescato and Antonini, 2008).Globally, $1.4x10^{14}$kg of waste biomass are generated from agricultural activities every year (Mohlala et al. 2016). Making use of this enormous amount of biomass in the oil and gas industries will provide a better and more economical alternative for its management. This review therefore presents an overview of some of the common sources of biomass wastes in Nigeria and their applications in oilfield operations.

2.0 BIO-DERIVED MATERIALS FOR DRILLING FLUIDS FORMULATION AND ADDITIVES

Drilling fluid is a complex mixture of several chemical compounds that are used as circulating fluid in oil and gas drilling operations. Its functions include carrying of cuttings from the bottom of the hole; cooling and cleaning of the drill and the bit; maintaining borehole stability; lubricating the gap between the drilling string and the wall of the hole; and preventing the inflow of fluids from surrounding rocks by forming a thin and low-permeable filter cake (Elkatatny et al. 2017; Hermoso et al. 2014; Nasiri et al. 2009)

The cost of the drilling fluid system often represents one of the single greatest capital outlays in oil and gas recovery (Nasser et al. 2013). The operational challenges that are encountered during drilling have contributed to the development of different types of fluids: water-based fluids, oil or synthetic-based fluid. Water-based fluids are the most widely used type in drilling operations. Some of the primary ingredients of these fluids are water, gas, oil, barite, polymer and other chemical additives (Al-yasiri and Al-sallami, 2015; Sadeghalvaad and Sabbaghi, 2016).The materials used to satisfy some of the challenges encounter during drilling operations include corrosion inhibitor, weighing agents, lubricants, biocides, detergents, deformer, emulsifiers, surfactants, loss circulation agents, viscosifiers, shale inhibitors and others (Ololade, 2016).

Drilling experience of many years have shown that water-based polymer mud system has a good comprehensive performance in reducing drilling related accidents, improving drilling efficiency, shortening drilling cycle, and saving cost (Luheng, 2014). Synthetic as well as natural polymeric additives are usually added to water-based drilling mud in order to improve its performance properties. There is a global campaign against the use of synthetic additive of petroleum feedstock. This is due to their contribution to environmental pollution and toxicity. Agricultural biomass is a cheap, non-toxic, sustainable and renewable

source of natural polymeric additive (Alsabagh et al. 2015; Fink 2012).

The use of natural polymers for oil field operations can be traced back to the 1930's. More natural polymers have been investigated in recent years for drilling fluids applications. The use of soy protein (one of the most abundant plant proteins) was investigated by Mei-chun et al (2015), as Soy Protein Integration (SPI) at various concentrations. Details of SPI performance in improving drilling fluids properties are summarized in Table2.1.At low concentration, (1and 1.5wt%) the addition of SPI was observed to result into thick, loose highly permeable filter cake. However, at relatively higher concentration, thin and low permeability filter cake was formed leading to better drilling fluid with improved fluid loss control property.

In a similar research, rice husk(containing approximately 20% opaline silica and phenyl propanoid structural polymer (lignin)) have also been used in formulating drilling fluid (Okon et al 2014). The blend of silica and lignin compound makes the rice husk to have high resistance to water penetration, thermal and fungal decomposition. The results of using this husk as additive are shown in Table 2.2. The addition of rice husk lead to continuous decrease in both the amount of fluid loss and filter cake thickness. The decrease in volume of fluid loss is a direct indication of drilling fluid with improved fluid loss control properties. On the other hand, the increase in filter cake thickness, which occurred from above 0.005kg of rice husk, is bad with respect to drilling fluid performance. It can therefore be concluded that rice husk additive is best used at low concentration in order to get a balanced fluid loss performance with respect to the volume of fluid loss and filter cake thickness.

Table 2.1: Effect Of SPI Concentration On Drilling Fluids

SPI concentration (%)	Thickness (m)	Filter rate $x10^{-6}(m^3/s)$	Permeability (mD)	Porosity (%)
0.0	0.014	0.75	3.77	89.7
1.0	0.069	0.16.3	40.5	94.6
1.5	0.065	13.8	32.3	92.5
3.0	0.017	6.00	3.66	86.8
6.0	0.007	2.50	0.63	72.8

Table 2.2: Rice husk impact as additive to drilling fluid

Weight of Rice Husk(kg)	Fluid Loss Volume ($x10^{-6}m^3$)	Filter Cake Thickness (m)
0.000	47.0	0.001
0.005	42.5	0.001
0.010	35.0	0.0015
0.015	24.5	0.0024
0.020	16.5	0.0032

Other materials such as cellulosic polymers (such as carboxymethyl cellulose, guar gum, and starch) which are available in abundance and at low cost have also been investigated for drilling fluid formulation. The carboxymethy cellulose (CMC) is a cellulose derivative with carboxymethy groups (ACH_2ACOOH) bond to some of the backbone of cellulose while the guar gum belongs to a class of polysaccharide that contained the sugar galactose and mannose (Fink, 2012).Starch is usually used in drilling fluids in its modified forms due to its solubility in water. Starch materials are predominantly used as filtration and rheological properties modifier. The impacts of different types local (Nigeria) cassavas on viscosity of drilling mud were investigated (Taiwo and Kazeem, 2011). Results of this investigation are shown in Table 2.3.

Table 2.3: Mud samples from different cassava starch(Taiwo and Kazeem 2011)

Different Cassava starch	MUD SAMPLES	Viscosity(at 200rpm)		
		80˚F	120˚F	150˚F
TMS 30572	A	22	17	15
TME 419	B	23	16	13
TMS 95/0289	C	23	17	14

Different Cassava starch	MUD SAMPLES	Viscosity(at 200rpm)		
TMS 91/02324`	D	23	15	13
TMS 96/1642	E	23	15	13

*TMS-Tropical Manioc Selection; TME-Tropical ManihotEsculenta

Other natural polymers such as xanthan gum, polyester and modified cellulose such as carboxymethy-hydro ethyl cellulose have also been tested for drilling applications. Xanthan gum based drilling fluid system provides optimum hydraulic efficiency, reduces pressure losses within the drill string, and improves stability and cutting carrying capacity. Consequently, the addition of xanthan gum increases the rate of penetration (Cpkelko, 2008). Polyesterhas been tested as thickening agent in drilling fluids(Doolan and Cody, 2012) while carboxymethy-hydro ethyl cellulose is used to retard cement hardening(Lucas et al. 2009).

3.0 UTILIZATION OF BIO-DERIVED MATERIALS FOR CHEMICAL ENHANCED OIL RECOVERY (EOR)

Oil recovery operations can be subdivided into three stages namely: primary, secondary, and tertiary. Primary production results from the displacement energy that naturally exists in a reservoir, such as solution-gas drive, gas-cap drive and natural water drive. Secondary recovery processes are water flooding and gas injection. Tertiary processes use miscible gases, chemicals and or thermal energy to displace additional oil after the secondary recovery process(Sun et al. 2017). In this section, our attention is focused on chemical EOR. The details of this method are illustrated in Table 3.1.EOR usually refers to the recovery beyond primary production and water flooding. This is important in order to facilitate recovery of more than 70% of the oil which is normally left in the reservoir after primary and secondary methods (Noureddini, 1996).

Table 3.1: The categories of available EOR technologies (Patrizio et al. 2016)

Categories	Detailed methods	EOR mechanisms
Chemical method	Alkaline flooding	IFT reduction
	Surfactant flooding	Wettability
	Polymer flooding	alteration
	ASP flooding	Mobility control
	Micellar flooding	emulsion

Chemical flooding (such as polymer flooding) of oil reservoirs could be the one of the most successful method to increase oil recovery rate of the depleted reservoirs (Nagy et al. 2015).It can yield a significant increase in percentage recovery by reducing the water production and improving the recovery when compared to the conventional water flooding (Moawad and Elhomadhi, 2013). Two of the main challenges in the use of chemical method are the cost effectiveness and the cost sensitivity of polymers to oil prices. Therefore, there is a need to find alternatives to non-petrochemical source polymers for EOR applications (Adewole and Sultan, 2014).There are two basic categories of polymers which are used in the field applications: biopolymers and synthetic polymers. Some of the widely used biopolymers include xanthan gums, hydroxyethyl cellulose, glucan, and guar gum (Bedaiwi and Paiaman, 2009).The result obtained from the use of Xanthan gum for EOR is shown below in Table 3.2.

Table 3.2: Percentage of oil recovery for each concentration of Xanthan Gum in water.

Xanthan gum(ppm)	Oil recovery
250	30.65
500	52.08
1000	58.79

The potential of date pit for EOR was investigated by Adewole and Sultan (2015).The authors evaluated the capability of date pit for mobility ratio control. Thus, the effect of date pit powder on the viscosity of surfactant formulation was investigated. Table 3.3 contains the results of the investigation. It was observed that date powder (in aqueous NaOH solution) possesses some level of viscosity enhancement capability which is useful for EOR application.

Table 3.3: Effect of Date pit powder on the Viscosity of surfactant formulation at 38˚C
(Adewole and Sultan 2014)

Weight of Date pit powder ($x\ 10^{-3}$kg)	Viscosity (cP)
0	1.0
0.8	2.0
1.8	3.0
2.5	5.0
5.0	10
6.5	23

Lignin is another macromolecular compound from renewable sources such as wood waste. It can be used in

surfactant system without the need to modify it. Besides, the modification process is costly. Thus currently, the need to find a way to avoid modification step has led to the use of unmodified Kraft lignin, water soluble sulfonate, and the oil-soluble organic amine blend for chemical EOR (Sulaiman et al. 2016).

4.0 WATER AND GAS CONTROL IN OILFIELD USING NATURAL POLYMERS

Whenever water production exceeds economic limits of a given oil or gas field, the need arises for a process by which produced water is reduced. Published data indicate that the petroleum industry spends $40 billion every year to process excessive produced water. Moreover, water causes corrosion, scale and requires the construction of larger downstream handling facilities (Al-muntasheri, 2012).

Several types of materials and methods are used for water and gas control. One of the most commonly used materials are polymer gels. There are two types of gels that are commonly used for water- relative permeability modifier (RPM), and sealant. RPMs usually reduce the relative permeability of water without affecting the permeability of oil. The sealant type of gels seals all the fluids by creating a barrier. Fractures, high-permeability channels and other heterogeneities present in reservoirs are very likely to provide preferential paths to the fluid and therefore causes premature breakthrough. A common way to mitigate this problem and to maximize the production from the reservoir is to place sealants or blocking agents in such flow paths. Polymer gels and other types of conformance materials are permeability reducing agents that can fill fractures and high permeability channels to reduce fluid production (Swain et al. 2016).

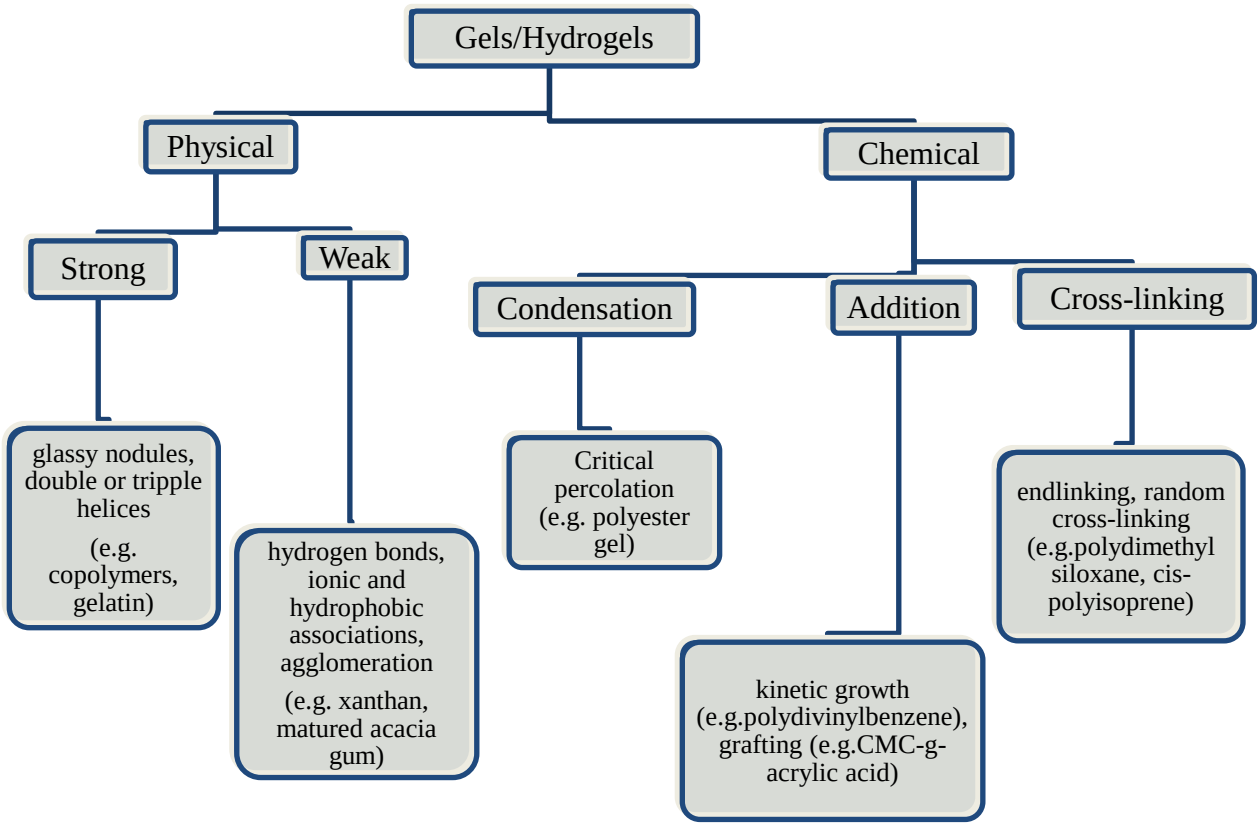

Fig 4.1: Classification of gelation mechanism and relevant examples (Gulrez et al. 2003)

Natural polymers could play a very important part in improving the performance of polymer gels. Adewunmi et al.(2015) investigated the potentials of cross-linked polyacrylamide composite hydrogels embedded with date seed powder for water control in oil reservoirs. The

authors examined the effect of date pit on the rheological behavior, morphological and structural properties of the hydrogels. The characterization results showed that the surface of the hydrogels filled with various concentration of date pit were smooth, homogeneous and dense.

Another challenge often faced by operators in the oilfield is the unwanted production of associated gas from oil wells. This is particularly worrisome if the extra gas does not have readily available access to a market, thereby making disposal becomes the only option. Most of the disposal solutions (such as flaring, well injection or liquid conversion) are environmentally unfriendly, technically challenging, and expensive. An alternative method commonly employed by oilfield operators is the gas shut-off. To shut off unwanted gas production in order to optimize the overall reservoir recovery, a wide range of technology is employed including cased-hole wireline, chemical treatments, and thru-tubing services. For problem which resides near the wellbore, mechanical solutions within the thru-tubing services portfolio often provide the best option. Studies were conducted by Adewole (2016) on gas transport properties of date pit/polysulfone composite for some associated gas components including CO_2, CH_4, N_2, He, and H_2 gases. The composite membranes were prepared by solvent casting method with 2 – 10 wt% date pit micro-sized particles. Gas shut-off performance of the membranes was done using high pressure gas permeation, X-ray diffraction, and thermogravimetric analyses. Time-dependent gas control performance properties were evaluated up to a pressure of 40 bar for 75 days. The resulting composite showed the highest decrease in overall gas permeability of 96% with 2wt% loading of the particles as compared to pure polysulfone membrane (Table 4.1). Thus, this composite possesses some potential for innovative fluid control technology which can lead to most significant cost reduction and improved oil production. This is especially important in solving the gas flaring related environmental pollution issues in the oil producing states in Nigeria.

Table 4.1: Effect of Date Pit Loading on Permeability and Selectivity (Adewole, 2016)

Sample	%wt	He	H_2	N_2	CH_4	CO_2
DP-PS- 0	0.00	600.454	633.873	230	318.229	240.292
DP-PSF-2	2.00	30.768	20.339	8.461	11.072	13.957
DP-PSF-5	5.00	151.264	213.773	76.165	115.697	94.949
DP-PSF-10	10.00	1130.918	1741.240	547.787	705.246	445.658

On a general note, the results of Table 4.1 showed that, date pit based membrane can be used for gas shut-off at low concentration (up to 2wt%) while at high concentration, the resulting membrane is better suited for natural gas processing (Adewole, 2016).

5.0 CONCLUSION AND RECOMMENDATION FOR FUTURE WORK

The importance of oilfield chemicals from macromolecular renewable resources in Nigeria was examined. The potential for integrating hydrocarbon recovery with bioresource utilization were reviewed. Considering the interest of the Nigerian government in agriculture, coupled with the private sector investment in the agriculture industry, the country will be generating a huge amount of agriculture-based biomass waste in the near future. Integration of hydrocarbon recovery with the utilization of these biomass wastes will create a smart solid management technique. By doing this, the country will be turning waste to wealth. Consequently, this will create jobs for the youths, increase the local content participation in the oil sector, reduce the cost of oil and gas exploration and production, and preserve our environment for the future generation.

It is recommended that research and development efforts be established (with collaboration between the oil and gas industry and the academics) to begin oilfield tests using the wastes from those agricultural products that were identified in this article.

REFERENCES

Adewole, J. K. 2016. “Transport Properties of Gases through Integrally Skinned Asymmetric Composite Membranes Prepared from Date Pit Powder and Polysulfone.” *Applied Polymer Science*, 43606:8–17.

Adewole, J. K. and A. S. Sultan. 2014. “A Study on Processing and Chemical Composition of Date Pit

Powder for Application in Enhanced Oil Recovery." *Defect and Diffusion Forum,* 353:79–83.

Adewunmi, Ahmad. A., Suzylawati Ismail, and Abdullah. S. Sultan. 2015. "Laboratory Scale Study on Rheological Behavior, Morphological and Structural Properties of Crosslinked Polyacrylamide Composite Hydrogels Embedded with Date Seed Powder." *Polymer Science,* 42110:1 – 9.

Agbota, Steve. 2016. "SunNews." Retrieved (http://sunnewsonline.com/agric-nigeria-can-earn-n2-5trn-from-sugarcane-farming/).

Aina, O., Ajijola, S., Ibrahim, I.,Musa I.A, and Bappah, T.M. 2015. "Economics Analysis of Sugarcane (Saccharum Officinarum) Production in Moro Local Government Area of Kwara State , Nigeria." *Reseach Journal of Plant Science*, 6(1):1–6.

Akuru, Udochukwu B. and Ogbonnaya I. Okoro. 2011. "A Prediction on Nigeria's Oil Depletion Based on Hubbert's Model and the Need for Renewable Energy." *ISRN Renewable Energy*, 2011(v), doi: 10.5402/2011/285649.

Al-muntasheri, Ghaithan A. 2012. "Conformance Control with Polymer Gels : What It Takes." *Arab J Sci Eng*, (37):1131–32.

Al-yasiri, Mortatha Saadoon and Waleed Tareq Al-sallami. 2015. "How the Drilling Fluids Can Be Made More Efficient by Using Nanomaterials." *American Journal of Nano Research and Applications* 3(3):41–45.

Alsabagh, Ahmed Mohamed, Mahmoud Ibrahim Abdou, Hany El Sayed Ahmed, Ahmed Abdel Salam Khalil, and Amany Ayman Aboulrous. 2015. "Evaluation of Some Natural Water-Insoluble Cellulosic Material as Lost Circulation Control Additives in Water-Based Drilling Fluid." *Egyptian Journal of Petroleum* 24(4):461–68.

Aregheore, Eroarome Martin. 2009. "Country Pasture / Forage Resource Profiles." *Food and Agriculture Organization of the United Nations (FAO)*.

Bedaiwi, E. and A. M. Paiaman. 2009. "Polymer Injection for Water Production Control through Permeability Alteration in Fractured Reservoir." *NAFTA* 60(4):221–31.

Cpkelko. 2008. "KELTROL ® / KELZAN Xanthan Gum." *Xanthan Book* 8:1–32.

Doolan, Joseph and Charles Cody. 1995. "Pourable Water Dispersible Thickening Composition for Aqueous Systems And a Method ff Thickening said Aqueous Systems." *US Patent 5,425,806* 2(12).

Elkatatny, Salaheldin, Mohamed Mahmoud, and Hisham A. Nasr-el-din. 2017. "Filter Cake Properties of Water-Based Drilling Fluids Under Static and Dynamic Conditions Using Computed Tomography Scan." *Journal of Energy Resources Technology* 135 (December 2013):1–9.

Fink,Johannes (2012). "Petroleum Engineer's Guide to Oil Field Chemicals and Fluids." 2:1–59. Retrieved (http://www.sciencedirect.com/science/book/9780123838445).

Francescato, Valter and Eliseo Antonini. 2008." *Wood Fuels Hand Book*.

Gulrez, Syed K. H., Saphwan Al-assaf, and Glyn O. Phillips. 2003. "Hydrogels : Methods of Preparation , Characterisation and Applications." *Advanced Research* 6(2):105–21. Retrieved (https://doi.org/10.1016/j.jare.2013.07.006).

Hermoso, J., Martinez-Boza, F., and Gallegos, C. 2014. "Influence of Viscosity Modifier Nature and Concentration on the Viscous Flow Behaviour of Oil-Based Drilling Fluids at High Pressure." *Applied Clay Science* 87:14–21.

Ibeawuchi, I.I, Okoli, N.A., Alagba, R.A., Emma-Okafor, L.C; Peter-Onoh, C.A and Obiefuna, J.C 2015. "Fruit and Vegetable Crop Production in Nigeria : The Gains , Challenges and The Way Forward." *Biology, Agriculture and Healthcare* 5(2):194–209.

Jan E.G. van Dam, Martien J.A. van den Oever, Edwin R.P. Keijsers (2004), "Production Process for High Density High Performance Binderless Boards from Whole Coconut Husk" *Industrial Crops and Products* 20: 97-101

Lucas, Elizabete F., Claudia R. E. Mansur, Luciana Spinelli, and Yure G. C. Queirós. 2009. "Polymer Science Applied to Petroleum Production." *Pure and*

Applied Chemistry 81(3):473–94.

Luheng, Qi. 2014. "The Application of Polymer Mud System in Drilling Engineering." *Procedia Engineering* 73 (May):230–36.

Moawad, Taha and Emad Elhomadhi. 2013. "A Novel Promising, High Viscosifier, Cheap, Available and Environmental Friendley Biopolymer (Polymtea) for Different Applications at Reservoir Conditions under Investigation. Part a: Polymer Properties." 1–16. Retrieved (http://citeseerx.ist.psu.edu/viewdoc/summary?doi=10.1.1.564.6153).

Mohlala, Lesego M. et al. 2016. "Beneficiation of Corncob and Sugarcane Bagasse for Energy Generation and Materials Development in Nigeria and South Africa : A Short Overview." *Alexandria Engineering Journal* 55(3):3025–36.

Nagy, Roland, Rubina Sallai, László Bartha, and Árpád Vágó. 2015. "Selection Method of Surfactants for Chemical Enhanced Oil Recovery." *Advances in Chemical Engineering and Sciences* 5(April):121–28.

Nasiri, M., S. N. Ashrafizadeh, and A. Ghalambor. 2009. "Synthesis of a Novel Ester-Based Drilling Fluid Applicable to High Temperature Conditions." *Energy Resources Technology* 131:13103-013103–10.

Nasser, Jamal et al. 2013. "Experimental Investigation of Drilling Fluid Performance as Nanoparticles." *World Journal of Nano Science and Engineering* 2013(September):57–61.

Ndubuisi, Eke, Okechukwu, and Nwoguikpe. 2011. "Waste to Wealth : Industrial Raw Materials Potential of Peels of Nigerian Sweet Orange (Citrus Sinensis)." *African Journal of Biotechnology* 10(33):6257–64.

NEPC. 2015. "Nigerian Missions in Vietnam and United Arab Emirates." *Nigeria Export Promotion Council* (February):1–12.

Noureddini, Hossein. 1996. "Pelargonic Acid in Enhanced Oil Recovery Pelargonic Acid in Enhanced Oil Recovery." *Papers in Biomaterials*.

Nwosu, Kingston. 2016. "Nigerian Palm Oil Sector Still a Promising Growth Story." *FBNQuest Research* 234 (October). Retrieved (http://www.fbnquest.com).

Ogunwusi, A. .. 2014. "Wood Waste Generation in the Forest Industry in Nigeria and Prospects for Its Industrial Utilization." *Civil and Environmental Research* 6(9):62–70.

Okon, Francis, and Perpetua. 2014. "Evaluation of Rice Husk as Fluid Loss Control Additive in Water-Based." *Society of Petroleum Engineers(SPE)* SPE-172379.

Ololade, Olatunji. 2016. Book of *Natural Polymers Industry Techniques and Applications*. edited by O. Ololade. Springer.

Patrizio Raffa, Antonius Broekhuis, and Francesco Picchioni. 2016. "Polymeric Surfactants for Enhanced Oil Recovery : A Review." *Petroleum Science and Engineering* 145:723–33.

Sadeghalvaad and Sabbaghi. 2016. "Synthesis and Application of the Drilling Mud Additive in the Presence of Surfactants." *Int. J. Nano Dimens* 7(4):321–28.

Sulaiman, WRW, AH Abbas, MZ Jaafar, and AK Idris. 2016. "Lignin Black Liquor in Chemical Enhanced Oil Recovery: A Review for Sacrificial Agent." *Petroleum & Environmental Biotechnology* 7(5):5–8.

Sun, Xiaofei, Yanyu Zhang, Guangpeng Chen, and Zhiyong Gai. 2017. "Application of Nanoparticles in Enhanced Oil Recovery : A Critical Review of Recent Progress." *Energies* 10(345):1–33.

Swain, Manasmita, Saroj Chaudhary, P. N. Meshram, V. V Manchalwar, and C. P. Singhal. 2016. "Water Control in Naturally Fractured Carbonate Reservoir with Novel Polymer Gel System." *Petrotech; Category: Drilling and Completion Technologies*.

Taiwo, Ademiluyi and Amuda A. Kazeem. 2011. "Investigation of Local Polymer (Cassava Starches) as a Substitute for Imported Sample in Viscosity and Fluid Loss Control of Water-Based Drilling Mud." *Engineering and Applied Sciences* 6(12):43–48.

ThisDay Newspaper. 2017."Long Contracting Cycle Threatens Multi-million dollar oilfield Investment" https://www.thisdaylive.com/index.php/2017/04/25/long-contracting-cycle-threatens-multi-million-dollar-oilfield-investments/.

Uwubanmwen, C. N. Nwawe, R. A. Okere, M. Dada, and E. Eseigbe. 2011. "Harnessing the Potentials of the Coconut Palm in the Nigerian Economy." *World Journal or Agricultural Sciences* 7(6):684–91.

Valentin, Kindomihou, Tatiana Windekpè Koura, Valentin Kindomihou, and Gustave Dagbenonbakin. 2016. "Quantitative Assessment of Palm Oil Wastes Generated by Mills in Southern Benin Quantitative Assessment of Palm Oil Wastes Generated by Mills in Southern Benin." *African Journal of Agricultural Research* 11(19).

RED AND METHYLENE BLUE DYES IN AQUEOUES SOLUTION USING COPPER (II) OXIDE NANOPARTICLES

[*]Oboh, I. O.[1], Inyang, U. E[2]., Aduak, O. J. [3] and Okon, E. E. [4]

[1,2,3]Department of Chemical and Petroleum Engineering, University of Uyo, Uyo, Nigeria.

[4]Department of Chemical and Petrochemical Engineering, Akwa Ibom State University, Mkpat-Enin, Akwa Ibom State, Nigeria.

Email: innocentoboh@uniuyo.edu.ng

ABSTRACT

The removal of Congo Red (CR) and Methylene Blue (MB) in aqueous solution using copper (II) oxide nanoparticles as the adsorbent has been studied. Copper (II) Oxide nanoparticles were synthesized by simple aqueous precipitation method and the surface area and bulk density were determined. Batch adsorption kinetic studies were carried out with varied initial dye concentration and varied adsorbent dosage. Non-linear regression method was used to fit experimental data to Pseudo-first order, Intra particle diffusion and Pseudo-second order kinetic models. The results obtained for varied adsorbent doses showed that when the three kinetics models studied were compared, the pseudo-second order kinetic model with R^2 values of 0.9999, 0.9981, 0.9798, 0.9378, 0.9858 and R^2 values of 0.9922, 0.9994, 0.9807, 0.9755 and 0.9960 for Congo red and Methylene blue respectively showed best fit for the sorption process. The results obtained for varied initial dye concentration showed that when the three kinetic models were compared, the intra particle diffusion model with R^2 values of 0.9966, 0.9959, 0.9998, 0.9999, and 0.9997 for the sorption of Congo red and R^2 values of 0.9815, 1.0000, 0.9999, 0.9988 and 0.9999 for Methylene blue, showed best fit. These results obtained showed that Copper (II) Oxide nanoparticles could be used as an adsorbent for the removal of Congo red and Methylene blue from aqueous solution.

Keywords: *Copper (II) Oxide nanoparticles, Congo red dye, Methylene Blue dye, Wastewater*

INTRODUCTION

Industries such as textile, leather, paper, plastics, etc., use dyes in order to colour their products and also consume substantial volumes of water. As a result, they generate a considerable amount of colored wastewater (Ravi *et al., 2005*).

Coloured wastewater from different industries affects the ecosystem in many ways. With the environmental regulations which become more and more stringent in recent years, how to eliminate hazardous materials (especially those highly toxic and carcinogenic contaminants) from wastewater and prevent them from entering environmental system is a focus of international concern (Akrout *et al., 2015*).

Nanomaterials, like nanoparticles, nanotubes, nanowires and thin films, are defined as very small aggregate of atoms with less than 100 nm in at least one dimension (Schmid *et al.,* 1994). Nanotechnology ("nanotech") is manipulation of matter on an atomic, molecular, and supramolecular scale. Nanotechnology is a multidisciplinary field, as it combines the knowledge from different disciplines: chemistry, physics, and biology amongst others (Hahens *et al.,* 2007).

During the past three decades, several physical, chemical and biological decolourization methods have been reported. A variety of physical, chemical, and biological methods have been applied for the treatment of wastewater, which contains dyes and heavy metals. Nanomaterials reveal good result than other techniques used in water treatment because of its high surface area (surface/volume ratio) (Maraval *et al.,* 2003).

Congo red (CR) and Methylene blue (MB) are the most commonly used substances for dyeing cotton, wood and silk. They have many uses in different fields, such as biology and chemistry. But, it is proved that these dye have many hazardous effect on human body such as hypertension, precordial pain, mental confusion, nausea, profuse sweating and methemoglobinemia, skin staining, dizziness, headache and anemia (Rafatullaha *et al.,* 2010; Mokhlesi *et al.,* 2003; Harvey & Keitt, 1983). They can also cause eye burns which may be responsible for permanent injury to human and animals. To purify wastewater contaminated by CR and MB

from solutions, various techniques including adsorption (Mittal *et al.,* 2009) photodegradation (Murcia *et al.,* 2011) chemical oxidation (Khadhraoui *et al.,* 2009) coagulation (Patel *et al*., 2012) electrochemical oxidation (Elahmadi *et al.,* 2009) and microbiological treatment (Ng *et al.,* 2014) have been employed. Among these techniques, adsorption has been intensively concerned and found to be superior to other techniques due to its simple operation, high efficiency, economy and convenience. A number of adsorbents, including activated carbon (Purkait *et al.,* 2007) acid activated red mud (Tor *et al*., 2006) fly ash (Mall *et al*., 2005) as well as polymers (Xiao *et al.,* 2013) have been studied for CR removal. Wastewater treatment using nanoparticles is one of the areas of concentration in nanotechnology among the various applications for the nanotechnology such as fuel cells, hydrogen storage and various clinical antibacterial activity applications (Schmid *et al.,* 1994; Suleiman *et al.,* 2003).

Varying sizes and shapes can be synthesized for CuO nanoparticles by different methods such as sonochemical technique, electrochemical method, high temperature combustion and novel quick precipitation method. CuO nanoparticles synthesis by novel quick precipitation (salt reduction) method is very interesting because it is safe, simple, environmentally friendly method and gives large scale of nanoparticles (Zhou *et al.,* 2006; Zhang *et al.,* 2006). CuO finds various applications in modern day science and technology, due to its unique features like high specific surface area, chemical stability, electrochemical activity, high electron communication features, optical switch, pigment, fungicide, metallurgy reagent, gas sensor, magnetic storage media, field emission (FE) emitter, etc (Ejhieh & Hushmandrad, 2010).

The objective of this study is to show the removal of Congo red and Methylene blue dyes from aqueous wastewater solution using Copper (II) Oxide nanoparticles as adsorbent and the experimental data obtained fitted to some selected kinetic models

MATERIALS AND METHODS

Preparation of adsorbent

CuO nanoparticles were synthesized by simple aqueous precipitation method using copper metal chips, nitric acid and caustic soda. Firstly, copper nitrate solution was prepared by dissolving 12g of copper metal chips with 48ml of nitric acid. The reddish-brown copper metal chips was first oxidized, the solution formed was very concentrated and gave a green colour and then later turned to greenish-brown colour. The nitrate solution was then diluted with distilled water. After which the solution changed to blue colour. Then 10% sodium hydroxide solution was added drop by drop to the diluted solution while stirring. Copper hydroxide was precipitated at pH≈10. The resulting precipitate was filtered and washed several times with distilled water until the pH was approximately neutral (~7) and finally dried in an oven at a temperature of 100℃. A black powder product was obtained (Mittal *et al.,* 2009).

Preparation of dye solutions

The stock solutions were prepared separately by dissolving 1g of Congo red and Methylene blue in 1000ml of distilled water. All the working solutions were obtained by diluting the stock solutions with distilled water into different concentration ranging from 10ppm to 30ppm.

Adsorption Experiment

The experiments were carried out in the batch mode for the measurement of adsorption capabilities. The bottles with 500ml capacity were filled with 50ml of the dye solution, and 10-50mg of Copper (II) Oxide nanoparticles. The bottles were shaken for a predetermined period of 2h at room temperature in a reciprocating shaker set at 240 rpm. The separation of the biosorbents and solutions was carried out by filtration with whatman filter paper No. 42 and the filtrate stored in sample cans in a refrigerator prior to analysis. The residual dye concentrations were determined using UV/VIS Spectrophotometer (model: Enway 7305) at wavelength 664 nm for Methylene blue (MB) and 496nm for Congo red (CR).

The concentration of dye adsorbed was determined using the following equation;

$$\%\,\text{Removal} = \frac{\text{Initial conc - final conc}}{\text{Initial conc}} \text{x}100 \qquad (2.1)$$

Kinetic models

The process was studied by fitting it on pseudo-first order, pseudo-second order and intra-particle diffusion kinetics.

The non-linear form of pseudo-first order model is given as

$$q_t = q_e[1-\exp(-k_f t)] \qquad (3.2)$$

Where

q_e = mass of the dye adsorbed at equilibrium

q_t = mass of adsorbed at equilibrium time t (mg/t)
k = equilibrium constant

The non-linear form of pseudo-second order model is given below as:

$$q_t = \frac{K_s.q_e^2.t}{1+K_s.q_e.t} \qquad (3.3)$$

Where
q_t = amount of dye ions on the adsorbent surface (mg/g) at any time t.
q_e = the amount of dye ions adsorbed at equilibrium (mg/g)
k_s = equilibrium constant

Where
K_s is the pseudo-second order rate constant (g/mg/min)
The linear plot of t/q_t against t confirms the model.

The intraparticle diffusion equation is expressed as:

$$q_t = k_{id}\sqrt{t} + C \qquad (3.5)$$

Where
k_i = Intra-particle diffusion rate constant (mg/g $min^{0.5}$); and
C = Constant.

Determination of Surface Area

The specific surface area of CuO nanoparticles was estimated using Sear's method by agitating 1.5g of the CuO nanoparticles in 100ml of diluted hydrochloric acid of a pH = 3. Then a 30g of sodium chloride was added with stirring and the volume was made up to 150ml with deionized water. The solution was titrated with 0.1M NaoH and the volume, V, needed to raise the pH from 5-10 was then recorded. The surface area according th this method was calculated by the following equation:

$S\ (m^2g^{-1}) = 32V-25$

Where, V is the volume of sodium hydroxide required to raise the pH of the sample from 5-10. This volume was measured in replicate and the average value was taken for the surface area calculation (Alzaydien, 2009).

Determination of Bulk Density of CuO Nanoparticles

The method of Okaka and Potter (1979) was used to determine the bulk density. 2g of CuO nanoparticles was put into a 10ml measuring cyclinder and tapped to a constant volume and the bulk density (gcm^3) calculated using the formula:

$$\text{Bulk density} = \frac{\text{Weight of Copper (II) Oxide nanoparticles (g)}}{\text{Copper (II) Oxide nanoparticles volume}(cm^3)}$$

Determination of optimum pH

The effect of pH on the adsorption of the dye ion on the adsorbent (CuO nanoparticles) was analyse by varying the pH of the solution 2.0, 4.0, 6.0, 8.0 and 10.0 with the addition of either HCl or NaOH. The experiment was carried out at constant adsorbent dosage of 10mg with constant concentration of 15ppm at a constant time of 60min.

RESULTS AND DISCUSSION

The physical properties of the Copper (II) Oxide nanoparticles adsorbent were analyzed. The properties analyzed are shown in Tables 1 and 2.

Table 1: Physical properties of Copper (II) Oxide nanoparticles adsorbent

Specific surface area (m^2g^{-1})	13.1
Bulk density (g/cm^3)	0.79

Table 2: Optimum pH for adsorption of dyes onto Copper (II) Oxide nanoparticles

Optimum pH	Value
Congo Red	2
Methylene Blue	8

Table 1 show the specific surface area and bulk density of the Copper (II) Oxide nanoparticles adsorbent prepared. The value of the specific surface area was $13.1m^2/g$ which is in agreement with literatures (Hedberg, 2016) and the bulk density was 0.79 g/cm^3. Table 2 show that the pH of the dyes for optimum adsorption onto the prepared Copper (II) Oxide nanoparticles adsorbent were 2 for Congo Red dye and 8.0 for Methylene Blue dye.

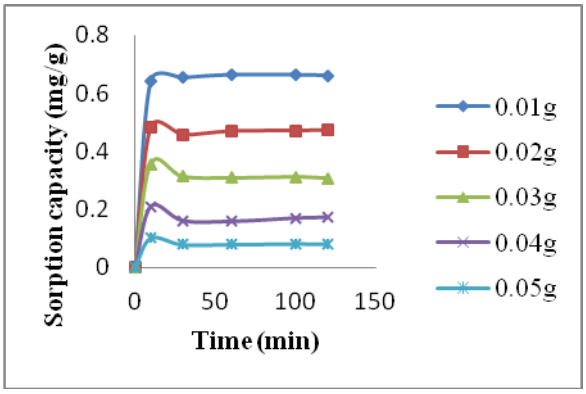

Figure 1: The sorbed capacity against time for the effect of varied doses on the sorption kinetics of Congo red dye onto Copper (II) Oxide nanoparticles at pH = 2.0

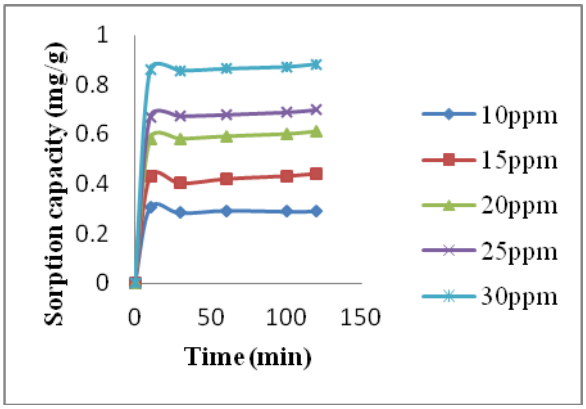

Figure 3: The sorbed capacity against time for the effect of varied concentration on the sorption kinetics of Congo red dye onto Copper (II) Oxide nanoparticles at pH = 2.0

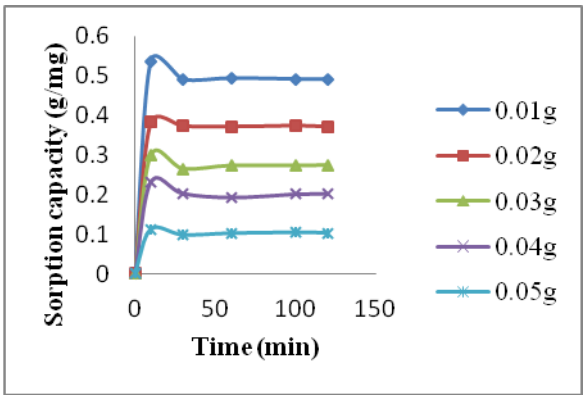

Figure 2: The sorbed capacity against time for the effect of varied doses on the sorption kinetics of Methylene blue dye onto Copper (II) Oxide nanoparticles at pH = 8.0

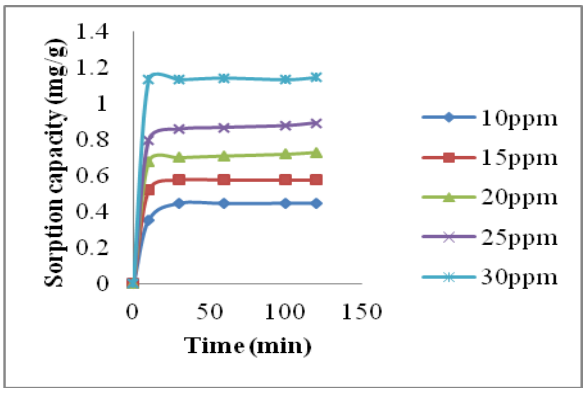

Figure 4: The sorbed capacity against time for the effect of varied concentration on the sorption kinetics of Methylene blue dye onto Copper (II) Oxide nanoparticles at pH = 8.0

Table 3: Congo red experimental data for dosage fit to models

Doses (g)	Pseudo-first order	Intra-particle diffusion	Pseudo-second order
0.01	q_e=0.66002853 k=0.360045534 r^2=0.999811313	K_{id}=0.002512 C=0.637658 $r^2$0.999812	q_e=0.664189 k=0.223483 r^2=0.999938
0.02	q_e=0.469748017 k=2.27599877 r^2=0.998114839	K_{id}=0 C=0.469258 r^2=0.998108	q_e=0.469754 k=0.219249 r^2=0.998114
0.03	q_e=0.31915494 k=2.070953451 r^2=0.979861084	K_{id}=0 C=0.319915 r^2=0.979861	q_e=0.319921 k=0.378505 r^2=0.979861
0.04	q_e=0.1746 k=0.024362 r^2=0.963288122	K_{id}=0 C=0.176668 r^2=0.93779	q_e=0.176672 k=0.866095 r^2=0.93779

Doses (g)	Pseudo-first order	Intra-particle diffusion	Pseudo-second order
0.05	q_e = 0.085732093 k = 2.141975737 r^2 = 0.941739684	K_{id} = 0 C = 0.08735 r^2 = 0.985834	q_e=0.085856 k=0.491574 r^2=0.985834

Table 4: Methylene blue experimental data for dosage fit to models

Doses (g)	Pseudo-first order	Intra-particle diffusion	Pseudo-second order
0.01	q_e=0.500655 k=2.44668 r^2=0.992266	K_{id}=0 C=0.500655 r^2=0.992266	q_e=0.500661 k=0.54888 r^2=0.992265
0.02	q_e=0.374638 k=2.133653 r^2=0.999392	K_{id}=0 C=0.374638 r^2=0.999392	q_e=0.374653 k=0.49931 r^2=0.999391
0.03	q_e=0.277309 k=0..483755 r^2=0.989652	K_{id}=0 C=2.77287 r^2=0.989652	q_e=0.277295 k=0.41778 r^2=0.989651
0.04	q_e=0.207085 k=0.579111 r^2=0.975471	K_{id}=0 C=975471 r^2=0.975471	q_e=0.207088 k=0.39131 r^2=0.975471
0.05	q_e=0.104004 k=0.759803 r^2=0.988485	K_{id}=0 C=0.104004 r^2=0.988485	q_e=0.104006 k=0.27336 r^2=0.996028

Table 5: Congo red experimental data for concentration fit to models

Concentration (ppm)	Pseudo-first order	Intra particle diffusion	Pseudo-second order
10	q_e=0.291958603 k=0.882438249 r^2=0.996647701	K_{id}=0 C=0.291964 r^2=0.996648	q_e=0.291886 k=0.38123 r^2=0.996643
15	q_e=0.425225511 k=0.922222022 r^2=0.994051412	K_{id}=0.002647 C=0.405322 r^2=0.995939	q_e=0.42704 k=0.32317 r^2=0.994159
20	q_e=0.594229398 k=0.231351999 r^2=0.997693536	K_{id}=0.003841 C=0.565338 r^2=0.999752	q_e=0.602402 k=0.949284 r^2=0.998843
25	q_e=0.681168214 k=0.570384829 r^2=0.998522485	K_{id}=0.003543 C=0.65456 r^2=0.999856	q_e=0.68892 k=0.193432 r^2=0.999316
30	q_e=0.86884384 k=0.459691068 r^2=0.999364004	K_{id}=0.004354 C=0.83453 r^2=0.999684	q_e=0.872498 k=0.125752 r^2=0.999504

Table 6: Methylene blue experimental data for concentration fit to models

Concentration (ppm)	Pseudo-first order	Intra particle diffusion	Pseudo-second order
10	q_e=0.449651 k=0.157349 r^2=0.999907	K_{id}=0.009904 C=0.357599 r^2=0.981478	q_e=0.468742 k=0.742193 r^2=0.996028
15	q_e=0.378806 k=0.232861 r^2=0.999997	K_{id}=0.165197 C=0 r^2=1	q_e=0.589627 k=1.407602 r^2=0.999263
20	q_e=0.717199 k=0.298608 r^2=0.99882	K_{id}=0.006038 C=0.664716 r^2=0.999913	q_e=0.726459 k=1.934329 r^2=0.999529
25	q_e=0.874796 k=0.243575 r^2=0.99882	K_{id}=0.010501 C=0.780967 r^2=0.998806	q_e=0.892232 k=0.945737 r^2=0.999759
30	q_e=1.139544 k=0.540399 r^2=0.999899	K_{id}=0.001043 C=1.130724 r^2=0.999921	q_e=1.141072 k=0.11424 r^2=0.999911

Congo red and Methylene blue dyes for varied dosages showed rapid dye sorbed increased with time in the early stage and very slowly towards the end as showed in Figures 1 and 2. The plot showed that large fractions of the total amount of the dye (Congo red and Methylene blue dyes) were removed within the first 10 minutes. Figures 1 and 2 also showed that sorption capacity increased as the dosage of Copper (II) oxide nanoparticles decreased at any given time.

The experimental data for the adsorption of Congo red and Methylene blue dyes onto Copper (II) oxide nanoparticles for varied dosages and initial dye concentrations were fitted to pseudo-first order, pseudo-second order, and intra-particle diffusion models. The data obtained were fitted into three kinetic models and the parameters and regression coefficients were obtained as shown in Table 3. This is in agreement with similar trend recorded where pseudo-second order kinetic model was more favourable than pseudo-first order kinetic for the adsorption of Methylene blue dye (Santi *et al*, 2009). The data obtained from the experiment for the varied Copper (II) oxide nanoparticles doses of 0.01g, 0.02g, 0.03g, 0.04g, and 0.05g at 240rpm with a fixed initial dye concentration of 15ppm for both dyes used showed that when the three kinetics models were compared, the pseudo-second order kinetic model with R^2 values 0.999938, 0.998114, 0.979861, 0.93779 and 0.985834 for Congo red and R^2 values 0.992265, 0.999391, 0.980651, 0.975471 and 0.996028 for Methylene blue respectively showed best fit for the sorption of Congo red and Methylene blue dyes as could be seen in Tables 3 and 4.

Intra-particle diffusion model is used to explain the rate of adsorption dye onto the surface of the adsorbent. In agreement with intra-particle diffusion model over pseudo-first and pseudo-second order (Nigam, 2000), Congo red and Methylene blue dyes for varied initial dye concentrations showed rapid dye sorbed increased with time in the early stage and very slowly towards the end as showed in Figures 3 and 4. The plot showed that large fractions of the total amount of the dye (Congo red and Methylene blue dyes) were removed within the first 10 minutes. Figure 3 and 4 also showed that sorption capacity increased as the dye concentrations increased at any given time. Three kinetic models were used for this study. The data obtained from the experiment where Copper (II) Oxide nanoparticles of fixed dosage of 0.01g at 240rpm was used for Congo red and Methylene blue dye concentrations of 10, 15, 20, 25, and 30ppm, showed that when the three kinetic models were compared, the intra particle diffusion model with R^2 values 0.996648, 0.995939, 0.999752, 0.999856, and 0.999684 for the sorption of Congo red and R^2 values 0.981478, 1.0, 0.999913, 0.998806 and 0.999921 showed best fit for the sorption of Methylene

blue dye onto Copper (II) Oxide nanoparticles as could be seen in Tables 5 and 6. Similar trend were recorded for the removal of dyes (Mishra *et al*, 2009; Santi *et al*, 2009 and Nigam, 2000).

CONCLUSION

The adsorbent, Copper (II) oxide nanoparticles was synthesized and physicochemical properties analysed. Adsorption behaviour of Congo red and Methylene blue dye onto Copper (II) oxide nanoparticles was investigated and was found to be spontaneous. The prepared Copper (II) oxide nanoparticles exhibited some adsorption capability for the removal of Congo red and Methylene blue dyes. The obtained experimental data were fitted into three kinetic models: Pseudo-first order, Intra particle diffusion and Pseudo-second order. Pseudo-second order was observed to have the best fit for both Congo red and Methylene blue at varied initial dye concentrations, while Intra particle diffusion showed best fit for varied doses of Copper (II) oxide nanoparticles with highest regression coefficient.

REFERENCES

Akrout, H., Jellal,i S., and Bousselmi, L. (2015). *Enhancement of Methylene blue removal by anodic oxidation using BDD electrode combined with adsorption onto sawdust*. C R Chimie. Vol. 18, pp. 110–120.

Alzaydien, A.S. (2009). *Adsorption of Methylene blue from aqueous solution onto lower cost natural Jordanian Tripoli*. American Journal of Engineering Science Vol. 5, no. 3, pp. 197-208.

Ejhieh, A. N., Shohreh, H. (2010). *Solar photodecolourization of methylene blue by CuO/X zeolite as a heterogeneous catalyst Applied Catalysis A*: Vol. 388, pp. 149–159.

Elahmadi, M. F., Bensalah, N. and Gadri, A. (2009). *Treatment of aqueous wastes contaminated with Congo red dye by electrochemical oxidation and ozonation processes*, J. Hazard. Mater. Vol. 168, pp. 1163–1169.

Hahens, W. I., Oomen, A. G., Dejong, W. H. and Cassee, F. R. (2007). *What do we (need to) know about the kinetic properties of nanoparticless in the body*? Regulatory Toxicology and Pharmacology. Vol. 49, p. 217-229.

Harvey, J. W., Keitt, A. S. (1983). *Studies of the efficacy and potential hazards of Methylene blue therapy in aniline-induced methaemoglobinaemia*, Br. J. Haematol. Vol. 54, No.1, pp. 29-41.

Hedberg,Y. S., Pradhan, S. Cappellini, F., M.-E. Karlssona, M-E, Blomberg,E. Karlsson, H.L., Odnevall Wallinder, I. Hedberg, J.F. (2016). *Electrochemical surface oxide characteristics of metal nanoparticles (Mn, Cu and Al) and the relation to toxicity*. Electrochimica Acta 212, 360–371.

Khadhraoui, M., Trabelsi, H., Ksibi, M., Bouguerra, S. and Elleuch, B. (2009). *Discolouration and detoxicification of a Congo red dye solution by means of ozone treatment for a possible water reuse*, J. Hazard. Material. Vol. 161, pp. 974–981.

Maraval, V., Pyzowski, J., Caminade, A. M. and Majora,l J. P. (2003). *LegoQ chemistry for the straightforward synthesis of dendrimers*, J. Org. Chem. Vol. 68, p. 6043-6046.

Mishra, S., Prakash, D.J. and Ramakrishma, G. (2009). *Characterization and Utilization of Mahua Oil Cake-A New Adsorbent for Removal of Congo red Dye from Aqueous phase*. Electronic Journal of Environmental, Agricultural and Food Chemistry Vol.8, no. 6, pp.425-436.

Mittal, A., Mittal, M. J. and Gupta, V. K. (2009). *Adsorptive removal of hazardous anionic dye ''Congo red'' from wastewater using waste materials and recovery by desorption*, J. Colloid Interf. Sci. Vol. 340, pp. 16–26.

Mokhlesi, B., Leikin, J. B, Murray, T. C. (2003). *Corbridge, Adult toxicology in critical care: Part II: specific poisonings, Chest*. Vol. 123, pp. 3897-922.

Murcia, M. D., Gomez, M. E., Gomez, J. L. and Gomez, N. (2011). *Photodegradation of Congo red using XeBr, KrCl and Cl_2 barrier discharge excilamps: a kinetics study, Desalination*. Vol. 281, pp. 364–371.

Ng, I.S., Chen, T., Lin, R., Zhang, X., Ni, C., Sun, D. (2014). *Decolorization of textile azo dye and Congo red by an isolated strain of the dissimilatory manganese-reducing bacterium Shewanella xiamenensis BC01*, Appl. Microbiol. Biotechnol. Vol. 98, pp. 2297–2308.

Nigam, P., Armou, G., Banat, I.M., Singh, D., and Marchant, R., (2000). *Physical removal of textile dyes and solid-state fermentation of dye-adsorbed agricultural residues*. Bioresource Technology, vol. 72, pp.219-226.

Okaka, J.C. and Potter, N.N (1979). *Physicochemical and Functional Properties of Cowpea Powders Processed to Reduce Beany Favours*. Journal of Food Science Vol. 44, pp. 1235-1240.

Patel, H. and Vashi, R. T. (2012). *Removal of Congo red dye from its aqueous solution using natural coagulants*, J. Saudi Chem. Soc. Vol. 16, pp. 131–136.

Purkait, M. K., Maiti, A. and DasGupta, (2007). *Removal of Congo red using activated carbon and its regeneration*, J. Hazard. Mater. Vol. 145, pp. 287–295.

Rafatullaha, M., Othman, S., Rokiah, H., Anees, A. (2010). *Adsorption of Methylene blue on low-cost adsorbents: A review*, Journal of Hazardous Materials. Vol. 177, pp. 70–80.

Ravi, K., Deebika, B. and Balu, K. (2005). *Decolourization of aqueous dye solutions by a novel adsorbent: application of statistical designs and surface plots for the optimization and regression analysis*, J. Hazard. Mater. B., Vol. 122, pp 75- 83.

Santi, T., Manonamani, S., Sugirtha, D., and Mahalakshmi, K., (2009). *Uptake of cationic dyes from aqueous solution by bio-adsorption onto granular cucumis sativa*, Journal of Applied Science in Environmental Sanitation, Vol.4, pp.29-35.

Schmid, G. (1994). *Clusters and Colloids: From Theory to Applications. New York*: Wiley& Sons. Weinheim/VCH Publishers. Pp. 753-754

Suleiman, M., Jisrawi, N. M., Dankert, O., Reetz, M. T., Bähtz, C., Kirchheim, R. and Pundt, A., (2003). Journal Alloys Comp, Vol. 356, pp. 644-648.

Tor, A., and Cengeloglu, Y., (2006). *Removal of Congo red from aqueous solution by adsorption onto acid activated red mud*, J. Hazard. Mater. Vol. 138, pp. 409 – 415.

Xiao, S. L., Li, Y. H., Ma, P. J. and Cui, G. H. (2013). *Synthesis and characterizations of two bis (benzimidazole) based cobaltous coordination polymers with high adsorption capacity for Congo red dye*, Inorg. Chem. Commun. Vol. 37, pp. 54–58.

Zhang, J., Liu, J., Peng, Q., Wang, X. and Li, Y. (2006). *Chem. Mater*. Vol. 18, No. 4, pp. 867-871.

Zhou K.,Wang, R., Xu, B. and Li, Y. (2006). *Nanotechnology*. Vol. 17, No. 15, pp. 3939.

PHAGO-REPELLENCY OF CULICIDAE BY APPLICATION OF NEEM SEED KERNEL EXTRACT

Sampson, I. E.
Department of Chemical Engineering, Rivers State University, Port Harcourt, Nigeria.
idongesit.sampson@ust.edu.ng

ABSTRACT

The extract from the seed of the Neem tree (Azadirachta indica) is known for its use by traditional medicine practitioners and its local use as mosquito repellent but little is known about its chemical properties. This research studies the efficacy of the use of the Neem Seed Kernel Extract (NSKE) as a mosquito (culicidae) repellent. Mosquito repellent is necessary considering that mosquitoes are detrimental to human health and economy. Local production and use of this repellent could enhance the Nigerian content in Phyto- chemical production and also increase the Nigerian Gross Domestic Product. NSKE mosquito repellent is better than synthetic mosquito repellent for its low mammalian toxicity. Activity test revealed an active area of 0.7855 m^2; active period of 3 hours of rubbing, 45 minutes for spraying and as long as the lantern keeps burning for burning. The repellent should be re - applied after the recommended active period. The repellent breaks away into harmless products within a reasonable time. By this, it cannot produce harmful effects on man nor pollute his environment. Chromatographic and spectrophotometric analysis revealed that NSKE contains four methyl esters with 11, 14 - Eicosadienoic acid being the most active. These were found to produce phago-repellent anti-feeding effect but majority of the mosquitoes still recovered after the active period when the repellent was completely metabolized. This was okay, as the real effect is to stop the mosquitoes from biting not necessarily killing the mosquitoes. Besides mosquitoes, the repellent can be used to repel other insect pests.

***Keywords**: Phago-repellent, Active Period, Active area, Active component, Spectrophotometric, Culicidae, Neem Seed Kernel Extract*.

1.0. INTRODUCTION

Sampson (1999) state that much work has been done on the production of insect repellent using petrochemicals but little has so far been done on the production of insect repellent from a natural source which has no acute toxicity to mammals but with negligible or no chronic effects. Sampson (1999) empirically found that the NSKE is not lethal, it repels the target mosquitoes without causing a total irreversible unresponsiveness to tactile stimulation. According to world health organization (WHO) "malaria takes life every fifteen seconds" it kills more than AIDS, Cancer or Asthma (Kristof, 1997).

Most seeds, farm animals and domestic animal kept indoors cannot be attacked by insect pests where the repellent is burnt or sprayed. This study is therefore of tremendous importance not only for improving the health of man but also for enhancing better storage not prone to attack by insect pest. Animal disease can also be prevented by the use of this product.

Moreover, the psychological state of man is improved when he is in the best state of health. According to World Health Organization (WHO) this has a relationship to intellectuality (World health report, 2001). It is therefore believed that if these disease vectors prevalent in the tropical region are gotten rid off or controlled effectively, the tropical man can easily measure up with the temperate men in terms of intellectuality. The result of this will be a fast developed technology, which of course we are yearning for. Besides an improved technological development, there will also be an improvement in the efficiency of the labour force. The workers work faster and more accurately under the best health conditions. Having examined the importance of the product, it has been realized that the product is low cost, so it is possible to produce it in commercial scale to meet the demands of Nigerians for the product. A chemical process plant can therefore be established to produce the product in large capacity.

The natural extract of neem seed kernel is phago-repellent (Buckingham & Cadogan,1982). The insect may starve to death while still remaining on its host in the presence of an anti-feeding compound (Green *et al*., 1987). Moreover, the larvae which do consume the

compound despite the repellency have both molting and growth delayed and eventually die. The repellent is very effective a short distance from its point of application, hence more effective for indoor pests. According to Food and Agricultural Organization (FAO) and World Health Organization (WHO) insecticides account for 500,000 poisonings and 500 deaths which occur annually in developing countries and this is a problem which the developing countries should address (WHO,2014).

1.0.1. Insect Repellency Component

NSKE contains a natural insect pest repellent called Azadirachtin, a methyl ester and a powerful antifeedant with empirical formula $C_{35}H_{44}O_{16}$. It is built up of 17 membered, 36 membered and 25 membered rings which can be represented in planar form but with two ringed bridge. Four of the oxygen atoms are ring members but there is only one double bond. Three carboxyl groups are attached, two esterified with methyl and one with enol form of butanone. Two hydroxyl and one acetyloxyl groups are attached. Simpler synthetic compounds related to this complex structure are being sought. Azadirachtin ($C_{35}H_{44}O_{16}$) is a constituent of the seeds of melia Azadirachta and the Indian neem tree (Azadirachta indica). Buckingham & Cadogan (1982) state that Azadirachtin is a very active phago- repellent and systematic disruptor. The repellent is effective over a reasonable time interval and acts over a short distance from the point of its application. It acts by displacement or morbidity of the insect pest but discontinuation of application after a short period of activity results in re-occurrence of the insect pests. Throughout the active period of the repellent the target pest is rendered inactive. This means that there will be no mosquito bites during the active period.

2.0. MATERIALS AND METHODS

2.1. Materials

The following materials were used for the study:
Ati Matson infra- red Spectrophotometer; Schimadzu 160 A Ultra-Violet Spectrophotometer; Carbon-13 Nuclear Magnetic Resonance Spectrophotometer; Proton Nuclear Magnetic Resonance Spectrophotometer; Schimadzu Gas Chromatograph-Mass Spectrophotometer; Round bottomed flask; Anti-bumping granules; Neem seed kernel extract; Petroleum ether; Sodium ethoxide; Methanol; Sodium hydrogen sulphate; Sodium sulphate.

Table 1: Spectrophotometric Methods of Analysis

Methods	Application
UV&IR	Detection of functional groups
NMR	Detection of position of functional groups on parent atom
GC-MS	Detection of major components of interest in a sample

2.2. Methods

2.2.1. Determination of Mosquito Repellency Component

2.2.1.1. Infra-red Spectrophotometry

The Neem Seed Kernel Extract was bombarded with infra – red radiation. The wave band corresponding to different functional groups were used to detect the functional groups

2.2.1.2. Ultra -violet Spectrophotometry

The ultra-violet spectrophotometer was used to confirm the functional groups detected by the infra-red spectrophotometry and to differentiate between them.

2.2.1.3. Nuclear Magnetic Resonance

Besides proton NMR, the carbon-13 NMR spectrophotometer was used for this analysis because it allows more detailed analysis of structural features of fairly large molecules. The extract was placed in a magnetic field and bombarded with electromagnetic radiation. The orientation of the magnetic nuclei changed as a result of resonance absorption of

electromagnetic radiation. From the NMR spectrum, the intensity of each peak was obtained as the area under each peak in the NMR spectrum. The position and intensity of lines in the NMR spectrum was used to locate the position of the functional groups as they are attached to the parent atom.

2.2.1.4. Gas Chromatograhpy-Mass Spectrophotometry

Methylation:

Methylation was carried out in order to make the extract volatile enough not to block the chromatographic column and damage the equipment.

5 ml of the sample oil was added to 10 ml of petroleum ether in a round bottomed flask. A few drops of anti-bumping granules were added after which 1 ml of sodium ethoxide and 0.5N dry methanol was added. The mixture was refluxed for 5 minutes at 40 ^{0}C in a water bath and 2 ml of $NaHSO_4$ added in order to neutralize excess sodium ethoxide. The mixture was allowed to settle and the upper layer taken. A little Na_2SO_4 was then added in order to absorb moisture.

Equipment:

The (GC-MS), a standard equipment, was used to detect the various components of the neem seed kernel extract. It has an inbuilt standard so it can
detect even the minutest components very efficiently. The interfacing of chromatographic columns to mass spectrophotometers permits instantaneous display of the spectrum of each species as it leaves the chromatographic column. The instrument is also interfaced with a computer so that each spectrum is digitalized and stored for later production. With a gas chromatograph alone, components with almost similar peak heights and retention times may be imbibed in the other components, hence the need to combine gas chromatograph with mass spectrophotometer. A Mass spectrophotometer bombards the substance under investigation with an electron beam and quantitatively records the result as a spectrum of positive fragments.

Procedure:

1 µL of the methylated extract was weighed and injected into a carrier (He) gas supplied from high-pressure cylinders at constant flow rate and pressure. The injected sample was heated to vapour and carried by the carrier gas to a hydrogen flame ionization detector maintained at constant temperature and supplied with combustion air and hydrogen. The detector retention time (time taken to elude the column) and a recorder recorded peak heights of each component. The retention time was used to identify the component but the peak height was used to determine the amount of each component.

UV and IR Spectrophotometry

The following Functional groups were detected:
CH_3; C = C; –COO; CO_2ME; AOC; –OH; –O; C-C; C-H

3.0. RESULTS AND DISCUSSION

3.1. U.V SPECTROPHOTOMETRY

According to Basler (1991) a peak range of 425 -445 Nm show the presence of methyl ester. 441.0 Nm confirm methyl ester group.

3.2. Nuclear Magnetic Resonance

The functional group detected by the ultraviolet (UV) and the infrared (I.R) spectrophotometry are attached at the following positions on the parent atom:

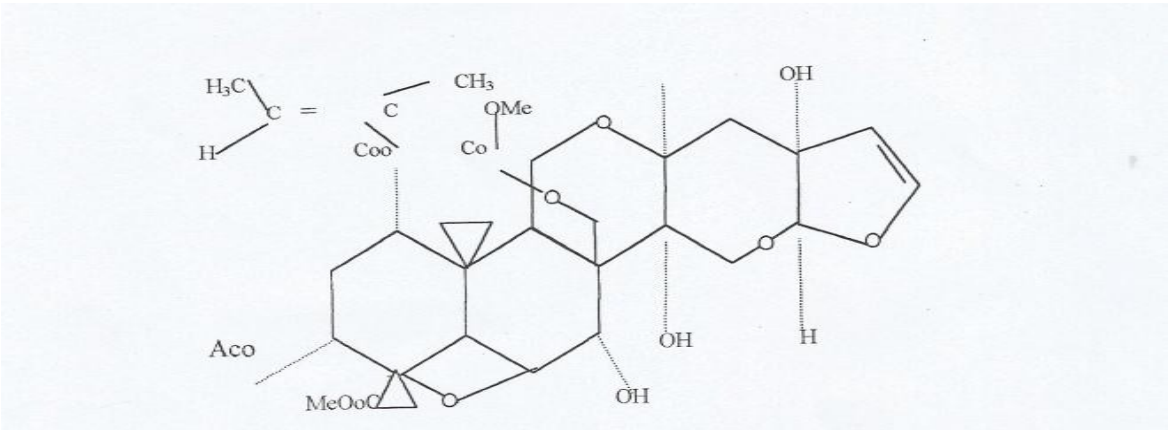

Chemical formula: $C_{35}H_4O_{16}$

Fig.1: Positions of Functional Groups on Parent Atom as detected by NMR

3.3. Gas Chromatography-Mass Spectrophotometry.

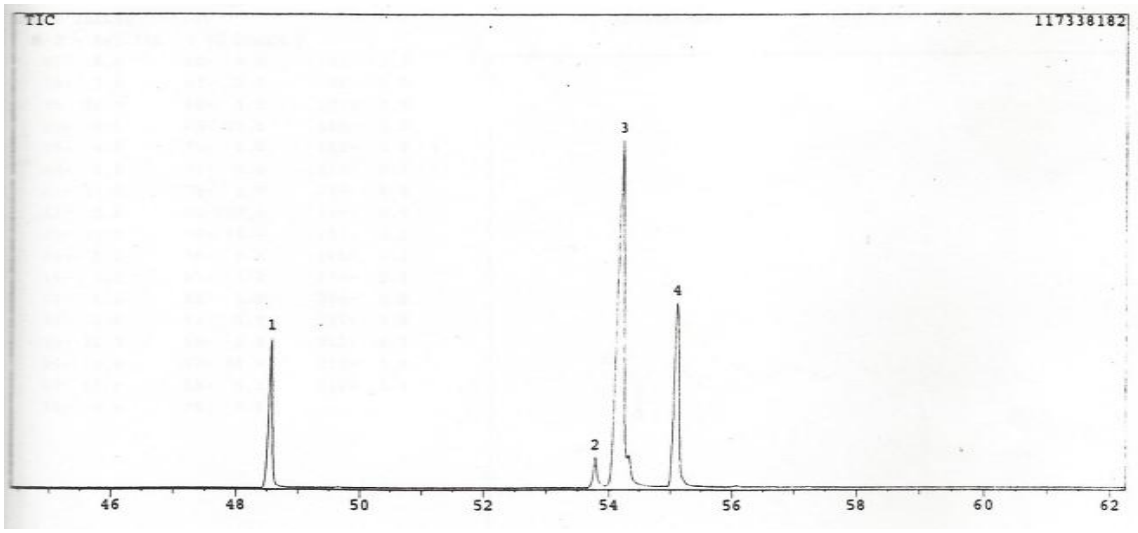

Fig 2: Gas Chromatography-Mass Spectrophotometry Waveform

From the GC –MS analysis and GC-MS library information the major components of the neem seed kernel extract were as follows:

Peak 1: **Tetradecanoic Acid (Methyl Ester)**

Structure:

$CH_3(CH_2)_{12}\,C(=O)\,–OCH_3$

Mol. Wt. 242 **Percentage**: 15.02 **Formula**: $C_{15}H_{30}O_2$

Peak 2: 11, 14 – Eicosadienoic Acid (Methyl Ester)

Structure:

$CH_3(CH_2)_4\,CH = CH\text{-}CH_2 = CH – (CH_2)_9\,C(=O) –OCH_3$

Mol.Wt. 322 **Percentage:** 2.95 **Formula**: $C_{21}\,H_{38}\,O_2$

Peak 3: 10 – Octadecenoic Acid (Methyl Ester)

Structure:

$CH_3(CH_2)_6CH =CH\,(CH_2)_8 – C(=O) – OCH_3$

Mol.Wt. 296 **Percentage**:59.10 **Formula:** $C_{19}H_{36}\,O_2$

Peak 4: Octadecanoic Acid, (Methyl. Ester) or Stearic Acid

Structure:

$CH_3\,(CH_2)_{16}\,C(=O) –OCH_3$

Mol.Wt. 298 **Percentage:** 22.92

Formula:$C_{19}H_{38}O_2$

Removal of one methyl group from each of the above methyl esters yield their corresponding free fatty acids which are palmitic. Arachidonic and oleic acids respectively, the fourth is stearic acid. According to Kenneth (1990) an insect repellent must have the following properties: A methoxyl group, Ester linkage to a leaving group, hydrophobicity and unsaturation. Another property that gives these methyl esters insect repellency property is that they are highly volatile, easily distilled and vaporized into air and hence effective in repelling the target mosquitoes. It is known that the presence of double bond show the level of unsaturation and hence reactivity, therefore among the four methyl esters 11, 14 – Eicosadienoic Acid appears to be the most active followed by 10-Octadecenoic Acid. Chromatographic and spectrophotometric analysis reveals that the neem seed kernel extract contains four methyl esters close to the structure of azadirachtin. These methyl esters are active, easily distilled and vaporized into air; hence their effectiveness in causing mosquito repellency action of the extract. 11, 14 – Eicosadienoic Acid is the most active because of the presence of two double bonds.

Combustion Products

These methyl esters detected by GC-MS react with indigenous groups and Oxygen to produce toxic metabolites. That is why it is more effective when burnt. The combustion reaction increases the toxicity of the repellent to the target mosquitoes. A further research to investigate the combustion products may require Air space chromatography which is not available in Nigeria.

3.4. Formulation

Being considered to be the most reactive 11, 14 – Eicosadienoic acid is considered the active component for this formulation.

$$Basis: 0.5\ ml\ oil + 1\ ml\ kerosene = 1.5\ ml\ (\mathbf{1})$$

Table 2: Formulation of the Repellent

Component	Calculation	Percentage
Kerosene	$\frac{1}{1.5} \times \frac{100}{1} = 66.6667$	66.6667
Eicosadienoic acid	$100 - 66.6667 = 33.33$ $\frac{2.95}{100} \times 33.33 = 0.9832\%$	0.9832
Other Components	100 – 66.6667 – 0.9832 = 32.3501%	32.3501
	Total	100

3.5. Applicability Characteristics

Subjecting a sample of the NSKE to extremes of temperature 0^0C, 50^0C and 100^0C, vibration, compression and to sunlight without the NSKE changing in physical properties proved that the NSKE is physically stable. Igniting a sample of the NSKE proved it has a high flash point and hence could be mixed with kerosene and burnt in lanterns without addition of synergist nor humectant. Without these additives, the advantage of low mammalian toxicity was maintained as most of these additives are toxic. Besides burning in lanterns, the repellent can equally be sprayed or rubbed.

Table 3: Active Period for different methods of Application

Method of Application	Active Period
Burning	**As long as the Lantern keeps burning**
Rubbing	3 hours
Spraying	45 minutes

Active Period

Burning is therefore a better method but the spraying and rubbing could frequently be renewed after the active period. The repellent was found to be non-toxic to man and his domestic animals but highly toxic to the target mosquitoes.

Active Area

$$Active\ area\ under\ closed\ door = Area\ of\ the\ room \quad (2)$$

$$Active\ area\ under\ open\ door = \pi r^2 \quad (3)$$

$$3.142 \times 50^2\ cm = 3.142 \times 2500 = 7855 cm^2 = 0.78855 m^2$$

$$The\ number\ of\ lanterns\ needed\ per\ 0.7855 m^2 = \frac{Area\ of\ the\ living\ room\ in\ m^2}{0.7855 m^2} \quad (4)$$

If the room is square or rectangle or triangular in shape, the area is calculated in terms of a circle circumscribing the room.

4.0. CONCLUSION

It is concluded that:

The Neem Seed Kernel Extract is best for use in the production of mosquito (culicidae) repellent considering that it is cheap and readily available, non-toxic to man and his domestic animals and contains an appreciable quantity of oil. Moreover, the extract can be stored for a reasonable long time without going rancid. Repellent produced from neem seed kernel is active within a short time over a small range of area. The advantage of this is that it is confined to the user at the time he needs it. Moreover, being biodegradable, the repellent breaks away to harmless products within a reasonable time. By this, it cannot produce harmful effects on man nor pollute his environment (soil, water and air). The repellent is non-hazardous and non-toxic to man and his domestic animals but highly toxic to the target

mosquitoes through the anti-feeding or phago-repellent action of the active component (Azadirachtin), a complex methyl ester, an unstable compound which transforms itself into four simpler methyl esters as confirmed by GC – MS analysis. These methyl esters are active in one way or the other, but 11, 14 – Eicosadienoic Acid has structure closest to azardirachtin. It is the most active because of the presence of two double bonds. Local production and use of the repellent could enhance the Nigerian content in phytochemical production,,increase the Nigerian Gross Domestic Product hence advancing the Nigerian economy.

5.0. RECOMMENDATIONS

The following recommendations are made:

(i) Considering the importance of neem in the control of insect pest which hampers economy, the government should set up an agency in the forestry department to promote the plantation of neem trees in large numbers by setting up neem forests.

(ii) Considering the deleterious effects of mosquitoes and other insect pests on the economy, the government should set up an industry for production of insect repellent from neem seed kernel extract in large capacity.

(iii) To increase level of awareness on the advantages of the new product, government should organize an extension education service to educate the masses on the NSKE mosquito repellent.

Besides the production of mosquito repellent, Neem Seed Kernel Extract (NSKE) can also be used for soap production, tooth paste, cream, waxes, lubricants and fuel; government should therefore encourage research on the use of NSKE for these products.

6.0. NOMENCLATURE

Abbreviation	Definition
AC	Active Component
EPA	Environmental Protection Agency
FAO	Food and Agricultural Organisation
GC-MS	Gas Chromatography- Mass Spectrophotometry
GDP	Gross Domestic Product
IR	Infra-red
NMR	Nuclear Magnetic Resonance
NSKE	Neem Seed Kernel Extract
UV	Ultra-Violet
WHO	World Health Organisation

REFERENCES

Basler, C.(1991) Spectrophotometry. USA: Basler Electrical Company.

Buckingham, J. B & Cadogan, R.A.(1982). Dictionary of organic Compounds.Vol1,5th edition, New York: Chapman & Hall.

Green, M. B; Hartley, G. S & West, T. F.(1987). Chemicals for Crop Improvement and Pesticide management. 3rd edition, New York: Pergamon Press.

Kenneth, A. H.(1990). The Chemistry and uses of Pesticides, Structure, Metabolism, Mode of action and uses in crop protection.1st edition, London: Macmillan Press Ltd.

Kristof N. (January 8,1997). *Malaria makes a come back, and is more deadly than ever*. New York times.

Sampson, I. (1999). Production of Mosquito Repellent using Neem Seed Kernel Extract. 1st edition, Yola, Nigeria: Federal University of Technology.

WHO.(2001). *Mental Health,New Understanding,New Hope*. World Health report.

WHO.(2014).*Mental Health;Strengthening our response*. World Health Organisation

COMPARATIVE STUDY BETWEEN SODIUM PERSULFATE AND SODIUM HYPOCHLORITE BREAKERS FOR HYDROXYETHYL CELLULOSE AND XANTHAN POLYMERS

***John, A.O.[1], Joel, O.F.[2] and Chukwuma, F.O.[3]**

[1]World Bank African Centre of Excellence for Oilfield Chemical Research, Institute of Petroleum Studies, University of Port Harcourt, Nigeria
[2]Centre for Petroleum Research and Training, University of Port Harcourt, Nigeria
[3]Department of Chemical Engineering, University of Port Harcourt, Nigeria
tonyomarie@yahoo.com, ogbonna.joel@ipsng.org and fochukwuma@yahoo.com

ABSTRACT

Sand production is undesirable during hydrocarbon production. Gravel pack is the most popular and most robust sand control technique. Slurry or viscous pack process enables large concentration of proppants to be transported to the wellbore. Hydroxyethyl cellulose and xanthan gums possess some qualities that make them to be the most popular polymers used to formulate viscous gravel carrier fluid. The viscous gravel pack fluid must be degraded after depositing the proppant to facilitate hydrocarbon production without impairment. Various types of gel breakers are available for effective polymer degradation. The choice of the type of breaker employed depends on wellbore conditions and the type of fluid system. The rate of polymer degradation is a function of many factors including the type and concentration of breaker. In this paper, the action of sodium persulfates and sodium hypochlorite oxidizer breakers on the degradation of hydroxyethyl cellulose and xanthan based polymer fluids at various temperatures was evaluated. Sodium persulfate was effective in degrading 40 and 60 lbs/1000gal hydroxyethyl cellulose and xanthan fluids at temperatures above 140^oF and 160^oF respectively but the breaker was ineffective below these temperatures. Sodium hypochlorite effectively degraded both polymer fluids at 120^oF. Therefore, sodium hypochlorite oxidizer breaker can be used for low temperature applications where sodium persulfate is not effective without using breaker activator.

Keywords: *Formation damage, gravel pack, hydroxyethyl cellulose, sodium persulfate, sodium hypochlorite, xanthan.*

INTRODUCTION

Sand production from hydrocarbon wells has a lot of consequences which include bridging of tubings, screens, casings, separators and reduced well production. It can cause environmental hazards, high maintenance cost, formation or casing collapse and damage to surface and subsurface equipment. Sand control techniques, used to prevent or minimize sand production from wells include optimization of production rate, selective perforation or production from more consolidated intervals, use of stand alone screens (SAS), use of resin coated proppants, formation sand consolidation by chemical means, frac packing and gravel packing (Abass et al, 2002; John et al. 2016). Selection of sand control method for a particular well depends on well's configuration, type of completion and the geo-mechanical properties of the formation.

Gravel pack is the most utilized and very reliable sand control technique (El-Dhabi and Bulgachev, 2011). Gravel packing sand control method can be done for both openhole and cased hole completions, irrespective of the angle of deviation of the well. Openhole gravel packing (OHGP) commonly used in horizontal wells is very reliable with high productivity (Jain et al. 2011). Gravel packing can be deplored using water packing or slurry packing methods. Water packing (alpha/beta) uses low viscosity fluids, mostly brine, to transport low concentration gravel (typically 1ppa), relying on the pump rate or fluid velocity to transport proppants, while slurry packing relies more on the fluid viscosity to transport high gravel concentration (typically 4 to 6ppa). Advantages and disadvantages of each method have been discussed in various literatures (Thibodeaux et al, 1991; Economides et al, 1997; Jones et al, 1997; John et al, 2016). Selecting the appropriate gravel-carrier fluid system is key to success of the sand control treatment.

Factors such as bottomhole temperature (BHT), rheology, frictional pressure, sand suspension capability,

fluid density for well control, viscosifier compatibility with base brine, formation damage tendency and fluid compatibility with formation and completion fluids are to be considered while selecting gravel carrier fluids. According to (Jain et al, 2011), the three most commonly used polymer based fluids are guar, hydroxyethyl cellulose (HEC) and xanthan gums, with maximum temperature stability of 200^{o}F, 225^{o}F and 350^{o}F respectively for regular grades of the products.

HEC is synthetized from cellulose by reaction with ethylene oxide while xanthan is produced from the fermentation of micro-organism xanthomanas campestris by bacteria (Lipton and Burnett, 1976; Underdown et al, 1989; Abbas et al, 2013). Xanthan and HEC have some excellent properties such as good solubility, excellent rheology, good leak off rate and insensitivity to salinity (Underdown et al, 1989). Formation damage is a major concern with viscous gravel pack fluids. Formation damage potential of HEC fluids is attributed to some unhydrated polymer powder known as fish eyes or micro-gels. Improvement in the manufacturing process and good mixing, shearing and filtration processes has greatly reduced the formation damage potentials of the polymers (Nguyen and LaFontaine, 1983; Cole and Ali, 1994; Volmer and Alleman, 2001). HEC is cost effective, easy to degrade and has the least potential to cause formation damage (El-Dhabi and Bulgachev, 2011). High grade clarified xanthan based fluids is highly shear thinning and possesses unique properties, such as pH insensitivity, good mechanical shear resistance, good thermal stability and inherent gel strength, which makes it candidate for packing deviated and/or long intervals (Nguyen and LaFontaine, 1983; Wellington, 1983; John et al, 2016).

After proppant placement in the desired interval in the wellbore, low viscosity is required for compact packing of the proppant bed and the viscous fluid must be removed to facilitate hydrocarbon production without impairment. This is achieved by gradual degradation of the viscous polymer fluid by reaction of gel breakers. The viscous fluid polymer degradation process depends on temperature, fluid pH, salinity, type of breaker, concentration of breaker, type and concentration of polymer (Cole and Ali 1994; Al-Muhammad et al, 2007; Sarwar et al, 2011; Al-Muntasheri 2014; John et al, 2016; John et al. 2016b; John et al, 2017). Available gel breakers can be grouped into enzymes, acids and oxidizers. Oxidizer breakers include peroxides, persulfates and chlorites. Enzymes are prone to denaturing if exposed to high temperature and very low or high pH (Jennings Jr, 1996; Montgomery, 2013). Encapsulation can be used to delay the action of the breakers at high temperatures while activators is often used to catalyzed the reaction of the breakers to make them effective at low temperatures (Harris and Sabhapondit, 2009).

Oxidizer breakers function by breaking the long backbone of the polymer into smaller fragments of lower molecular weights, resulting in decrease viscosity. Persulfates type of breaker undergoes thermal decomposition to produce free sulfate radicals, while oxygen is released as peroxides comes in contact with water (Montgomery, 2013). Therefore reaction of persulfate depends on temperature and often over reactive at high temperature while peroxide type of breakers can be used at low temperature since there reaction depends on dissolution in water.

In this paper, a comparative study was performed to determine the effectiveness of sodium persulfate and sodium hypochlorite gel breakers on the most commonly used polymer for gravel pack fluids, hydroxyethyl cellulose (HEC) and clarified xanthan gums, at various temperatures. This can serve as a guide in choosing effective breaker for a particular condition and for a particular polymer.

MATERIALS AND METHOD

Viscous fluids gelled with 40lbs/1000gal (40ppt) and 60lbs/1000gal (60ppt) hydroxyethyl cellulose polymer was prepared, using 2% by weight potassium chloride brine as mix fluid. The base fluid was measured into 1 litre blender jar and additives were added in the order as shown in Table 1, while mixing at speed high enough to create a vortex without allowing air entrainment. 5 minutes after adding the HEC polymer, the pH of the mixture was raised to between 8 to 9 with sodium carbonate to facilitate full gel hydration and mixed for 30 minutes. Similarly, 40ppt and 60ppt xanthan fluids where prepared, using the same procedure as specified above. The final fluid pH for the xanthan fluid was kept between 7 and 8.

Break time of the viscous HEC and xanthan fluids was determined by measuring 200cc of the hydrated gel into glass jar and required concentration of breaker added while mixing. The mixture was placed in water bath preset to the test temperature and the viscosity periodically measured. Acceptable break is taken as fluid viscosity of 10cP or below at 511 s^{-1} shear rate, using viscometer model 35 with F1spring B1 bob and R1 rotor configuration. The break test was conducted, using 20ppt sodium persulfate (SP) breaker at and

repeated with 3.5% w/v sodium hypochlorite breaker solution at equivalence of 20ppt, at 120°F, 140°F, 160°F and 180°F.

Table 1 - HEC Fluid Recipe

Chemical	Concentration (per 1000gal)	Amount per Litre
KCl brine (2%)	1000 gal	1000 cc
Biocide 1	0.015 lbs	0.018 g
Biocide - Preservative	0.015 lbs	0.018 g
Iron Chelating Agent	10 lbs	1.2 g
HEC Gelling agent	*40 lbs	4.8 g
Sodium carbonate	20 lbs	2.4 g
Surfactant	1 gal	1 cc

*60ppt HEC fluid was also prepared

Table 2 - Xanthan Fluid Recipe

Chemical	Concentration (per 1000gal)	Amount per Litre
KCl brine (2%)	1000 gal	1000 cc
Biocide 1	0.015 lbs	0.018 g
Biocide - Preservative	0.015 lbs	0.018 g
Iron Chelating Agent	10 lbs	1.2 g
Clarified Xanthan	*40 lbs	4.8 g
Sodium carbonate	15 lbs	1.8 g
Surfactant	1 gal	1 cc

*60ppt xanthan fluid was also prepared

RESULTS AND DISCUSSION

The results for the HEC and xanthan polymer fluids break test with sodium persulfate breaker at 140, 160 and 180°F are shown in Tables 3 and 4 respectively.

Table 3- Break Test for HEC Fluid

HEC (ppt)	40	40	40	60	60	60
Sodium Persulfate (ppt)	20	20	20	20	20	20
pH of brine	5.85	5.85	5.85	5.85	5.85	5.85
Final Gel pH	8.1	8.1	8.1	8.03	8.03	8.03
Temperature (°F)	140	160	180	140	160	180
Time (minutes)	**Viscosity (cP) at 511 s^{-1} shear rate**					
0	43	43	43	98	98	98
10	27	20	10	72	68	23
20	22	10	7	65	28	8
30	19	9	6	57	16	6
60	13			50	9	
90	10			42		
120				31		
150				25		
180				20		
210				15		
240				13		
270				11		
300				10		
Break Time (minutes)	**90**	**20**	**10**	**300**	**45**	**20**

Table 4 - Break Test for Xanthan Fluid

Xanthan (ppt)	40	40	40	60	60	60
Sodium Persulfate (ppt)	20	20	20	20	20	20
pH of brine	5.85	5.85	5.85	5.85	5.85	5.85
Final Gel pH	8.21	8.21	8.21	8.14	8.14	8.14
Temperature (°F)	140	160	180	140	160	180

Time (minutes)	Viscosity (cP) at 511 s^{-1} shear rate					
0	28	28	28	42	42	42
30	23	21	16	41	36	18
60	22	20	10	40	35	12
90	22	18		40	34	10
120	21	16		40	33	
150	21	14		40	32	
180	21	13		39	31	
210	21	12		39	30	
240	21	11		38	29	
270	21	10		38	28	
300	21			38	27	
330	21			38	26	
360	21			38	26	
Break Time (minutes)	**ND**	**270**	**60**	**ND**	**ND**	**90**

The test results showed that break time decreases with increase in temperature and decrease in polymer loadings as described in other literatures (Cole and Ali 1994; Sarwar et al, 2011; Al-Muntasheri 2014; John et al, 2016; John et al, 2016b; John et al, 2017). More so, no break was observed for the 40ppt xanthan fluid at 140^{o}F and for the 60ppt xanthan fluid at 140^{o}F and 160^{o}F with 20ppt SP breaker. Incomplete or partial polymer degradation can affect the permeability of the proppant pack and restrict hydrocarbon production (Morales et al, 2001).

However, xanthan polymer fluids exhibited better fluid stability compared to the same HEC polymer concentration at the same condition. Fluid stability is needed, especially when packing long intervals, as the carrier fluid is expected to suspend and transport the proppant deep into the desired interval. Fluid instability can cause ineffective packing or premature screen out as result of settling out and deposition of the proppants before getting to the target location.

HEC and xanthan polymer degradation test with sodium hypochlorite was conducted for the lower temperatures of 120^{o}F and 140^{o}F and the result shown in Tables 5 and 6. The HEC polymer fluid showed faster degradation than xanthan with sodium hypochlorite breaker at the same condition, the same trend with the result with sodium persulfate. Therefore, xanthan polymer is more resistant than HEC to degradation at the same condition. The rate of degradation of HEC polymer is faster than that of xanthan at the same conditions, suggesting that HEC will be easier to clean out from the wellbore.

20ppt equivalent of 35% w/v of sodium hypochlorite was able to break the 40ppt and 60ppt xanthan polymer fluid at 140^{o}F in 30 and 75 minutes respectively. A good break was also achieved at 120^{o}F with equivalent breaker concentration of 30ppt. The comparative performance of sodium persulfate and sodium hypochlorite breakers is shown in Figures 1 and 2 for HEC and xanthan polymer fluids respectively. At the same condition, polymer degradation rate by sodium hypochlorite was faster than that of the sodium persulfate for both HEC and xanthan polymers. Therefore, sodium hypochlorite was effective in degrading xanthan polymers at low temperatures where sodium persulfate was not effective.

Table 5 - Break Test for HEC Fluid

HEC (ppt)	40	40	60	60
Sodium Hypochlorite 3.5%W/V (ppt)	30	20	30	20
pH of brine	5.85	5.85	5.85	5.85
Final Gel pH	8.15	8.15	8.11	8.11
Temperature (^{o}F)	120	140	120	140
Time (minutes)	**Viscosity (cP) at 511 s^{-1}**			
0	43	43	98	98
15	22	9	53	30
30	20	5	48	22
45	17	4	44	10
60	14	3	37	7
75	12		33	4
90	10		29	
105	8		21	
120	5		17	
135	3		13	
150			10	
165			8	
180			6	
Break Time (minutes)	**90**	**15**	**150**	**45**

Table 6 - Break Test for Xanthan Fluid

Xanthan (ppt)	40	40	60	60
Sodium Hypochlorite 3.5%W/V (ppt)	30	20	30	20
pH of brine	5.85	5.85	5.85	5.85
Final Gel pH	8.15	8.15	8.11	8.11
Temperature (^{o}F)	120	140	120	140
Time (minutes)	**Viscosity (cP) at 511 s^{-1}**			
0	28	28	42	42
15	24	19	39	32
30	20	9	34	21
45	17	7	28	16
60	15	5	26	12
75	13	3	22	10
90	11		19	8
105	10		18	
120	6		17	
135			18	
150			14	
165			12	
180			7	
Break Time (minutes)	**105**	**30**	**180**	**75**

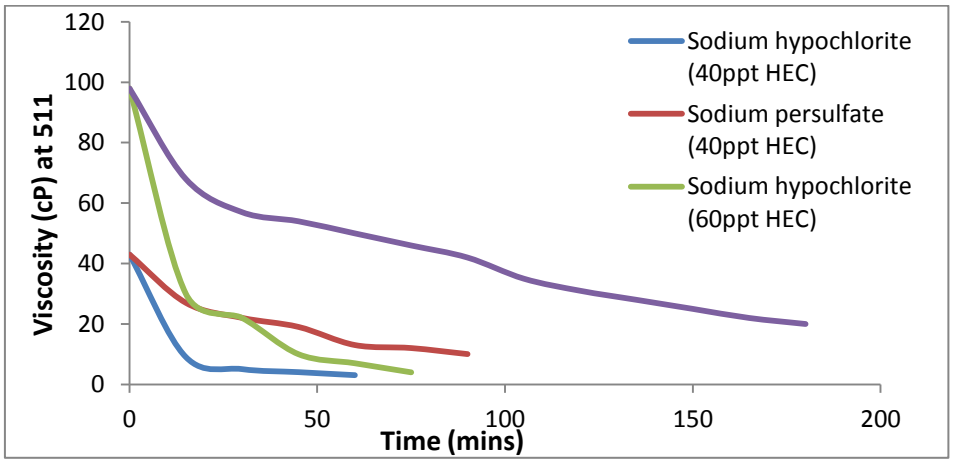

Figure 1 – Comparative Degradation for HEC

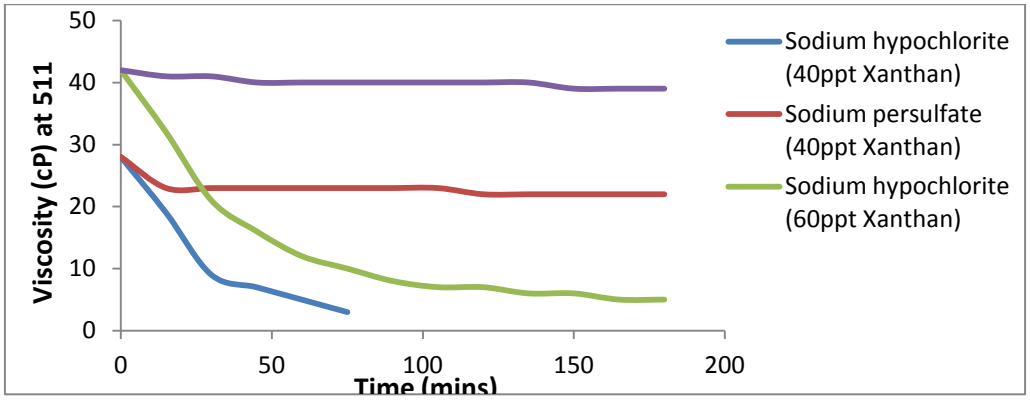

Figure 2 – Comparative Degradation for xanthan

CONCLUSION

Polymer fluid degradation rate depends on a lot of factors including type and the concentration the polymer and breaker. Xanthan resist degradation more than HEC at the same conditions. Sodium persulfate oxidizer breaker was effective in degrading HEC polymer fluids throughout the test temperature range from 140^{o}F to 180^{o}F but was difficult to degrade the xanthan fluids, especially the 60ppt loading from 160^{o}F and below.

Sodium hypochlorite demonstrated effective degradation of the HEC and xanthan polymers at 120^{o}F and 140^{o}F, unlike sodium persulfate that was not effective in degrading the xanthan at 140^{o}F.

Therefore, the optimum polymers concentration, the correct breaker type and appropriate breaker concentration must be used to achieve effective polymer degradation in gravel pack operations, depending on temperature application.

ABBREVIATIONS

cc – cubic centimeter
cP - centipoise
HEC – Hydroxyethyl cellulose
mins - minutes
ppa – pounds of proppant additive per thousand gallons
ppt – pounds per thousand gallons
SP – Sodium persulfate
w/v – weight per volume

ACKNOWLEDGEMENT

The authors which to thank the management and staff of World Bank Africa Centre of Excellence in Oilfield Chemical Research, University of Port Harcourt for the providing the platform to perform this study.

REFERENCES

Abass, H.H., Nasr-El-Din, BaTaweel, M.H. (2002). Sand Control: Sand Characterization, Failure Mechanisms, and Completion Methods. *SPE 77686*, San Antonio, Texas, 29 September-2 October 2002.

Abbas, S., Sander, A.W. and Danovan, J.C. (2013). Applicability of HEC Polymer for Chemical EOR. *SPE 165311*, Kuala Lumpur, Malaysia, July 2-4 July.

Al-Mohammed, A.M., Nasr-El-Din, H.A., Al-Fuwaires, O.A. and Al-Aamri, A.D. (2007). Degradation of High pH Borate Gels. *IPTC 11585*, Dubai, U.A.E., December 4-6.

Al-Muntasheri, G.A. (2014). A Critical Review of Hydraulic Fracturing Fluids over the Last Decade. *SPE 169552*, Denver, Colorado, U.S.A., April 16-18.

Cole, R.C. and Ali, S.A. (1994). A Comparative Study of Succinoglycan Gravel Pack Gel Properties to Those of HEC. *SPE 28533*, New Orleans, Louisiana, September, 25-28.

Economides, M.J., Walters, L.T., and Dunn-Norman, S. (1997). *Petroleum Well Construction. Halliburton*, Released 1997.

El-Dhabi F. and Bulgachev, R. (2011). Gravel Packing Depleted Reservoirs. *SPE 143929*, Noordwijk, The Netherlands, June 7-10.

Jain, S., Gadiyar, B., Stamm, B., Abad, C., Parlar, M. and Shah, S. (2011). Friction Pressure Performance of Commonly used Viscous Gravel Packing Fluids. *SPE 134386*, Florence, Tuscany, Italy, September 20-22, 2010.

Jennings Jr., A.R. (1996). Fracturing Fluids - Then and Now. *SPE 36166-Technology Today Series, JPT*, 604-610.

John, A.O., Joel, O.F and Chukwuma, F.O. (2016). Evaluating the Effect of Temperature and Polymer Concentration on Properties of Xanthan Gravel Pack Fluid. *SPE 184312*, Lagos, Nigeria, August 2-4.

John, A.O., Joel, O.F and Chukwuma, F.O. (2016b). Comparative Study of Gravel Suspension Properties of Hydroxyethyl Cellulose and Xanthan Gravel Pack Fluids. *International Journal of Engineering and Management Research (IJEMR)*, Vol. 6, Issue-5, September – October 2016, pg. 427-434.

John, A.O., Joel, O.F and Chukwuma, F.O. (2017). Evaluating the Effect of Temperature and Polymer Concentration on Properties of Hydroxyethyl Cellulose Gravel Pack Fluid. *American Journal of Chemical Engineering*, S(3-1): 21-27. http://sciencepublishinggroup.com/j/ajche

Harris, P.C. and Sabhapondit, A. (2009). Chemistry Applied to Fracturing Stimulation of Petroleum Wells. *SPE 120029*, Bahrain, Bahrain, March 15-18.

Lipton, D. and Burnett, D.B. (1976). Comparisons of Polymers Used in Workover and Completion Fluids. *SPE 5872, AIME*, Long Beach, California, April 8-9, 1976.

Montgomery, C. (2013). Fracturing Fluids. *ISRM Specialized Conference Paper*, Brisbane, Australia, May 2013.

Morales, R.H., Gadiyar, B.R., Bowman, M.D., Wallace, C., and Norman, W.D. (2001). Fluid Characterization for Placing Effective Frac/Pack. *SPE 71658*, New Orleans, Louisiana, 30 September to 3 October, 2001.

Nguyen, H.T and Lafontaine, J.M. (1990). Effect of Various Additives on the Properties of the Clarified XC

Polymer System. *SPE 19404-MS*, Louisiana, February 22-23, 1990.

Sarwa, M.U., Cawiesel, K.E. and Nasr-El-Din, H.A. (2011). Gel Degradation Studies of Oxidative and Enzyme breakers to Optimize Breaker Type and Concentration for Effective Break Profile at Low and Medium Temperature Ranges. *SPE 140520*, Woodlands, TX, January 24-25.

Thibodeaux, G.A., Gill, S.B., Richard, B.M. and Bowman, C.W. (1991). Comparative Study of Gravel/Water Packing 12 Gulf Coast Wells. *SPE 22794*, Dallas, TX, October 6-9.

Underdown, D.R., Calvert, A.L. and Newhouse, D.P. (1989). Comparison of HEC and XC Polymer Gravel Pack Fluids. *SPE 19751*, San Antonio, Texas, October 8-11, 1989.

Vollmer, D.P. and Alleman, D.J. (2001). HEC No Longer the Preferred Polymer. *SPE 65398*, Houston, Texas, February 13-16.

Wellington, S.L. (1983). Biopolymer Solution Viscosity Stabilization – Polymer Degradation and Antioxidant Use. *SPE 9296*, Dallas, Texas, USA, September 21 – 24.

IDENTIFICATION OF NEW CONTROL STRUCTURES FOR A TUBULAR AMMONIA REACTOR-HEAT EXCHANGER SYSTEM USING DYNAMIC RESILIENCE ANALYSIS

***Williams, A.O.F and Adeniyi, V.O.**
Department of Chemical & Petroleum Engineering
University of Lagos, Akoka, Lagos
Email: afwilliams@unilag.edu.ng; bmnpsvg@gmail.com

ABSTRACT

The task of control structure selection for a tubular ammonia reactor-heat exchanger system using dynamic resilience analysis is presented. Based on the linearized ninth-order state-space model of the reactor-heat exchanger system presented in the literature, sixty (60) 2×2*, twenty (20)* 2×3*, and thirty (30)* 3×3 *alternate control structures corresponding to the choice of two controlled outputs and two manipulated inputs (square system); two controlled outputs and three manipulated inputs (i.e. non-square system); and three controlled outputs and three manipulated inputs (i.e. square system) respectively, were analyzed. The dynamic resilience analysis identified new control structures for this reactor-heat exchanger system which have not been previously reported in the literature. These new control structures have potential for improved control design and closed-loop performance for the tubular reactor-heat exchanger system beyond what is achievable using the* 2×2 *control structure previously reported in the literature.*

1 INTRODUCTION

Control system design involves two subtasks(Manousiothakis *et al.*, 1986):

1. selection of a control structure i.e. set of measurements and manipulated variables
2. decision on the structure interconnecting the measured and manipulated variables, along with the control law governing the interconnections.

For large-scale systems such as lumped models of distributed parameter systems, the first subtask which is to select a control structure i.e. choosing the number and location of measured and manipulated variables is not a trivial one (Bonvin, 1986). The choice of inputs and outputs affects the performance, complexity and cost of the control system (Van de Wal and de Jager, 2001).

This problem has usually been solved by experienced engineers (Govind and Powers, 1982) who have the ability to simultaneously consider the economic, safety and reliability goals of a given process; the interactions which might occur between control structures; possible changes in the process to improve control etc. Traditionally, however, dynamic simulations are often employed to evaluate and compare alternate control schemes, to verify that proposed design are adequate, or to examine the effect of changes to an existing control system, or plant design. Unfortunately, the large number of alternative schemes, or sets of controller parameters, and/or disturbance conditions which may have to be examined make dynamic simulations a time consuming task, even for moderately small problems(Johnstone and Barton, 1987). Furthermore, as Morari (1985) *et al.* note, "simulations require that quite arbitrary decisions about controller structure and parameters be made which could very well bias the results. Specific disturbances and/or set points have to be selected which might or might not represent the worst case scenarios for the plant, and thus give an entirely incorrect impression of its steady-state and dynamic behaviour".

The prohibitive manpower and computational requirements for the simulation approach led Morari and co-workers (Morari, 1983a,b; Morari *et al.*, 1985; Morari & Holt, 1985a,b); to develop a much more efficient method called dynamic resilience analysis (DRA) technique. The technique is based on identifying system characteristics that limit control quality, or which give rise to control difficulties independent of the selected or installed controller. These characteristics are non-minimum phase behaviour, manipulated input constraints, and sensitivity to model/plant mismatch. The dynamic resilience analysis framework allows one to quickly examine several alternative designs or control schemes about their performance than can dynamic simulations, and at a considerably lower computational cost based on input-output controllability of the system. Thus, the technique has successfully been used in a number of studies to assess dynamic operability characteristics of various alternative process design, and

for control structure selection (Morari, 1983b; Morari *et al.*, 1985; Shimizu *et al.*, 1985; Perkins and Wong, 1985; Mandler *et al.*, 1986; Levien and Moarari, 1987; McAvoy, 1987; Williams and Adeniyi,1991; Ogunnaike and Ray, 1994; Dadhe *et al.*, 2002; Engel *et al.*, 2004; Skogestad and Postllethwaite, 2005; Williams and Adeniyi, 2017). A review of some of the other methods for input/output selection such as accessibility, state controllability and state observability, input-output controllability, efficiency of manipulation and estimation and their applications is presented by Van de Wal and de Jager (2001), while Yuan *et al.* (2011) provide a recent review of the extensive literature on controllability analysis of chemical processes in general and dynamic resilience in particular.

The purpose of this paper is to use dynamic resilience analysis technique to determine the appropriate control structure(s) for a tubular ammonia synthesis reactor-heat exchanger system. The ammonia synthesis reactor is the heart of an ammonia plant for the manufacture of ammonia based on the Haber process. Because it is the major process in the manufacture of nitrogenous fertilizers, an ammonia plant and hence the ammonia reactor, is a very important industrial process unit. Consequently, studies relating to the control and safe operation of the reactor are of immense practical importance. The approach here is motivated by the realization that the studies of Patnaik *et al.* (1980a,b; 1981) and Viswanadham *et al.* (1979), whose models are employed in the present paper predates the development of the DRA for control structure selection. Thus, it is suspected that the control structure selection reported in their work may not necessarily be the best from the point of view of dynamic resilience considerations. The implication of such possibly poor choice of control structure on the control system design and closed loop performance is obvious. The work reported here is part of the larger task of the design of an advanced control system such as a model predictive controller for the regulation of the tubular ammonia reactor system in the presence of disturbances entering the system. A key step in this task is the selection of the resilient control structure(s) that shall form the basis of the controller design. The selection of the resilient control structure(s) is addressed in this paper. A future paper shall present the design and simulated evaluation of the advanced controllers using the selected control structures.

2 PROCESS DESCRIPTION AND MODEL OF THE AMMONIA REACTION SYSTEM

Ammonia as manufactured in the Haber process, is formed according to the catalysed exothermic reaction:

$$N_2 + 3H_2 \rightarrow 2NH_3$$

A schematic diagram of the ammonia synthesis reactor under consideration as presented by Patnaik *et al.* (1980a,b; 1981) is shown in Figure 1.

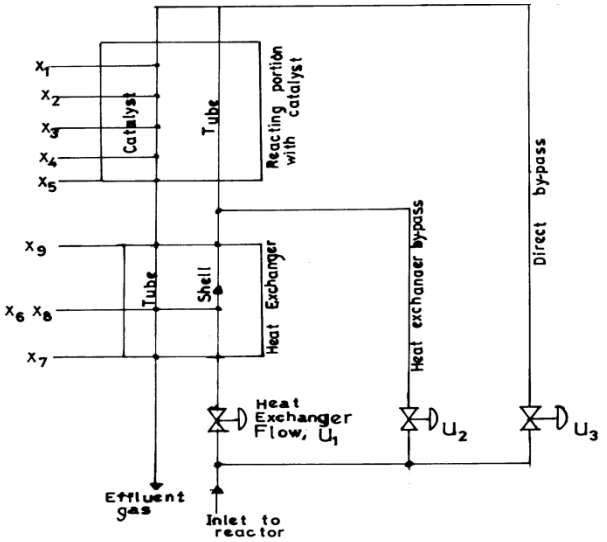

Figure 1: Schematic of ammonia synthesis reactor-heat exchanger system (Patnaik *et al.*, 1980a,b,1981; Viswanadham *et al.*, 1979).

The synthesis gas, which consists of hydrogen and nitrogen in the stoichiometric ratios of 3:1, is prepared in the reformer section of the plant. This gas mixture is compressed to a pressure of 200–300 atm, and enters the synthesis reactor which consists of two parts: (i) the catalyst bed section shown in the upper part of the diagram, and (ii) the heat exchanger section in the lower part of the diagram.

To ensure stable operating conditions with maximum yield, it is necessary to bring the feed gases to a temperature of about 420^{o}C before they enter the catalyst bed. This is economically achieved by pre-heating the feed gases first in the bottom heat exchanger, and subsequently in the tubes of the reacting portion. The inlet gaseous mixture is split into three separate streams: (i) the main stream called the heat exchanger flow, F_1; (ii) the second stream called the heat exchanger by pass flow, F_2; and (iii) the third stream called the direct by pass flow, F_3.

The feed gases flowing down the catalyst bed react to produce ammonia. The outlet gases from the reacting zone enter the tubes of the heat exchanger and finally leave the reactor. The three flow rates can be varied using valves. The reactor-heat exchanger system is also well instrumented to measure process variables of interest e.g. the temperature at various points along the axial length of the reactor-heat exchanger system are measured using thermocouples; while the inlet flows are measured using differential pressure type flow meters (Patnaik, *et a*l., 1980a,b, 1981; Viswanadham *et al*., 1979).

A simplified, state-space model of the reactor system obtained by linearizing around the steady-state corresponding to the maximum yield and discretization along the axial lenght is given as (Patnaik *et al.,* 1980a,b, 1981; Viswanadham *et al.,* 1979):

$$\frac{d\mathbf{x}}{dt} = \mathbf{A}\mathbf{x}(t) + \mathbf{B}\mathbf{u}(t) + \mathbf{D}\mathbf{d}(t) \qquad (1)$$

$$\mathbf{y} = \mathbf{C}\mathbf{x} \qquad (2)$$

where $\mathbf{x}(t)$ is a 9×1 state vector representing the deviation temperature along the reactor-heat exchanger unit, $\mathbf{u}(t)$ is a 3×1 control inputs representing the three deviation flow rates, and $\mathbf{d}(t)$ is a 2×1 disturbance vector of feed gases inlet deviation temperature, and inlet deviation of ammonia composition. The matrices $\mathbf{A},\mathbf{B}$, and $\mathbf{D}$ are given in Viswanadham *et al.* (1979), while matrix $\mathbf{C}$ depends on which of the nine states are selected as controlled variables.

3 DYNAMIC RESILIENCE ANALYSIS (DRA)

Morari (1983a,b) defined the term ``dynamic resilience" qualitatively to mean the ability of a process to move quickly and smoothly from one operating condition to another and reject disturbances effectively. Since resilience is defined as an inherent property of the system, it is independent of the quality of controller design. Using the internal model control (IMC) structure introduced by Garcia and Morari (1982), Morari and co-workers (Morari, 1983a,b; Morari *et al.*, 1985; Morari & Holt, 1985a,b) provided insights/understanding into the sources or system characteristics which limit process resilience, as well as quantitative measures for these. Grossmann *et al.* (2014) give a historical sketch of the methods for the analysis of flexibility and resilience in process plants. They note that "steady-state flexibility or resilience addresses the general flexibility of operation of a plant over a range of conditions, with the ultimate goal being on how to design a process for guaranteed /resilient operation", while, "Dynamic Resilience is concerned with fast and smooth changeover and recovery from process disturbance, with the ultimate goal of determining the inherent dynamic characteristics of a plant independent of the selection of a particular controller". The attraction of dynamic resilience analysis is that it can be easily used to assess alternative designs during the development stage, and in making selection of control structures, and thereby eliminating the need for extensive simulations.

For a system model without explicit time delay elements, the essential elements of DRA are as presented below.

Given a transfer function model $G(s)$ which is open-loop stable (or which has been stabilized), DRA essentially involves the following (Morari, 1983a,b; Morari *et al.*, 1985; Morari & Holt, 1985a,b);

1. Analysis of the process model, $G(s)$, to determine the presence of NMP elements.
2. Analysis of the minimum singular value, $\underline{\sigma}(G)$ and the sensitivity function, $\gamma(G)$ as a function of frequency, ω; $\underline{\sigma}(G)$ and $\gamma(G)$ being defined as follows:

$$\underline{\sigma}(j\omega) = \left[\lambda_{min}(\mathbf{G}^*\mathbf{G})\right]^{1/2},\quad \gamma(j\omega) = \frac{\bar{\sigma}(j\omega)}{\underline{\sigma}(j\omega)},\quad \bar{\sigma} = \left[\lambda_{max}(\mathbf{G}^*\mathbf{G})\right]^{1/2} \qquad (3)$$

in which $\bar{\sigma}(j\omega)$ is the maximum singular value, and $\mathbf{G}^*$ is the conjugate transpose of $\mathbf{G}$.

At steady state i.e. at zero frequency, $\omega = 0$, the model $\mathbf{G}$ is simply the steady state gain matrix i.e. $\mathbf{G}(0)$, and the sensitivity function $\gamma(j\omega)$ becomes the condition number, $\gamma(0)$. This is simply given by

$$\gamma = \frac{\bar{\sigma}(0)}{\underline{\sigma}(0)} \qquad (4)$$

where $\bar{\sigma}(0)$ and $\underline{\sigma}(0)$ are the maximum and minimum singular values of $G(0)$, respectively.

The minimum singular value, $\underline{\sigma}$ (also known as the Morari Resiliency Index, MRI) is proportional to the magnitude of the largest disturbance input which can be handled without causing the manipulated variables to saturate, while the condition number and the sensitivity function, $\gamma(0)$ and $\gamma(j\omega)$, give a measure of how sensitive the system will be to significant model/plant mismatch (i.e. modelling errors).

It is pertinent to note that the condition number $\gamma(0)$ and the sensitivity function $\gamma(j\omega)$ are scaling dependent. In using these to screen alternative structures, $\gamma(0)$ and $\gamma(j\omega)$ must be minimized by scaling. The recommendations of Morari *et al.*(1985) and Levien and Morari (1987) have been used i.e. choose diagonal scaling factors such that the maximum entry in each row and column of G is unity.

4 APPLICATION TO THE AMMONIA REACTOR-HEAT EXCHANGER SYSTEM

For this system, the main control objective is stable and fast regulation of the temperature profile of the reactor close to the steady-state optimal values in the face of disturbances entering the system. In other words, it is necessary to design a controller to achieve asymptotic behaviour of the reactor temperatures, x_1 to x_9, around the origin. Since there are only three manipulated variables for this system, we obtain trivially from the condition for the existence of the right inverse of the process transfer function, that only three outputs can be perfectly controlled. Thus we can only select one, two or three of the state-variables for output feedback control.

In this paper, we consider various 2×2 (2 outputs, 2 inputs), 2×3 (2 outputs, 3 inputs), and 3×3 (3 outputs, 3 inputs) alternate control structures resulting from selecting the appropriate number of controlled variables from the nine possible state variables and the three manipulated variables.

As shall be seen shortly, a total number of sixty (60) square (2×2), twenty (20) non-square (2 × 3) and thirty (30) square (3 × 3) control structures are to examined for the ammonia reactor-heat exchanger system under study. This is clearly a very formidable task if conventional simulation and trial and error procedures were the only tools available. The question concerning which of these control structures is the most resilient, and should therefore be selected for feedback controller design for this ammonia reactor system, shall be addressed below through application of the dynamic resilience analysis framework presented above.

4.1 STEP 1: GENERATION OF (2 × 2), (2 × 3) AND (3 × 3) CONTROL STRUCTURES & DETERMINATION OF NMP CHARACTERISTICS

The sixty (60) square (2 × 2), twenty (20) non-square (2 × 3) and thirty (30) square (3 × 3) control structures generated for DRA of the ammonia reactor-heat exchanger system are shown in Tables 1, 2 and 3 (See Appendix A). Engineering judgement and physical intuition/reasoning were used to generate all these control structures for the objective of regulatory control of the reactor temperature in the presence of disturbances entering the system. These control structures correspond to different transfer function models, $\mathbf{G}$, which are easily determined from the system matrices $\mathbf{A,B,C}$ for the different $\mathbf{B}$ and $\mathbf{C}$ of each control structure.

The DRA of these control structures is greatly facilitated by the availability of computer software to carry out the computations. Williams and Adeniyi (2001) describe a suite of FORTRAN 77 programs which were utilized for the computations reported in this work. However, the computations could also be carried out using Matlab (commercialize software) or using its open-source counterparts such as Octave or Scilab.

In the first step, we analyzed the various control structures for the presence of non-minimum phase characteristics which translated to determination of right-half plane (RHP) zeros for the systems.

1. (2 × 2) Control Structures.

The results from the computer analysis show that the following control Structures: E, F, G, I, J, L, M, N, Q, R, S, AD, AH, AM have RHP transmission zeros. These structures are therefore rejected according the discussion above. Furthermore, we found that the following control structures: O, T, AI, AN, BC, BH are degenerate cases i.e. each has rank =1, which is lower than the expected normal rank of 2 for each. Control structures with this rank degeneracy are not controllable. This was confirmed by the singular value analysis of the steady-state system matrix which indicated that the control structures in question, are actually singular. Consequently, they are eliminated from further consideration. Thus on the basis of the presence of RHP zeros and rank degeneracy, alone, we have been able to eliminate twenty (20) control structures with poor resiliency characteristic. This is one-third of the total control structures that we started with, and is clearly a significant reduction in the number of structures to be analysed in the next step on singular value analysis.

2. (2 × 3) and (3 × 3) Control Structures

No RHP zeros were found for all these control structures. However, the following 2 × 3 control structures: CA, CB; and the following 3 × 3 control structures: CO, CP, CX, CY, DC, DD, DE, DF were found to be degenerate cases, each structure having rank lower than the expected normal rank. Similar to the

remarks made earlier about rank degeneracy control structures, these control structures are eliminated from further consideration.

4.2 STEP 2: STEADY-STATE SINGULAR VALUE ANALYSIS

Tables 4, 5 and 6 show the results of the steady-state singular value analysis where we have indicated the minimum singular value $\underline{\sigma}(0)$, unscaled condition number, $\gamma(0)$, and the scaled condition number, $\gamma_s(0)$, for the remaining 2 × 2, 2 × 3, and 3 × 3 control structures, respectively.

Table 4: Minimum singular values, $\underline{\sigma}(0)$ and condition numbers, $\gamma(0)$ and $\gamma_s(0)$ for the ammonia reactor system. 2 × 2 control structures.

Control structure	$\underline{\sigma}(0)$	$\gamma(0)$	$\gamma_s(0)$	Control structure	$\underline{\sigma}(0)$	$\gamma(0)$	$\gamma_s(0)$
A	0.730	212.09	28.48	AK	7.063	32.35	10.53
B	2.711	54.96	5.97	AL	6.561	30.56	11.32
C	6.346	22.07	1.57	AO	0.708	476.76	29.42
D	13.545	9.58	1.52	AP	2.571	125.17	6.20
H	3.602	29.76	1.039	AQ	6.113	49.16	1.52
K	4.303	28.77	1.88	AR	12.958	21.26	1.71
P	8.201	15.30	1.88	AS	1.743	155.02	7.44
U	0.308	1203.89	878.86	AT	5.218	46.85	1.42
V	2.093	169.31	119.34	AU	12.478	17.06	1.25
W	4.284	77.34	48.67	AV	3.580	62.15	1.00
X	12.046	25.251	10.42	AW	11.562	16.20	1.08
Y	1.638	181.90	138.07	AX	9.272	15.96	1.96
Z	3.779	71.49	51.51	AY	4.016	67.06	2.08
AA	11.681	20.21	10.53	AZ	3.929	52.14	2.14
AB	2.285	108.09	82.01	BA	3.685	48.32	2.05
AC	10.750	19.458	11.318	BB	3.059	44.45	2.26
AE	3.749	78.98	10.42	BD	7.709	35.16	2.08
AF	3.704	60.90	10.53	BE	7.508	27.59	1.98
AG	3.455	57.07	11.32	BF	7.017	25.75	1.27
AJ	7.188	41.51	10.42	BG	5.763	24.18	1.87

These results show that on the basis of $\underline{\sigma}(0)$ values (which is desirable to be as large as possible) and $\gamma_s(0)$ values (which is desirable to be as low as possible), the most promising control structures are as follows:

1. **2 × 2 Control Structures**

The most promising 2 × 2 control structures are D (i.e. control x_1, x_5 with u_1, u_2), AR (i.e. control x_1, x_5 with u_2, u_3), AU (i.e. control x_2, x_5 with u_2, u_3), and AW (i.e. control x_3, x_5 with u_2, u_3), with ($\underline{\sigma}(0)$, $\gamma_s(0)$) = (13.545, 1.52), (12.958,1.71), (12.478, 1.25), and (11.562, 1.08), respectively (see Table 4). On the basis of these results, we can eliminate all the other control structures from further considerations. Notice that on the basis of the steady-state singular value analysis, we have been able to eliminate thirty six (36) control structures with poor resiliency characteristic, leaving just four (4) control structures whose dynamic singular value analysis are to be assessed in the next step.

Table 5: Minimum singular values, $\underline{\sigma}(0)$ and condition numbers, $\gamma(0)$ and $\gamma_s(0)$ for the ammonia reactor system. 2 × 3 control structures.

Control structure	$\underline{\sigma}(0)$	$\gamma(0)$	$\gamma_s(0)$	Control Structure	$\underline{\sigma}(0)$	$\gamma(0)$	$\gamma_s(0)$
BI	0.776	478.37	31.32	BR	5.431	41.54	1.86
BJ	3.335	106.30	6.92	BS	10.359	22.06	1.75
BK	7.500	44.19	1.93	BT	4.251	58.10	1.40
BL	17.779	17.11	1.55	BU	15.768	13.26	1.52
BM	5.532	53.55	1.80	BV	5.067	39.91	1.88
BN	10.608	28.14	1.80	BW	9.625	20.83	1.40
BO	2.404	123.96	8.21	BX	12.823	13.06	2.44
BP	6.463	41.81	1.83	BY	4.279	35.52	2.33
BQ	17.135	13.78	1.37	BZ	8.035	19.467	2.16

2. 2 × 3 Control Structures.

The most promising 2 × 3 control structures are BL (i.e. control x_1, x_5 with u_1, u_2, u_3), BQ (i.e. control x_2, x_5 with u_1, u_2, u_3) and BU (i.e. control x_3, x_5 with u_1, u_2, u_3), with ($\underline{\sigma}(0)$, $\gamma_s(0)$) = (17.78 1.55), (17.14,1.37), and (15.77, 1.578), respectively (see Table 5). Control structure BX (i.e. control x_4, x_5 with u_1, u_2, u_3) is excluded because its $\gamma_s(0)$ is higher than those selected.

Table 6: Minimum singular values, $\underline{\sigma}(0)$ and condition numbers, $\gamma(0)$ and $\gamma_s(0)$ for the ammonia reactor system. 3 × 3 control structures.

Control structure	$\underline{\sigma}(0)$	$\gamma(0)$	$\gamma_s(0)$	Control structure	$\underline{\sigma}(0)$	$\gamma(0)$	$\gamma_s(0)$
CC	0.218	1923.62	1314.11	CN	0.862	387.77	191.30
CD	0.158	2541.88	1830.99	CQ	0.322	1036.99	702.42
CE	0.257	1469.93	901.50	CR	1.771×10^{-3}	1.73×10^{5}	1.00×10^{5}
CF	0.255	1456.64	956.88	CS	1.624×10^{-3}	1.84×10^{5}	1.12×10^{5}
CG	0.257	1452.21	956.88	CT	1.735×10^{-3}	1.73×10^{6}	1.10×10^{5}
CH	0.238	1620.16	990.58	CU	0.805	347.57	188.23
CI	0.221	1630.62	918.87	CV	0.537	505.12	230.72
CJ	0.192	1847.10	972.68	CW	0.723	378.51	221.68
CK	0.215	1659.78	972.68	CZ	0.789	326.49	184.28
CL	0.980	346.21	175.13	DA	0.614	403.24	238.69
CM	0.617	538.19	191.30	DB	0.744	336.85	195.83

3. 3 × 3 Control Structures

The most promising 3 × 3 control structures are CL (i.e. control x_1, x_2, x_5 with u_1, u_2, u_3), CN (i.e. control x_1, x_4, x_9 with u_1, u_2, u_3) and CU (i.e. control x_2, x_4, x_5 with u_1, u_2, u_3), with ($\underline{\sigma}(0)$, $\gamma_s(0)$) = (0.98 175.13), (0.862,191.30), and (0.81, 188.23), respectively (see Table 6). These values of $\underline{\sigma}(0)$ and $\gamma_s(0)$ suggest that a controller designed on the basis of these control structures will be easily subject to

manipulated variable saturation and will exhibit high sensitivity to modeling errors. Thus, even from this steady-state singular value analysis, we are able to obtain valuable insight for the choice of the controller structure.

Thus all other control structures are eliminated from further consideration. It is to be noted that the values of $\underline{\sigma}(0)$ and $\gamma_s(0)$ for the 2 × 3 control structures are much better than those of the 2 × 2 and the 3 × 3 control structures, but final choice will await the outcome of the dynamic singular value analysis to be sure that this is also the case in the dynamic case.

4.3 STEP 3: SCREENING FOR POOR DYNAMIC PERFORMANCE

1. 2×2 control structures.

Looking at the plots of $\underline{\sigma}(j\omega)$ for the four most promising control structures in Figure 2a, we see that structure D has the highest $\underline{\sigma}(j\omega)$ at low frequencies up to about 0.1 rad/s. However, beyond a frequency of about 0.1 rad/s, the value of $\underline{\sigma}(j\omega)$ for structure D drops below that for structure AR which now becomes the structure with the highest $\underline{\sigma}(j\omega)$ for the remaining range of frequency values. Thus at steady-state and at low frequencies (up to 0.1 rad/s), structure D is the best in terms of the magnitude of disturbances that can be handled followed by structures AR, AU, and AW in that order. However, at high frequencies (>0.1 rad/s), the ordering or ranking of the best structure changes to AR, followed by D, while that of AU and AW, remains the same.

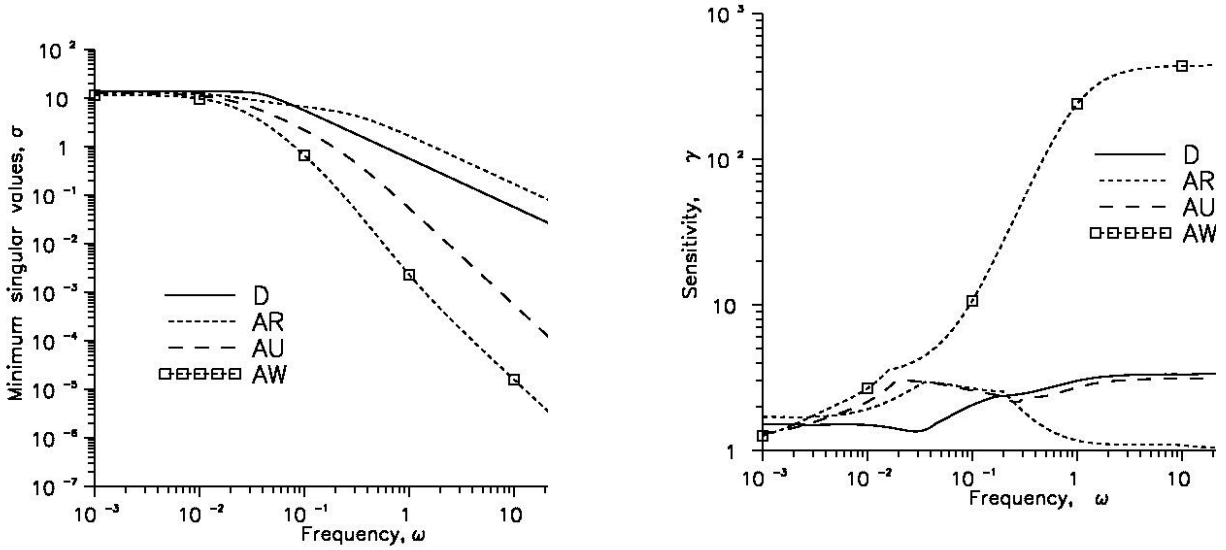

Figure 2: (a) Left: Minimum singular values, $\underline{\sigma}$, (b) Right: Sensitivity function γ_s for the 2 × 2 control structures D, AR, AU, and AW of ammonia reactor -heat exchanger system

Next we consider sensitivity to modelling errors: similar to the ordering predicted by considering the minimum singular values, we also find in this case that at low frequencies, the best structure (with lowest $\gamma_s(j\omega)$) is D, followed by structures AR and AU. However, at high frequencies, structure AR becomes the best while structures AU and D are comparable. The value of $\gamma_s(j\omega)$ for structure AW is very large and increases with frequency, thus indicating severe sensitivity to modelling errors; it is therefore rejected. These results should be compared with the ranking based on the steady-state analysis (i.e. $\gamma_s(0)$) which indicates that the best structure is AW followed by AU, D, and then AR. This points out that an assessment of the sensitivity to modelling errors based on $\gamma_s(0)$ alone can lead to erroneous conclusions. On the basis of the steady-state and dynamic singular value analysis results presented above, it is clear that the best 2 × 2 control structures are D (i.e. control x_1 and x_5 with u_1 and u_2) and AR (i.e. control x_1 and x_5 with u_2 and u_3). Structure D is the best at steady-state and at low frequencies(up to about 0.2 rad/s), while structure AR is the best at high frequencies.

It is interesting to point out that based on the following: (a) the model not having right half plane transmission

zeros, (b) relative influence of each control input pairs on the reactor temperature profile, (c) the flows employed as manipulated variables in actual practice, and (d) choice of two temperature points in anticipation that, if offsets at these points are maintained at zero, then the offsets at all intermediate points would lie within tolerable bounds, and insights from extensive closed-loop computer simulations, Viswanadham *et al.*(1979) and Patnaik *et al.* (1981) chose x_1 and x_5 as the controlled variables, and u_2 and u_3 as the manipulated variables. This turns out to be one of the structures i.e. AR identified above. However, contrary to their claim, our analysis indicated that not all structures with u_1 and u_2 as manipulated variables have right half plane transmission zeros. While our analysis confirmed the choice of the control structure by Viswanadham *et al.*(1979) and Patnaik *et al.* (1981), we have also been able to determine that this structure is best only at high frequencies. At steady-state and low frequencies, the best control structure is D. The dynamic resilience analysis has also indicated that the magnitude of disturbances which can be handled by the two control structures (D and AR) are about 13.5 and 12.96, respectively. For all practical purposes, both structures can handle disturbances of about the same magnitude.

2. 2×3 **control structures.**

The results of the dynamic singular value analysis are shown in Figures 3 for the three most promising 2×3 control structures i.e. BL, BQ and BU.

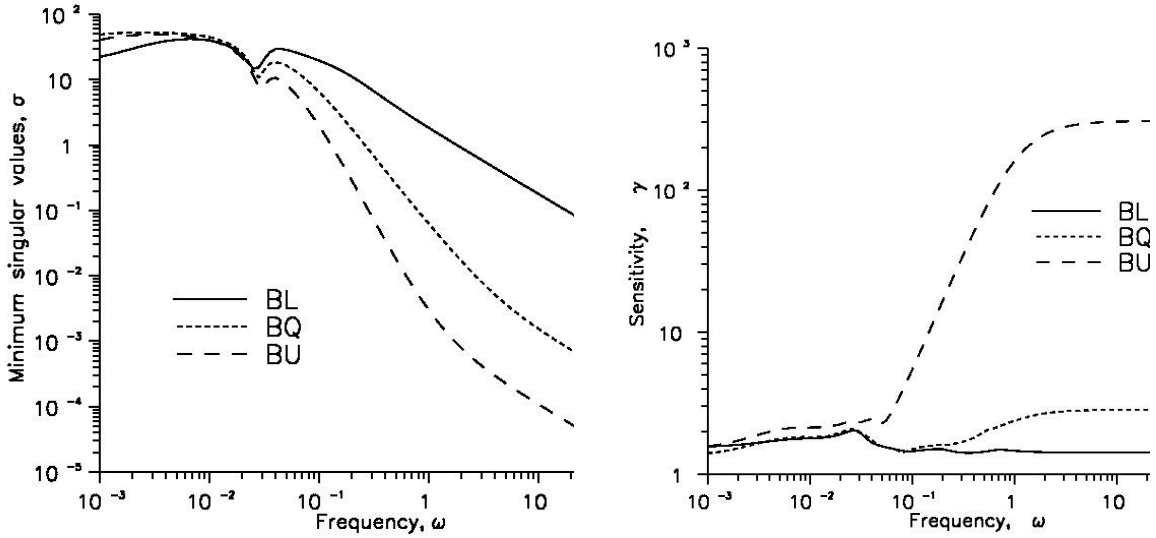

Figure 3: (a) Left: Minimum singular values, $\underline{\sigma}$, (b) Right: Sensitivity function γ_s for the 2 × 3 control structures BL, BQ, and BU: Ammonia reactor-heat exchanger system

When we examine the plots of $\underline{\sigma}(j\omega)$ for the 2 × 3 control structures in Figure 3, we see that structure BQ has the highest value up to a frequency of about 0.04 rad/s. However, for frequencies higher than 0.04 rad/s, BL becomes the structure with the highest $\underline{\sigma}(j\omega)$, followed by structures BQ and BU, respectively. Thus at low frequencies up to 0.03 rad/s, structure BQ is the best followed by structures BU and BL, respectively. However, at high frequencies (>0.03 rad/s), the ranking of the best structures changes to BL, followed by BQ, and then BU. This ranking agrees with that indicated by the assessment of $\underline{\sigma}(0)$. The plots of $\gamma_s(j\omega)$ shown in Figure 3b indicates that the values for structures BL and BU are small and comparable at frequencies up to about 0.1 rad/s. Beyond this point, the $\gamma_s(j\omega)$ values for structure BL drops below that for structure BQ. On

the other hand, the $\gamma_s(j\omega)$ values for structure BU are much larger (than those for structures BL and BQ), and also increases significantly with frequency. These plots of $\gamma_s(j\omega)$ indicate that structure BL is the best, followed by structure BQ. Structure BU is rejected as it is likely to be very sensitive to modelling errors. On the basis of the overall information from the steady-state and dynamic singular value analysis, it is clear that the best 2×3 control structure is BL (i.e. control x_1, x_5

with u_1, u_2, u_3), followed by control structure structure BQ (i.e. control x_2, x_5 with u_1, u_2, u_3).

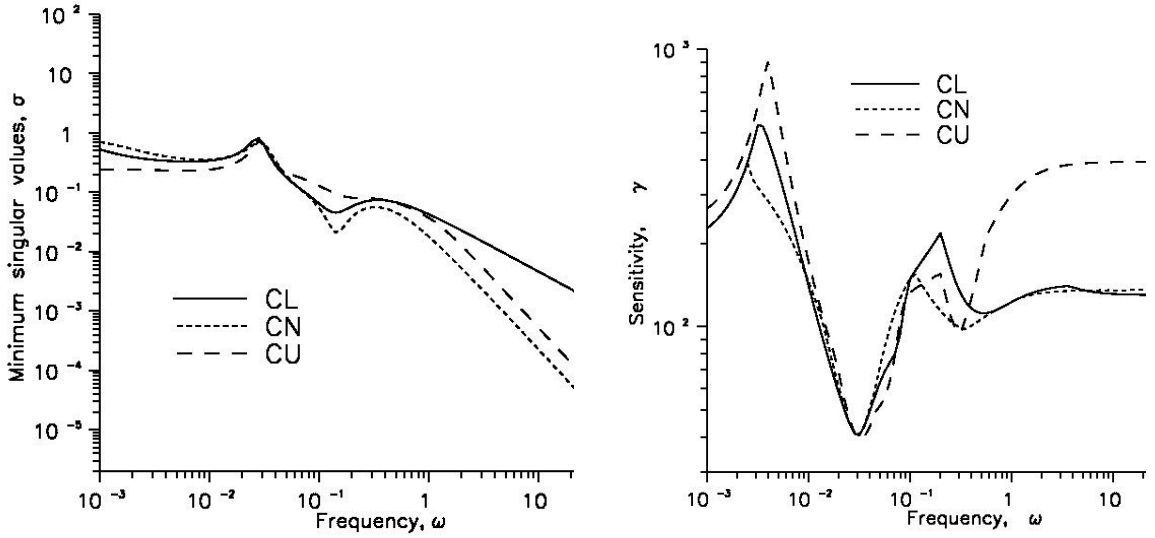

Figure 4: (a) Left: Minimum singular values, $\underline{\sigma}$; (b) Right: Sensitivity function γ_s for the 3 × 3 control structures CL, CN, and CU of ammonia reactor -heat exchanger system

Examining Figure 4 and following similar considerations and arguments as for the 2×3 control structures above, we can easily identify that the best 3×3 control structures are CL (i.e. control x_1, x_4, x_5 with u_1, u_2, u_3), followed by, CN (i.e. control x_1, x_4, x_9 with u_1, u_2, u_3) . Control structure CU is also rejected since the dynamic sensitivity to modeling errors is also very poor.

When we compare the results of $\underline{\sigma}$ and γ_s) (for both the static and dynamic cases) for the 2×3 and 3×3 control structures, it is clear that the former has much greater potential for control design and closed-loop performance and are therefore to be recommended above the latter.

From a dynamic resilience point of view, the foregoing results show that the 3×3 control structures should not be employed for controller design as any of the structures would lead to controllers that easily saturate and that exhibit significant sensitivity to modeling errors. On the other hand, for the 2×2 control

3. 3×3 control structures

The corresponding results for the three most promising 3 × 3 control structures (i.e. CL. CN, and CU) are shown in Figure 4.

structures, the most attractive candidates are D (i.e. control x_1, x_5 with u_1, u_2), AR (i.e. control x_1, x_5 with u_2, u_3) and AU (i.e. control x_2, x_5 with u_2, u_3) in that order, at low frequencies; while at high frequencies, the preference order is AR, D, AU.

For the 2×3 control structures, the best candidates are BL(i.e. control x_1, x_5 with u_1, u_2, u_3) and BQ (i.e. control x_2, x_5 with u_1, u_2, u_3). For these control structures, the values of $\underline{\sigma}$ and γ_s suggest that controllers designed on this basis will be able to respond without the manipulated variables getting easily saturated, and will tolerate modeling errors much better. Apart from control structure AR which was selected for controller design for the ammonia reactor system by Viswanadham *et al.* (1979) and Patnaik *et al.* (1981), the other control structures that we have identified here using dynamic resilence analysis have not appeared in the open literature to the best of our knowledge.

5 CONCLUSIONS

Sixty (60) 2 × 2, twenty (20) 2×3, and thirty (30) 3×3 alternate square and non-square control structures

for the tubular ammonia reactor-heat exchanger system, were analyzed. The DRA identified new control structures (for the 2×2 and 2×3 sub-systems) for this reactor-heat exchanger system which have not been previously reported in the literature. The DRA of the 3×3 control structures suggest that this would lead to controllers with poor performance due to manipulated variable saturation and sensitivity to modeling errors.

The new 2×3 control structures have potential for improved control design and closed-loop performance for the tubular reactor system beyond what is achievable using the 2×2 control structures previously reported in the literature. As to be expected, model predictive control(MPC) design for the reactor-heat exchanger system based on the most promising control structures confirmed the outcome of the DRA. The results of these shall be presented in a future paper.

REFERENCES

Bonvin, D. (1986). Cost Decomposition of Large-Scale Systems and Scaling of Input and Output Variables, *4th. IFAC Symp. Large-Scale Systems*, Zurich.

Dadhe, K., Engell, S., Gesthuisen R., Pegel, R. and Volker, M.(2002). Control Structure Selection for a Reactive Distillation Column, *Proc. 15th. IFAC Triennial World Congress*, Barcelona, Spain.

Engell, S., Trierwenter, J. O., Volker, M. and Pagelic (2004), in *The Integration of Process Design and Control*, Seferlis, P.and Geogiadis, M.C. (Eds.)

Garca, V. M., Serra, M., & Llorca, J. (2011). Controllability study of an ethanol steam reforming process for hydrogen production, *Journal of power sources*, **196** (9), pp. 4411-4417.

Garca , V. M., Serra, M., Llorca, J., & Riera, J. (2013). Design of linear controllers applied to an ethanol steam reformer for PEM fuel cell applications, *International journal of hydrogen energy*, **38**(18), pp. 7640-7646.

Garcia , C. E., and Morari, M. (1982). Internal Model Control. 1. A Unifying Review and Some New Results, Ind. Eng. Chem. Process Des. Dev., **Vol. 21**, pp. 308{323.

Govind , R., and Powers, G. J. (1982). Control System Synthesis Strategies, *AIChE J.*, **Vol. 28**, No. 1, pp. 60–72.

Grossmann , I. E., Calfa, A., Garcia-Herreros, P. (2014). Evolution of Concepts and Models for Quantifying Resiliency and Flexibility of Chemical Processes, *Computers & Chem. Eng.* **Vol. 70**, 5, Nov., pp. 22–34

Holt, B. R. and Morari, M., Design of Resilient Processing Plants - V. The Effect of Deadtime on Dynamic Resilience, *Chem. Eng. Sci.*, **Vol. 40**, pp. 1229–1237, (1985a).

Holt, B. R., and Morari, M. (1985b). Design of Resilient Processing Plants–VI. The Effect of Right–Half–Plane Zeros on Dynamic Resilience. *Chem. Eng. Sci.*, **40**, pp. 59–74.

Johnston, R. D., and Barton, G. W. (1987). Design and Performance Assessment of Control Systems Using Singular Value Analysis, *Ind. Eng. Chem. Res.*, **26**, pp. 830–839.

Levien, K. L., and Morari, M. (1987). Internal Model Control of Distillation Columns, *AIChE J.*, **Vol. 33**, No. 1, pp. 83–98.

Mandler, J. A., Morari, M., and Seinfeld, J. H. (1986). Control System Design for a Fixed-Bed Methanation Reactor, *Chem. Eng. Sci.*, **Vol. 41**, pp. 1577–1597.

Manousiothakis, V., Savage, R., and Arkun, Y. (1986). Synthesis of Decentralized Process Control Structures Using the Concept of Block Relative Gain, *AIChE J.*, **Vol. 32**, No. 6, pp. 991–1003.

McAvoy, T. J. (1987). Integration of Process Design and Process Control, in *Recent Developments in Chemical Process and Plant Design*, Liu, Y. A., McGee, H. A.(Jr.), and Epperly, W. R. (Eds.), Chap. 8, John Wiley & Sons, New York.

Morari, M. (1983a). Design of Resilient Processing Plants-III. A General Framework for the Assessment of Dynamic Resilience. *Chem. Eng. Sci.*, **38**(11), 1881-1898.

Morari, M. (1983b). Flexibility and Resiliency of Process Systems, *Comput. & Chem. Eng.*, **Vol. 7**, No. 4, pp. 423–437.

Morari , M., W. Grimm, M. J. Oglesby and Prosser, I. D. (1985). Design of Resilient Processing Plants – VI. Design of Energy Management Systems for Unstable

Reactors – New Insights. *Chem. Eng. Sci.*, **40**(2), pp. 187–198.

Ogunnaike , B. A. and Ray, W. H.(1994), *Process Dynamics, Modeling and Control* , Oxford University Press,New York.

Patnaik, L. M. Viswanadham, N., and Sarma, I. G. (1980a). State Space Formulation of Ammonia Reactor Dynamics, *Comput. & Chem. Eng.*, **Vol. 4**, pp. 215–222.

Patnaik , L. M., Viswanandham and Sarma, I. G. (1980b). Computer Control Algorithms for a Tubular Ammonia Reactor, *IEEE Trans. Autom. Control.*, **AC-25**, No. 4, August, pp. 642–651.

Patnaik, L. M., Viswanandham and Sarma, I. G. (1981). Design of Multiloop Controllers for an Ammonia Reactor, IEEE Trans. on Inds. Elec. and Control Inst., **Vol. IECI-28**, No. 4, Nov. pp. 353-358.

Perkins , J. D., and Wong, M. P. F. (1985). Assessing Controllability of Chemical Plants, *Chem. Eng. Res. Des.*, **63**, pp. 358–362.

Shimizu, K., Holt, B. R., Morari, M., and Mah, R. S. (1985). Assessment of Control Structures for Binary Distillation Columns with Secondary Reflux and Vaporization, *Ind. & Eng. Chem. Process Design Dev.*, **24**, pp. 852–858.

Skogestad, S., and Postlethwaite, I. (2011). *Multivariable Feedback Control: Analysis and Design*, 3rd ed., Wiley, New York

Van de Wal, M. and de Jager, B. (2001), A Review of Methods for Input/Output Selection, *Automatica*, **37**, pp. 487-510.

Viswanadham, N., Patnaik, L. M., and Sarma I. G. (1979). Robust Multivariable Controllers for a Tubular Ammonia Reactor, *ASME J. Dynamic Syst. Meas. & Control*, **Vol. 101**, pp. 290 –298. Dec., (1979).

Williams, A. O. F., and Adeniyi, V. O. (1991). Dynamic Resilience Analysis of the Measurement Structures for a Distributed Parameter Heat conduction System, *Proc. Nig. Soc. Chem. Engrs. 21st. Ann. Conf.*, Otta, Ogun State, pp. 39–47.

Williams, A. O. F. and Adeniyi, V. O. (2001). Development of Some Fortran 77 Programs for Linear System Analysis, *NSE Technical Transactions*, **Vol. 36**, No. 1., pp. 68–80

Williams, A. O. F. and V. O. Adeniyi (2017). Identification of New Control Structures for a Tubular Ammonia Reactor System Using Dynamic Resilience Analysis, paper presented at the 2017 Ann. Conf. of NSChE, Port Harcourt

Yuan, Z., Chen, B., and Zhou, J. (2011). An Overview on Controllability Analysis of Chemical Processes, AIChE J., **Vol. 57**, No. 5, May, pp. 1185–1201.

Appendix A

Table 1: List of the possible sixty 2 × 2 2 control structures for the tubular ammonia reactor- heat exchanger system

Control structure	Manipulated variables, u	Controlled variables	Control structure	Manipulated variables, u	Controlled variables
A	u_1, u_2	x_1, x_2	AE	u_1, u_3	x_1, x_8
B	,,	x_1, x_3	AF	,,	x_2, x_8
C	,,	x_1, x_4	AG	,,	x_3, x_8
D	,,	x_1, x_5	AH	,,	x_4, x_8
E	,,	x_2, x_3	AI	,,	x_5, x_8
F	,,	x_2, x_4	AJ	,,	x_1, x_9
G	,,	x_2, x_5	AK	,,	x_2, x_9

Table 1: List of the possible sixty 2 × 2 2 control structures for the tubular ammonia reactor- heat exchanger system

Control structure	Manipulated variables, u	Controlled variables	Control structure	Manipulated variables, u	Controlled variables
H	,,	x_3, x_4	AL	,,	x_3, x_9
I	,,	x_3, x_5	AM	,,	x_4, x_9
J	,,	x_4, x_5	AN	,,	x_5, x_9
K	,,	x_1, x_8	AO	u_2, u_3	x_1, x_2
L	,,	x_2, x_8	AP	,,	x_1, x_3
M	,,	x_3, x_8	AQ		x_1, x_4
N	,,	x_4, x_8	AR	,,	x_1, x_5
O	,,	x_5, x_8	AS	,,	x_2, x_3
P	,,	x_1, x_9	AT	,,	x_2, x_4
Q	,,	x_2, x_9	AU	,,	x_2, x_5
R	,,	x_3, x_9	AV	,,	x_3, x_4
S	,,	x_4, x_9	AW	,,	x_3, x_5
T	,,	x_5, x_9	AX	,,	x_4, x_5
U	u_1, u_3	x_1, x_2	AY	,,	x_1, x_8
V	,,	x_1, x_3	AZ	,,	x_2, x_8
W	,,	x_1, x_4	BA	,,	x_3, x_8
X	,,	x_1, x_5	BB	,,	x_4, x_8
Y	,,	x_2, x_3	BC	,,	x_5, x_8
Z	,,	x_2, x_4	BD	,,	x_1, x_9
AA	,,	x_2, x_5	BE	,,	x_2, x_9
AB	,,	x_3, x_4	BF	,,	x_3, x_9
AC	,,	x_3, x_5	BG	,,	x_4, x_9
AD	,,	x_4, x_5	BH	,,	x_5, x_9

Table 2: List of the possible twenty 2×3 control structures for the tubular ammonia reactor-heat exchanger system

Control structure	Manipulated variable, u	Controlled variables	Control structure	Manipulated variable, u	Controlled variables
BI	u_1, u_2, u_3	x_1, x_2	BS	u_1, u_2, u_3	x_2, x_9
BJ	,,	x_1, x_3	BT	,,	x_3, x_4
BK	,,	x_1, x_4	BU	,,	x_3, x_5
BL	,,	x_1, x_5	BV	,,	x_3, x_8

Table 2: List of the possible twenty 2×3 control structures for the tubular ammonia reactor-heat exchanger system

Control structure	Manipulated variable, u	Controlled variables	Control structure	Manipulated variable, u	Controlled variables
BM	,,	x_1, x_8	BW	,,	x_3, x_9
BN	,,	x_1, x_9	BX	,,	x_4, x_5
BO	,,	x_2, x_3	BY	,,	x_4, x_8
BP	,,	x_2, x_4	BZ	,,	x_4, x_9
BQ	,,	x_2, x_5	CA	,,	x_5, x_8
BR	,,	x_2, x_8	CB	,,	x_5, x_9

Table 3: List of the possible thirty 3×3 control structures for the tubular ammonia reactor-heat exchanger system

Control structure	Manipulated variables, u	Controlled variables	Control structure	Manipulated variables, u	Controlled variables
CC	u_1, u_2, u_3	x_1, x_2, x_3	CR	u_1, u_2, u_3	x_2, x_3, x_5
CD	,,	x_1, x_2, x_4	CS	,,	x_2, x_3, x_8
CE	,,	x_1, x_2, x_5	CT	,,	x_2, x_3, x_9
CF	,,	x_1, x_2, x_8	CU	,,	x_2, x_4, x_5
CG	,,	x_1, x_2, x_9	CV	,,	x_2, x_4, x_8
CH	,,	x_1, x_3, x_4	CW	,,	x_2, x_4, x_9
CI	,,	x_1, x_3, x_5	CX	,,	x_2, x_5, x_8
CJ	,,	x_1, x_3, x_8	CY	,,	x_2, x_5, x_9
CK	,,	x_1, x_3, x_9	CZ	,,	x_3, x_4, x_5
CL	,,	x_1, x_4, x_5	DA	,,	x_3, x_4, x_8
CM	,,	x_1, x_4, x_8	DB	,,	x_3, x_4, x_9
CN	,,	x_1, x_4, x_9	DC	,,	x_3, x_5, x_8
CO	,,	x_1, x_5, x_8	DD		x_3, x_5, x_9
CP	,,	x_1, x_5, x_9	DE	,,	x_4, x_5, x_8
CQ	,,	x_2, x_3, x_4	DF	,,	x_4, x_5, x_9

MODELLING AND SIMULATION OF REACTIVE DISTILLATION SYSTEMS USING MATLAB AND ASPEN PLUS

[*]Bamikole, J.O. and Taiwo, O.
Process Systems Engineering Laboratory, Obafemi Awolowo University, Ile-Ife, Nigeria
(E-mails: johnbamy@yahoo.com and femtaiwo@yahoo.com)

ABSTRACT

A systematic but simple approach for modeling reactive distillation columns using the Material Equilibrium, Summation and Heat (MESH) equations was developed. The unsteady state model involves Differential Algebraic Equations (DAE), in order to avoid initial value and convergence error, the solution of a model with more simplifying assumptions was used as initial values for the complicated model. The model was simulated in MATLAB using the solver ode15s with MTBE, ETBE and methyl acetate reactive distillation systems as case studies. The results of the model are very similar to those obtained from Aspen Plus simulation and the literature. The model was used to study the effect of different reaction kinetics and activity models on the compositions, temperatures, activity coefficients, percentage purity and percentage conversion in the column. The model is simple, easy to implement without complicated algorithm, useful in studying, simulating and predicting reactive distillation systems with no initial value problem and convergence error.

Keywords: Modeling, MATLAB, Aspen Plus, Reactive distillation, MTBE, ETBE, Methyl Acetate

1. INTRODUCTION

The recent trend for economic and environmental considerations in the chemical process industries has led to the development of the concept of process intensification. Process intensification is a technological development of improving processes for chemical and high energy efficiency. Process intensification has led to the increasing interest in the reactive distillation. (Luyben and Yu, 2008).

Reactive distillation is a process that combines reaction and separation into a single unit. This unit can be said to be a combination of a reactor and a conventional distillation column. It is a hybrid process with dual process objectives of reactants conversion and products compositions, (Sneesby *et al*., 1999). This system can be viewed as a process which begins with reaction of reactants in the reactor after which its effluents are separated based on their relative volatilities in the distillation column.

Reactive distillation process is preferred to conventional process of a reactor then follow by a separator because; it drives reaction to completion, it reduces the tendency for formation of side-reactions and by-products, reduces the quantity of catalysts, heat is integrated (heat of an exothermic reaction can be used for vaporization) and azeotrope can be avoided. (Taylor and Krishna, 2000).

Despite the increasing interest and benefits of reactive distillation, its design and operation are challenging. The high degree of interaction between the vapour-liquid equilibrium, vapour-liquid mass transfer, chemical kinetic and intra-catalyst diffusion from the reaction and separation processes make the column complex. (Taylor and Krishna, 2000). The complexity is conspicuous with the occurrence of multiple steady states and complex dynamics.(Isao,1971; Jacobs and Krishna, 1993; Ciric and Miao, 1994; Mohlet al., 1999; Guttinger and Morari, 1997 Chen et al.,2002).

The production of Methyl tertiary buthyl ether (MTBE) from methanol and isobutene in a reactive distillation column is a handy example of reactive distillation that has been extensively studied. This system is a ternary reactive distillation in the presence of an inert. The modeling and simulation of this system has been studied using different algorithms as given by Chen et al.(2002) and commercial software packages like Speedup, Chemcad and Aspen plus (Abufares and Douglas, 1995; Isla and Irazoqui,1996; Pilavachi et al., 1997; Bao et al., 2002; Wang et al., 2003). Different kinetics and activity models have also been used to study the system. Jhon and Lee, (2003) developed a rigorous algorithm for simulating reactive distillation dynamically. Raful *et al.,* (2008) developed an algorithm for solving the DAE system of equations for reactive distillation, in an attempt to increase the speed of convergence, analytical differentiation was carried out in order to obtain the rate change of enthalpy. Enthalpies functions are complex and analytical differentiation of these functions are tedious.

The focus of this work is to develop a mathematical model for reactive distillation that will be simulated using inbuilt solvers in MATLAB, compare the results of the model with that of Aspen plus and check the

impact of reaction kinetics and activity models on the systems.

In section 2 the mathematical modeling that was used for the work was presented. Section 3, deals with illustrative examples of MTBE, ETBE and methyl acetate reactive distillation systems to validate model. Conclusions from the work are considered in section 4.

2. MODELING

The equilibrium model was adopted in the modeling of reactive distillation in this work. The Material Equilibrium Summation and Heat (MESH) balance was adopted in the modeling of the system. The MESH model leads to a set of differential and algebraic equations (DAE) system. The material balance includes the overall mole balance and component mole balance. In this work in order to maintain a DAE system for all the models, the component mole balance equations were used in their unsteady state forms and serve as the differential part of the DAE system.

To develop the model for this work the following assumptions were made:

1. There is vapour-liquid equilibrium between vapour and liquid leaving a stage.
2. Constant liquid molar hold-up in all stages.
3. Vapour molar hold-up is negligible
4. Pressure drop in the column is negligible.
5. Reaction takes place in the liquid phase.
6. Ideal Vapour phase.

The top-bottom convention was used in modeling this work with the condenser as stage 1 and the reboiler as last stage. The schematic representation of reactive distillation that was used for modeling the system is shown in Figure 1. The total mole balance for the condenser, other stages and reboiler are shown in the Equations (1), (2) and (3) respectively.

Total mole balance;

For the condenser

$$V_2 = L_1 + D \qquad (1)$$

For stage i

$$L_{i-1} + V_{i+1} + F_i = L_i + V_i + \delta_i R_i \qquad (2)$$

For the reboiler

$$L_{N-1} = B + V_N \qquad (3)$$

L_i is the molar liquid flow on stage *i*, V_i is vapour molar flow on stage *i*, D is the distillate flowrate, B is the bottom flowrate, R_i is the total rate of reaction on stage *i* and F_i is the feed rate in stage *i*.

δ_i can take a value of 1 or 0 for reactive and non-reactive stages respectively.

It should be noted that L_1 and V_N are the reflux and boil up flow rate respectively

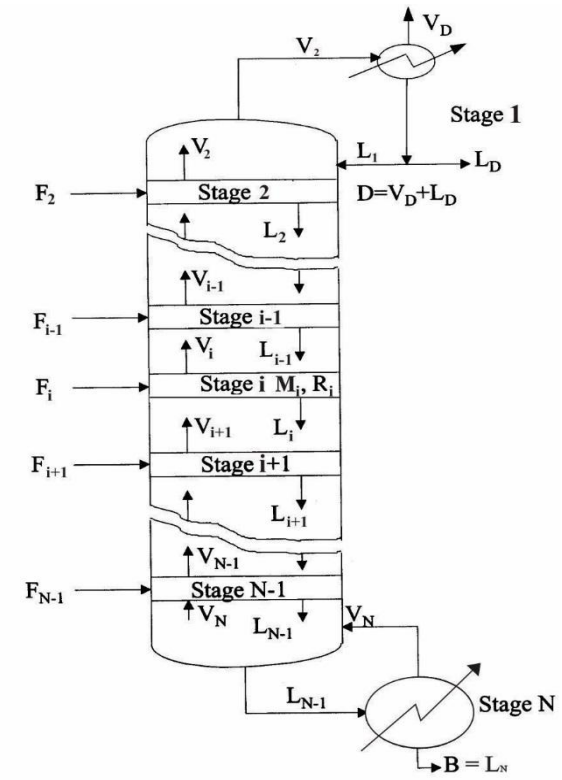

Figure 1: A Schematic Diagram of Reactive Distillation

The overall mole balance for the column is given as

$$\sum_{i=1}^{N} F_i + \sum_{i=1}^{N} R_i = B + D \qquad (4)$$

The component mole balance for component j in the condenser, stage i and the reboiler are shown in Equations (5), (6) and (7) respectively.

For condenser

$$\frac{M_1 dx_{1,j}}{dt} = V_2 y_{2,j} - L_1 x_{1,j} - D x_{1,j} \qquad (5)$$

For stage i

$$\frac{M_i dx_{i,j}}{dt} = L_{i-1} x_{i-1,j} - L_i x_{i,j} + V_{i+1} y_{i+1,j} - V_i y_{i,j} - F_i z_{i,j} + \delta_i v_j r_{i,j} \qquad (6)$$

for the reboiler

$$\frac{M_N dx_{N,j}}{dt} = L_{N-1} x_{N-1,j-} - B x_{N,j} - V_N y_{N,j} \qquad (7)$$

$x_{i,j}$ and $y_{i,j}$ are the mole fractions in liquid and vapour phases in stage *i* and component *j* respectively. v_j is the stoichiometric coefficient of component *j*, $r_{i,j}$ is the rate of production or consumption of component *j* via reaction in stage *i*.

The equilibrium balance between the liquid and vapour phase is shown below

$$y_{i,j} = \frac{\gamma_{i,j} P^0_{i,j} x_{i,j}}{\emptyset_{i,j} P} \quad (8)$$

Where γ is the activity coefficient, P^0 is the saturated vapour pressure calculated from the Antoine equation, $\emptyset$ is the fugacity coefficient and P is the total pressure of the column.

The summation equations in the liquid and vapour phase in stage i are shown in Equations (8) and (9) respectively.

$$\sum_{j=1}^{nc} x_{i,j} = 1 \quad (9)$$

$$\sum_{j=1}^{nc} y_{i,j} = 1 \quad (10)$$

The heat balance

For condenser

$$V_2 H_2 = (L_1 + D)h_1 + Q_c \quad (11)$$

For stage i

$$L_{i-1}h_{i-1} + V_{i+1}H_{i+1} + F_i h_i^f = L_i h_i + V_i H_i + \delta_i R_i H_i^R \quad (12)$$

For reboiler

$$L_{N-1}h_{N-1} + Q_R = Bh_N + V_N H_N \quad (13)$$

Where Q_c and Q_R are the condenser and reboiler heatduties respectively. H_i and h_i are the vapour enthalpy and liquid enthalpies respectively for stage *i*, h_i^f enthalpy of feed in stage *i*, H_i^R is the heat of reaction in stage *i*. The total enthalpy is a summation of all the partial enthalpies as shown in Equations (14) and (15).

$$H_i = \sum_{j=1}^{nc} y_{i,j} H^0_{i,j} + \Omega_V \quad (14)$$

$$h_i = \sum_{j=1}^{nc} x_{i,j} H^0_{i,j} + \Omega_L \quad (15)$$

Where Ω_V and Ω_L are departure functions of actual gas and liquid from ideal gas respectively. These departures can be estimated with equations of state. (Holland,1980; Henley and Seader,1981).

The above set of equations form a set of differential and algebraic equations (DAE) which were solved using the MATLAB ode15s solver. The algorithm involves making the unspecified variables i.e. y, V and L functions of the liquid mole fraction x and the temperature T.

Solving these set of equations using algorithm like ode15s could lead to initial and convergence problem, the solver will require a good set of initial values. To overcome this problem, the model was further simplified by the assumption of constant vapour and liquid flows except in the reactive section of the column. The following equations were used in developing the simplified model for a good set of initial values; the distillate flowrate is calculated from the overall mole balance in the column in (4) and it is given in (16)

$$D = \sum_{i=1}^{NT} F_i + \sum_{i=1}^{NT} R_i - B \quad (16)$$

Calculate reflux flow L_1 from Equation (17)

$$L_1 = rD \quad (17)$$

Where *r* is the reflux ratio

Calculate V_2 from Equation (1)

Calculate all the other V_i from Equation (18)

$$V_i = D(r+1) + \sum_{i=2}^{i} (1 - q_i)F_i \quad (18)$$

Calculate all the L_i from Equation (19)

$$L_i = rD + \sum_{2}^{i} q_i F_i + \sum_{1}^{i} R_i \quad (19)$$

The algorithm is summarized as follows
Calculate y(x,T) from Equation (8)
Calculate D(x,T) from Equation (16)
Calculate reflux flow L_1 from Equation (17)
Calculate V_2 from Equation (1)
Calculate all the $L_i$from Equation (19)
Calculate x from the differential Equations (5) to (7)
Calculate T by solving the algebraic Equation (10)
Calculate V from Equations (1) to (3)

3.0 EXAMPLES

3.1 Example 1: MTBE Reactive Distillation

3.1.1 Process Description

In the MTBE reactive distillation system, the MTBE is produced from the reversible reaction between isobutene (IB) and methanol (MeOH). The isobutene contains

normal butene (NB) which serves as an inert for the reactive system. The major reaction in the system is given in (20)

$$(CH_3)_2C = CH_2 + CH_3OH \leftrightarrow (CH_3)_3COCH_3 \qquad (20)$$

The reaction kinetics are taken from Rehfinger and Hoffmann, (1990) and Seader and Henley, (1998). Two types of reaction kinetics are commonly used; one in terms of mole fractions and the other in terms activities. The first reaction kinetic in terms of mole fractions is given in Equations (21), (22) and (23) and the other is in terms of activities is given in Equation (24).

$$rate = WqK_f(r_f - r_b) \qquad (21)$$

$$r_f = 3.67 \times 10^{12} exp\left(\frac{-92440}{RT}\right)\left(\frac{x_{IB}}{x_{MeOH}}\right) \qquad (22)$$

$$r_b = 2.67 \times 10^{17} exp\left(\frac{-134454}{RT}\right)\left(\frac{x_{MTBE}}{x_{MTBE}^2}\right) \qquad (23)$$

W is the weight of catalyst (kg) on each stage, q is the amount of acid groups on the resin per unit mass (4.9 equiv/kg), r_f and r_b are the rate of forward and backward reactions in moles per second per equivalent of acid groups.

The reaction in terms of activities is given as

$$rate = WqK_f\left[\frac{a_{IB}}{a_{MeOH}} - \frac{a_{MTBE}}{K_{eq}\, a_{MeOH}^2}\right] \qquad (24)$$

K_f and K_{eq} are the rate of forward and reaction and equilibrium constant which is a complex function of temperature $f(T)$ as shown in Equations (25) and (26) respectively. The temperature function of the equilibrium constant is given in Equation (27).

$$K_f = 3.67 \times 10^{12} exp\left(-\frac{11110}{T}\right) \qquad (25)$$

$$K_{eq} = 284 exp[f(T)] \qquad (26)$$

$$f(T) = A_1\left(\frac{1}{T} - \frac{1}{T_0}\right) + A_2 ln\left(\frac{T}{T_0}\right) + A_3(T - T_0) + A_4(T^2 - T_0^2) + A_5(T^3 - T_0^3) + A_6(T^4 - 704 \qquad (27)$$

Where $T_0 = 298.15K$, $A_1 = -1.49277 \times 10^3 K$,

$A_2 = -77.4002$, $A_3 = 0.507563K^{-1}$,

$A_4 = 9.12739 \times 10^{-4}K^{-2}$, $A_5 = 1.10649 \times 10^{-6}K^{-3}$, $A_6 = -6.27996 \times 10^{-10}K^{-4}$

3.1.2 SIMULATION

The column configuration and specification given by Seader and Henley (1998) was used for the simulation and it is shown in Table 1. The column has a total number of 17 stages including the reboiler and condenser.

Seader and Henley (1998) used Aspen plus to simulate the system using reaction kinetics in terms of mole fractions given in Equations (21), (22) and (23) and UNIQUAC activity model.

This specification was used as the base case in our study, the reaction kinetic in terms of mole fractions in Equation (21), (22) and (23) were used. The set of modeling Equations and algorithm given in the previous section were used in simulating the system in MATLAB while in Aspen plus the RADFRAC model was used in simulating the system using design specification given by Jana (2011). The Peng Robinson equation of state was used to estimate enthalpy departure. The Extended Antoine equation was used for the vapour pressure calculation.

3.1.3 CASE 1

Case 1 uses the reaction kinetics in equations (21), (22) and (23). This case was chosen as the base and reference case in order to validate the mathematical modeling in MATLAB and Aspen Plus by comparing the results obtained with that of Seader and Henley (2006). The initial values for both composition and temperature are shown in Figures 2 and 3. These values were used for dynamic simulation of the system until it converges to a new steady state. The steady state liquid mole fractions of the components for MATLAB and Aspen Plus are shown in the Figures 4 and 5 respectively. The compositions profile from both MATLAB and Aspen Plus are similar to that of Seader and Henley, (2006) and those reported in the literature. The temperature profiles for the simulation in MATLAB and Aspen Plus are shown in Figures 6 and 7 respectively. The reaction profiles are also shown in Figures 8 and 9 for simulation in MATLAB and Aspen Plus respectively.

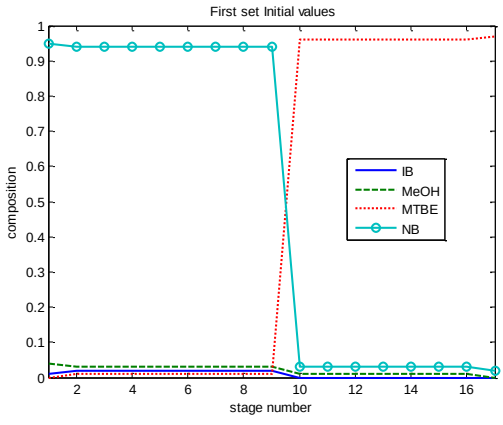

Figure 2: Initial Values for Liquid Compositions for MTBE

Table 1: MTBE System Column Configuration and Feed Specification

	Units		
Number of stages		17	
Number of Reactive tray		8	
Pressure	bar	11	
Bottom flow rate (B)	mol/s	197	
Reflux ratio		7	
		Feed 1	Feed 2
Flow rate		215.5	549
Temperature	K	320	350
Pressure	Bar	11	11
Stage		11	11
x_{IB}		0.0	0.356
x_{MeOH}		1	0.0
x_{MTBE}		0.0	0.0
x_{NB}		0.0	0.644

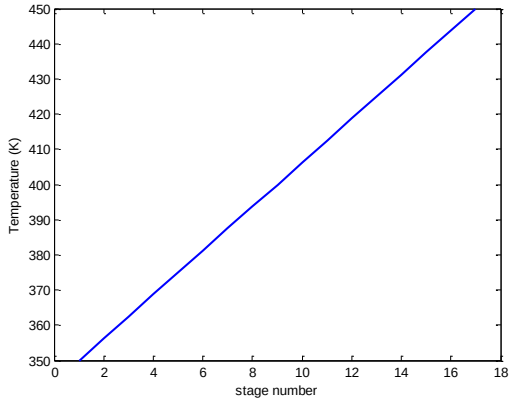

Figure 3: Initial Values of Temperature profile for MTBE

All these results are similar to those given in the literature and in the work of Seader and Henley (2006). A summarized comparison for the terminal products (top and bottom) of the base case is presented in Table 2. The values are so close for all the results and the percentage conversion are very close, this shows that the assumptions in the mathematical modeling done in MATLAB are valid and can be compared with standard commercial simulation software package like Aspen plus and results in the literature.

The temperature profiles are shown in Figures 6 and 7 for both MATLAB and Aspen Plus. The profiles are also similar to that of Seader and Henley, (2006).

The compositions and temperatures of terminal products are summarized and compared with those of Seader and Henley, (2006) as shown in Table 2. From close observation of the result, the result of the simulation of MATLAB and Aspen Plus are close to that of Seader and Henley (2006).

The activity coefficient profile of all the components are plotted in Figure 10, the activity coefficient show that the system is highly non-ideal, from the plot it can be seen that the activity coefficients of all other components except that of MeOH are close to unity, while that of MeOH ranges from least value of 2.39 in stage 17 to highest value of 13.04 in stage 5. This shows that the main non-ideality in the system is as a result of methanol, this agrees with previous observations in the literature. (Jacobs and Krishna, 1993; Seader and Henley, 2006; Murat,et al, 2003)

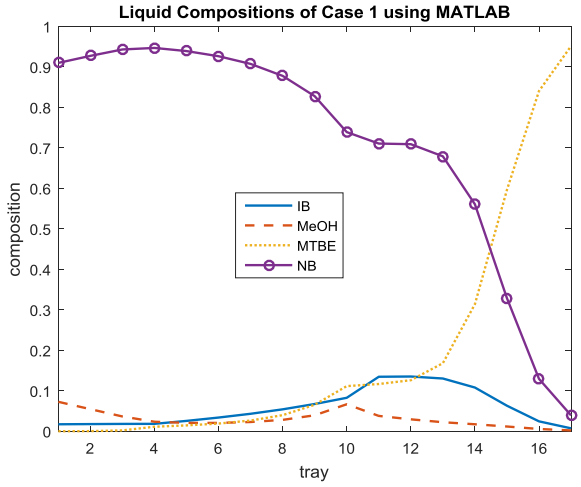

Figure 4: Liquid Composition Profile for MTBE Case 1 using MATLAB

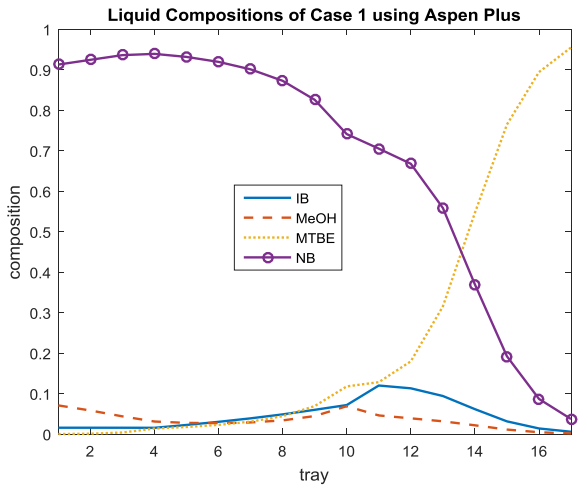

Figure 5: Liquid Composition Profile for MTBE Case 1 using Aspen Plus

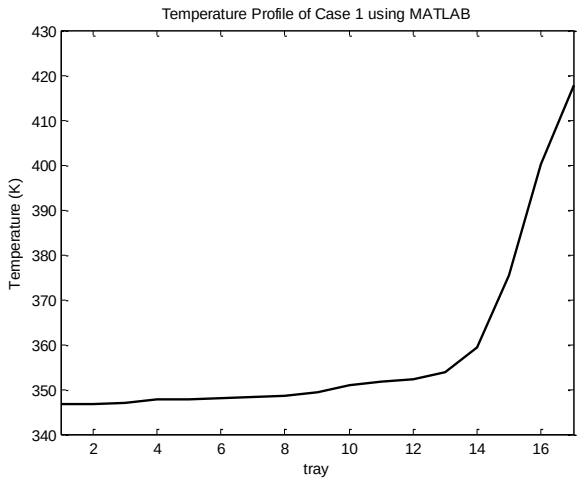

Figure 6: Temperature Profile for MTBE Case 1 using MATLAB

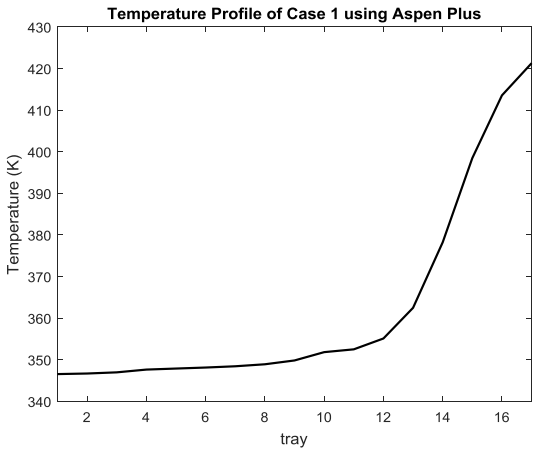

Figure 7: Temperature Profile for MTBE Case 1 using Aspen Plus

Table 2: Comparison of Simulation for MTBE Base Case

		Seader and Henley (2006)		MATLAB		Aspen	
Quantity	Units	Top	Bottom	Top	Bottom	Top	Bottom
x_{IB}		0.0191	0.0066	0.0175	0.0072	0.0161	0.0074
x_{MeOH}		0.0744	0.0016	0.0726	0.0028	0.0718	0.0020
x_{MTBE}		0.0003	0.9479	0.0001	0.9509	0.0001	0.9534
x_{NB}		0.9062	0.0439	0.9098	0.0391	0.9120	0.0371
Flow	mol/s	380.63	197	380.14	197	379.26	197
Temperature	K	347	420	347.70	418.72	346.54	421.27
% conversion		95.5443		95.8704		96.1298	

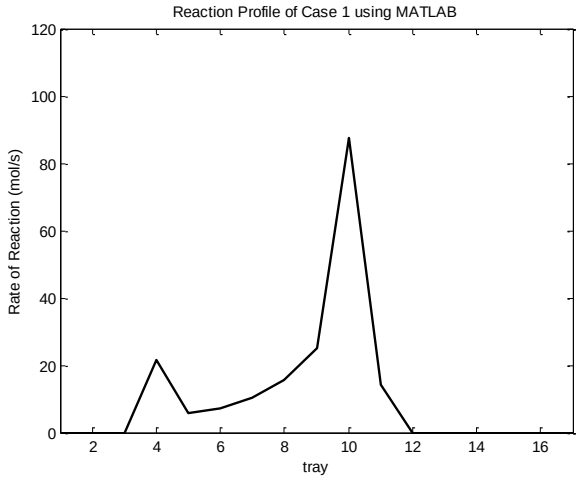

Figure 8: The Reaction Profile for MTBE Case 1 using MATLAB

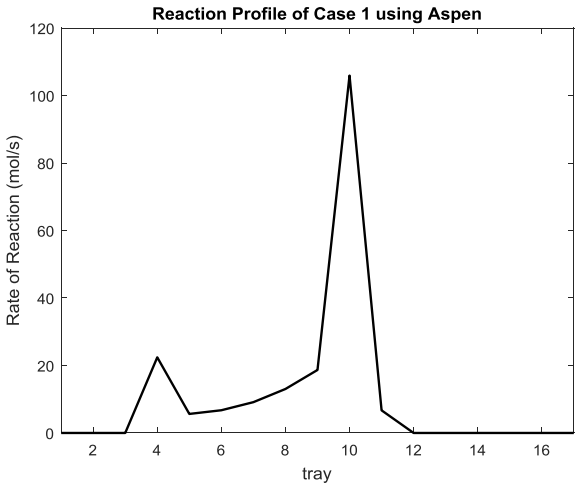

Figure 9: The Reaction Profile for MTBE Case 1 using Aspen Plus

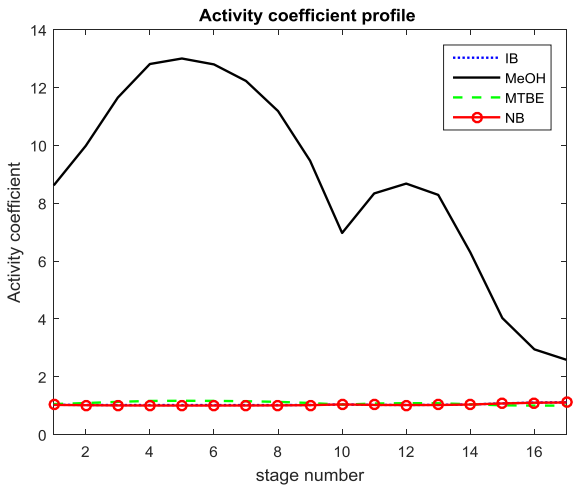

Figure 10 Activity Coefficients Profile for MTBE Case 1

3.1.4 CASE 2

Further simulation was done by using the base specification to simulate a second case study in which the reaction kinetic in terms of activities and complex temperature dependence equilibrium constant was used with the UNIQUAC activity coefficient model as given in (24) to (27). To simulate this reaction kinetic in RADFRAC model in Aspen plus, a fortran subroutine was used. The result of the simulation for the composition profiles using both MATLAB and Aspen plus are shown in Figures 11 and 12. The profiles are similar to each other and these are similar to the simulation result of case1. The percentage purity of MTBE at the top and percentage conversion of IB in case 2 are higher than that of case 1. The rate of reaction profiles shown in Figures 13 and 14 for case 2 show that the rate of reaction increases down the reactive stages with the peak at stage 10 in the MATLAB model while in Aspen Plus simulation stage 11 has the highest rate of reaction.

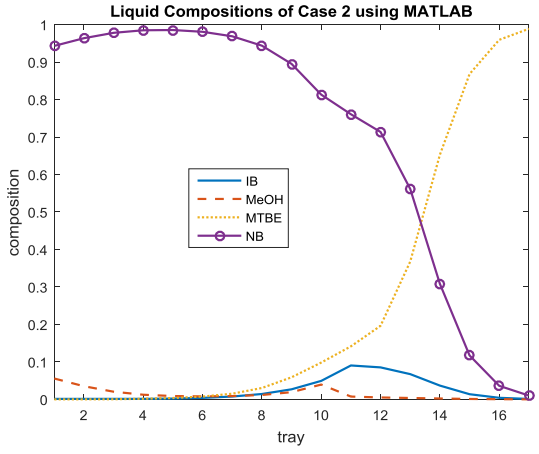

Figure 11: Liquid Composition Profile for MTBE Case 2 using MATLAB

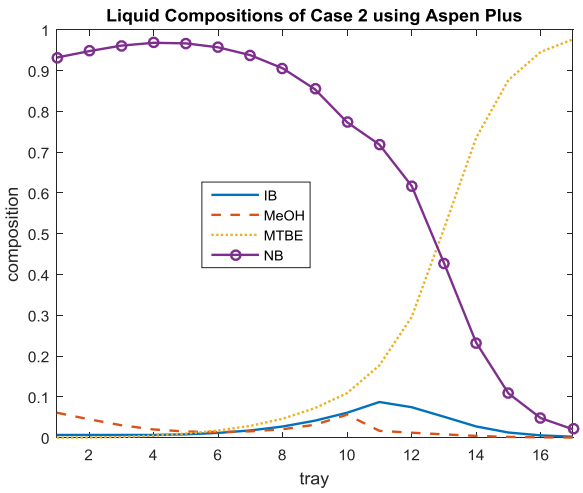

Figure 12: Liquid Composition profile for MTBE Case 2 using Aspen Plus

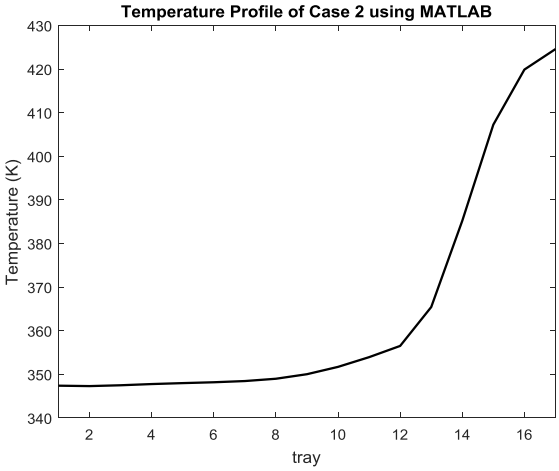

Figure 13: Temperature profile for MTBE Case 2 using MATLAB

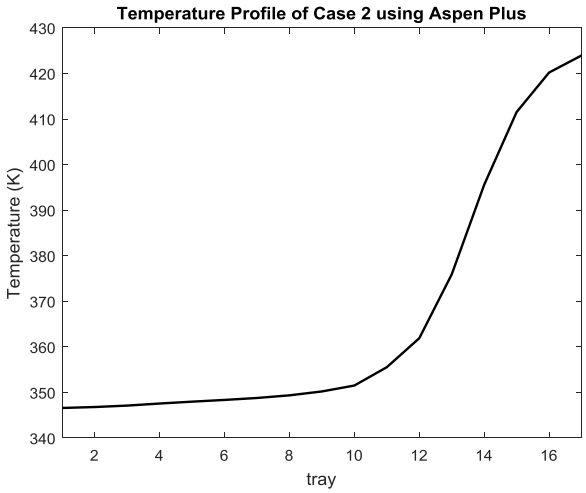

Figure 14: Temperature Profile for MTBE Case 2 using Aspen Plus

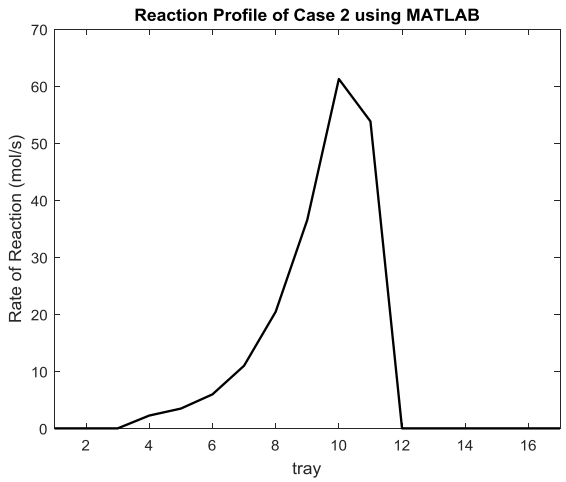

Figure 15 Reaction profile for MTBE Case 2 using MATLAB

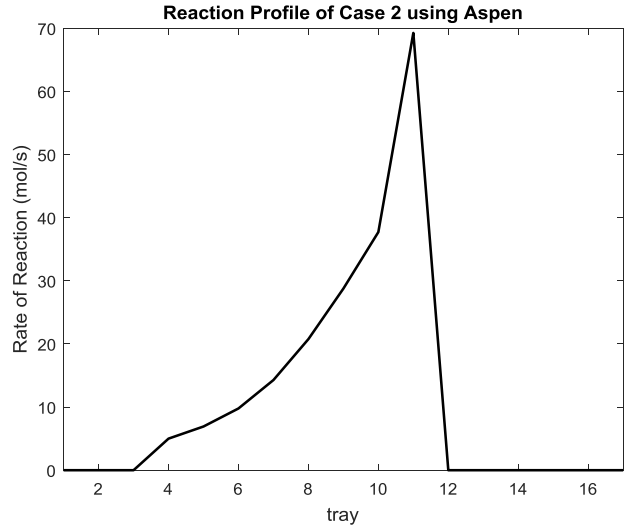

Figure 16: Reaction profile for MTBE Case 2 using Aspen Plus

3.1.5 Activity Models

Four activity models were used for both cases 1 and 2 using MATLAB and Aspen Plus, the result of MATLAB simulation of case 1 is shown in Table 3. NTRL has the least MTBE purity at the top followed by UNIQUAC, UNIFAC and Wilson with the highest, the percentage conversion of IB in an increasing order of NTRL, UNIFAC, UNIQUAC and Wilson. The Aspen Plus simulation for this case is shown in Table 4, the percentage purity of MTBE in increasing order of UNIFAC, NTRL, UNIQUAC and Wilson and the conversion of IB follows the same order. From previous discussion, it was shown that MeOH is the major reason for the non-ideality of the MTBE system. Therefore to check the impact of the various activity models, Methanol activity coefficient profile for all the activity models used are shown in Figure 17, from the plot it can be seen that NRTL activity profile has the highest set of values which varies from a lowest value of 2.6 at stage 17 to the highest value of 14.14 at stage 5, the MeOH activity models for UNIQUAC and UNIFAC profile are similar and they superimpose each other. The MEOH Wilson activity model has the lowest set of values which ranges from 2.57 in stage 17 to 9.53 in stage 5. The result of the simulation shown in Tables 3 and 4 for case 1 using MATLAB and Aspen plus for all the models considered show that the Wilson model has the highest MTBE percentage purity and IB percentage conversion than any other model, while in Case 2, MTBE percentage purity and IB percentage conversion are similar for all activity models. This shows that all the activity models are suitable for correlation of the activity coefficients in the liquid phase.

3.1.6 OTHER CASES

In this section, two additional cases based on modifications in the reaction kinetics were studied; cases 3 and 4. In case 3 the reaction kinetics of case 1 given in Equations 22 and 23 were modified by replacing all the mole fractions with activities as shown in Equations 28 and 29.

$$r_f = 3.67 \times 10^{12} exp\left(\frac{-92440}{RT}\right)\left(\frac{a_{IB}}{a_{MeOH}}\right) \quad (28)$$

$$r_b = 2.67 \times 10^{17} exp\left(\frac{-134454}{RT}\right)\left(\frac{a_{MTBE}}{a_{MTBE}^2}\right) \quad (29)$$

In case 4 all the activities in Cases 2 reaction kinetics in Equation 24 are replaced with mole fraction as shown in Equation (30)

$$rate = WqK_f\left[\frac{x_{IB}}{x_{MeOH}} - \frac{x_{MTBE}}{K_{eq}\, x_{MeOH}^2}\right] \quad (30)$$

The result of all the cases using the MATLAB simulation for the base specification are shown in Table 7 The cases in which the reaction kinetics are in terms of activities have higher percentages than those in mole fractions, the percentages in case 2 are higher than case 4 and similarly the percentages in case 3 are higher than those in case 1. The cases with reaction kinetics using the complex temperature dependence equilibrium constant have higher MTBE percentage purity and IB percentage conversion as can be seen in comparison of Cases 4 and 1 and comparison between cases 2 and 3.

3.2 Example 2: ETBE Reactive Distillation

3.2.1 Process description

The ETBE reactive distillation is similar to that of MTBE studied in the example 1 both MTBE and ETBE are used for increasing the octane rating in fuel. ETBE is produced from the reversible reaction between isobutene (IB) and ethanol (EtOH). The isobutene contains normal butene (NB) which serves as an inert for the reactive system. The major reaction in the system is given in (31)

$$(CH_3)_2C = CH_2 + C_2H_5OH \leftrightarrow (CH_3)_3COC_2H_3 \quad (31)$$

The reaction kinetics based Langmuir-Hinshelwood-Hougen-Watson (LHHW) model by Zhang *et al* (1997) is given as

Table 3: Comparison of Activity Models for MTBE Case 1 using MATLAB

	UNIQUAC		UNIFAC		WILSON		NTRL	
	Top	Bottom	Top	Bottom	Top	Bottom	Top	Bottom
x_{IB}	0.0175	0.0072	0.0175	0.0075	0.0070	0.0019	0.0220	0.0104
x_{MeOH}	0.0726	0.0028	0.0732	0.0020	0.0578	0.0071	0.0793	0.0010
x_{MTBE}	0.0001	0.9509	0.0001	0.9506	0.0000	0.9768	0.0001	0.9387
x_{NB}	0.9098	0.0391	0.9092	0.0399	0.9352	0.0142	0.8986	0.0499
Flow	380.14	197	380.21	197	375.07	197	382.54	197
Temperature	347.70	418.72	347.72	418.60	348.1	422.88	347.52	416.79
% conversion	95.8704		95.8396		98.4651		94.6456	

Table 4: Comparison of Activity Models for MTBE Case 1 using Aspen Plus

	UNIQUAC		UNIFAC		WILSON		NTRL	
	Top	Bottom	Top	Bottom	Top	Bottom	Top	Bottom
x_{IB}	0.0161	0.0074	0.0279	0.0120	0.0090	0.0049	0.0187	0.0153
x_{MeOH}	0.0718	0.0020	0.0857	0.0007	0.0585	0.0017	0.0786	0.0007
x_{MTBE}	0.0001	0.9534	0.0003	0.9249	0.0004	0.9694	0.0001	0.9404
x_{NB}	0.9120	0.0371	0.8860	0.0624	0.9321	0.02412	0.9026	0.0436
Flow	379.264	197	385.166	197	376.51	197	382.20	197
Temperature	346.54	421.27	345.58	417.63	347.02	420.68	346.41	415.64
% conversion	96.1298		93.2920		97.7722		94.8008	

Table 5: Comparison of Activity Models for MTBE Case 2 using MATLAB

	UNIQUAC		UNIFAC		WILSON		NTRL	
	Top	Bottom	Top	Bottom	Top	Bottom	Top	Bottom
x_{IB}	0.0013	0.0011	0.0013	0.0011	0.0015	0.0010	0.0013	0.0012
x_{MeOH}	0.0556	0.0001	0.0556	0.0001	0.0557	0.0003	0.0557	0.0001
x_{MTBE}	0.0000	0.9887	0.0000	0.9887	0.0000	0.9884	0.0000	0.9885
x_{NB}	0.9431	0.0101	0.9431	0.0101	0.9427	0.0104	0.9430	0.0102
Flow	372.7452	197	372.74	197	372.8239	197	372.7730	197
Temperature	347.40	424.58	347.40	424.58	348.05	424.54	347.1342	424.5578
% conversion	99.6412		99.6414		99.6131		99.6311	

Table 6: Comparison of Activity Models for MTBE Case 2 using Aspen Plus

	UNIQUAC		UNIFAC		WILSON		NTRL	
	Top	Bottom	Top	Bottom	Top	Bottom	Top	Bottom
x_{IB}	0.0066	0.0023	0.0062	0.0025	0.0064	0.0023	0.0042	0.0031
x_{MeOH}	0.0612	0.0002	0.0340	0.0001	0.0610	0.0002	0.0594	0.0040
x_{MTBE}	0.0001	0.9770	0.0005	0.9777	0.0001	0.9774	0.0000	0.9770
x_{NB}	0.9321	0.0205	0.9592	0.0197	0.9325	0.0201	0.9364	0.0159
Flow(mol/s)	375	197	375	197	374.91	197	375.23	197
Temperature (K)	346.59	420.2	345.74	424.06	346.59	423.99	347.85	422.96
% conversion	98.5018		98.5584		98.5404		98.4798	

Table 7: Comparison of Different Reaction Kinetics for MTBE System

	Case 1		Case 2		Case 3		Case 4	
	Top	Bottom	Top	Bottom	Top	Bottom	Top	Bottom
x_{IB}	0.0175	0.0072	0.0012	0.0011	0.0014	0.0011	0.0170	0.0070
x_{MeOH}	0.0726	0.0028	0.0556	0.0002	0.0557	0.0002	0.0793	0.0026
x_{MTBE}	0.0001	0.9509	0.0000	0.9887	0.0000	0.9885	0.0001	0.9522
x_{NB}	0.9098	0.0391	0.9432	0.0100	0.9430	0.0102	0.9109	0.0381
Flow	380.14	197	372.75	197	372.79	197	379.89	197
Temperature	347.70	418.72	347.3998	424.5945	347.43	424.56	347.69	418.90
	95.8704		99.6602		99.6220		95.99	

$$rate = \frac{M_{cat} K_{rate} a_{EtOH}^2 \left(a_{IB} - \frac{a_{ETBE}}{K_{ETBE}}\right)}{(1 + K_A a_{EtOH})^3} \quad (32)$$

Reaction equilibrium constant

$$K_{ETBE} = 10.387 + \frac{4060.59}{T} - 2.89055 lnT - 0.0191544T + 5.28586 \times 10^{-5} T^2 - 5.32977 \times 10^{-8} T^3 \quad (33)$$

Absorption equilibrium constant

$$lnK_A = -1.0707 + \frac{1323.1}{T} \quad (34)$$

Reaction rate constant

$$K_{rate} = 7.418 \times 10^{12} \exp\left(\frac{-60.4 \times 10^3}{RT}\right) \quad (35)$$

3.2.2 Simulation

The column specification is taken from Luyben and Yu (2008) and is shown in Table 8. The column has a total number of 25 stages including the reboiler and condenser. UNIFAC activity model was used.

The compositions and temperatures of terminal products are summarized and compared with those of Luyben and Yu, (2008) as shown in Table 9, from close observation of the result, the results of the simulation of MATLAB and Aspen plus are similar to those obtained by Luyben and Yu (2008).

The composition and temperature profiles shown in Figures 18 and 19 respectively are also similar. The activity profile is shown in Figure 20, from the plot it can be seen that the activity coefficients of all the other compounds are close to unity except that of ethanol. This shows that ethanol is the major reason of the non-ideality of the system. The rate of reaction plot is shown in Figure 21. The rate reaction increases down the column with stage 19 having the highest rate of reaction.

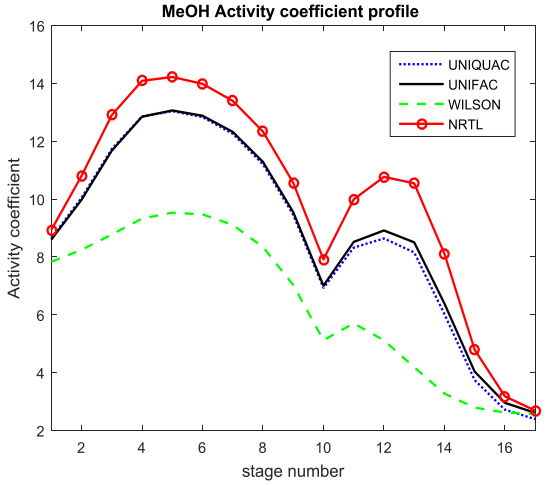

Figure 17: MeOH Activity Coefficient Profiles for Different Activity Models in MTBE System

Table 8: ETBE System Column Configuration and Feed Specification

	Units		
Number of stages		25	
Number of Reactive tray		15	
Pressure	Atm	7.5	
Bottom flow rate (B)	Kmol/h	706	
Reflux ratio		2.94	
		Feed 1	Feed 2
Flow rate		1767	549
Temperature	K	320	350
Pressure	Atm	7.5	7.5
Stage		6	20
x_{IB}		0.0	0.4
x_{MeOH}		1	0.0
x_{MTBE}		0.0	0.0
x_{NB}		0.0	0.6

The impact of different activity models was also explored, the compositions and temperature profiles of the system for all the activity model that were used were very similar but NRTL activity model has the highest percentage conversion of IB and the highest percentage purity for ETBE. Since the activity coefficients of all the other components are closed to unity, the effects of activity model on the activity coefficients on Ethanol were explored. It was observed that ethanol activity coefficients for all the models are similar except for NRTL which has least ethanol activity coefficients as shown in Figure 22.

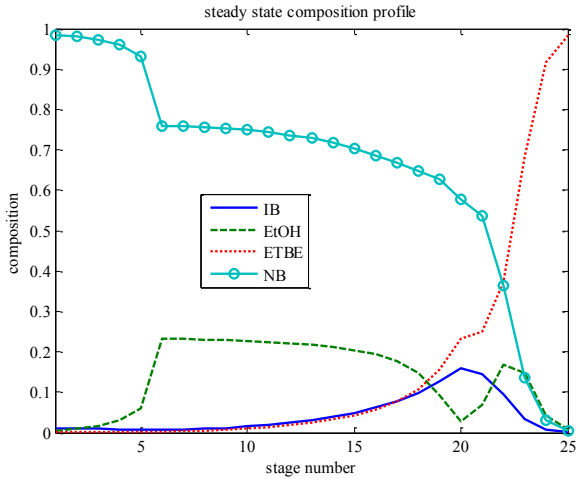

Figure 18: Liquid Composition for ETBE System

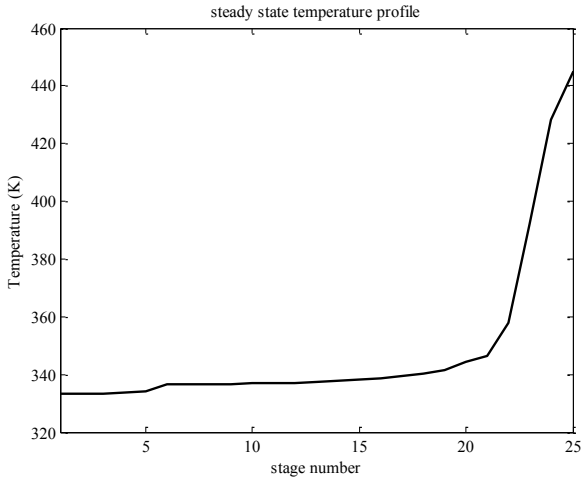

Figure 19: Temperature Profile for ETBE System

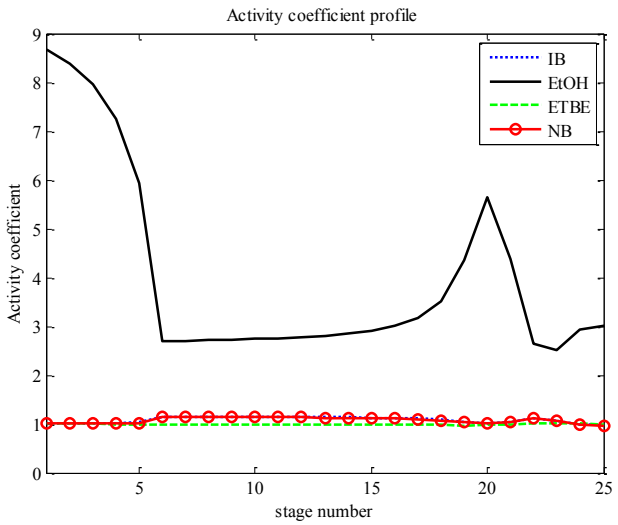

Figure 20: Activity Coefficient Profile for ETBE System

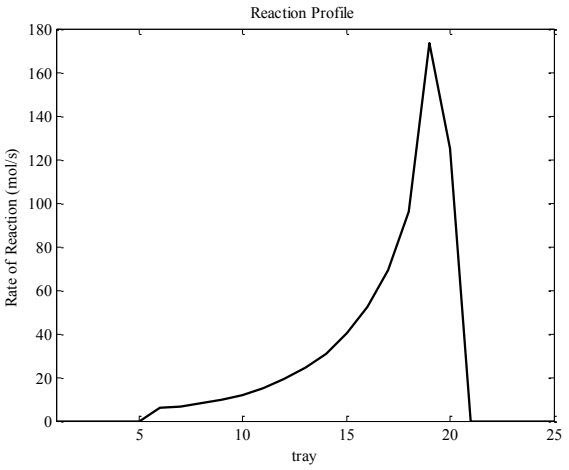

Figure 21: Rate of Reaction Profile for ETBE System

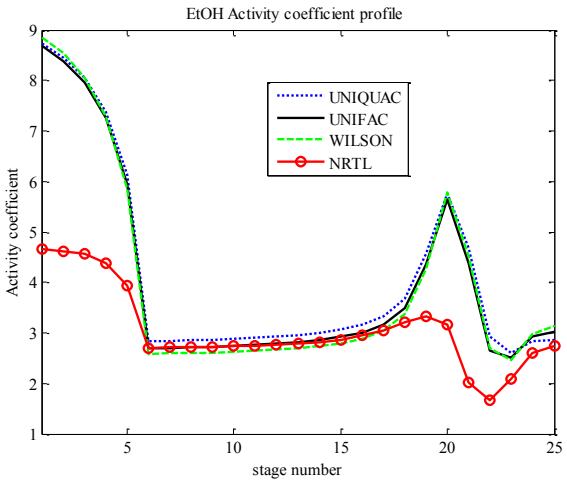

Figure 22: Comparison of Different Activity Models

Table 9: Comparison of Simulation for ETBE Base Case

		Luyben and Yu		MATLAB		Aspen	
Quantity	Units	Top	Bottom	Top	Bottom	Top	Bottom
x_{IB}		0.0050	0.0020	0.0095	0.0014	0.0045	0.0015
x_{EtOH}		0.0050	0.0020	0.0052	0.0081	0.0046	0.0013
x_{ETBE}		0.0000	0.9910	0.0000	0.9848	0.0000	0.9926
x_{NB}		0.9900	0.005	0.9851	0.0057	0.9909	0.0046
flow	Kmol/h	1068	706	1073	706	1067	706
Temperature	K	333	447	333.23	445.12	336.54	447.536
% conversion		99.4444		98.6982		99.4786	

Table 10: Comparison of Different Activity models for ETBE System

	UNIFAC		UNIQUAC		WILSON		NTRL	
	Top	Bottom	Top	Bottom	Top	Bottom	Top	Bottom
x_{IB}	0.0087	0.0012	0.0097	0.0014	0.0084	0.0012	0.0073	0.0001
x_{EtOH}	0.0046	0.0074	0.0052	0.0081	0.0044	0.0072	0.0009	0.0097
x_{ETBE}	0.0000	0.9865	0.0000	0.9848	0.0000	0.9869	0.0000	0.9896
x_{NB}	0.9867	0.0049	0.9851	0.0057	0.9872	0.0046	0.9918	0.0006
Flow(Kmol/h)	1071	706	1073	706	1071	706	1069	706
Temperature (K)	333.22	445.52	333.225	445.12	333.21	445.42	333.16	446.73
% conversion	98.5622		98.388		98.6076		98.8862	

3.3 Example 2: Methyl Acetate Reactive Distillation

3.3.1 Process description

Methyl acetate reactive distillation is quaternary reactive distillation system with two reactants and two products. In system, methyl acetate (MeAc) and water (H_2O) are produced from the reversible reaction between acetic acid (HAc) and methanol (MeOH). The esterification reaction in the system is given as

$$CH_3COOH + CH_3OH \leftrightarrow CH_3COOCH_3 + H_2O \quad (36)$$

The pseudo homogenous model reaction kinetic by Tang *et al.* (2005) is given as

$$rate = M_{cat}\left(K_f a_{HAc} a_{MeOH} - K_b a_{MeAc} a_{H_2O}\right) \quad (37)$$

$$K_f = 2.961 \times 10^4 \exp\left(\frac{-49190}{RT}\right) \quad (38)$$

$$K_b = 1.348 \times 10^6 \exp\left(\frac{-69230}{RT}\right) \quad (39)$$

Where M_{cat} is mass of catalyst (kg), K_f and K_b rate constant for forward reaction and backward reactions in kmole per kg per second.

3.3.2 Simulation

The operating conditions for the simulation are taken from Al-Arfaj and Luyben (2002). The column has a total number of 37 stages including reboiler and condenser. UNIFAC activity model was used for the liquid activity coefficients. Table 11 shows the operating conditions that were used.

The steady state composition and temperature profiles are shown in Figures 23 and 24, these profiles are similar to those reported in the literature. Table 12 shows distillate and bottom compositions for different activity models. The compositions, percentage purities and conversions for the activity models are very close. This shows that the activity models can be used interchangeable for correlation of the activity coefficients in the liquid phase. It can also be seen from Table 12 that the distillate and bottom flowrates are not affected by activity models and reactions, this is as result of zero net reaction.

Table 11: Methyl Acetate System Column Configuration and Feed Specification

	Units		
Number of stages		37	
Number of Reactive tray		18	
Pressure	Atm	1.25	
Distillate flow rate (D)	Kmol/h	310	
Reflux ratio		1.875	
		Feed 1	Feed 2
Flow rate		300	300
Stage		9	26
x_{HAc}		1.0	0.0
x_{MeOH}		0.0	1.0
x_{MeAc}		0.0	0.0
x_{H_2O}		0.0	0.0

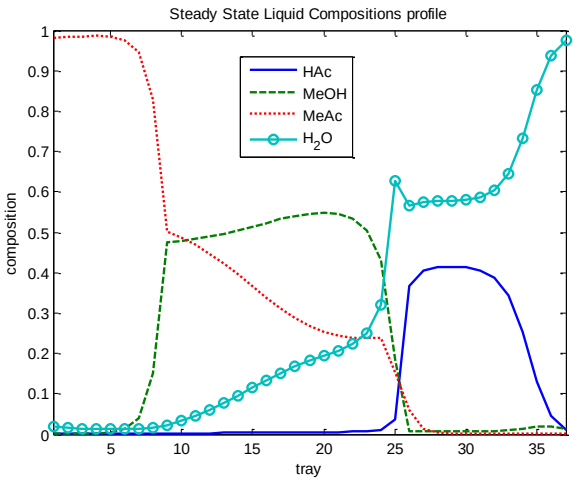

Figure 23: Liquid Composition for Methyl Acetate System

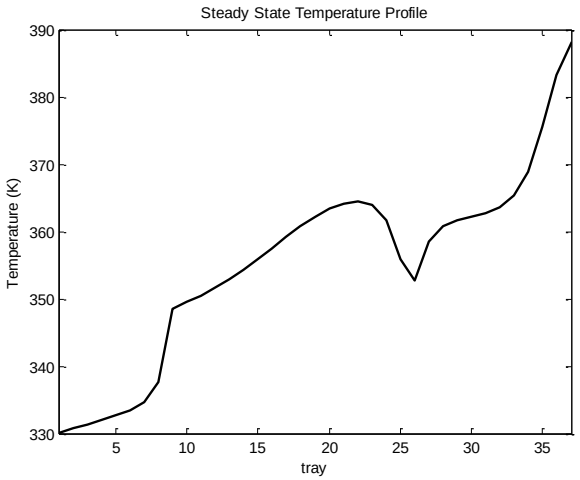

Figure 23: Temperature Profile for Methyl Acetate System

Table 10: Comparison of Different Activity Models for Methyl Acetate System

	UNIFAC		UNIQUAC		WILSON		NTRL	
	Top	Bottom	Top	Bottom	Top	Bottom	Top	Bottom
x_{HAc}	0.0000	0.0012	0.0002	0.0008	0.0000	0.0032	0.0000	0.0032
x_{MeOH}	0.0038	0.0074	0.0029	0.0080	0.0030	0.0000	0.0030	0.0000
x_{MeAc}	0.9640	0.9865	0.9648	0.0000	0.9647	0.0000	0.9647	0.0000
x_{H_2O}	0.0322	0.0049	0.0321	0.9912	0.0323	0.9968	0.0323	0.9968
Flow(Kmol/h)	310	290	310	290	310	290	310	290
Temperature (K)	336.022	380.87	336.32	381.03	334.66	381.02	336.18	380.93
% conversion	99.884		99.900		99.691		99.691	

4 CONCLUSION

The Mathematical model developed from the fundamental principle of material and energy balance lead to a system of DAE that can be systematically solved with commercial DAE solvers like MATLAB ode15s with no initial value and convergence error. The simulation converges dynamically to steady state results. These steady state results are very similar to those obtained using Aspen Plus and are in agreement with results in literature. Therefore the model can be used to study and predict reactive distillation systems.

NOMENCLATURE

B bottom flowrate (mol/s)
D distillate flowrate (mol/s)
F_i feed rate (mol/s)
H_i vapour enthalpy for stage (J/mol)
h_i liquid enthalpy for stage (J/mol)
h_i^f enthalpy of feed (J/mol)
H_i^R heat of reaction in stage (J/mol)
L_i molar liquid flow (mol/s)
P^0 saturated vapour pressure (bar)
P total pressure of the column (bar)
Q_c condenser heat duties (J/s)
Q_R reboiler heat duties (J/s)
R_i total rate of reaction (mol/s)
$r_{i,j}$ rate of production or consumption of component (mol/s)
$.v_j$ stoichiometric coefficient of component
V_i vapour molar flow (mol/s)
$x_{i,j}$ liquid mole fractions of component
$y_{i,j}$ vapour mole fractions of component
δ_i Coefficient of reaction occurrence
γ activity coefficient,
$\emptyset$ fugacity coefficient
Ω_V departure functions of actual gas from ideal gas
Ω_L departure functions of actual liquid from ideal gas

Subscript
i stage i
j component j
c condenser
N last stage
b backward

Superscript
f *Feed*

REFERENCES

Abufares, A.A., Douglas, P.L., 1995. Mathematical modeling and simulation of an MTBE catalytic distillation process using speedup and Aspen plus. *Chemical Engineering Research and Design* 73A, 3–12

Al-Arfaj, M.A. and Luyben, W.L., (2002), Comparative control study of ideal and methyl acetate reactive distillation, *Chemical Engineering Science*, 57: 5039 – 5050.

Bao, J., Gao, B., Wu, X., Yoshimoto, M., Nakao, K., (2002). Simulation of industrial catalytic-distillation process for production of methyl tertbutyl ether by developing user's model on aspen plus platform. *Chemical Engineering Journal* 90, 253–266.

Chen F., Huss R. S., Malone M. F., Doherty M. F., (2002) "Simulation of kinetic effects in reactive distillation" *Computer and Chemical Engineering*, 24, 2457 – 2472

Ciric, A.R. and Miao, P.,(1994), Steady state multiplicities in an ethylene glycol reactive distillation column, *Industrial and Engineering Chemistry Research*, 33(11): 2738–2748.

Guttinger, T.E. and Morari, M., (1997), Predicting multiple steady states in distillation: Singularity analysis and reactive systems, *Computer and Chemical Engineering*, 21(1): 995 – 1000

Henley, E.J. and Seader, J. D. (1981) Equilibrium-stage Separation Operation in Chemical Engineering, Wiley, New York

Holland, C. D. (1980) Fundamentals of Multicomponent Distillation. New York: McGraw-Hill Book Company.

Isla, M.A., Irazoqui, H.A., (1996). Modeling, analysis, and simulation of a methyl tert-butyl ether reactive distillation column. *Industrial and Engineering Chemistry Research* 35, 2696–2708.

Isao, S. Yagi, H., Komatsu, H. and Hirata, M. (1971) "Calculation of Multi-Component Distillation Accompanied by Chemical Reaction" *Journal Chemical Engineering Japan* 4 26-33.

Jacobs, R. and Krishna, R.,(1993). Multiple solutions in reactive distillation for methyl tert-butyl ether synthesis, *Industrial and Engineering Chemistry Research*, 32: 1706–1709

Jana, A. K., (2011), Control of a reactive distillation process: MTBE synthesis. *International Journal of Automation and Control*. 5(1), 61 – 78

Jhon, Y. H., & Lee, T. H. (2003). Dynamic simulation for reactive distillation with ETBE synthesis. *Separation and Purification Technology*, 31, 301–317.

Luyben, W. L. and Yu, C.-C. (2008). Reactive Distillation Design and control. New Jersey: John Wiley & Sons Inc.

Mohammed, M. Z. (2009). Mathematical Modelling and Production of MTBE by Reactive Distillation .Thesis

Mohl, K., Kienle, A., Gilles, E., Rapmund, P., Sundmacher, K. and Hoffmann, U., (1999), Steady-state multiplicities in reactive distillation columns for the production of fuel ethers MTBE and TAME: theoretical analysis and experimental verification, *Chemical Engineering Science*, 54(8): 1029–1043.

Murat M. N., Mohamed A. R., and Bhatia S. (2003) "Modeling of reactive distillation column: methyl tertiary butyl ether (MTBE) simulation studies," *IIUM Engineering Journal*, 4(2), 13 – 30.

Nijhuis S. A Kerkhof, F.P.J.M. and Mak, A.N.S. (1993) "Multiple steady states during reactive distillation of methyl tert-butyl ether," *Industrial and Engineering. Chemistry Research*., 32, 2767-2774.

Pilavachi, P.A., Schenk, M., Perez-Cisneros, E., Gani, R., (1997). Modeling and simulation of reactive distillation operations. *Industrial and Engineering Chemistry Research* 36, 3188–3197.

Rahul, M., Kumar, M. V. P., Dwivedi, D. and Kaistha, N. (2009.) An efficient algorithm for rigorous dynamic simulation of reactive distillation columns. *Computers and Chemical Engineering* 33, 1336–1343

Rehfinger A. and Hoffmann U., (1990) "Kinetics of methyl tertiary butyl ether liquid phase synthesis catalyzed by ion exchange resin-I. Intrinsic rate expression in liquid phase activities," *Chemical Engineering Science*, 45(6), 1605-1617.

Seader, J.D. and Henley, E.J. (1998) Separation Process Principles. New York: John Wiley & Sons.

Sneesby, M. G., Tade, M. O and Smith, T. N. (1999). Two-point control of reactive distillation column for composition and conversion. Journal of Process Control, 9(1), 19-31

Tang, Y. T.; Hung, S. B.; Chen, Y. W.; Huang, H. P.; Lee, M. J.; Yu, C. C. (2005). Design of Reactive Distillations for Acetic Acid Esterification with Different Alcohols . *American Institute of Chemical Engineers Journal* , 51, 1683-1699.

Taylor R. and Krishna R.(2000) "Review: Modelling reactive distillation," *Chemical Engineering Science*, 55, 5183-5229.

Ung, S., and Doherty, M. F. (1995). Vapor – liquid phase equilibrium in systems with multiple chemical reactions. *Chemical Engineering Science*, 50(1), 23

Wang, S. J., Wong, D. S. H. and Lee, E. K. (2003) . Effect of interaction multiplicity on control system design for a MTBE reactive distillation column. *Journal of Process Control*, 13, 503-515

Zhang T., Jensen K., Kitchaiya P., Phillips C. and Datta R. (1997). Liquid-Phase Synthesis of Ethanol-Derived Mixed Tertiary Alkyl Ethers in an Isothermal Integral Packed-Bed Reactor. *Industrial Engineering and Chemistry Research*, 36, 4586-4594

JOURNAL OF THE NIGERIAN SOCIETY OF ENGINEERS
INSTRUCTION TO AUTHORS

1. TYPES OF PUBLICATION

The Journal of the Nigerian Society of Chemical Engineers will publish articles on the original research on the science and technology of Chemical Engineering. Preference will be given to articles on new processes or innovative adaptation of existing processes. Critical reviews on current topics of Chemical Engineering are encouraged and may be solicited by the Editorial Board. The following types of articles will be considered for publication:

a. Full length **articles or review papers**.
b. **Communication** – a preliminary report on research findings.
c. **Note** – a short paper describing a research finding not sufficiently completed to warrant a full article.
d. **Letter to the Editor** – comments or remarks by readers and/or authors on previously published materials.

The authors are entirely responsible for the accuracy of data and statements. It is also the responsibility of authors to seek ethical clearance and written permission from persons or agencies concerned, whenever copyrighted material is used.

2. MANUSCRIPT REQUIREMENTS

a. The **Manuscript** should be written in clear and concise English and typed in Microsoft Word using double spacing on A4-size paper, Times New Romans font and 12 point. A full length article or review should not exceed 15 pages. Margin should be Normal (i.e. 2.54cm for Top, Bottom, Left & Right margins).
b. The **Manuscript** should be prepared in the following format: Abstract, Introduction, Materials and Methods, Results, Discussion, Conclusion, Acknowledgements, and References..
c. The **Manuscript** must contain the full names, address and emails of the authors. In the case of multiple authorship, the person to whom correspondence should be addressed must be indicated with functional email address. As an examples, authors' names should be in this format:
Momoh, S. O., Adisa, A. A. and **Abubakar, A. S.**
If the addresses of authors are different, use the following format:
***Momoh, S. O.[1], Adisa, A. A.[2]** and **Abubakar, A. S.[3]**
Use star * to indicate the corresponding author.
d. **Symbols** should conform to America Standard Association. An abridged set of acceptable symbols is available in the fourth edition of Perry's Chemical Engineering Handbook. Greek letters, subscripts and superscripts should be carefully typed. A list of all symbols used in the paper should be included after the main text as **Nomenclature**.
e. All **Units** must be in the SI units (kg, m, s, N, etc).
f. The **Abstract** should be in English and should not be more than 200 words. The Abstract should state briefly the purpose of the research, methodology, results, major findings and major conclusions. Abstracts are not required for Communications, Notes or Letters.
g. **Citation** must be in the Harvard Format i.e. (Author, Date). Examples are (Smith, 1990) or (Jones et al, 2011). (Kemp, 2000) demonstrated that …..; (Mbuk, 1985; Boma, 1999; Sani, 2000) if more than two authors. (Telma, 2001a), (Telma, 2001b); etc if the citation have the same author and year of publication.
For more information on **Harvard Referencing: Guide** visit
http://www.citethisforme.com/harvard-referencing
h. **References** must also be in the Harvard Format i.e. (Author, Date, Title, Publication Information). References are listed in alphabetical order. Examples are shown below:
Haghi, A. K. and Ghanadzadeh, H. (2005). A Study of Thermal Drying Process. *Indian Journal of Chemical Technology*, Vol. 12, November 2005, pp. 654-663
Kemp, I.C., Fyhr, C. B., Laurent, S., Roques, M. A., Groenewold, C. E., Tsotsas, E., Sereno, A. A., Bonazzi, C. B., Bimbernet, J. J. and Kind M.(2001). Methods for Processing Experimental Drying Kinetic Data. *Drying Technology*, 19: 15-34.
i. **Tables** should contain a minimum of descriptive materials. Tables should be numbered in Arabic numerals (1, 2, 3, etc), and should be placed at the referenced point with captions (centralised) placed at the top of the table.
j. **Figures**, charts, graphs and all illustrations should be placed at the referenced point, numbered in Arabic numerals (1, 2, 3, etc) and incorporated in the text. Caption for Figures should be placed at the bottom of the Figure (centralised). Lettering set or symbols should be used for all labels on the figures, graphs, charts, photographs even when drawn in colours. (Note that figures drawn in colours may be unreadable if printed in black and white).
k. **Equations** should be typed using MS Word Equation Editor and should be centred with number (in Arabic numeral) at the right margin.
l. Wherever possible, **Fractions** should be shown using the oblique slash. E.g. x/y
m. **Footnotes** should not be incorporated in the text.
n. **Acknowledgements** should appear at the end of the paper, before the list of references.

Instruction to Authors

3. SUBMISSION OF MANUSCRIPTS

Manuscripts should be submitted by sending a Microsoft Word document (taking into account the Manuscript Requirements described in section 2 above) to the following email address: nschejournal@yahoo.com and copy stevmomoh@yahoo.com**.**
All correspondences are directed to the Editor-in-Chief using the submission emails addresses: nschejournal@yahoo.com and copy stevmomoh@yahoo.com.

4. ACCEPTED PAPERS

On acceptance, authors will be required to submit a copy of their manuscripts using Microsoft Word by emails to nschejournal@yahoo.com and copy stevmomoh@yahoo.com.

The following additional information should be observed for accepted papers: (i) Typed in Microsoft Word using 1.15 spacing on A4-size paper, Times New Romans font and 10 point; (ii) Margin should be 2.54cm for Top & Bottom; 2.20cm for Left & Right margins; (iii) The abstract should be one column document while the body of the manuscript should be double columns with 0.5cm gutter spacing except some tables and figures that may have to go in for one column document.

5. PUBLICATION

Full NSChE Journal edition in hard copy will be published twice annually.

6. REPRINT

Reprints are available on request at a moderate fee per page. Orders must be placed before the paper appears in Print.

7. READER'S INFORMATION

The papers are wholly the view of their author(s) and therefore the publishers and the editors bear no responsibility for such views.

8. SUBSCRIPTION INFORMATION

The subscription price per volume is as follows:

a.	Individual Reader	-	N1,500.00
b.	Institutions, Libraries, etc.	-	N2,500.00
c.	Overseas Subscription	-	$30.00

Request for information or subscription should be sent to the Editor-in-Chief through the following emails addresses: nschejournal@yahoo.com and copy stevmomoh@yahoo.com.

9. COPYRIGHT NOTICE

Copyright of published material belongs to the journal

10. PRIVACY STATEMENT

The names and email addresses entered in this journal site will be used exclusively for the stated purposes of this journal and will not be made available for any other purpose or to any other party**.**